P2X RECEPTOR FUNCTION IN *LYMNAEA STAGNALIS* AND OTHER LOWER ORGANISMS

Thesis submitted for degree of

Doctor of Philosophy

at the University of Leicester

by

Selvan Bavan

Department of Cell Physiology & Pharmacology

University of Leicester

September 2010

Selvan Bavan

P2X receptor function in *Lymnaea stagnalis* and other lower organisms

The mollusc *Lymnaea stagnalis* has a relatively simple central nervous system (CNS) consisting of large and easily identifiable neurons. This feature together with well characterized neuronal circuitry for important physiological processes and an established adenosine 5'-triphosphate (ATP) release system puts *Lymnaea* forward as an attractive model to examine the CNS function of P2X receptors. Furthermore, lower organism P2X receptors may provide structure function insights by virtue of conservation of functionally important domains. Following the identification of a P2X receptor-like sequence (*Lym*P2X) in the *Lymnaea* CNS, the cloned complementary deoxyribonucleic acid encoding *Lym*P2X when heterologously expressed in *Xenopus* oocytes exhibited ATP-evoked inward currents (EC_{50}: 6.2 μM) with slow desensitisation. 2', 3'-O-(4-Benzoylbenzoyl) adenosine 5'-triphosphate (BzATP) was a partial agonist (EC_{50}: 2.4 μM), whilst pyridoxalphosphate-6-azophenyl-2', 5'-disulphonic acid (PPADS) and suramin were antagonists (IC_{50}: 8.1 and 27.4 μM respectively). A P2X receptor from another invertebrate *Hypsibius Dujardini* (*Hd*P2X) was also characterised in a comparative study. This tardigrade receptor displayed ATP-evoked currents (EC_{50}: 28.5 μM) with extremely rapid activation and desensitization kinetics, which were concentration-dependently inhibited by copper and zinc. Histidine 306 in *Hd*P2X was found to have a minor role in copper inhibition. Quantitative reverse transcription-polymerase chain reaction and *in situ* hybridization detected *Lym*P2X expression in all CNS ganglia, including buccal suggesting a possible role in the feeding network. Intracellular recording of motoneuron activity demonstrated that application of ATP (1 mM) to buccal ganglia increased the rate of fictive feeding whereas PPADS abolished this response. The application of BzATP, in an attempt to selectively activate P2X receptors, did not trigger fictive feeding, suggesting that *Lym*P2X activation alone does not initiate the feeding rhythm. BzATP however did cause a significant hyperpolarisation of a key feeding motoneuron, suggesting that *Lym*P2X activation may be required for the latter phase in the ATP-evoked feeding cycle.

Acknowledgments

I would like to express my gratitude to my supervisors Dr. Steve Ennion and Dr. Volko Straub for selecting an exciting research project, for their support, and advice through the Ph.D. Dr. Steve Ennion's molecular biology work has been of great assistance in allowing me to generate data for this thesis. Dr. Volko Straub's guidance in experiments and thesis writing has been very beneficial in terms of my development as a scientist. I would also like to thank BBSRC for funding this studentship.

In addition I would like to show my appreciation to members of the Department of Cell Physiology and Pharmacology, who have provided an approachable working environment. Particularly I would like to thank Prof. Richard Evans for his role in my thesis committee and providing advice for my research. Also to Dr. Michael Sereda for guiding me through the quantitative RT-PCR technique, Waheeda Nasreen for helping me carry out some of the quantitative RT-PCR experiments, Matt Barker for his assistance in using the cryostat, Dr. Martine Hamann for her help in photomicroscopy, and Susan Giblett from the Department of Biochemistry for taking considerable time to provide paraffin-embedded sections for *in situ* hybridization experiments.

Finally I would like to thank my family for their support and encouragement through my academic career.

Publications

Abstract:

BAVAN, S., STRAUB, V. A., & ENNION, S. J. (2008) Pharmacological characterisation of a P2X receptor cloned from the central nervous system of *Lymnaea stagnalis*. *Purinergic Signal*. 2008 May; 4(Suppl 1): 1–210.

Purines 2008, Copenhagen.

Journal paper publication:

BAVAN, S., STRAUB, V. A., BLAXTER, M. L. & ENNION, S. J. (2009) A P2X receptor from the tardigrade species *Hypsibius dujardini* with fast kinetics and sensitivity to zinc and copper. *BMC Evol Biol*, 9**,** 17.

Contents

Contents of figures

Chapter 1

Chapter 2

Chapter 3

Chapter 4

Chapter 5

Abbreviations

ACh	acetylcholine
ADP	adenosine 5’-diphosphate
AFM	atomic force microscopy
AF-792	5-(5-ethynyl-2-isopropyl-4-methoxy-phenoxy)-pyrimidine-2, 4-diamine
AMP	adenosine 5’-monophosphate
ASIC	acid sensing ion channel
ATP	adenosine 5’-triphosphate
αβmeATP	α,β-methylene adenosine 5’-triphosphate
*Bm*P2X	P2X receptor identified from *Boophilus microplus*
BzATP	2’, 3’-O-(4-Benzoylbenzoyl) adenosine 5’-triphosphate
B4Cl	buccal ganglia B4 cluster neuron
cAMP	cyclic AMP
cDNA	complementary deoxyribonucleic acid
CFA	complete Freund’s Reagent
CGC	cerebral giant cell
CNS	central nervous system
CNQX	6-cyano-7-nitroquinoxaline-2,3-dione
CODEHOP	COnsensus-DEgenerate Hybrid Oligonucleotide Primer
CPG	central pattern generator
cRNA	complementary ribonucleic acid
C_t	number of PCR cycles to reach exponential phase
CFP	cyan fluorescent protein
DEG/ENaC	degenerin / epithelial sodium channel family

DEPC	diethyl-pyrocarbonate
DIG	digoxigenin
DNA	deoxyribonucleic acid
DNP	dinitrophenyl
dsRNA	double stranded ribonucleic acid
ERK	extracellular-regulated signal kinase
EST	expressed sequence tags
FlAsH	fluorescein arsenical hairpin spectroscopy
FRET	fluorescence resonance energy transfer
FT	phenylalanine threonine motif
GABA	gamma-amino butyric acid
GFP	green fluorescent protein
*Hd*P2X	P2X receptor identified from *Hypsibius dujardini*
HEK-293	human embryonic kidney cell line
IP3	input 3 (*Lymnaea* neuron)
KCl	potassium chloride
KirBac1.1	bacterial inward rectifier potassium channel
*Lym*P2X	P2X receptor identified from *Lymnaea stagnalis*
LPeD1	left pedal dorsal 1 (*Lymnaea* neuron)
min	minute
ml	millilitre
mM	millimolar
mRNA	messenger ribonucleic acid
MscL	mechanosensitive channel
MTS	methanethiosulfonate

MTSEA	2-aminoethyl-methanethiosufonate, a positively charged MTS
MTSES	2-sulfonatoethyl-methanethiosufonate, a negatively charged MTS
MTSET	2-trimethylammonioethyl-methanethiosufonate, a positively charged MTS
MTSM	methyl-methanethiosulfonate, a neutral MTS
mV	millivolt
mV.s	millivolt x second
nAChR	nicotinic acetylcholine receptor
NBT/BCIP	nitro blue tetrazolium chloride / 5-bromo-4-chloro-3-indolyl phosphate
NFR	asparagine phenylalanine arginine motif
Ni^{2+}-NTA	nickel-nitrilotriacetic acid
NF02	8, 8'-(carbonylbis(imino-3, 1-phenylene carbonylimino)bis(1, 3, 5-naphthalenetrisulfonic acid naphthalenetrisulfonic acid
$NMDG^{+}$	N-methyl-D-glucamine
NOS	nitric oxide synthase
ng	nanogram
ORF	open reading frame
PAGE	polyacrylamide gel electrophoresis
PBS	phosphate buffered saline
PCO_2	partial pressure of carbon dioxide
PCR	polymerase chain reaction
PFA	paraformaldehyde
pg	picogram
PKC	protein kinase C

PSFHSWSamide	leucokinin-like Peptide
PPADS	pyridoxalphosphate-6-azophenyl-2', 5'-disulphonic acid
qRT-PCR	quantitative reverse transcription PCR
RACE	rapid amplification of complementary DNA ends
RFP	red fluorescent protein
RNA	ribonucleic acid
RPeD1	right pedal dorsal 1
RT-PCR	reverse transcription PCR
s	second
SCAM	substituted cysteine accessibility mutagenesis
S. D.	standard deviation of the mean
S. E.	standard error of the mean
ssRNA	single stranded RNA
TM	transmembrane domain
TNP-ATP	2′,3′-O-(2,4,6- trinitrophenyl) adenosine 5′-triphosphate
tRNA	transfer RNA
TSA	tyramide signal amplification
UTP	uridine 5’-triphosphate
µg	microgram
µM	micromolar
VD4	visceral dorsal 4 (*Lymnaea* neuron)
YFP	yellow fluorescent protein
2-MeSATP	2-(methylthio) ATP
7TM GPCR	seven transmembrane domain G-protein coupled receptor

Chapter 1: General Introduction

1.1 Cellular roles of ATP

Adenosine 5'-triphosphate (ATP) is a purine nucleotide molecule and its primary function is to act as a source of energy to drive cellular processes. ATP also functions as a building block for many important intracellular molecules such as DNA and as a phosphate group donor in phosphorylation reactions. In addition to these intracellular roles, ATP also has a role outside of the cell where it acts as an extracellular signalling molecule in many physiological processes in both the animal and plant kingdoms.

The structure of ATP consists of an adenine ring as the purine base, which is bonded to the first (1') carbon atom of ribose, a pentose sugar. The 5' carbon atom of the pentose sugar is bonded to three negatively charged phosphate groups. ATP has a chemical formula ($C_{10}H_{16}N_5O_{13}P_3$), with a molecular weight of 507.2. ATP is produced in glycolysis, the Krebs cycle and oxidative phosphorylation stages of cellular respiration.

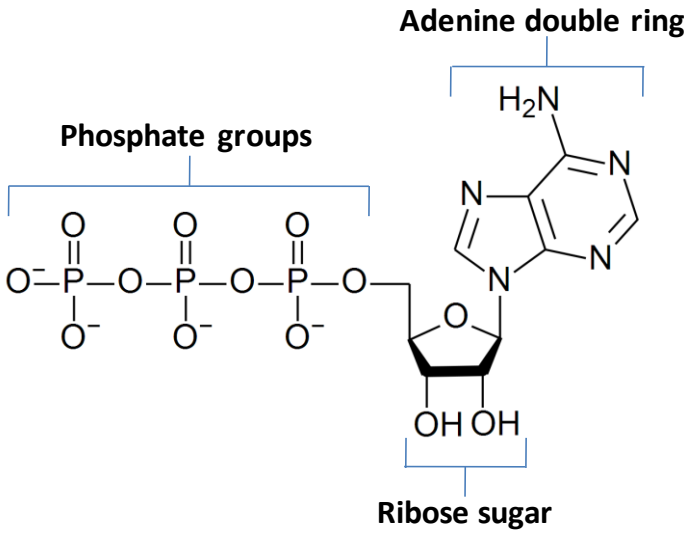

Figure 1.1. Chemical structure of ATP, composed of an adenine ring bonded to a ribose sugar attached to three phosphate groups.

-30.5 kJ of net enthalpy change occurs following the breakdown of a single molecule of ATP into adenosine 5'-diphosphate (ADP) and inorganic phosphate (Pi), providing energy for the cell to carry out its functions (Berg J. M., 2007). This inorganic phosphate is also known as gamma phosphate, and it is located furthest from the ribose.

Extracellular ATP concentration varies widely between species and among the different tissues within an organism, depending on the requirements for energy expenditure used for processes such as muscle contraction. ATP concentrations can be measured by various ATP sensors such as luciferin (Yegutkin, 2008). In the presence of ATP as a co-factor, the luciferase enzyme catalyses the conversion of luciferin substrate into oxyluciferin and emits light which acts as an indicator of the amount of ATP in a sample. Concentrations of extracellular ATP are usually in the nanomolar range (10^{-9} to 10^{-7} mol/L), however following inflammation or traumatic shock, extracellular ATP concentrations can reach up to 10^{-5} to10^{-4} mol/L (Yegutkin, 2008).

1.2 The identification of ATP as a signalling molecule

Over fifty years ago it was discovered that ATP and its breakdown products are the vasodilators which mediate the transmission of impulses from both central and peripheral sensory nerve endings in horse dorsal spinal root (Holton and Holton, 1954). Acetone-dried powders prepared from the dorsal and ventral spinal roots were assessed for vasodilator activity at various stages of purification in comparison to ATP, followed by paper chromatography that showed an ultraviolet absorption of between 260 - 265

mμ, positions corresponding to ATP and ADP (Holton and Holton, 1954). Later it was found that rabbit nerves release ATP after electrical or mechanical stimulation of the great auricular sensory nerve to cause vasodilatation (Holton, 1959, Burnstock, 1972). ATP was detected using the firefly luciferase method that emits light in the presence of ATP (Holton, 1959). Further studies suggested that ATP was the transmitter released from non-adrenergic and non-cholinergic nerve endings for the inhibitory control of mammalian gastrointestinal smooth muscle (Burnstock *et al.*, 1970). The conclusion that ATP acts as a neurotransmitter led to the definition of purinergic nerves (Burnstock, 1972).

ATP satisfies the criteria for classification as a neurotransmitter (Dale, 1934), by virtue of the following characteristics:

1) The neurotransmitter substance (ATP) and enzymes for its synthesis are located in the neuron

2) ATP is released from nerve endings following nerve activation

3) The effect of released ATP on nerve stimulation is mimicked by exogenous application of the transmitter to the effector neuron

4) The existence of mechanisms for inactivation of the transmitter

5) The effects of the exogenously applied transmitter being modulated by drugs to increase or decrease the response.

Prior to its release into the synaptic cleft, ATP is loaded into readily releasable

presynaptic vesicles by an ADP/ATP translocase. ATP can be released from the presynaptic terminal through several mechanisms such as Ca^{2+}-mediated exocytosis upon nerve depolarization. Gap channels, hemichannels, volume sensitive chloride channels, or flow through dilation pores of highly permeable receptors serve as other routes for ATP entry into the synaptic cleft. ATP can be released from nerve terminals as a co-transmitter with acetylcholine (Van der Kloot, 2003). ATP can also be packaged in separate pools of presynaptic vesicles to GABA, glutamate or other transmitters that also enter the synaptic cleft upon arrival of a presynaptic action potential (Pankratov *et al.*, 2006, Pankratov *et al.*, 2007).

ATP in the synaptic cleft is hydrolysed to ADP, AMP or adenosine by removal of phosphate groups through the action of ectonucleotidases such as the E-NTPDase (ectonucleoside triphosphate diphosphohydrolase) family, E-NPP (ectonucleotide pyrophosphatase/phosphodiesterase) family, or by alkaline phosphatases (Zimmermann, 1996, Zimmermann, 2001, Huxtable *et al.*, 2009).

1.3 Receptors that bind ATP

In order for ATP to carry out its extracellular functions as a ligand, binding to specific receptors must occur. P2 purinergic receptors are divided into ion channels and G protein-coupled receptors that bind nucleotides such as ATP, leading to their activation. The existence of ATP-gated ion channels was first suggested when application of the non-hydrolysable ATP analogue α,β-methylene adenosine 5'-triphosphate (αβmeATP)

to the rat medial habenula gave rise to membrane currents with a time course faster than that which would be expected from indirect G protein-coupled receptor activation (Edwards *et al.*, 1992). The medial habenula that was exposed to glutamate, GABA, muscarinic and sodium channel blockers had amplitudes of the fast minature synaptic currents further reduced upon application of suramin, a known ATP channel blocker (Edwards *et al.*, 1992). This was the first time that ATP was shown to be a fast acting transmitter to mediate synaptic currents in the brain (Edwards *et al*., 1992).

It is now known that these ATP-gated ion channels, subsequently called P2X receptors, form part of a family of purinergic receptors for extracellular nucleotides and nucleosides. This family also consists of P1 receptors (Fredholm *et al.*, 2001) and P2Y receptors (Burnstock, 1996), which are both seven transmembrane domain G protein-coupled receptors. P1 receptors are adenosine sensitive and are classified as P1 A_1, A_{2A}, A_{2B} and A_3 (Fredholm *et al*., 2001). A_1 and A_3 receptors couple to G_s and A_{2A} and 2_B couple to $G_{i/o}$ (Fredholm *et al*., 2001). P2Y receptors are grouped into $P2Y_1$ to $P2Y_{14}$ subtypes, the majority of which couple to phospholipase C through G-proteins, which leads to increases in intracellular calcium (North and Barnard, 1997).

Following the binding of ATP to P2X receptors, the ion channel becomes activated to open and non-selectively allow positively charged ions to flow down their electrochemical gradient. P2Y receptors are a family of G protein-coupled receptors that couple to intracellular second-messenger systems and have a wider agonist profile in that they can also be activated by UTP and ADP.

1.4 Cloning of P2X receptors

$P2X_1$ from rat *vas deferens* was the first P2X receptor-encoding complementary DNA (cDNA) to be cloned (Valera *et al.*, 1994). The existence of this receptor was first suggested from ATP-evoked responses in *Xenopus* oocytes injected with poly(A)+ RNA isolated from rat *vas deferens* using oligo(dT) cellulose chromatography. Subsequent generation of a unidirectional *vas deferens* cDNA library allowed subdivisions of this library to be transcribed and analyzed in *Xenopus* oocytes. A single clone encoding a functional ATP-gated channel of 399 amino acids was identified and named $P2X_1$ (Valera *et al*., 1994).

A second P2X receptor, termed $P2X_2$ with a length of 472 amino acids was identified shortly after the discovery of $P2X_1$ from a cDNA expression library constructed from rat pheochromocytoma PC12 messenger RNA (Brake *et al.*, 1994). The presence of this $P2X_2$ receptor in PC12 cells was first suggested from ATP-evoked currents in these cells (Nakazawa *et al.*, 1990). A cDNA clone isolated from the PC12 cDNA library also produced functional ATP-gated channels when expressed in *Xenopus* oocytes (Brake *et al.*, 1994).

The detection of ATP-evoked nociceptive effects on sensory neurons led to the discovery of a third P2X receptor, $P2X_3$ (Chen *et al.*, 1995). $P2X_3$ was identified from a 3.8kb transcript from rat dorsal root ganglion sensory neurons, and an *in-vitro* coupled transcription translation system revealed a protein product of 397 amino acids with sequence homology to $P2X_1$ and $P2X_2$ (Chen *et al*., 1995). $P2X_4$ was originally isolated

by low stringency screening of a rat hippocampal cDNA library brain with probes derived from sequence data of $P2X_1$ and $P2X_2$ DNA clones (Bo *et al.*, 1995). This receptor when injected into oocytes gave rise to slow inward currents. A cDNA of $P2X_4$ isolated from rat superior cervical ganglion shortly after that was transfected into HEK293 cells to produce functional P2X receptors also exhibited similar slow kinetic currents (Buell *et al.*, 1996). The $P2X_5$ receptor subunit was isolated from rat celiac ganglia as well as rat heart, and $P2X_6$ from a superior cervical ganglion cDNA library and a rat brain (Collo *et al.*, 1996, Garcia-Guzman *et al.*, 1996, Soto *et al.*, 1996). Lastly, a $P2X_7$ receptor subunit of 595 amino acids was identified, and this receptor possessed an interesting property of increased pore size following agonist activation (Surprenant *et al.*, 1996, Rassendren *et al.*, 1997b). This allowed the flow of large molecules of 600-900Da such as the propidium dye YO-PRO1 (Surprenant *et al.*, 1996, Rassendren *et al.*, 1997b). These seven P2X receptor subunits ($P2X_1$ – $P2X_7$) represent the full complement of P2X receptors identified and cloned from mammals (North, 2002).

The first instance of cloning of an invertebrate P2X receptor was from the parasitic blood fluke *Schistosoma mansoni* (Agboh *et al.*, 2004). The expansion in genomic and EST sequence databases consisting of sequences from a range of species had allowed a bioinformatics approach to screen a variety of lower organisms for P2X receptor-like protein encoding sequences. A cDNA clone from the *Schistosoma mansoni* cDNA library of 1492 bp contained an open reading frame of 1314 bp (Agboh *et al.*, 2004). Introduction of a Kozak sequence at the initiation codon and substitution of the 5′-untranslated region of the *Schistosoma mansoni* gene with the 5′-untranslated region of the human $P2X_1$ gene generated functional ATP-gated channels in *Xenopus* oocytes

(Agboh *et al*., 2004).

P2X receptors were subsequently identified from a range of non-vertebrate organisms such as the slime mould *Dictyostelium discoideum* (Fountain *et al.*, 2007) and the single celled green algae *Ostreococcus tauri* (Fountain *et al.*, 2008). *Ostreococcus tauri* represents one of the smallest existing eukaryotes (Derelle *et al.*, 2006), and the identification of a P2X receptor from this organism that emerged over a billion years ago gives insight into the evolution of P2X receptors and their functionality in various species over time. P2X receptors have yet to be discovered in a prokaryote and given the large number of complete prokaryotic genomes that have been fully sequenced, it is expected that, unlike other ion channel families, the P2X receptors are restricted to eukaryotes. Not all eukaryotic species however possess P2X receptors as *A. gambiae, C. elegans* and *D. melanogaster* for which complete genomic data are available lack P2X-like protein sequences (Fountain and Burnstock, 2009). The future identification of P2X receptors from other eukaryotic phyla will provide information that will allow a better estimate of the pattern of loss of P2X receptors from various species during the course of eukaryotic evolution.

1.5 P2X receptor structure

The first structure of a P2X receptor was recently determined to a resolution of 3.1 Å by crystallization of the zebrafish $P2X_4$ receptor ($zP2X_4$) in a closed, resting state (Kawate *et al.*, 2009). The high potential for crystallization of this P2X receptor was

indicated by its ability to aggregate in a well-ordered arrangement in the presence of detergents, and its monodisperse diffraction profile in fluorescence spectroscopy analysis (Ostermeier and Michel, 1997, Kawate and Gouaux, 2006). Among the P2X subtypes screened, $P2X_4$ was selected as a suitable candidate for crystallization studies following fluorescence-detection-size-exclusion chromatography (FSEC) experiments on green fluorescent protein (GFP)-tagged versions of the receptor, which proved to be a fast and efficient pre-crystallization screening procedure (Kawate and Gouaux, 2006). FSEC of $zP2X_4$ displayed a sharp, symmetrical elution profile demonstrating its purity and stability in a complex (Kawate *et al*., 2009).

The $zP2X_4$ receptor complex consists of an arrangement of three subunits, each composed of a dolphin shape (Figure 1.2). α-helices form the transmembrane domains (TM) and β-sheets mainly constitute the extracellular body, with smaller structurally distinct extensions from the body forming subunit contacts (Kawate *et al*., 2009). The extracellular domain emerges ~70 Å above the membrane surface, and ~28 Å of subunit structure forming the transmembrane helix is buried in the membrane. N- and C- termini regions of the channel previously shown to be intracellular domains were truncated from the receptor-encoding sequence to make the zebrafish $P2X_4$ receptor more amenable to crystallization. While maintaining ATP-gated currents, further point mutations and exposure to gadalonium ions (Gd^{3+}) were carried out to facilitate structural determination of the receptor at higher resolutions (Figure 1.2C). Despite the lack of primary amino acid sequence similarity, many aspects of the P2X atomic structure are similar to that of the acid-sensing ion channel (ASIC) that was also elucidated by the same research group (Gonzales *et al*., 2009).

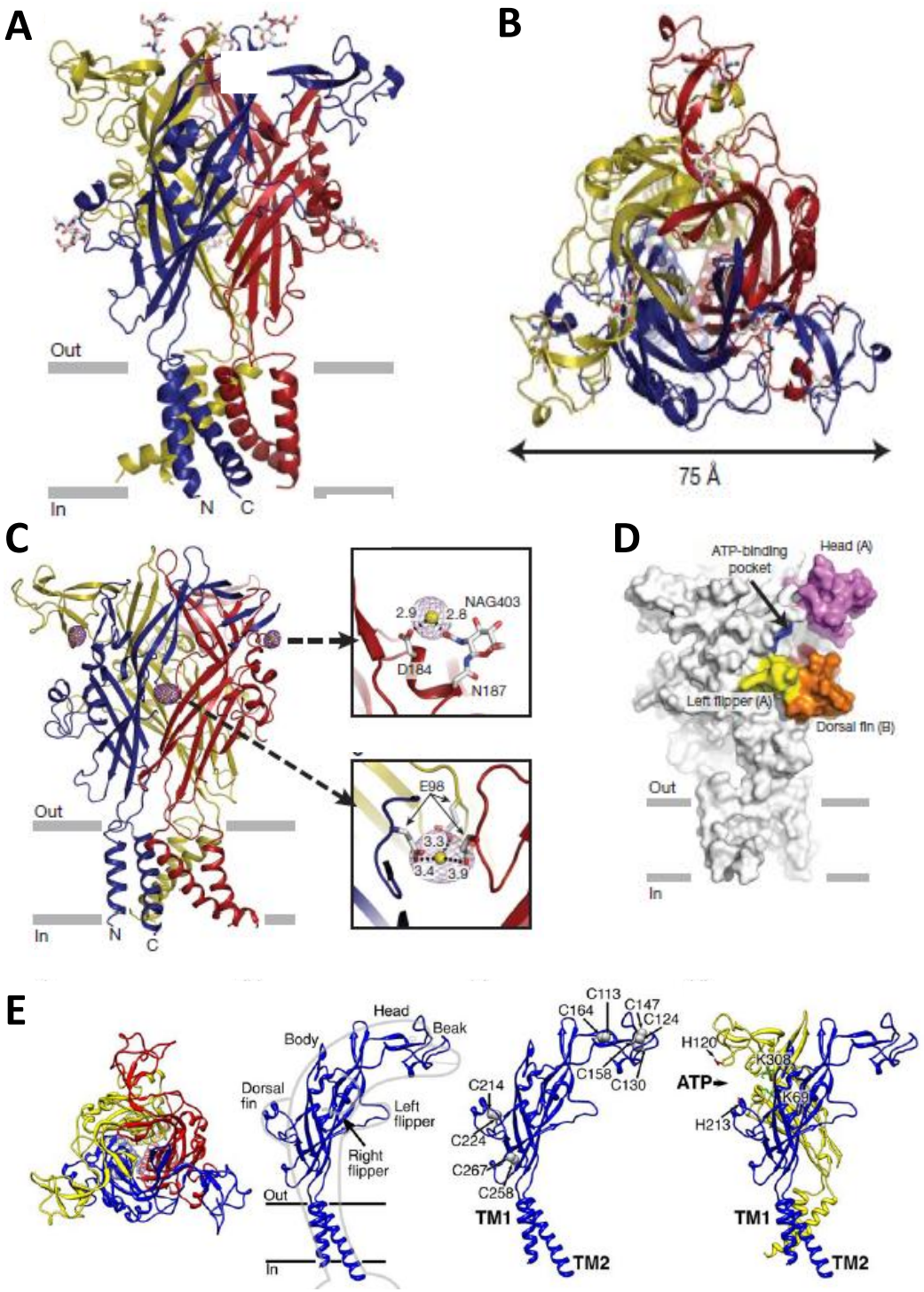

Figure 1.2. $zP2X_4$ receptor structure taken from Kawate *et al.*, (2009) and Browne *et al.*, (2010). A, $zP2X_4$ viewed parallel to the membrane plane. B, $zP2X_4$ structure viewed from above the membrane plane. C, position of Gd^{3+} binding sites. D, surface representation model with putative ATP binding site. E, subunit fold structure is shaped like a dolphin, with α-helical transmembrane domains, and β-sheets forming the extracellular body. Head, flipper and dorsal fin structures are attached to the extracellular body. For A, B, C, and E the red, yellow and blue colours highlight the different subunits of the P2X receptor.

Acquiring the P2X receptor crystal structure has not only increased knowledge of the mechanisms behind P2X receptor functionality, but will also help discover the molecular principles that underlie agonist and antagonist binding. This will accelerate the design and development of drugs targeting P2X receptors for therapeutic applications.

A year previous to the crystal structure elucidation, the methods of fluorescence resonance energy transfer (FRET) with electron microscopy were used to determine the three dimensional structure of $P2X_4$ to a resolution of 21 Å (Figure 1.3)(Young *et al.*, 2008). $P2X_4$ receptors histidine-tagged at their intracellular C-termini were purified by non-denaturing gel-electrophoresis, followed by negative staining for electron microscopy (Young *et al.*, 2008). Addition of Ni^{2+}-NTA-Nanogold particles were used to orientate $P2X_4$ receptors for electron microscopy, and lectins were applied to label the extracellular domain in order to obtain more electron density for the ectodomain (Young *et al.*, 2008). This procedure judged the $P2X_4$ structure to be a globular torpedo-like molecule with dimensions of 12 nm long by 8 nm wide with an estimated volume of 270 nm^3, in agreement with the crystal structure of $zP2X_4$ (Young *et al.*, 2008, Young, 2009). The distance between the intracellular C- terminals was determined by FRET and electron microscopy to be about 6.1nm apart (Young *et al.*, 2008). However this approach was not successful in the determination of transmembrane regions due to the binding of detergent micelles at this region of the receptor (Young *et al.*, 2008). Subsequently the $P2X_2$ structure was determined to a resolution of 15 Å by cryo-electron microscopy in combination with a helium cooled stage (Mio *et al.*, 2009). The structural information gathered suggested that the receptor was vase-shaped, 202 Å in height and 160 Å in diameter, possessed a two-layered

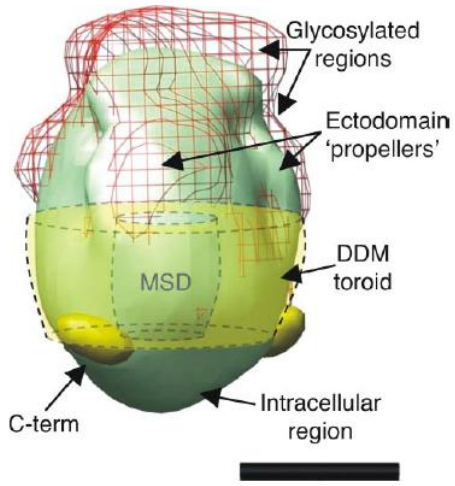

Figure 1.3. Model of human $P2X_4$ receptor, based on electron microscopy data from Young *et al*., (2008). Lectin labelling that reported further density, expected to be regions of glycosylation on the ectodomain, is displayed as a *dark pink mesh*, and the gold particles highlighting the position of the C termini (*C*-term) are also displayed towards the bottom of the molecule. The approximate location of a toroidal β-D-dodecyl maltoside (DDM) micelle surrounding the membrane-spanning domain (MSD) is also present in the model.

internal structure, and that the subunits are loosely associated with each other (Mio *et al.*, 2009).

Obstacles and challenges previously encountered with attempted crystallization of membrane proteins including P2X receptors were the expression of sufficient protein quantities and purification of stable trimers required for structural determination (Tate, 2001, Young, 2009). Prior to the elucidation of the P2X receptor three dimensional organization, structural information of the P2X subunit and receptor complex were obtained by mutagenesis approaches. How these earlier approaches were used to discover functionally important residues and domains, subunit assembly to form a functional receptor complex and how the recently determined crystal structure is in agreement with these earlier findings will be discussed in more detail in the following sections.

1.5.1 P2X subunit structure topology

A basic schematic diagram for P2X subunit topology was first proposed from the identification of $P2X_1$ and $P2X_2$ (Brake *et al.*, 1994, Valera *et al.*, 1994). Subsequent mutagenesis studies confirmed the subunit topology to consist of intracellular N- and C- termini, and two transmembrane domains separated by a large extracellular ATP-binding 'loop' domain (Figure 1.4). This topology is also similar to inwardly rectifying potassium channels (Kubo *et al.*, 1993, Doupnik *et al.*, 1995) and epithelial sodium / degenerin (ENaC/DEG) channel family members (Kellenberger and Schild, 2002).

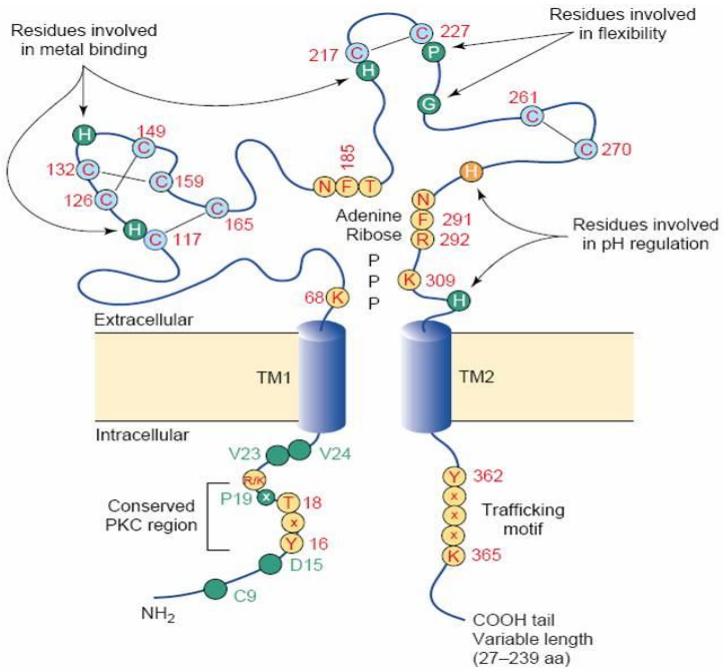

Figure 1.4. Schematic diagram of a P2X receptor subunit proposed before determination of three-dimensional structure, displaying the intracellular N- and C-termini, 2 TM domains, extracellular binding loop and the important amino acid residues that have functional properties in these regions. Highlighted residues include prolines and glycines that influence the flexibility of the extracellular loop, histidines that are involved in metal binding and cysteines take part in disulphide bonding with each other. Figure taken from Vial *et al.*, (2004)

Hydrophobicity plots displaying a high proportion of hydrophobic residues in two areas of the receptor sequence first suggested the presence of two transmembrane domains (Valera *et al*., 1994). Evidence of two transmembrane domains was extended by an N-glycosylation site tagging approach that targeted residues that are only present in the extracellular domain, followed by a gel shift assay to detect glycosylated residues (Newbolt *et al.*, 1998). Residues in the $P2X_2$ sequence towards the amino-terminal were mutated to an asparagine-containing artificial consensus sequence for glycosylation (N-X-S/T), and absence of glycosylation of N-terminal sites at positions 9, 16 or 26 suggested their intracellular location. Further, glycosylation consensus sequences introduced at positions K324N, I328N and A335T towards the carboxy-terminal of $P2X_2$ failed to be glycosylated, indicating that the C-terminal does not have an extracellular location that is accessible to glycosylating enzymes (Newbolt *et al*., 1998). Additional evidence of the intracellular location of the amino and carboxy-termini came from studies in HEK293 cells expressing N- and C- termini epitope-tagged $P2X_2$ receptors, where antibodies only bound the introduced epitope after the cells were permeabilized (Torres *et al.*, 1998a).

The extracellular domain of P2X receptors also contain asparagine residues that are sites for N-glycosylation (Newbolt *et al*., 1998). Functional receptors were maintained when only one of the three asparagines of $P2X_2$ was mutated, whereas mutation of more than one asparagine residue resulted in receptors with significantly lower current amplitudes or non-functional channels (Newbolt *et al*., 1998). The N-terminus contains a conserved protein kinase C consensus site that has been proposed to be involved in

phosphorylation, and has been found to regulate the time course of responses in $P2X_2$ receptors (Boue-Grabot *et al.*, 2000) and $P2X_1$ receptors (Ennion and Evans, 2002b). The length of the C-terminal intracellular domain varies amongst the seven P2X subunits, with $P2X_7$ possessing an unusually long C-terminus (North, 2002, Yan *et al.*, 2005). The C-terminus also plays a role in current desensitization (Koshimizu *et al.*, 1999, Yan *et al.*, 2005).

1.5.2 Three subunits combine to form a functional P2X receptor complex

Early studies by both chemical-cross linking (Nicke *et al.*, 1998, Aschrafi *et al.*, 2004, Barrera *et al.*, 2005) and atomic force microscopy (AFM) (Barrera *et al.*, 2005) suggested that three P2X subunits combine non-covalently to form a functional channel.

In chemical cross-linking studies, $P2X_1$ and $P2X_3$ receptor subunits with histidine tags attached to their intracellular termini were cross linked by analogues of the P2X antagonist PPADS, followed by Ni^{2+} agarose chromatography and blue native PAGE to reveal band sizes corresponding to trimers (Nicke *et al.*, 1998). AFM allows direct imaging of receptor proteins and measurement of the mean molecular volume of rat $P2X_2$, which was found to be 409 nm^3, corresponding to the size of a trimeric receptor (Barrera *et al.*, 2005). This size of 409 nm^3 is in agreement with the electron microscopy measurement for human $P2X_4$ of 270 nm^3, when the difference in molecular mass between the two receptor subtypes, 165 kDa for human $P2X_4$ trimers

compared to 210 kDa for rat $P2X_2$ trimers, is taken into consideration (Young *et al.*, 2008).

An angle of ~120 degrees between subunits was observed after antibodies were targeted against introduced epitopes at the N-termini, which is in agreement with the trimeric assembly of the channel (Barrera *et al.*, 2005). The crystal structure of the $zP2X_4$ subunits was shown to be arranged in a three-fold axis of symmetry when viewed from the extracellular side, perpendicular to the membrane plane, and therefore in agreement with Barrera's earlier findings.

1.5.3 Transmembrane domains

Amino acid residues spanning positions near 30 to 50 and 330 to 353 form the transmembrane domains TM1 and TM2 respectively (North, 2002). TM1 and the external half of TM2 were proposed to adopt alpha-helical secondary structures (Li *et al.*, 2004, Silberberg *et al.*, 2005), with the rest of TM2 being relatively unstructured (Li *et al.*, 2004). For TM1, this was found using alanine scanning mutagenesis where every third or fourth substituted residue significantly affected the receptor potency, consistent with the turn of an α-helix every 3 - 4 residues (Li *et al.*, 2004).

This proposed TM domain structure turned out to be in agreement with the $zP2X_4$ crystal structure which additionally showed that the transmembrane helices are oriented

roughly antiparallel to one another and are angled almost 45 ° from the membrane plane within each subunit (Kawate *et al*., 2009). This arrangement of transmembrane domains is similarly observed in ASICs (Gonzales *et al*., 2009). The inner TM2 helices are co-ordinated around a threefold axis of symmetry and cross each other approximately halfway across their membrane-spanning lengths. This has the effect of narrowing the transmembrane pore and defining the gate as well as the closed, resting state of the ion channel. The outer positioned TM1 helices surround the TM2 helices (Kawate *et al*., 2009).

1.5.4 Extracellular domain

Secondary structure predictions and sequence alignment analysis had suggested that residues 170 - 330 of the P2X extracellular loop contain structural similarities with the catalytic domain of class II aminoacyl-tRNA synthetases (Freist *et al*., 1998). This region was predicted to have β-pleated sheets in an antiparallel arrangement with α-helices in between, and a metal binding domain on the outside for both P2X and aminoacyl-tRNA synthetases (Freist *et al*., 1998).

Crystallographic data further illustrated that the upper region of the extracellular body consists of conserved residues of β-sheets having contacts with neighbouring subunits, and upon trimer formation one subunit buries about 3,750 Å squared of its surface area. The central part of the extracellular body region is composed of extensive contacts between β-sheets of a β-sandwich motif, conferring a rigid structure to this domain.

However, in the lower extracellular body region there are no contacts present between neighbouring subunits, an arrangement that could possibly allow for conformational changes of the transmembrane domains following ligand binding. An extracellular head domain composed of three antiparallel β-strands with an α-helix and three structurally distinct components known as the dorsal fin, the right flipper and the left flipper are attached above the extracellular body domain. Subunit interactions within a heteromeric receptor take place between body-body and head-body, and within a homotrimeric P2X receptor the same interactions are thought to occur in addition to between the less conserved residues of the left flipper and dorsal fin (Kawate *et al.*, 2009).

Ten cysteine residues are also present in the extracellular loop, and this feature is conserved among P2X receptors (Hansen *et al.*, 1997). By analysing the accessibility of free cysteine residues in $P2X_1$ receptors with one or two extracellular cysteines mutated, it was proposed that Cys^{117}-Cys^{165}, Cys^{126}-Cys^{149}, Cys^{132}-Cys^{159}, Cys^{217}-Cys^{227}, and Cys^{261}-Cys^{270} formed five disulphide bonds (Ennion and Evans, 2002a). These cysteine bonds at equivalent positions were later confirmed in the $zP2X_4$ crystal structure (Kawate *et al.*, 2009). The disulphide bonds predicted to be present in $P2X_2$ by analysing concentration-response curves for $P2X_2$ receptors with a single cysteine mutated were Cys^{113}-Cys^{164}, Cys^{214}-Cys^{224}, and Cys^{258}-Cys^{267}(Clyne *et al.*, 2002b). The disulphide bonding of the other four cysteines in $P2X_2$ were not predicted with certainty (Clyne *et al.*, 2002b).

1.5.5 ATP binding site

ATP is thought to bind to P2X receptors through hydrogen bonds and electrostatic interactions with the polar side chains and charged residues of the extracellular domain (Jiang *et al.*, 2000b). Binding of ATP to the channel is thought to induce a conformational change in the protein, resulting in gating and subsequent flow of ions through the pore. The absence of consensus ATP-binding domain sequences such as the Walker type A motif (Walker *et al.*, 1982), have made the exact nature of the ATP binding site elusive. Early experiments strongly suggested that ATP binds to the extracellular loop through positive and aromatic residues. Mutagenesis studies suggested that positive residues Lys^{68} and Lys^{309} of $P2X_1$ (Ennion *et al.*, 2000), Lys^{69} and Lys^{71} of $P2X_2$ (Jiang *et al.*, 2000b) and aromatic residues Phe^{185} and Phe^{291} of $P2X_1$ (Roberts and Evans, 2004) are involved in binding ATP, as substitution of these residues resulted in very significant decreases in ATP potency. When Lys^{309} was mutated to arginine the decrease in ATP potency was about 25-fold, however when mutated to alanine the decrease in ATP potency was over 1000-fold, revealing that both charge and chemical properties of the residue at this position are important for function (Ennion *et al.*, 2000). Hence, it was proposed that lysine residues bind and co-ordinate the negative charges of the phosphate chain groups of ATP (Jiang *et al.*, 2000b, Roberts and Evans, 2004), while phenylalanines sandwich the adenine ring (Roberts and Evans 2004). This proposed function of aromatic phenylalanine residues is parallel to that demonstrated for the crystal structure of 5'-nucleotidases, where the adenine ring of ATP is stacked between two aromatic phenylalanine residues (Knofel and Strater, 2001). The $P2X_1$ extracellular loop has four proline residues, which can confer a more rigid structure to the extracellular domain by forming *cis* peptide bonds (Roberts and Evans, 2005). It has also been found that the conformation of the receptor around

residue Pro^{272} for $P2X_1$ contributes to the binding of ATP at the receptor, as mutation of Pro^{272} to alanine, glutamic acid or lysine gives rise to non-functional receptors, whereas substitution to glycine or phenylalanine still produces functional receptors with increased agonist potency (Roberts and Evans, 2005).

The location of residues suggested to be important for ATP binding at opposite ends of the extracellular loop indicated the possibility of an intersubunit ATP binding site. Subsequently it was found that the ATP binding site is at the interface of two adjacent P2X subunits, rather than one subunit providing the binding site for one ATP molecule. This was shown using an approach where aromatic and positive residues that were previously suggested to bind ATP were substituted with cysteines, followed by observation of their ability to form dimers through disulphide bonds. Pairs of cysteine-substituted residues that formed a disulphide bond with each other would suggest the close proximity of residues at these positions on adjacent subunits and therefore give further indication of the nature of the ATP binding site. The most pronounced dimer formation was formed by a bond between K68C and F291C, and a double K68C F291C mutant also formed disulphide-linked trimers (Marquez-Klaka *et al.*, 2007). Disulphide cross-linking between these mutated subunits was reported to prevent or reduce ATP binding and opening of the channel (Marquez-Klaka *et al.*, 2007). Disulphide bond formations between K68C and F291C to produce dimers and trimers were prevented in the presence of ATP, unlike disulphide bonds between V48C and I329C, further confirming the location of the ATP binding site to be inter-subunit and close to residues Lys^{68} and Phe^{291}.

As the crystal structure of $zP2X_4$ was determined in a closed, agonist unbound state (Kawate *et al.*, 2009), the definitive location of the agonist binding site remains elusive. However, the information gathered so far from the crystal structure is supportive of earlier studies and suggests that the ATP binding site is located in intersubunit deep grooves at the outside of the trimer at a distance of 45 Å from the ion channel domain and across adjacent subunits. These grooves contain the same conserved residues, previously proposed to be part of the ATP-binding site. Lys^{70}, Lys^{72}, Phe^{188} and Thr^{189} from one subunit, and residues Asn^{296}, Phe^{297}, Arg^{298} and Lys^{316} from the neighbouring subunit are present in the head, body, dorsal fin and flipper regions that surround the ATP binding site (Kawate *et al.*, 2009). Some of these residues are positioned towards the grooves and possibly bind ATP directly. Phe^{188} and Phe^{297} are positioned away from the groove and could transduce ATP binding into conformational changes for ion flow. ATP binding may close the head, flipper and dorsal fin structures from adjacent subunits to surround the agonist, and the consequent changes between subunits allow ions to flow (Kawate *et al.*, 2009).

1.5.6 Access of ions into the channel

Ions have been proposed to flow through the P2X channel by two possible routes. The more likely passage for ion flow is through three fenestrations of a diameter as large as 8 Å that are situated directly above the membrane bilayer. This can occur after cations are drawn to acidic patches in the extracellular domain by electrostatic attractions. The second potential pathway is along the length of the extracellular domain and three-fold axis of symmetry of the channel. Following agonist binding it is proposed that an

increase in the diameter of the constricted gate region occurs. Ions in the intracellular side can cross the channel to the extracellular side through a pore of an intracellular vestibule that includes Asp^{357}, a residue previously shown to play a role in receptor assembly (Duckwitz *et al.*, 2006, Kawate *et al.*, 2009).

1.5.7 Ion selectivity

The crystal structure shows acidic residues in the central vestibule, immediately above the ion channel, along with Asp^{59} and Asp^{61} close to the extracellular fenestrations, which are thought to confer ion selectivity for the channel (Kawate *et al*., 2009). These negative residues may possibly form a long-range negative electrostatic potential to accumulate cations in close proximity to the extracellular entrance of the ion channel, in addition to direct binding of cations. An alternative proposal is that ions which permeate the length of the extracellular region and channel interact with main-chain and side-chain oxygen atoms of the transmembrane region, for example with the side chain oxygen atom of Asn^{341} (Kawate *et al.*, 2009).

1.5.8 Channel pore

Regions of the channel forming the ion-conducting pore were first indicated by cysteine scanning mutagenesis of the TM2 domain combined with the action of charged and neutral methanethiosulfonates (MTS) to react with the cysteines (Rassendren *et al.*,

1997a). $P2X_2$ I328C, N333C and T336C mutant receptors had significantly reduced ion flow after exposure to all MTS reagents, suggesting these residues are located at the outer vestibule of the channel pore. N333C and T336C were proposed to lie in a pore region that has some extent of charge selectivity as they were more greatly inhibited by the smaller positively charged MTS derivatives (Rassendren *et al*., 1997a). Two further mutations, L338C and D349C inhibited current flow after application of only the smaller membrane permeant positively charged ethylamine derivative, indicating that these residues are located on the intracellular side of the channel gate (Rassendren *et al*., 1997a). $P2X_2$ receptors with cysteines introduced at positions that are N-terminal side of Ile^{328} could not be significantly modified by any MTS reagents, implying that residues in this region do not form part of the aqueous channel pore (Rassendren *et al*., 1997a). The data also suggested that TM2 residues that form the pore are not always part of a polar face of an amphipathic helix as the distribution of cysteine-substituted mutants with altered channel function did not always follow the same face of an α-helical turn (Rassendren *et al*., 1997a). A similar experiment further suggested the presence of the pore region in rat $P2X_2$ TM2 domain by observing the rate of modification of Ag^+ and MTSET (a positively charged MTS derivative) on TM2 residues that had certain residues substituted to cysteine (Li *et al.*, 2008). Residues in between Thr^{336} and Phe^{346} were found to have much higher modification rates and have currents more strongly inhibited by Cd^{2+} in the presence of ATP than in the absence, suggesting that ATP-evoked opening of the channel allows exposure of pore residues to thiol-reactive compounds and ions (Li *et al*., 2008).

An approach that tested the Ag^+ and MTSEA (a positively charged MTS derivative) accessibility of TM2 residues that were substituted with cysteine gave more

information about the pore domain (Egan *et al.*, 1998). Ag^+ and MTSEA are modifying reagents that react only with sulfhydryls exposed to aqueous environments, and cysteine substituted TM2 residues around Gly^{342} exposed to these reagents generated some of the greatest augmentation or inhibition in current during channel gating, hence the close proximity of these residues to the hydrophilic pore (Egan *et al*., 1998).

Involvement of TM1 residues to the pore was found by using MTS reagents on TM1 cysteine-substituted residues of $P2X_2$ (Jiang *et al.*, 2001). Treatment of positive, negative and neutral MTS agents on Val^{48}-substituted receptors strongly inhibited ATP-evoked currents, suggesting that this residue is located outside the membrane field and towards an extracellular position (Jiang *et al*., 2001). Repeated ATP application increased the effectiveness of MTSET and MTSM (a neutral MTS derivative) inhibition of $P2X_2$ V48C receptors, indicating that conformational changes move Val^{48} into a more accessible position during ATP-evoked channel opening (Jiang *et al*., 2001). V48C was able to form a disulphide bond with I328C to demonstrate the close proximity of Val^{48} and Ile^{328}, and this led to channels that were constitutively open and not gated by ATP (Jiang *et al*., 2001).

1.5.9 Channel gate

The channel gate is proposed to be near a conserved glycine residue in TM2 corresponding to Gly^{342} in rat $P2X_2$ (Khakh *et al.*, 1999a). Glycine has a single hydrogen atom as a side chain and therefore this residue will confer conformational

flexibility that may underlie pore diameter changes in the channel. Mutating Gly^{347} of $P2X_4$ to a positively charged residue reduced the initial I_1 current component, whereas substitution to tyrosine removed the slower I_2 current component. These mutants also have altered $NMDG^+$ permeability, altogether suggesting that Gly^{347} of TM2 has an important role for the channel pore and activation gate (Khakh *et al.*, 1999a).

Subsequently it was suggested that hydrophobic residues adjacent to the glycine residue of TM2 may form the activation gate by restricting the flow of water and hydrated ions (Khakh and North, 2006). Hydrophobic residues have been found previously to form gates of nicotinic acetylcholine receptors, mechanosensitive receptor MscL and the bacterial inward rectifier KirBac1.1 channel (Doyle, 2004). MscL tilts its helices, the nicotinic ACh receptor rotates its helices, and KirBac1.1 bends its helices to displace the hydrophobic gate and permit ion flow (Doyle, 2004).

Information from the $zP2X_4$ crystal structure in the closed state suggests the pore resembles an hour glass shape where the transmembrane domains traverse each other (Kawate *et al.*, 2009). The boundary of the channel gate at the extracellular side is possibly defined by Leu^{340} and Asn^{341}, with the side chain of Leu^{340} occluding the pore. The cytoplamsic side of the gate boundary is judged to consist of residue Ala^{347} and side chain of Leu^{346}. The ion channel gate consists of hydrophobic residues within two turns of α-helix of TM2 domains, with Ala^{344} expected to be at the centre of the gate as this residue is where TM2 helices converge to their nearest positions to each other.

Further information about the nature of the P2X channel gate was obtained by recent findings of the closed channel gate being located between residues Thr^{336} and Thr^{339} in rat $P2X_2$ (Kracun *et al.*, 2010). A substituted cysteine accessibility mutagenesis (SCAM) experiment on rat $P2X_2$ had showed accessibility of cadmium ions (Cd^{2+}) in the closed state for $rP2X_2$ I332C and T336C mutants, however cysteine mutations at more C-terminal regions were only accessible in the open state (Kracun *et al.*, 2010). $rP2X_2$ Thr^{336} was determined to be the position of maximum occlusion of ion flow, and this location is present at one helical turn away from the equivalent residue judged from the crystal structure to have the same function in zebrafish $P2X_{4.1}$ (Kracun *et al.*, 2010). This indicates that the position of the gate can vary at different P2X sequences. The same investigation also demonstrated that the distance between cytosolic ends of the TM2 domains are reduced in the open state, after interactions between Cys^{348} and D349C resulted in tighter binding of Cd^{2+} compared to C348T D349C double mutants (Kracun *et al.*, 2010).

1.5.10 Residues responsible for gating

The roles of transmembrane residues in gating was earlier suggested when αβmeATP-sensitivity was maintained after the extracellular domain of the αβmeATP-sensitive rat $P2X_1$ was replaced with that of the αβmeATP-insensitive rat $P2X_2$ (Haines *et al.*, 2001). The αβmeATP-sensitivity of receptors containing rat $P2X_1$ TM1 sequence in a rat $P2X_2$ sequence background was further evidence of TM1 domain role in gating (Haines *et al.*, 2001).

Single channel recordings showed that rat $P2X_2$ with the T339S mutation have channels that spontaneously open in the absence of ATP as well as having ATP potency many fold higher than wildtype channels (Cao *et al.*, 2007) When this Thr^{339} residue was mutated to alanine or cysteine there was no spontaneous activity of the channel, demonstrating the importance of residue 339 in the molecular rearrangements that constitute gating (Cao *et al.*, 2007). Lys^{69}, previously suggested to play a role in ATP binding when mutated and served as a rat $P2X_2$ sequence background for study of further mutations had receptors with different functionalities (Cao *et al.*, 2007). The K69A / T339S double mutant was also constitutively active, unlike K308A / T339S, implying a gating role for Lys^{308} in addition to its agonist binding role and suggesting that this residue may serve as a link between agonist binding and TM domain movements in rat $P2X_2$ (Cao *et al.*, 2007).

Further mutagenesis studies on the rat $P2X_2$ central TM2 residues Asn^{333}, Thr^{336} and Ser^{340} gave rise to channels with spontaneous activity in the absence of agonist (Cao *et al.*, 2007, Cao *et al.*, 2009), implying the location of the channel gate lies within this region. Asn^{333} when substituted to positive or nonpolar residues, Thr^{336} when mutated to almost any other residue, and Ser^{340} when mutated to either aspartate, glutamate, lysine, asparagine, or glutamine led to spontaneous channel openings, providing more information about the nature of the channel gate (Cao *et al.*, 2009). Therefore the hydroxyl group of Asn^{333} may be important to stabilise the closed conformation of the channel (Cao *et al.*, 2009). Asn^{333} is predicted to lie in the external vestibule, corresponding to Asn^{341} of the zebrafish sequence (Cao *et al.*, 2009, Kawate *et al.*,

2009). T336C displays spontaneous unitary currents that were further increased upon ATP application (Cao *et al.*, 2009). Thr^{336} is therefore suggested to lie in a packed region of the channel as it can tolerate substitutions of by various residues (Cao *et al.*, 2009). Thr^{339} and Ser^{340} can tolerate substitutions by large or uncharged residues without largely affecting the closed state as they lie at the turn of the TM2 helix (Cao *et al.*, 2009).

Arginine or cysteine substitutions with subsequent MTSEA or MTSET (both positive MTS derivatives) treatment at positions Thr^{336}, Thr^{339} and Ser^{340} exhibited noticeable outward rectification of basal or ATP-evoked currents compared to wildtype, and this was independent of extracellular calcium or magnesium (Cao *et al.*, 2009). This suggests that these residues form part of the permeation pathway for the receptor, and positive charge introduced at these positions facilitates outward flow of positive ions (Cao *et al.*, 2009). The channel in the open state is predicted to be narrower at Thr^{336} compared to at Thr^{339} or Ser^{340}, as lysine substitution at this Thr^{336} does not cause outward rectification unlike at Thr^{339} or Ser^{340} (Cao *et al.*, 2009).

With this information it was predicted that the open channel widens at Thr^{336} and Thr^{339}, and these residues form the selectivity filter, whose properties are influenced by Ser^{340} (Cao *et al.*, 2009). TM2 helices are expected to slide against each other to rotate anticlockwise during channel opening (Cao *et al.*, 2009). Asn^{333} and Asp^{349} may function to concentrate positively charged ions in the outer and inner vestibules (Cao *et al.*, 2009).

1.5.11 Homo- and heteromeric assembly of receptors

The same or different subunits can co-assemble to form homotrimeric or heterotrimeric channels respectively, resulting in receptors that have a range of distinct pharmacological properties such as their sensitivity to agonists, antagonists and pH. Whilst several mammalian heteromeric P2X receptor combinations have been studied, heteromeric P2X receptors are yet to be reported in invertebrates. Occurrence of heteromeric assembly of P2X receptors is much more predominant over homomeric assembly. Heteromeric P2X ion channels have been clearly established for $P2X_{2/3}$, $P2X_{4/6}$, $P2X_{1/5}$, $P2X_{4/7}$, $P2X_{1/2}$, $P2X_{1/4}$, and $P2X_{2/6}$ (Gever *et al.*, 2006). Biochemical studies have suggested other hetero-oligomeric P2X receptors, observed by their co-immunoprecipitation, and these include $P2X_{1/3}$, $P2X_{1/6}$, $P2X_{2/5}$, $P2X_{3/5}$, $P2X_{4/5}$, and $P2X_{5/6}$ (Torres *et al.*, 1999).

$P2X_1$ and $P2X_5$ were first suggested to form a heteromeric channel after *in situ* hybridization studies showed co-expression of these subunits in similar areas of cervical cells of the spinal cord, and sensory ganglia (Collo *et al.*, 1996). Co-expression of $P2X_1$ and $P2X_5$ and recordings in HEK293 cells revealed a P2X channel with novel pharmacological characteristics, with confirmation of $P2X_{1/5}$ assembly extended by co-immunoprecipitation studies (Torres *et al.*, 1998b). $P2X_{1/2}$ heteromeric channels were demonstrated after the co-expression of $P2X_1$ and $P2X_2$ in *Xenopus* oocytes gave rise to channels with an initial fast desensitizing component that is similar to $P2X_1$ homotrimers, followed by a slower desensitizing component that is similar to $P2X_2$ homomeric channels (Brown *et al.*, 2002). $P2X_1$ and $P2X_4$ were shown to form heteromeric channels after antibody detection of $P2X_4$ subunits after its co-expression

with Histidine-tagged $P2X_1$, and co-purification with $P2X_1$ containing receptors by Ni^{2+}-NTA agarose resin and PAGE (Nicke *et al.*, 2005). Electrophysiological analysis further confirmed the association of $P2X_1$ and $P2X_4$ in a heterotrimer, observed by these co-expressed receptors exhibiting similar current kinetics to $P2X_4$, and agonist and antagonist sensitivity to $P2X_1$ (Nicke *et al.*, 2005).

$P2X_2$ and $P2X_3$ forming functional heteromeric trimers were discovered after baculovirus infection of cell cultures, and detection of co-immunoprecipitation by western blotting (Radford *et al.*, 1997). These heteromeric receptors were αβmeATP-sensitive with current kinetics intermediate of $P2X_2$ and $P2X_3$ homomeric receptors (Radford *et al.*, 1997). $P2X_{2/6}$ heteromers were found after the co-expression of $P2X_2$ and $P2X_6$ in *Xenopus* oocytes gave rise to ATP-evoked currents with lower potency than $P2X_2$ homomeric receptors (King *et al.*, 2000).

$P2X_4$ has been shown to form heteromeric channels with $P2X_6$ that have sensitivity to αβmeATP, and are more sensitive to suramin inhibition compared to homomeric $P2X_4$ receptors (Le *et al.*, 1998). $P2X_7$ was first reported to be incapable of forming heteromeric channels in studies showing lack of co-immunoprecipitation with other subtypes (Torres *et al.*, 1999). Further, co-expression of $P2X_7$ and $P2X_4$ receptors displayed co-immunoprecipitation, and higher $P2X_4$ membrane localization than cells only expressing only $P2X_4$ subtype, and currents of the receptors exhibiting ivermectin and 2′,3′-O-(2,4,6- trinitrophenyl)-ATP (TNP-ATP) sensitivity to demonstrate the ability of $P2X_7$ to form a heteromeric channel (Guo *et al.*, 2007). However, the predominant assembly of $P2X_7$ was found to be homomeric, as heteromeric $P2X_{4/7}$

receptor complexes were identified as being less stable than homomeric $P2X_7$ (Nicke, 2008).

$P2X_6$ subunits have a very low propensity to form trimers, observed by the lack of ATP-evoked currents at $P2X_6$–injected *Xenopus* oocytes (Soto *et al.*, 1996). The observed non-functionality of $P2X_6$ homotrimers can be conceivably explained by the lack of nine residues in the 'left flipper', therefore preventing subunit–subunit contacts and hence the receptor is unable to couple agonist binding to ion channel gating (Kawate *et al.*, 2009).

The close proximity of the TM1 domain of one subunit to the TM2 domain of an adjacent subunit in the receptor trimeric complex was demonstrated by the formation of intersubunit disulphide bonds between cysteine residues introduced at Val^{48} of $P2X_2$ and Ile^{319} of $P2X_3$ (Jiang *et al.*, 2003). This led to the proposal that P2X subunits within a receptor have a 'head-to-tail' arrangement, where the outer end of TM1 of one subunit is in contact with the outer end of TM2 of an adjacent subunit (Jiang *et al.*, 2003). This study also illustrated that $P2X_2/P2X_3$ heteromeric receptors only have a single $P2X_2$ subunit, as $P2X_2$ V48C/I318C double mutants failed to form disulphide bonded pairs when co-expressed with wildtype $P2X_3$, whereas $P2X_3$ V42C/I319C double mutants formed disulphide bonded pairs when co-expressed with wildtype $P2X_2$ (Jiang *et al.*, 2003).

1.6 Trafficking of P2X receptors to the cell membrane

Correct folding and trafficking of P2X proteins to the cell membrane are essential for receptor function. The disulphide bonds formed between the ten extracellular cysteine residues appear to be important in trafficking of the P2X receptor to the cell membrane since disruption of the Cys^{261}-Cys^{270} disulfide bond or disruption of Cys^{117}-Cys^{165} with another disulphide bond broken results in reduced membrane expression (Ennion and Evans, 2002a).

In the human $P2X_7$ receptor, an Ile^{568} to asparagine polymorphism has been found to be responsible for preventing surface expression in lymphocytes (Wiley *et al.*, 2003). Subjects that were heterozygous for I568N had reduced surface expression in lymphocytes, found by using FITC-conjugated monoclonal antibody against the extracellular domain of $P2X_7$ (Wiley *et al.*, 2003). $P2X_7$ I568N mutant receptors transfected into HEK293 cells showed no membrane expression, whereas confocal microscopy displayed strong intracellular staining, demonstrating the importance of Ile^{568} in trafficking of $P2X_7$ to the membrane (Wiley *et al.*, 2003).

Using a luminescent-based assay, surface expression of $P2X_2$ receptors with Y362A or K366A mutations were significantly reduced in HEK cells, whereas no decrease in surface expression was observed when residues 363, 364 and 365 were mutated (Chaumont *et al.*, 2004). $P2X_3$, $P2X_4$ and $P2X_5$ also had reduced membrane expression but unaltered quantity of total cellular protein when tyrosine or lysine at equivalent positions were mutated to alanine, leading to the proposal for an intracellular C-

terminal trafficking motif YXXXK (Chaumont *et al*., 2004). $P2X_2$ Y362A or K366A mutant receptors display increased rates of internalisation, showing that Tyr^{362} and Lys^{366} are important for stability at the membrane (Chaumont *et al*., 2004).

For $P2X_1$, the intracellular C-terminal residue His^{355} has also been shown to be important for trafficking, as the low current amplitudes of H355A mutants were due to reduced cell surface expression (Vial *et al.*, 2006).

1.7 P2X receptor pharmacology

P2X receptors differ in their sensitivity to agonists and antagonists, and this is due to the variation of residues at particular positions involved in binding of these molecules. Knowledge of the pharmacology of a P2X ion channel will give indications about the presence of that particular P2X subtype in functional studies. In addition to their universal sensitivity to ATP, all P2X receptors are sensitive to the ATP analogue 2-(methylthio) ATP (2-MeSATP) (Gever *et al.*, 2006).

$P2X_1$ has strong sensitivity to the ATP analogues BzATP and αβmeATP, the antagonists PPADS, suramin and TNP-ATP (Valera *et al.*, 1994, Gever *et al.*, 2006). NF023 has been shown to be a selective antagonist at $P2X_1$ (Soto *et al.*, 1999). Purified ADP was shown to not activate $P2X_1$ receptors (Mahaut-Smith *et al.*, 2000).

$P2X_2$ is not activated by αβmeATP, and reduced sensitivity to BzATP (Evans *et al.*, 1995). $P2X_2$ currents are potentiated by acidic pH, unlike other P2X receptors (King *et al.*, 1997). No selective inhibitors for $P2X_2$ are presently available, and $P2X_2$ currents are antagonised with equal potency by PPADS, suramin, and TNP-ATP (Evans *et al.*, 1995). $P2X_{2/6}$ heteromeric receptors have similar agonist and antagonist sensitivity profile as $P2X_2$ (King *et al.*, 2000).

$P2X_3$ has almost identical pharmacology with $P2X_1$, with the exception of sensitivity to beta,gamma-methylene ATP (βγmeATP) (Garcia-Guzman *et al.*, 1997). $P2X_1$ has much stronger sensitivity than $P2X_3$ for βγmeATP (Garcia-Guzman *et al.*, 1997). $P2X_{2/3}$ heteromers have similar pharmacology to $P2X_3$ and $P2X_1$ (Lewis *et al.*, 1995, Liu *et al.*, 2001).

$P2X_4$ is weakly activated by αβmeATP, and has no sensitivity to inhibition by the well known P2 receptor antagonists PPADS and suramin (Bo *et al.*, 1995). $P2X_4$ currents are known to be potentiated by the antiparasitic agent ivermectin (Khakh *et al.*, 1999b). $P2X_{4/6}$ heteromers are similar to $P2X_4$ homomeric receptors, in that they are also potentiated slightly by ivermectin (Khakh *et al.*, 1999b) and insensitive to antagonism by PPADS and suramin (Le *et al.*, 1998).

$P2X_5$ is weakly sensitive to αβmeATP, however unlike $P2X_4$ is sensitive to antagonism by PPADS and suramin (Garcia-Guzman *et al.*, 1996). $P2X_5$ is the only P2X receptor that responds to hexokinase purified-ADP, UTP, and GTP with inward currents

(Wildman *et al.*, 1997). $P2X_{1/5}$ heteromers respond to αβmeATP application with currents, and suramin and PPADS inhibition of these receptors is stronger than by TNP-ATP (Haines *et al.*, 1999).

$P2X_7$ has higher sensitivity for BzATP than ATP (Chessell *et al.*, 1998). PPADS effectively inhibits $P2X_7$ currents, however suramin is a weak antagonist (Hibell *et al.*, 2001). Brilliant Blue G has been shown to be a selective antagonist at $P2X_7$ (Jiang *et al.*, 2000a).

Among the invertebrate P2X receptors, *Schistosoma* P2X is sensitive to PPADS and suramin inhibition (Agboh *et al.*, 2004), whereas PPADS and suramin are insensitive at *Ostreococcus tauri* P2X (Fountain *et al.*, 2008) and *Dictyostelium discoideum* P2XB and E subtypes (Ludlow *et al.*, 2009). BzATP evokes no currents at *Ostreococcus tauri* P2X (Fountain *et al.*, 2008).

1.8 Localization of P2X receptor expression

The widespread and almost universal localization of P2X receptors in different cellular components, cell types and tissues have been investigated by a range of approaches. These include *in situ* hybridization, reverse-transcription-polymerase chain reaction (RT-PCR), northern blot to detect mRNA transcripts of the receptor, immunocytochemistry to detect the receptor protein, or Fura-2 fluorescence

measurements to measure Ca^{2+} flow through P2X-expressing cells. The location of a P2X receptor can also be indicated through functional studies by recording the effect that follows application of an agonist or antagonist for that receptor. The distribution of a particular P2X subtype most often overlaps with other P2X subtypes such as in the spinal cord or sensory ganglia (Collo *et al*., 1996). However other areas can display discrete expression of a single subtype (Collo *et al*., 1996). The distribution of P2X ion channels plays a role in determining their function by their co-localization with important components of a physiological pathway.

$P2X_1$

$P2X_1$ mRNA expression was observed in spinal cord, vas deferens, and bladder by northern blot and in trapezius muscle artery, carotid artery and umbilical artery by *in situ* hybridization with digoxigenin (DIG)-labeled cRNA probes (Valera *et al*., 1994). $P2X_1$ receptors were further found in cardiac muscle cells by *in situ* hybridization (Vulchanova *et al.*, 1996), and suggested in platelets by Fura-2 fluorescence measurements of Ca^{2+} entry after application of the $P2X_1$ agonist αβmeATP (MacKenzie *et al.*, 1996). The expression of $P2X_1$ in platelets was first demonstrated by western blotting (Sun *et al.*, 1998). Western blots and electrophysiological studies with applications of $P2X_1$ agonists αβmeATP and βγmeATP demonstrated the presence of $P2X_1$ in human neutrophils (Lecut *et al.*, 2009).

$P2X_2$

Northern blot analysis displayed $P2X_2$ expression in the adrenal gland, brain, bladder

and stronger expression in the spinal cord, pituitary and *vas deferens* (Brake *et al.*, 1994). *In situ* hybridization with a radiolabelled probe indicated $P2X_2$ mRNA in some neurons of the adult rat superior cervical ganglion (Brake *et al.*, 1994). Immunohistochemistry of cultured neurons showed that $P2X_2$ receptors are strongly expressed in neurons of the rat superior cervical (sympathetic) ganglia (Li *et al.*, 2000).

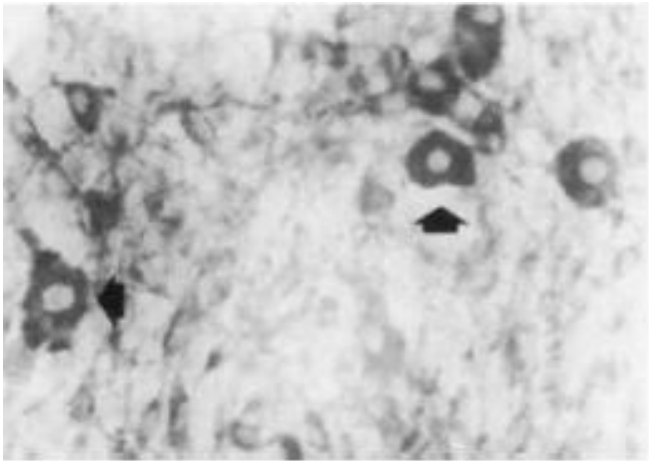

Figure 1.5. *In situ* hybridization using DIG-labelled cRNA probes against $P2X_3$ sequences in primary cultures of neonatal rat dorsal root ganglia. Dark stained cell bodies of neurons highlight areas of $P2X_3$ mRNA expression. Taken from Chen *et al.*, (1995).

$P2X_3$

Transcripts of $P2X_3$ were found in rat dorsal root ganglion sensory neurons by northern blots and by *in situ* hybridization using DIG-labelled cRNA probes (Chen *et al.*, 1995) (Figure 1.5). *In situ* hybridization using radioactive cRNA probes showed $P2X_3$ mRNA in the Purkinje cells and granule cells of the rat brain cerebellum (Seguela *et al.*, 1996). $P2X_3$ immunoreactivity was also found by antisera targeting the carboxy-terminus of $P2X_3$ in rat nociceptors and their peripheral endings (Cook *et al.*, 1997). $P2X_3$

immunoreactivity was observed in sensory neurons that innervate the suburothelial sensory nerve plexus of the mouse urinary bladder, with nerve terminals leading to the urothelium (Cockayne *et al.*, 2000).

$P2X_4$

$P2X_4$ mRNA has been localised by *in situ* hybridization to the olfactory bulb and hippocampal pyramidal cells of the rat brain, Purkinje cells in the cerebellar cortex, peripheral ganglia, acinar cells of the submandibular gland, and olfactory epithelia of the rat embryo (Bo *et al.*, 1995, Buell *et al.*, 1996). $P2X_4$ mRNA expression in the spinal cord, lung, vas deferens, bladder, testis, thymus and adrenal gland was highlighted by northern blot (Bo *et al*., 1995). Northern blots and RT-PCR indicated the presence of $P2X_4$ transcripts in human vascular endothelial cells (Yamamoto *et al.*, 2000).

$P2X_5$ and $P2X_6$

In situ hybridization detected $P2X_5$ mRNA expression in the mesencephalic nucleus of the trigeminal nerve of the brain, and in ventral horn motoneurons of the cervical spinal cord of the rat (Collo *et al*., 1996). $P2X_6$ receptor mRNA was discovered to be expressed most strongly in cerebellar Purkinje cells, ependyma as well as located in the lateral spinal nucleus and several lamanae of the rat spinal cord such as in spinal neurons of lamina IX, medium and large sized neurons of lamina IV, V, VII, VIII (Collo *et al*., 1996). $P2X_6$ mRNA was also localised to the cortex, dendate gyrus, all hippocampal fields, trigeminal and dorsal root ganglia and celiac ganglia (Collo *et al*.,

1996). Outside of the nervous system, $P2X_6$ mRNA expression was high in gland cells of the uterus, granulosa cells of the ovary and in bronchial epithelia (Collo *et al*., 1996).

$P2X_7$

In situ hybridization and immunohistochemistry experiments displayed heavy $P2X_7$ labelling of ependymal cells in both newborn and adult brain (Collo *et al.*, 1997). Microglia, which are activated in acute pathological events such as the necrosis after occlusion of cerebral arteries and develop into phagocytes, also were found to express $P2X_7$ (Collo *et al*., 1997). $P2X_7$ receptor expression has been reported in glial satellite cells by immunohistochemistry, Western blot, and calcium imaging (Chen *et al.*, 2008).

Intracellular localization of Dictyostelium P2X receptors

A P2X receptor from *Dictyostelium discoideum*, *Dd*P2X has been shown by green fluorescent protein (GFP)-tagging, immunoblotting and immunostaining to be expressed on the membranes of an intracellular organelle known as the contractile vacuole where it co-localizes with calmodulin (Fountain *et al*., 2007). Later studies on the other four members of the *Dictyostelium discoideum* P2X family indicated that all five subunits when RFP-labelled and visualised by confocal microscopy had intracellular vacuole locations (Ludlow *et al.*, 2009). These receptors were subsequently found to be orientated with their ligand-binding domain in the vacuole lumen and N- and C- termini facing the cytoplasm using protease-protection assays (Ludlow *et al*., 2009).

Co-localization of P2X receptors

In most cases P2X receptor subtypes are co-localized. In the olfactory system which plays a role in sensing odor, RT-PCR showed expression of $P2X_2$ mRNA in the rat olfactory epithelium and bulb (Hegg *et al.*, 2003). Immunohistochemistry displayed $P2X_1$ and $P2X_4$ antibody staining in the plasma membrane, cell soma and axons of olfactory receptor neurons and basal cell layers of the mouse olfactory epithelia (Hegg *et al.*, 2003). $P2X_2$ and $P2X_7$ were shown to be expressed in mouse taste bud cells by RT-PCR, immunohistochemistry, calcium imaging, dye uptake, and electrophysiological studies (Hayato *et al.*, 2007). Immunohistochemistry displayed the expression of $P2X_2$ and $P2X_3$ in the central terminals of the rat trigeminal ganglion neurons (Staikopoulos *et al.*, 2007). $P2X_1$, $P2X_4$ and $P2X_7$ transcripts were identified in human lung mast cells and leukemia-derived human mast cells by RT-PCR (Wareham *et al.*, 2009). The presence of P2X receptors in human lung mast cells suggest that they play a role in Ca^{2+} influx to influence the initiation of mast cell activation and secretion of pro-inflammatory cytokines (Wareham *et al.*, 2009). $P2X_2$ and $P2X_4$ receptors have been shown by RT-PCR and functional studies to be present in GABAergic neurons derived from mouse embryonic stem cells (Khaira *et al.*, 2009).

P2X receptors have been found to be distributed in glial cells. Voltage-clamped astrocytes were found to respond to ATP and αβmeATP application with inward currents consisting of rapid and steady state phases, which were blocked by PPADS and therefore suggested the presence of P2X receptors (Lalo *et al.*, 2008). $P2X_1$ and $P2X_5$ subtypes were found at high levels almost equal to each other in astrocytes by quantitative RT-PCR, implying that $P2X_{1/5}$ heteromers may be the functional receptors

in these cells (Lalo *et al*., 2008). The presence of P2X receptors in astrocytes was supported by previous findings that showed $P2X_1$ receptor protein immunoreactivity in rat cerebellar astrocytes (Loesch and Burnstock, 1998).

In rodent immune cells, $P2X_4$ is less abundant in the plasma membrane and located predominantly in intracellular compartments, whereas $P2X_7$ is more present at the plasma membrane (Boumechache *et al.*, 2009). These differences are due to the extent of $P2X_4$ traffic to and from the membrane as lipopolysacharides, and endocytosis inhibitors such as hypertonic sucrose and Dynasore increase the plasma membrane localization of $P2X_4$ in microglia as determined by surface biotinylation experiments (Boumechache *et al*., 2009). Punctate distribution of $P2X_4$ receptors was also reported from confocal images of the soma and dendrites of neurons (Bobanovic *et al.*, 2002). Postembedding immunocytochemistry was used to show the presence of $P2X_2$, $P2X_4$ and $P2X_6$ at postsynaptic specialisations of cerebellum and hippocampus (Rubio and Soto, 2001).

P2X receptors have also been discovered to be located in retinal ganglion cells (Taschenberger *et al.*, 1999), Muller glial cells of the human retina (Pannicke *et al.*, 2000), skeletal muscle (Meyer *et al.*, 1999), cardiac muscle (Hu *et al.*, 2002), smooth muscle (Vial and Evans, 2000), and lymophocytes (Sluyter *et al.*, 2001).

P2X receptors have been shown to have altered localization upon ligand binding. ATP application to the dendrites of embryonic hippocampal neurons resulted in

redistribution and formation of varicose hot spots (clustering) of functional GFP tagged-$P2X_2$ receptors in dendrites, with alterations in dendrite morphology, viewed by confocal microscopy (Khakh *et al.*, 2001). This property of $P2X_2$ is affected by protein kinase C, as mutation of the protein kinase C site at Thr^{18} which prevents the occurrence of the I_2 state also prevents redistribution of the receptors and changes in morphology (Khakh *et al*., 2001).

1.9 Physiological roles of P2X receptors

The widespread localization of P2X receptors implies that they participate in a wide range of processes. The location of P2X receptors together with knowledge of their function can highlight their therapeutic potential for disease treatments. Benefits may arise by either enhancing or blocking P2X receptor functionality, depending on the effect P2X activation has on the particular health condition.

P2X receptors have been reported to play roles in aggregation and adhesion of platelets (Hechler *et al.*, 2003, Gever *et al.*, 2006), synaptic transmission (Gu and MacDermott, 1997, Khakh and Henderson, 1998, Sim *et al.*, 2006), long term potentiation (Pankratov *et al.*, 2002), sensing pain (Cook *et al.*, 1997, Hamilton *et al.*, 2000) (Figure 1.6), cardiovascular functions, regulating airway ciliary motility (Korngreen *et al.*, 1998) and osmoregulation (Fountain *et al*., 2007).

Activation of P2X receptors present in dorsal root ganglion (DRG) nerve terminals by endogenous ATP released from superficial laminae of the dorsal horn has been found to function in synaptic transmission. This activation of P2X receptors located on presynaptic sites of DRG neuron nerve terminals and subsequent ion flow trigger action potentials and calcium channel openings, leading to increased frequency of spontaneous glutamate release across the synapse to dorsal horn neurons This was deduced after localized ATP application by focal puffs on cultured DRG nerve terminals with their associated dorsal horn neurites gave rise to inward currents in these dorsal horn neurites that were blocked not only by the P2 receptor antagonist PPADS, but also by the glutamate channel blocker CNQX (Gu and MacDermott, 1997). This implied that glutamate was released from DRG neurons into the synaptic cleft to activate receptors on the dorsal horn neurons as a consequence of P2X activation (Gu and MacDermott, 1997). These studies showed that P2X receptor activation at DRG central terminals can modify sensory transmission with their connections to dorsal neurons of the spinal cord, and that sensory signals at central synapses can be possibly initiated without direct peripheral input (Gu and MacDermott, 1997). Therefore presynaptic P2X receptors may be suggested as a target for pain therapy to painful stimuli. P2X activation in the trigeminal mesencephalic nucleus (MNV) in the brain stem similarly depolarized the nerve terminals and opened calcium channels to increase frequency of spontaneous glutamate release from MNV neurons to trigeminal mesencephalic motor nucleus (MoV) neurons (Khakh and Henderson, 1998).

A small role of P2X in long term potentiation was found after application of PPADS as a P2X inhibitor or αβmeATP as a desensitizing agonist induced LTP in CA1 pyramidal neurons during brief high frequency stimulation (HFS) delivered towards Schaffer

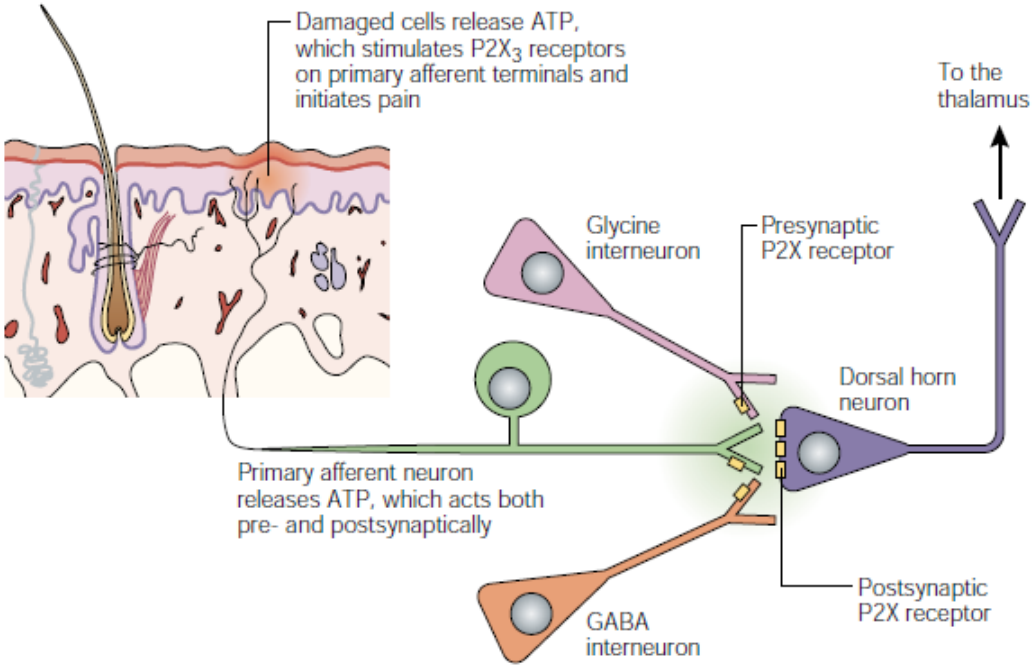

Figure 1.6. Diagram demonstrating P2X function. A pseudomonopolar pain-sensing neuron is shown above with its primary afferent terminal present in the periphery, in close proximity to skin cells. ATP that is released from damaged cells or exogenous application of a P2X agonist will activate primary afferents to raise the firing rate of these sensory neurons, subsequently leading to pain sensation. The central terminals of sensory neurons have synaptic connections with dorsal horn neurons. These dorsal horn neurons also have P2X receptors that are postsynaptic that bind ATP released from the primary afferent neurons. This ATP also binds to presynaptic P2X receptors on GABA and glycine interneurons to facilitate the release of these neurotransmitters to the dorsal horn cell. Taken from Khakh, (2001).

collaterals (Pankratov *et al*., 2002). In the absence of PPADS or αβmeATP, only continuous HFS and not brief HFS was able to trigger LTP. Therefore P2X functions as a dynamic low-frequency filter to prevent LTP and alterations in synaptic efficacy from being triggered by weak stimuli (Pankratov *et al*., 2002).

ATP is able to reduce odor sensitivity through P2X activation in olfactory receptor neurons of the peripheral olfactory system (Hegg *et al*., 2003). P2X selective agonists were shown to suppress the amplitude of calcium transients evoked by odor application, whereas PPADS further potentiated these odor-evoked calcium transients in mouse olfactory epithelial slice preparations (Hegg *et al*., 2003). This shows that endogenous ATP plays a role in modulating odor sensitivity of olfactory receptor neurons (Hegg *et al*., 2003). In this case P2X receptors may serve a neuroprotective function as extensive exposure to concentrated odors or noxious fumes can impair olfactory receptor neurons (ORNs) and also trigger expression of stress indicators (Hegg *et al*., 2003).

Application of αβmeATP and βγmeATP to neutrophils in Boyden chamber assays showed $P2X_1$ to play a role in promoting neutrophil chemotaxis, in a process involving Rho kinase-dependent actomyosin-mediated contraction at the cell rear (Lecut *et al.*, 2009). This implies the possible function of $P2X_1$ in host defense and inflammation.

The role of $P2X_2$ receptors in formation of the neuromuscular junction and synapses was suggested after $P2X_2$ knockout mice exhibited morphological abnormalities of the neuromuscular junction, as well as muscle fibre atrophy and increases in the proportion

of the fast type muscle fibres in the sloeus muscle (Ryten *et al.*, 2007).

Expression of $P2X_3$ in nociceptive sensory neurons suggested roles for P2X in the initiation of pain sensation (Burnstock and Wood, 1996). $P2X_3$ was further suggested to mediate pain sensation after ATP and αβmeATP were found to cause action potentials at $P2X_3$-containing nociceptive rat sensory neurons (Cook *et al.*, 1997). Currents at these nociceptors evoked by ATP and αβmeATP had similar kinetics as $P2X_3$ currents expressed in HEK293 cells (Cook *et al.*, 1997). Acute nociception mediated by P2X receptors on small diameter primary afferent neurons was elucidated by the occurrence of hindpaw lifting and paw licking in rats following the subplantar injection of αβmeATP, which were similar effects seen after injection of nociceptive triggering agents bradykinin or formalin (Bland-Ward and Humphrey, 1997). Therefore ATP released by tissue damage following noxious stimuli can activate these P2X receptors to cause acute nociception (Bland-Ward and Humphrey, 1997).

$P2X_3$-deficient ($P2X_3$ -/-) mice were prepared by deletion of over 1kb of the $P2X_3$ gene to further investigate roles of $P2X_3$ in sensory processing (Cockayne *et al.*, 2000). Neurons from $P2X_3$ -/- dorsal root ganglion did not respond to ATP or αβmeATP with fast desensitizing currents, unlike wildtype DRG neurons suggesting that $P2X_3$ receptors mediate rapid responses in these neurons (Cockayne *et al.*, 2000). $P2X_3$ -/- mice exhibited reduced hindpaw lifting, which is a nociceptive behavioural response, to ATP injected into the hindpaw compared to $P2X_3$ +/+ mice (Cockayne *et al.*, 2000). Bladder capacity was increased and bladder contractions in response to infusion of saline was reduced in $P2X_3$ -/- mice compared to $P2X_3$ +/+ mice, showing that $P2X_3$ -/-

mice have micturition hyporeflexia and that $P2X_3$ has a function in urinary bladder sensation (Cockayne *et al*., 2000). Therefore $P2X_3$ antagonists have the potential to be used as therapeutic agents for the treatment of urine storage or overactive bladder disorders (Cockayne *et al*., 2000). Subsequent studies demonstrated that presynpatic $P2X_3$ and $P2X_{2/3}$ receptors in the spinal cord were able to control bladder micturition reflex neurotransmission via activation of the extracellular-regulated signal kinase (ERK) pathway after acute noxious stimulation of the bladder (Kaan *et al.*). This was found following the intrathecal application of AF-792, a selective antagonist for $P2X_3$ and $P2X_{2/3}$ significantly inhibited micrutuition reflex contractions recorded by *in vivo* cystometry, and also the reduced phosphorylation of ERK1 and ERK2 in the spinal cord (Kaan *et al*., 2010).

$P2X_4$ has roles in tactile allodynia following neuropathic pain (spinal cord injury) and inflammatory pain (CFA-triggered swelling of hindpaw) in the rat (Tsuda *et al.*, 2009). ATP acts on microglial $P2X_4$ receptors to release brain derived neurotrophic factor (BDNF) from microglia and subsequently trigger a reduction in intracellular chloride and a depolarizing shift in annion reversal potential of nearby spinal lamina I neurons of the rat dorsal spinal cord (Coull *et al.*, 2005). The altered chloride gradient causes the GABA transmitter to switch its role from inhibitory to excitatory transmitter to increase intracellular calcium concentration and cause peripheral nerve injury-induced tactile allodynia (Coull *et al*., 2005). $P2X_4$ was also found to play a role in microglia migration evoked by morphine, observed by the reduction in morphine-induced microglial migration by TNP-ATP and not by PPADS (Horvath and DeLeo, 2009).

The C-terminal of $P2X_7$ is responsible for the increase in pore size to allow the flow of large molecules (Rassendren *et al.*, 1997b). There is evidence to indicate that these permeability changes are possibly associated with morphological changes and cell death through lysis (Surprenant *et al.*, 1996, Virginio *et al.*, 1999). Activation of $P2X_7$ receptors has also been found to result in cytokine IL-1β vesicle shedding from human THP-1 monocytes (MacKenzie *et al.*, 2001). $P2X_7$ has also been shown to have a trophic role in the activation and proliferation of microglia, due to the expanding pore forming property rather than the cation channel conductance of the $P2X_7$ receptor (Monif *et al.*, 2009). This was shown by a $P2X_7$ G345Y mutant which has impaired pore formation, and this lead to a reduced microglial activation and proliferation, characteristics which can affect the progression of neuroinflammatory diseases such as Alzheimer's (Monif *et al.*, 2009). $P2X_7$-knockout mice demonstrated roles of $P2X_7$ in pancreatic and salivary secretions (Novak *et al.* 2010).

Activation of $P2X_7$ receptors in glial satelite cells have been reported to have a function in reducing inflammation-induced allodynias by downregulating the expression of $P2X_3$ in the dorsal root ganglion (Chen *et al.*, 2008). This was shown by silencing $P2X_7$ expression by RNA interference that displayed increased $P2X_3$ expression and responsiveness to αβmeATP, whereas $P2X_7$ activation reduced levels of $P2X_3$ expression (Chen *et al.*, 2008).

1.10 Regulation of P2X receptors

In order to prevent constitutive activation of P2X receptors that could have possible harmful effects on the cell or to increase P2X currents for beneficial effects, regulatory mechanisms are required to modulate the amount of current that flows through P2X receptors. These regulatory procedures can be beneficial in a number of functions such as pain suppression or prevention of neurotoxicity. The mechanisms of regulation can reflect the intracellular signalling pathways that follow P2X receptor activation.

Carbon monoxide has been shown to act as a second messenger with reversible effects to inhibit currents flowing through the $P2X_{2/3}$ and $P2X_4$ receptors and activate $P2X_2$ currents through a soluble guanylyl cyclase independent pathway (Wilkinson *et al.*, 2009). It is not known whether the effects of carbon monoxide are due to direct binding to the P2X receptor or through an indirect mechanism.

$P2X_3$ receptor currents in both HEK cells and mouse trigeminal sensory neurons are depressed by a regulator of the Src signalling pathway called C-terminal Src inhibitory kinase, which carries out its inhibitory effect through phosphorylation of the C-terminal Tyr^{393} residue of the $P2X_3$ C-terminus (D'Arco *et al.*, 2009). C-terminal Src inhibitory kinase activity is inhibited by the allogen nerve growth factor (NGF), therefore NGF functions to prevent phosphorylation of Tyr^{393} and potentiate $P2X_3$ current amplitudes (D'Arco *et al.*, 2009).

Mercury is able to potentiate $P2X_2$ currents by crossing the membrane and binding to

its site of action at the intracellular C-terminal Cys^{430} residue, which may act to increase ATP binding affinity of the receptor (Coddou *et al.*, 2009). This finding shows that P2X receptors not only sense extracellular ligands and modulators but also act as a sensor for intracellular molecules to modify responses evoked by ATP (Coddou *et al*., 2009). Divalent metal ions as well as protons have been previously shown to modulate P2X currents, and this will be discussed in more detail in Chapters 2 and 3.

1.11 Invertebrate P2X receptors

The first instance of cloning and subsequent characterization of a P2X receptor from a non-vertebrate organism was from the parasitic blood fluke *Schistosoma* (Agboh *et al*., 2004). Since the discovery of this *Schistosoma mansoni* P2X receptor, several other P2X receptors from lower organisms have been found.

Many regions of the P2X sequences in invertebrates are dissimilar to vertebrate P2X sequences due to accumulation of random mutations and other mechanisms. However, evolutionary pressure has led to the conservation of residues that are important for essential P2X receptor properties such as ligand-binding, channel gating and permeation across evolutionary distant species. Alignment of various P2X sequences and differences in sequences can guide site-directed mutagenesis of suitable candidate residues that may impart a functional role for the receptor.

These invertebrate P2X receptors may possess a novel pharmacological profile, and differences in sequence with other P2X receptors will enhance understanding of agonist or antagonist binding sites. P2X receptors from invertebrates may also serve a potential route to elucidate P2X structure in the ligand-bound state. The Tardigrade species *Hypsibius dujardini* is an invertebrate that can withstand extreme temperatures, pressures and low water availability, and a P2X receptor identified from this organism may prove to be stable enough for determination of the ATP—bound P2X atomic structure.

The study of P2X receptors from non-vertebrates will allow better estimation of the pattern of P2X receptor sequence loss from organisms that are known to not possess P2X receptors. Organisms with a fully sequenced genome without P2X receptor sequences include *Anopheles gambiae, Caenorhabditis elegans, Drosophila melanogaster*, and *Apis mellifera.* The study of P2X receptors in invertebrates may lead to the discovery of novel functional roles or downstream signalling pathways which may have analogy to P2X receptor functions in mammals. Characterization of P2X receptor sequence and pharmacology from invertebrate organisms also allows structure-function analysis and therefore a comparative model for the better understanding of P2X receptors.

1.12 Lymnaea stagnalis

The freshwater snail *Lymnaea stagnalis* provides an attractive model system to further

investigate P2X receptors and their potential CNS functions in response to ATP acting as a neuromodulator or neurotransmitter. *Lymnaea* belongs to the order of molluscs, which have branched off at early stages of the evolution of bilaterians (Adoutte *et al.*, 2000, Raouf *et al.*, 2005). *Lymnaea stagnalis*, which is an invertebrate lacking a central brain structure, has the advantage of possessing a simple nervous system with about 20,000 large neurons that are easily identifiable by their cell bodies, features which makes research on this organism more accessible to investigate. The cell bodies of *Lymnaea stagnalis* neurons are up to 150 µm in diameter, compared to mammalian neurons that are about 10 - 60 µm in size (Moroz, 2000), making *Lymnaea* neurons easy to carry out intracellular electrophysiological recordings. Another advantage of using *Lymnaea* as a model organism is that neuronal networks underlying processes such as feeding and respiration have been well studied and characterised, allowing study of the functions of ATP and its receptors in these pathways (Benjamin and Rose, 1979, Syed *et al.*, 1990, Benjamin *et al.*, 2000).

Lymnaea has been used previously to investigate the effects of exposure to rotenone, a pesticide (Vehovszky *et al.*, 2007). Behavioural experiments showing a decreased spontaneous movement and feeding activity, immunocytochemistry experiments displaying reduced tyrosine hydroxylase levels, and electrophysiological recordings of dopaminergic neurons showing an absence of inhibitory inputs into VD4 neurons from RPeD1 neuron stimulation were the features of rotenone treated *Lymnaea* (Vehovszky *et al*., 2007). These findings correlate to the symptoms of Parkinson's disease seen in mammals, and therefore demonstrate the use of *Lymnaea* to model pathological diseases.

The role of presynaptic cyclic AMP and protein kinase A in the regulation of synapse number and efficacy of synaptic transmission was determined by experiments on the visceral dorsal 4 (VD4) and left pedal dorsal (LPeD1) neurons of *Lymnaea stagnalis* (Munno *et al.*, 2003). Incubating the presynaptic VD4 neuron with the protein kinase A antagonist H-89 had allowed the VD4 neuron to make connections with many postsynaptic LPeD1 neurons, whereas prior exposure of VD4 to the cAMP analog 8Br-cAMP had permitted innervations of only a single postsynaptic target with a reduced excitatory postsynaptic potential (EPSP) amplitude (Munno *et al.*, 2003).

The presence of purinergic receptors in *Lymnaea* is suggested by the presence of ATP release systems releasing ATP concentrations of 3 - 50nM, detected by luciferase-catalysed ATP chemiluminescence signals in imaging studies (Gruenhagen *et al.*, 2004). ATP was released in *Lymnaea* through methods such as stimulation of nerves by potassium chloride (KCl) to depolarize neurons, through serotonin application or physical stimulation. Prolonged ATP release was observed from *Lymnaea* neurons, whereas ATP release decreased to diminish over few minutes after physical stimulation of *Lymnaea* astrocytes (Gruenhagen *et al.*, 2004). Of all the *Lymnaea* CNS ganglia, ATP release varied most in the visceral ganglia, reaching as high as 50nM ATP (Gruenhagen *et al.*, 2004), suggesting purinergic receptors play role in functions in which visceral ganglia neurons form a component such as respiration. However, these recorded concentrations of ATP are far lower than that reported in mammalian systems, and it is almost certain that the actual ATP concentrations present in *Lymnaea*, especially near the receptor sites are many fold higher, as explained in Chapter 5.

Preliminary work in the lab also showed that *Lymnaea* neurons respond to ATP application, further suggesting the presence of purinergic receptors.

Receptors previously cloned from the *Lymnaea stagnalis* genome include the nicotinic acetylcholine receptor (van Nierop *et al.*, 2006), neuropeptide receptor PSFHSWSamide (Cox *et al.*, 1997), and the voltage-gated calcium channel (Senatore and Spafford, 2010).

1.13 Research aims

The underlying objective of this project is to utilise the freshwater snail *Lymnaea stagnalis* as a model system to investigate the roles played by ATP-gated P2X ion channels in central nervous system (CNS) function. *Lymnaea stagnalis* was selected as a model system due to the relative simplicity of the CNS in this organism, large size of its neurons, and the ability to link behavioural responses with neuronal activation.

Since P2X receptors have not previously been cloned from this organism, the initial stage of the project was to clone a P2X receptor from *Lymnaea* CNS, and characterize the physical and pharmacological properties of the receptor in the *Xenopus* oocyte expression system by electrophysiological techniques. These experiments to characterise the heterologously-expressed *Lymnaea* P2X will provide the pharmacological information necessary to explore the possible *in vivo* function of the

receptor in *Lymnaea* CNS and also serve as a comparative tool to provide additional insights into structure-function relationships in P2X receptors in general. In addition to characterising *Lymnaea* P2X, a P2X receptor recently identified from another invertebrate species *Hypsibius dujardini* was also cloned and its functional properties determined alongside *Lymnaea* P2X in oocytes. Comparison of the amino acid sequence and functional properties of these evolutionary remote invertebrate P2X receptors with P2X receptors from vertebrates will assist approaches to determine key residues and functional domains responsible for properties such as current kinetics/desensitisation, pore formation and sensitivity to zinc.

In order to identify the distribution of neurons expressing mRNA corresponding to the *Lymnaea* P2X receptor, *in situ* hybridization and RT-PCR on isolated ganglia will be carried out. This information will be used to direct *in vivo* experiments to determine the physiological function of this receptor and investigate links with behavioural responses such as the feeding network.

Chapter 2: Identification, cloning and characterization of P2X receptors from two invertebrate organisms: *Lymnaea stagnalis* and *Hypsibius dujardini.*

2.1 INTRODUCTION

P2X receptors play roles in a number of important physiological processes in the central nervous system such as synaptic transmission (Khakh and Henderson, 1998, Sim *et al.*, 2006), long term potentiation (Pankratov *et al.*, 2002) and taste sensation (Finger *et al.*, 2005).

A current handicap in this field is the availability of a simple model system to provide a test bed to probe fundamental aspects of P2X function in the CNS. The pond snail *Lymnaea stagnalis* has a relatively simple CNS containing ~20,000 readily identifiable neurons and has historically proved to be an extremely useful and accessible model system to study several fundamental aspects of CNS functionality such as synaptic plasticity (Munno *et al.*, 2003) and associative memory (Wan *et al.*, 2010). Furthermore, the neuronal pathways underlying complex processes such as feeding and respiration have been elucidated in this organism (Benjamin and Rose, 1979, Syed *et al.*, 1990, Benjamin *et al.*, 2000), making it an attractive model for investigating neural networks.

The demonstration of ATP release in the *Lymnaea stagnalis* CNS (Moroz, 2000) suggests the presence of an ATP-signalling system and it is therefore likely that *Lymnaea* could also provide a simple model system to study purinergic receptor

function in the CNS. With this potential benefit in mind, one of the initial aims in this study was to determine whether *Lymnaea* possess functional P2X receptors.

The vertebrate P2X receptors were originally identified and cloned through a variety of strategies. The first P2X receptors to be discovered ($P2X_1$ and $P2X_2$) were identified by expression cloning (Brake *et al.*, 1994, Valera *et al.*, 1994). PCR using degenerate primers based on sequence data from $P2X_1$ and $P2X_2$ was subsequently used to isolate $P2X_4$ (Buell *et al.*, 1996). This degenerate PCR succeeded because closely related sequences with high homology allowed the design of PCR primers from conserved sequences. This degenerate PCR based approach in its simplest form however would not have been suitable for the identification of P2X receptors from evolutionary remote species such as *Schistosoma* and *Dictyostelium*, which show a high level of sequence divergence from mammalian P2X receptors. These invertebrate P2X receptors were isolated using EST clone and genomic data, respectively (Agboh *et al.*, 2004, Fountain *et al.*, 2007).

In the absence of extensive genomic or expressed sequence tag (EST) data for *Lymnaea*, it is not possible to design primers to perform the rapid amplification of cDNA ends (RACE) PCR technique similar to that used for the isolation of *Schistosoma mansoni* P2X (Agboh *et al.*, 2004). The approach used for the isolation of P2X receptors from *Lymnaea stagnalis* therefore was that of CODEHOP-PCR (Rose *et al.*, 2003). This method incorporates the use of a pool of primers that contain two distinct regions. One region contains a 3' degenerate core region containing a variety of nucleotide combinations encoding 3-4 amino acids from a conserved region of the protein. This region of the primer is adjacent to a longer 5' consensus clamp containing

only one sequence consisting of bases judged most likely to be present at each position in the sequence, using information from the alignment of P2X sequences from a variety of organisms. The 3' degenerate core binds to the sequence first, and annealing of the 5' consensus clamp stabilises the primer interaction. This primer then becomes incorporated in subsequent amplification cycles.

In addition to trying to clone a P2X receptor from *Lymnaea stagnalis*, a P2X receptor from the tardigrade species *Hypsibius dujardini* was also cloned and studied as part of a comparative study with *Lymnaea* P2X. A partial P2X-like EST sequence from *Hypsibius dujardini* was identified in the GenBank database providing a straightforward route to obtaining the full clone for this P2X receptor. Tardigrades are microscopic animals around 200 to 500 μm in length which inhabit marine and fresh water habitats (Nelson DR, 1990, Gabriel *et al.*, 2007). They have an ability to desiccate into a reversible state of metabolic suspension called cryptobiosis, allowing them to endure many decades in harsh environments such as extreme temperatures, high pressure, lack of oxygen, before returning to an active state following rehydration (Kichin, 1994). These properties potentially make the tardigrade P2X receptor an attractive candidate for future structural determination as the robustness of tardigrade proteins may possibly make them more amenable to crystallographic studies. Tardigrades are placed in their own phylum, Tardigrada and share some phenotypic characteristics with arthropods and nematodes. Similar to arthropods they possess legs and a distinctly segmented body. However they possess a triradiate pharynx that is reminiscent of the nematodes. Molecular phylogenetic analyses strengthen the hypothesis that tardigrades can be classified as part of the Ecdysozoa (Aguinaldo *et al.*, 1997, Dopazo and Dopazo, 2005).

Functional confirmation that P2X receptors are present in molluscs and tardigrades would expand our emerging knowledge of P2X phylogeny. From the gathered information on non-vertebrate P2X receptors, it would be easier to estimate the pattern of loss of P2X-like sequences in nematodes and arthropods. Similarities and differences of the pharmacological characteristics of these receptors will be compared with other known P2X receptors, which may highlight functionally important residues. The pharmacology of *Lym*P2X in *Xenopus* oocytes obtained in this chapter will subsequently help elucidate the role of *Lym*P2X in the *Lymnaea* central nervous system.

2.2 METHODS

2.2.1 Identification of the Hypsibius dujardini P2X receptor

Searches by my supervisor using BLAST software of the GenBank EST database identified a partial *Hypsibius dujardini* EST sequence [GenBank:CO741227], which encoded a peptide with significant sequence relatedness to the N-terminus of vertebrate P2X receptors. The insert of the corresponding clone for this EST sequence (Hd_mx23_13F10) was fully sequenced on both strands (Automated ABI sequencing service, Leicester University, U.K.) using vector (pSPORT1) and insert specific primers, and was shown to contain a full length coding sequence for a P2X receptor which was named *Hd*P2X.

2.2.2 Identification and cloning of Lymnaea stagnalis P2X receptor

Prior to my commencement in the laboratory, total RNA from *Lymnaea stagnalis* CNS was isolated and reverse transcribed into cDNA using oligo-dT as primer. Degenerate CODEHOP primers designed using the BLOCKS programme were then used in an RT-PCR reaction to amplify an internal sequence of the *Lymnaea* P2X receptor (Rose *et al.*, 2003). Once this internal gene specific sequence had been obtained, the 5' and 3' sequences of the gene were obtained by performing 5' RACE-PCR and 3'RACE-PCR respectively (Graham *et al.*, 1991). This cloning strategy is summarised in Figure 2.1.

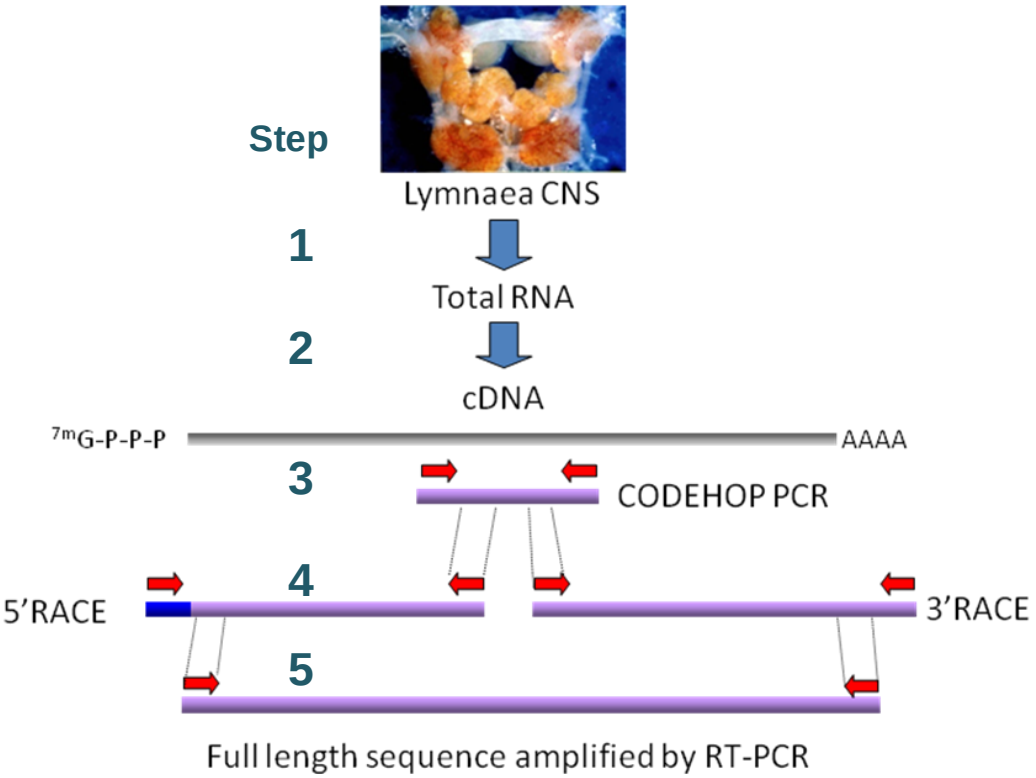

Figure 2.1. Cloning strategy for the *Lymnaea* P2X receptor. Total RNA was extracted and reverse transcribed into cDNA. CODEHOP PCR followed by 5' and 3' RACE was carried out, and the sequence information obtained allowed the design of primers to amplify the entire *Lym*P2X sequence. Steps 1, 2, 3 and 4 of the cloning strategy for *Lymnaea* P2X were carried out by my supervisor prior to my commencement in the laboratory. Step 5 (cloning of the full length receptor) and all subsequent methods were carried out by myself during the course of this chapter.

2.2.3 Cloning of the full length Lymnaea stagnalis P2X receptor

Sequence from the 5'RACE PCR product (Figure 2.1, step 4) revealed the possibility of two potential start codons in close proximity to one another at the 5' end of the gene. It was therefore decided to generate clones for both these possible start sites in order to determine whether they differed in function, and subsequent steps in this protocol were carried out by myself. RT-PCR was performed on cDNA prepared from *Lymnaea* CNS

using a forward primer consisting of either LymKOZMTTfor (5' GCCGCCACC**ATG**ACTACTAAGATGGCTGAC 3') (corresponding to the first potential start site) or LymKOZMADfor (5' GCCGCCACC**ATG**GCTGACCCAAAACACTG 3') (corresponding to the second potential start site) and a reverse primer *Lym*FULLrev_outer (5' ATTGATATATTCTAGGCTCG 3'). In both forward primers a Kozak sequence (Kozak, 1987) was included in the sequence 5' to the start ATG codon (bold underlined in primer sequences above). As a positive control, primers designed to amplify 867 bp of the *Lymnaea* nicotinic acetylcholine receptor (which subunit) (LymnACHFOR 5' GAATGACCTGGAATGCTGCTAA 3' and LymnACHREV 5' CTTTCACCTGGGCTCTTTGG 3') were also utilised. PCR reactions consisted of: 0.25 µl first strand *Lymnaea* CNS cDNA, 6.25 pmoles forward primer, 6.25 pmoles reverse primer, 0.2 mM dNTPs, 2 mM $MgCl_2$, 1 X Reaction Buffer (Bioline Bio-X-act) and 1.6 Units Bio-X-Act DNA polymerase (Bioline U.K.) in a 12.5 µl reaction. Thermal cycling consisted of 30 repetitions of 94 ^{o}C for 30 s, 50 ^{o}C for 1 min, and 72°C for 1.5 min. Amplicons were visualised on a 0.8 % agarose gel and purified using a QiaQuick gel extraction kit according to the manufacturer's instructions (Qiagen, U.K.). PCR products were cloned into pcDNA3.1 (Invitrogen, USA.) and independent clones sequenced on both strands (University of Leicester automated sequencing service).

2.2.4 Xenopus oocyte preparation and injection of P2X cRNA

*Lym*P2X and *Hd*P2X plasmids were digested with *MluI* and *NotI* restriction enzymes respectively in order to linearise the DNA, and sense strand cRNA was synthesised

using a T7 mMessage mMachine™ kit (Ambion, U.S.A.) according to the manufacturer's instructions. The concentration of the cRNA obtained was measured using a spectrophotometer at 260 nm. *Xenopus* oocytes at stage V - VI were manually defolliculated using forceps and injected with 5ng cRNA (50 nl at a concentration of 0.1 μg/μl) using an Inject +Matic micro injector (J. Alejandro Gaby, Genève). After injection, oocytes were stored in an incubator at 18 °C in ND96 buffer (96 mM NaCl, 2 mM KCl, 1.8 mM $CaCl_2$, 1 mM $MgCl_2$, 5 mM sodium pyruvate, and 5 mM HEPES, pH 7.5). Electrophysiological recordings were carried out 3 – 6 days following injection of cRNA. *Xenopus* oocytes are widely used as a suitable heterologous system to study functional characteristics of ion channels and receptors (Bianchi and Driscoll, 2006). This is due to their ability to translate injected cRNA into mature protein that is expressed in the membrane of the oocyte, and their accessibility to electrophysiological recordings (Bianchi and Driscoll, 2006).

2.2.5 Two-electrode voltage clamp

Two-electrode voltage clamp recordings were carried out on *Xenopus* oocytes using a Turbo TEC 10C amplifier (NPI Electronic Instruments, Germany) with a Digidata 1200 analogue to digital converter (Axon Instruments U.S.A.) and WinWCP acquisition software (Dr J. Dempster University of Strathclyde, Scotland). Microelectrodes were filled with 3 M KCl. The external recording solution consisted of ND96 buffer in which 1.8 mM $CaCl_2$ was replaced with 1.8 mM $BaCl_2$ to prevent endogenous calcium-activated chloride channel activation. Membrane currents were recorded at -60 mV holding potential. Agonists, ATP (Mg^{2+} salt), 2',3'-O-4-Benzoylbenzoyl ATP (BzATP) and α,β-methylene-adenosine 5'-triphosphate (αβmeATP) (Sigma, Poole, U.K.) were

applied through a U-tube perfusion system, whereas ivermectin, pyridoxal-phosphate-6-azophenyl-2',4'-disulfonic acid (PPADS), suramin,and altered pH solutions were bath-perfused as well as being present at the same concentration in the U-tube solution along with the agonist. Concentration-response curves were obtained by having a 5-min recovery period between agonist applications and by normalizing data points to two applications of a bracketing concentration of ATP (one preceding and one following the test agonist/antagonist concentration). 10 µM ATP for *Lym*P2X and 100 µM ATP for *Hd*P2X was used for normalisation as these concentrations produced reproducible responses with a 5 min recovery interval at the respective receptors. In the case of analysing the effect of PPADS, which is a irreversible antagonist, the response to ATP in the presence of PPADS was normalised to the preceding ATP-evoked response at concentrations of PPADS that significantly reduced the subsequent ATP-evoked response (10 µM, 100µM, and 300 µM).

2.2.6 Data analysis

Data are presented as means ± S.E. Differences between means were analysed by the Student's t-test. Concentration-response data were fitted with the Hill equation $Y = ((X)^H \cdot M)/((X)^H + (EC_{50})^H)$, where Y is response amplitude, X is agonist concentration, H is the Hill coefficient, M is maximum response, and EC_{50} is the concentration of agonist evoking 50 % of the maximum response. pEC_{50} is the $-\log_{10}$ of the EC_{50} value. All concentration-response curves, bar charts, EC_{50} values and Hill coefficients were obtained using GraphPad Prism software (La Jolla, USA).

2.2.7 Current kinetics

The desensitization of currents during the continued presence of agonist were fitted either by a double:

$(t) = A_1\exp(-t/\tau_{desen1}) + A_2\exp(-t/\tau_{desen2}) + Ss$

or a single:

$y(t) = A\exp(-t/\tau_{desen}) + Ss$

exponential equation where A_1 and A_2 = relative amplitudes of the first and second exponential, τ_{desen1} and τ_{desen2} = time constant of desensitization for first and second exponentials, t = time, and Ss = plateau. Time constants of desensitization were measured by fitting curves from 95 % peak amplitude to the end of ATP application. Currents that failed to reduce in amplitude by > 50 % peak were not fitted, and only T_{10} (time from peak to 90 % peak current amplitude) values were obtained.

Current rise times (from 10 – 90 % peak current amplitude) and T_{50} (time from peak to 50 % peak current amplitude) were also calculated using WinWCP analysis software.

2.3 RESULTS

Sequence analysis of LymP2X and HdP2X

2.3.1 RT-PCR to amplify full length Lymnaea P2X

RT-PCR reactions on *Lymnaea* cDNA resulted in amplicons of 1368 bp and 1356 bp for the LymKOZMTTfor / LymFULLrev_outer and LymKOZMADfor / LymFULLrev_outer primer combinations respectively (Figure 2.2). A PCR amplicon of 867 bp was obtained for the nicotinic acetylcholine receptor positive control and no PCR amplification was present in the no DNA template negative control (Figure 2.2). The two *Lymnaea* P2X PCR products were cloned into pcDNA3.1 plasmid and sequencing revealed coding sequences of 435 and 439 amino acids for the shorter and longer clones respectively (Figure 2.2 and 2.3).

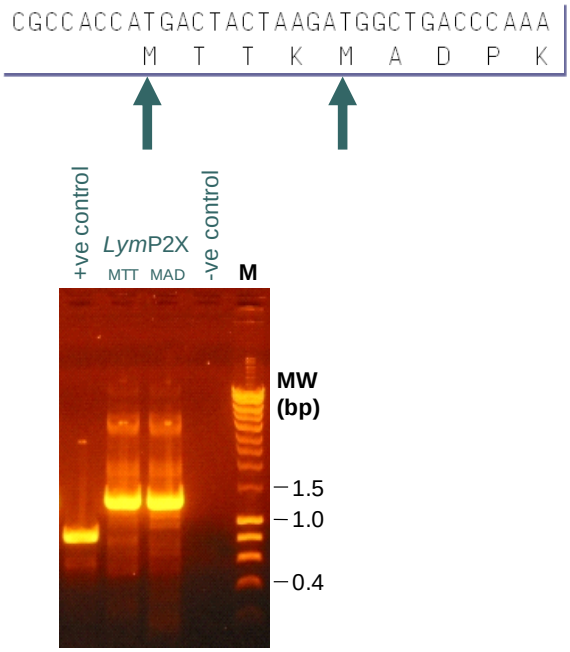

Figure 2.2. Agarose gel of PCR product of the two cloned versions of the *Lym*P2X receptor (MTT – shorter, MAD - longer), with a positive control clone on the left lane - *Lymnaea* nicotinic acetylcholine receptor (van Nierop *et al.*, 2006) and negative control (no template) on the right lane. Hyperladder I bands are shown on the far right with band sizes noted in bps.

```
ATATGACTACTAAGATGGCTGACCCAAAACACTGGTTGCGATCTGGCTTCGCCCTCTTTTTTGAGTATAA 70
   M  T  T  K  M  A  D  P  K  H  W  L  R  S  G  F  A  L  F  F  E  Y  N
TACTCCAAGAATTGTTCATATACGAAGCAAAAAAGTTGGGATCATCAATCGCTTTTTACAGCTTGTTATT 140
  T  P  R  I  V  H  I  R  S  K  K  V  G  I  I  N  R  F  L  Q  L  V  I
                                      └──────────────TM1──────────────┘
ATTTCTTACATAGCTGTGTATGCCATCTACTACAAAAAGGGATACCAAGAGTTTGATGATGTCCAAAGTG 210
 I  S  Y  I  A  V  Y  A  I  Y  Y  K  K  G  Y  Q  E  F  D  D  V  Q  S
└──────────────TM1──────────────┘
CTGTGACCACCAAAGTTAAAGGAATTGTTTTTTCCAATTATAGTCACATTCCTGAGATTGGTATGAGAAC 280
A  V  T  T  K  V  K  G  I  V  F  S  N  Y  S  H  I  P  E  I  G  M  R  T
ATGGGATGTGGCCGATTATGTCATTCCACCGCAGGAAAACAGTGCATTTTTCGTCATGACAAATGTCATT 350
  W  D  V  A  D  Y  V  I  P  P  Q  E  N  S  A  F  F  V  M  T  N  V  I
CCAACACTTGGACAAACTCAGTCAATGTGTTCTGAGGATCCAACAATAAAAAATATCAAGTGTGAAAATG 420
 P  T  L  G  Q  T  Q  S  M  C  S  E  D  P  T  I  K  N  I  K  C  E  N
ATGATTATTGTGAACGCCTGAAAGGGACTATAATGCCAGGAGGAAATGGTCCCCTTACTGGGAAATGTGT 490
D  D  Y  C  E  R  L  K  G  T  I  M  P  G  G  N  G  P  L  T  G  K  C  V
GAACTCTACAGGAGCTTTGAAAGTCTGTGAAATATATGGTTGGTGTCCTGTAGAGAATGGCAGCCCATAT 560
  N  S  T  G  A  L  K  V  C  E  I  Y  G  W  C  P  V  E  N  G  S  P  Y
AAAAACTTGACTCAACCTATATTGGCTGGGTCTCAAAATTTCACAGTTTTTATCAAGAACAACATAGAGT 630
 K  N  L  T  Q  P  I  L  A  G  S  Q  N  F  T  V  F  I  K  N  N  I  E
TTCCAAAGTTTGACGTTAGAAGGCGCAATATTTTGGACTTATATGAAAATGATACAGATTTTGGAAATTG 700
F  P  K  F  D  V  R  R  R  N  I  L  D  L  Y  E  N  D  T  D  F  G  N  C
TCGATGGAACCGCAATGATTCCAAAGGAAAATTTTGCCCCATATTTGTTTTAAATGATATTGCAAAAGAT 770
  R  W  N  R  N  D  S  K  G  K  F  C  P  I  F  V  L  N  D  I  A  K  D
GCTGGGGTAAATTATGATGACCTGACTCTTCAGGGTGGCGTAATGCAAATAATTATTGACTGGACGTGTA 840
 A  G  V  N  Y  D  D  L  T  L  Q  G  G  V  M  Q  I  I  I  D  W  T  C
ATCTGGACCAAAGTGTTGATAACTGCCTACCTGAGTACAGCTTCAGAAGACTGGACAGAGGGGATTATGT 910
N  L  D  Q  S  V  D  N  C  L  P  E  Y  S  F  R  R  L  D  R  G  D  Y  V
CATATCAAGAGGATTCAATTTCAGATATGCTGACAAGTTTGCAGTAAAAGAAAACAACACCTTCGTCCAG 980
  I  S  R  G  F  N  F  R  Y  A  D  K  F  A  V  K  E  N  N  T  F  V  Q
TACAGAAACCTGTACAAGGCAACAGGGATCGTCTTCGTGGTGACTGTCCAAGGGAAGGCTGGGAAGTTCA 1050
 Y  R  N  L  Y  K  A  T  G  I  V  F  V  V  T  V  Q  G  K  A  G  K  F
GCTTCTTTCCTCTAGTGATCAATATTGGCAGCGGTTTGGCCATGTTGGCACTGGCAACCATCGCCTGTGA 1120
S  F  F  P  L  V  I  N  I  G  S  G  L  A  M  L  A  L  A  T  I  A  C  D
            └──────────────────────────────TM2──────────────────────────────┘
TATCATCGTGCTCTATCTGTTGAAGGCCAGGAACTTCTACAGAGACAAGAAATATTTGGATGTGCAAGGC 1190
  I  I  V  L  Y  L  L  K  A  R  N  F  Y  R  D  K  K  Y  L  D  V  Q  G
└──────────TM2──────────┘
CAGGATGCATTCAGGATACTCGAAGAAGAGTCGCCTCAGGACAGGATGGAGGGGAGCAGCAGCAGCATTA 1260
 Q  D  A  F  R  I  L  E  E  E  S  P  Q  D  R  M  E  G  S  S  S  S  I
AAAAAAGAAATGTGACCCATTCTTATGATGGCAACCTGGAAGGGGATGGCACTGATACCTAGGATAACAT 1330
K  K  R  N  V  T  H  S  Y  D  G  N  L  E  G  D  G  T  D  T  .
TTGATAAGTCCCGAGCCTAGAATATATCAATTAAATTCTAAAAAAAAAAAAAAAAAAAAAA 1390
```

Figure 2.3. Amino acid (above) and DNA nucleotide sequences (below) of *Lymnaea* P2X. Putative transmembrane domains are highlighted by solid black lines underneath, determined by the web programme TmPred (Hofmann, 1993).

2.3.2 Sequencing of Hypsibius dujardini EST clone Hd_mx23_13F10

Existing GenBank sequence data for *Hypsibius dujardini* clone Hd_mx23_13F10 consisted of a 330 bp sequence from the 5' end of a cDNA showing similarity to vertebrate P2X receptor sequences. Sequencing of the full length clone showed that it contained an insert of 1743 bp. Contained within this insert was an open reading frame of 1440 bp corresponding to a full length P2X receptor of 480 amino acids (Figure 2.4) which was subsequently named *Hd*P2X. This P2X receptor is predicted to contain intracellular amino and carboxy termini and two transmembrane helices (residues 47 - 67 and 345 – 365) by the TMPred algorithm (Hofmann, 1993) (Figure 2.4).

2.3.3 Sequence analysis of LymP2X and HdP2X

Alignment of the *Lym*P2X and *Hd*P2X cDNA sequences with the human $P2X_{1-7}$ and *Schistosoma* P2X sequences, (Figure 2.5) indicates several conserved functionally important residues. These include the 10 extracellular cysteines that take part in disulphide bonding (yellow), N-terminal protein kinase C site, and an NFR motif (pink, blue, red in sequence), positive (red) and phenylalanine (dark blue) residues which are thought to play roles in ATP binding. The evolutionary relationships between P2X receptors are represented in a dendrogram (Figure 2.6). The percentage amino acid sequence identity between *Lym*P2X and human $P2X_{1-7}$ sequences range from 31.0 – 45.9, with highest similarity with $P2X_4$. The percentage sequence identity between *Hd*P2X and human $P2X_{1-7}$ sequences vary from 24.7 - 38.4 %, with greatest sequence identity also with $P2X_4$. *Lym*P2X and *Hd*P2X have 33.9 % sequence identity with each other.

```
GTACGGTCCGGATTCCCGGGTCGACCCACGCGTCCGCCCACGCGTCCGGGACACTGACATGGACTGAAGG 70
AGTAGAAAAGTTTCAGAGGCGATCAAGACTGAAGTTTCTTATACAGAGTGGCCGCAAAGGCTGCGGCAGT 140
AATTACTGCGCTAATAATAATGACGAATTTCACTAATACGAACGAGCAGGAGAAGCTCTCGTCATATGCC 210
                    H  T  N  F  T  N  T  N  E  Q  E  K  L  S  S  Y  A
AAACGGAAAGCTTTGGACTTTTTCTTTGAATACGAAACTCCCAAGGTCGTCAAGGTCTACAGCACTCGTT 280
 K  R  K  A  L  D  F  F  F  E  Y  E  T  P  K  V  V  K  V  Y  S  T  R
TGGGCGCCATCAATCGGACAGTACAGTTCCTGGTCATCGGATATGTTATCGGGTACATCTTCATCTATGC 350
L  G  A  I  N  R  T  V  Q  F  L  V  I  G  Y  V  I  G  Y  I  F  I  Y  A
                   ├──────────────────────────────────────────────────┤
                   └──────────────────────── TM1 ──────────────────────┘
GAAAGGGTACCAGGCCTTCGAGAAAGCCGAATCGACGACGATAGCGAAAGTCAAAGGGATGATTAAGACC 420
  K  G  Y  Q  A  F  E  K  A  E  S  T  T  I  A  K  V  K  G  H  I  K  T
┌──┐
- TM
AACTTTTCCGCCAGCACCGGTGCTAACAACGTGTGGGACGCCACGGACCTGGTAATTCCATCTGCGGAAA 490
 N  F  S  A  S  T  G  A  N  N  V  W  D  A  T  D  L  V  I  P  S  A  E
ACGATGCGGTCTTCATCACAACAAACTTCATTCAGACACCTAGCCAGCAGAGTGGAAAATGCCCCGAGGA 560
N  D  A  V  F  I  T  T  N  F  I  Q  T  P  S  Q  Q  S  G  K  C  P  E  D
CACCAACAACAAGTTCGCGAGGTGTCGAACGGATTCCGGCTGCACAGCCGGCGAACAAGTACTGCTGGGC 630
  T  N  N  K  F  A  R  C  R  T  D  S  G  C  T  A  G  E  Q  V  L  L  G
AACGGCTTCAAGACCGGACAGTGCGTGCAGGCTACCGGTACCTGCGAAATTGACGGATGGTGTCCGGCGG 700
 N  G  F  K  T  G  Q  C  V  Q  A  T  G  T  C  E  I  D  G  W  C  P  A
AAGTGGACGACAAGCCAGAGCCGCCGATCTTTATGGAGGCTGAAAACTTCACAATCATGGTGAAGAATTA 770
E  V  D  D  K  P  E  P  P  I  F  H  E  A  E  N  F  T  I  H  V  K  N  Y
CGTGACTTTCCCGGAGTTCGACGTCAAGCGGCGGAATATACCGGATGACATGAAGGGTGCGTACATCAAC 840
  V  T  F  P  E  F  D  V  K  R  R  N  I  P  D  D  H  K  G  A  Y  I  N
ACTTGCCGGTACCATCCCGTGTCCGACCCTTACTGCCCGATATTCACCGTGCAACGCTTGGTGGAGTTGG 910
 T  C  R  Y  H  P  V  S  D  P  Y  C  P  I  F  T  V  Q  R  L  V  E  L
CACATGAAAACTTCTCCGTCGTTGCCCGCACCGGAGCAATCTTCGGCTTCATCATTGAATGGGACTGCAA 980
A  H  E  N  F  S  V  V  A  R  T  G  A  I  F  G  F  I  I  E  W  D  C  N
CTTGGACTTCTCGGTGGAATATTGCCTCCCAAAGTACCAGATACGTCGGATAGATTCCGTTGAAGAGAAG 1050
  L  D  F  S  V  E  Y  C  L  P  K  Y  Q  I  R  R  I  D  S  V  E  E  K
ATAGCGAAGGGCTGGAACTTTCGTCATGCTGACTATTGGAATGCACCAGACGGCACACGACGCAGAACGT 1120
 I  A  K  G  W  N  F  R  H  A  D  Y  W  N  A  P  D  G  T  R  R  R  T
TATACAAGTTTTACGGGATCAAATTCGTCTTCATGGTTTACGGAAAAGCCGGTCGATTCAGCCCCGAGGA 1190
L  Y  K  F  Y  G  I  K  F  V  F  H  V  Y  G  K  A  G  R  F  S  P  E  E
GCTCGCCATGAATTTAGGTTCCGGAATCGGTCTTCTTGGCATTGCAACCATTCTATGCGACTTTTTAACG 1260
  L  A  H  N  L  G  S  G  I  G  L  L  G  I  A  T  I  L  C  D  F  L  T
  ├──────────────────────────────────────────────────────────────────┤
  └──────────────────────────────── TM2 ──────────────────────────────┘
GACTTCCTGCTGAGAACAGACGCATTTGGCAAGTCCAAGTTCGAGAGGATTCGCGATACCAAGAAAAAAG 1330
 D  F  L  L  R  T  D  A  F  G  K  S  K  F  E  R  I  R  D  T  K  K  K
GCCCCCCGACGTTGAAGACCATGCTGGAAAATGCAAAGCCGCCGGGTGCAGTCATGGTCATCGAAAATGA 1400
G  P  P  T  L  K  T  H  L  E  N  A  K  P  P  G  A  V  H  V  I  E  N  E
GCCCGATGCCGACCCAGACGCCTCAACGCTGGATGATGATTCCTCGAGCTCGGATGAGGATGGCAGCACT 1470
  P  D  A  D  P  D  A  S  T  L  D  D  D  S  S  S  S  D  E  D  G  S  T
CGCCGCGGTTTGCCCGAGCAAACACCCAGTGGCGATTCCGGCTTTGGTGTTGCCCGTCCGGAGAAGCATT 1540
 R  R  G  L  P  E  Q  T  P  S  G  D  S  G  F  G  V  A  R  P  E  K  H
TTCTGCTGGATGACCCGGTGAAGCCGGTCCACTTTCAAAGAACGAGAGTGACAAGCCTATGATGATGGGG 1610
F  L  L  D  D  P  V  K  P  V  H  F  Q  R  T  R  V  T  S  L  .
GACCCGGAAATCAGGGGAGGTCCGCGCTTGATGGGGCGGTCTGTGCGCTACCAAAACTCCATCTGTTTCG 1680
CAGCTCTCTGATGAATTTATTCTGGTTCAGTTGATCTCATTCTCCTCCCCTTTTTAGTCTATCCAAAGTC 1750
CATTAGTAGGTTACACAAAACTGTTTTATCGCATGCTGATAAAAGATTTACCTTAAAAAAAAAAAAAAAA 1820
AGGGCGGCCGCTCTAGAGGATCCAAGCTTACGTACGCGTGCATGC 1865
```

Figure 2.4. Amino acid and DNA nucleotide sequence of *Hypsibius dujardini* P2X, with transmembrane regions highlighted above solid black lines.

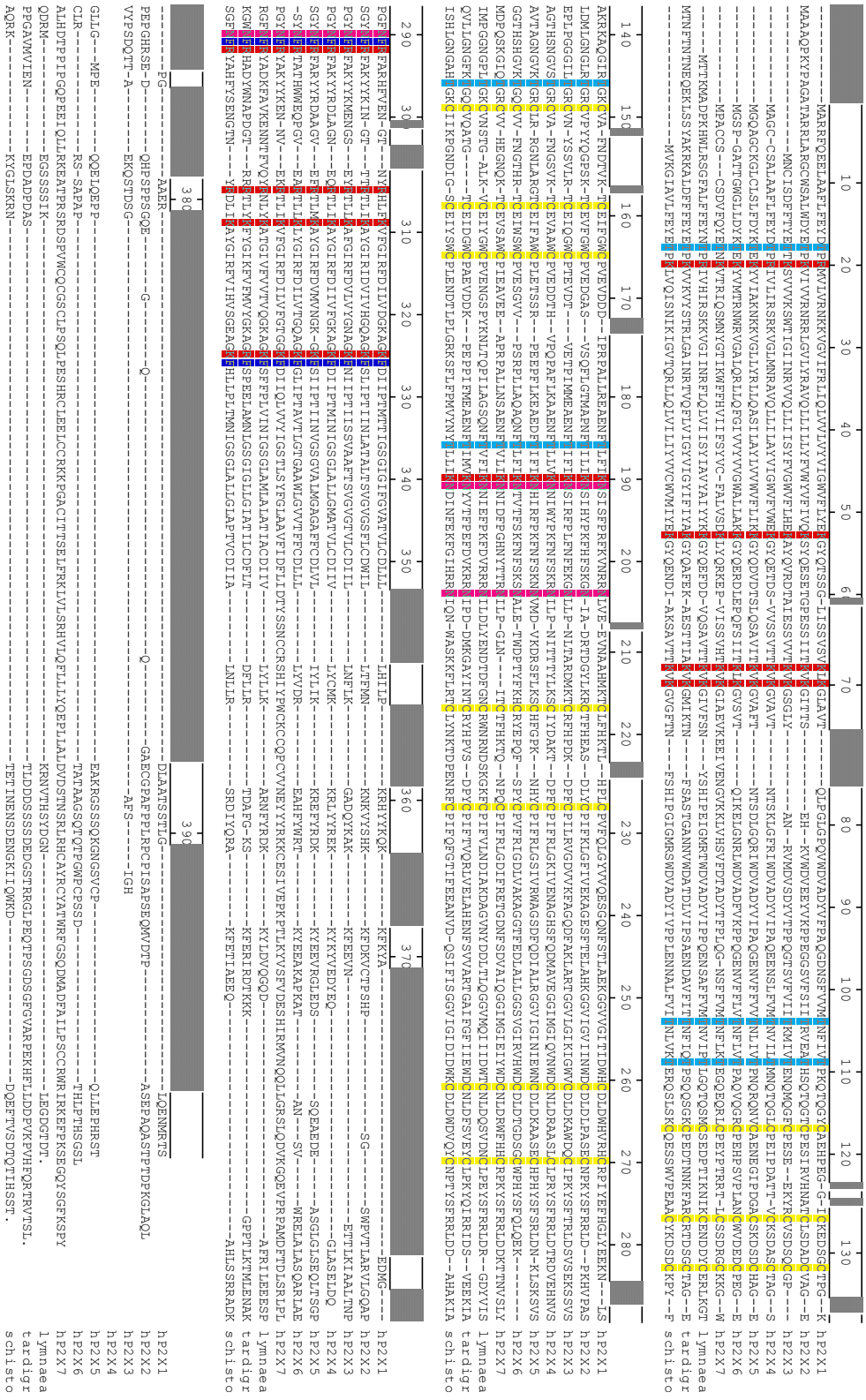

Figure 2.5. Alignment of *Lym*P2X and *Hd*P2X with human $P2X_{1-7}$ and *Schistosoma*P2X, showing the conserved residues, highlighted as cysteine residues (yellow), asparagine residues (pink), threonine residues (light blue), positive residues (red), and phenylalanine (blue).

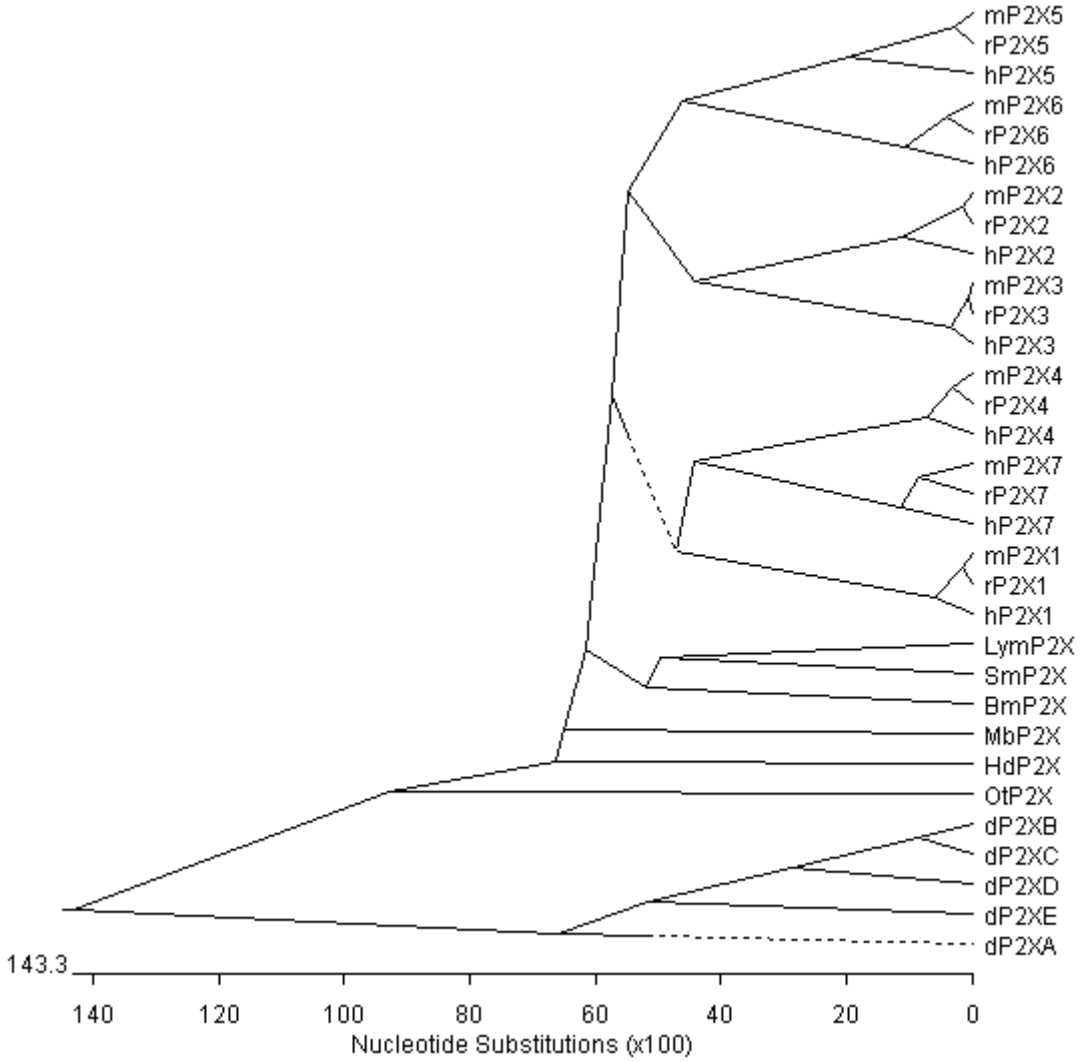

Figure 2.6. A dendrogram generated by Clustal W, displaying the evolutionary relatedness of P2X receptors across different species. Bm = *Boophilus microplus,* d = *Dictyostelium discoideum,* h = human, Hd = *Hypsibius dujardini,* Lym = *Lymnaea stagnalis,* m = mouse, Ot = *Ostreococcus tauri***,** r = rat, Sm = *Schistosoma mansoni,*

LymP2X pharmacology

2.3.4 Agonists

Application of 100 µM ATP to *Xenopus* oocytes expressing either the long or short form of the *Lym*P2X receptor evoked an inward current that decayed in amplitude during the continued presence of agonist (Figure 2.7), demonstrating that this *Lymnaea* receptor corresponds to a functional ATP-gated P2X ion channel.

For the shorter clone, the current rise time (from 10 – 90 % peak amplitude) was 207.7 ± 20.7 ms, the desensitizing current (T_{50} = 884.32 ± 49.3 ms) was quite slow and can be fitted by a single exponential and had a τ_{desen} of 1.5 ± 0.2 s (n = 10). The longer clone had a rise time of 209.7 ± 17.4 ms, the desensitizing current (T_{50} = 995.8 ± 50.5 ms) was also fitted by a single exponential and had a τ_{desen} of 1.6 ± 0.2 s (n = 8). There were no significant differences in these current kinetics between the longer and shorter versions of the cloned *Lym*P2X receptor ($p > 0.05$ for each current kinetic parameter). *Lym*P2X currents had a slow rise time, peak and relatively slow rate of desensitization, being similar to ATP-evoked currents of the mammalian $P2X_4$ subtype (Bo *et al.*, 1995).

*Lym*P2X currents evoked by 100 µM ATP at 5 min intervals resulted in marked run-down in current amplitudes and a slow rate of recovery from desensitization (Figure 2.7A). *Lym*P2X currents evoked by 100 µM ATP at 15 min intervals had slightly higher amplitude at the first application ($p < 0.05$), whereas subsequent applications did not significantly differ from each other (Figure 2.7B). However 10 µM ATP application at 5 min intervals gave currents of equal amplitudes. As seen in figure 2.7C, following two pulses of 100 µM ATP at 5 min intervals, subsequent 10 µM ATP applications at 5

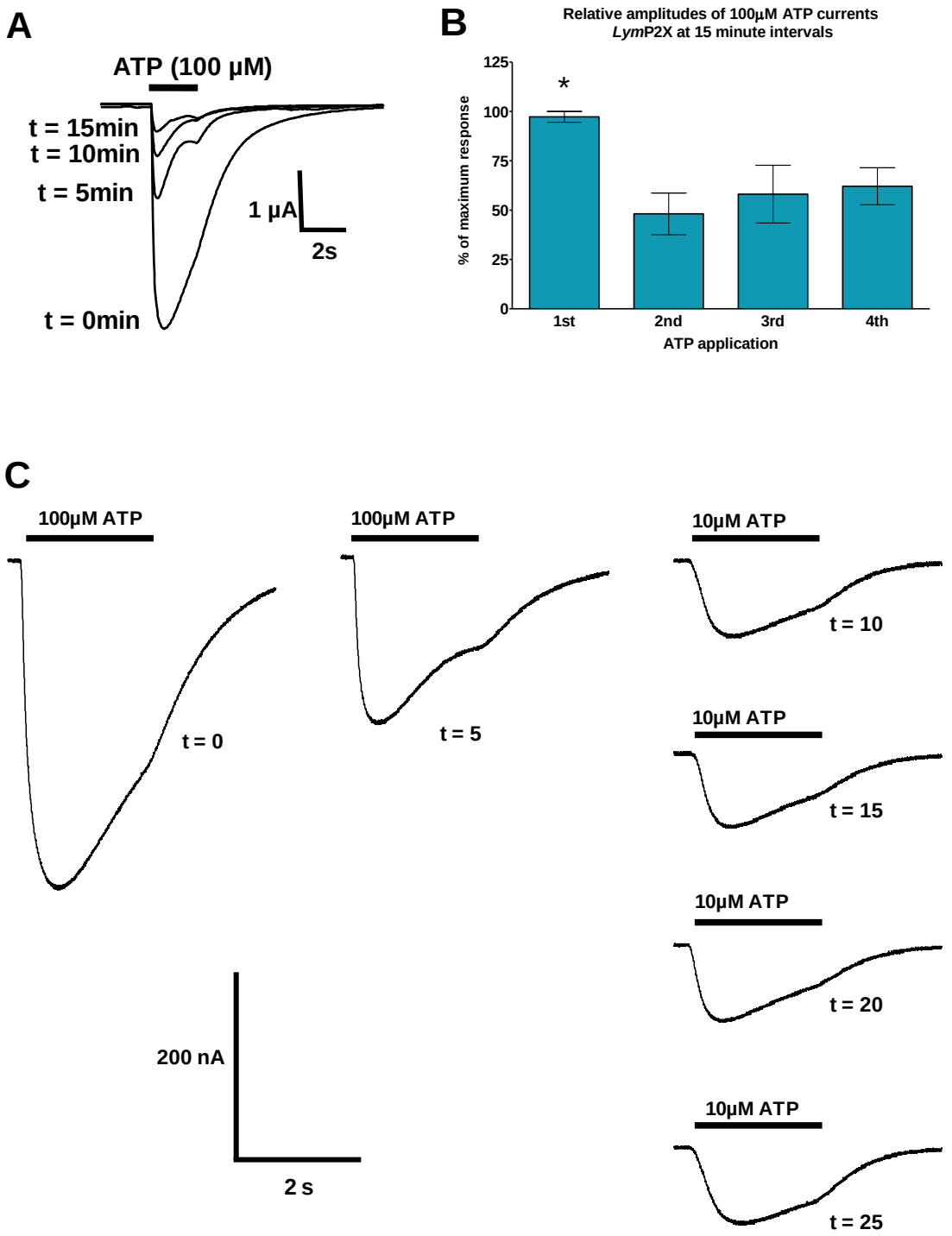

Figure 2.7. A, representative *Lym*P2X currents evoked by ATP. Amplitudes decrease after repeated 100 µM ATP applications at 5 min intervals. B, *Lym*P2X currents stimulated by 100 µM ATP at 15 min intervals have slightly better recovery from desensitization, though the 1st application still has significantly higher amplitude than subsequent applications. 3rd and 4th applications do not reduce in amplitude from the 2nd application (n = 4 - 5). C, currents are almost same amplitudes by 10 µM applications at 5 min intervals following an initial two applications of 100 µM ATP at 5 min intervals.

min intervals gave reproducible responses, and therefore 10 µM ATP was used as a bracketing concentration to construct concentration response curves. The initial two 100 µM ATP pulses served to reduce variation in amplitude of subsequent responses. Current responses evoked by ATP concentrations other than 10 µM are expressed as a percentage of the bracketing concentration's response (see methods). In order to gather reliable current responses by all analysed ATP concentrations it is important for the bracketing concentration to give almost equal responses at 5 min intervals. The bracketing assay is advantageous as it takes into consideration the level of desensitization of the receptor at different time points of the recording, and therefore allows more accurate analysis of the current responses.

2.3.5 Comparison of clones 11 and 14 of LymP2X

Application of ATP to both clones of the *LymP2X* receptor evoked inward currents in a concentration-dependent manner, and a range of ATP concentrations were applied to obtain concentration-response curves.

For ATP-evoked currents at clone 14 (shorter clone) of the *Lym*P2X receptor, the EC_{50} was 6.2 µM (pEC_{50}: -5.2 ± 0.07, n = 9 or 10) with a Hill Slope of 1.1 ± 0.2 and a maximum response that was 164.3 ± 6.2 % of the 10 µM ATP-evoked response (Figure 2.8). For clone 11 (longer clone), the EC_{50} was 5.8 µM (pEC_{50}: -5.2 ± 0.04, n = 5 or 6) with a Hill Slope of 1.4 ± 0.2 and a maximum response that was 143.0 ± 3.3% of the 10 µM ATP-evoked response. There was no significant difference in the EC_{50} values between the two clones ($p > 0.05$). The shorter clone was therefore chosen for all subsequent studies as the start methionine in the longer clone was only 2 nucleotides

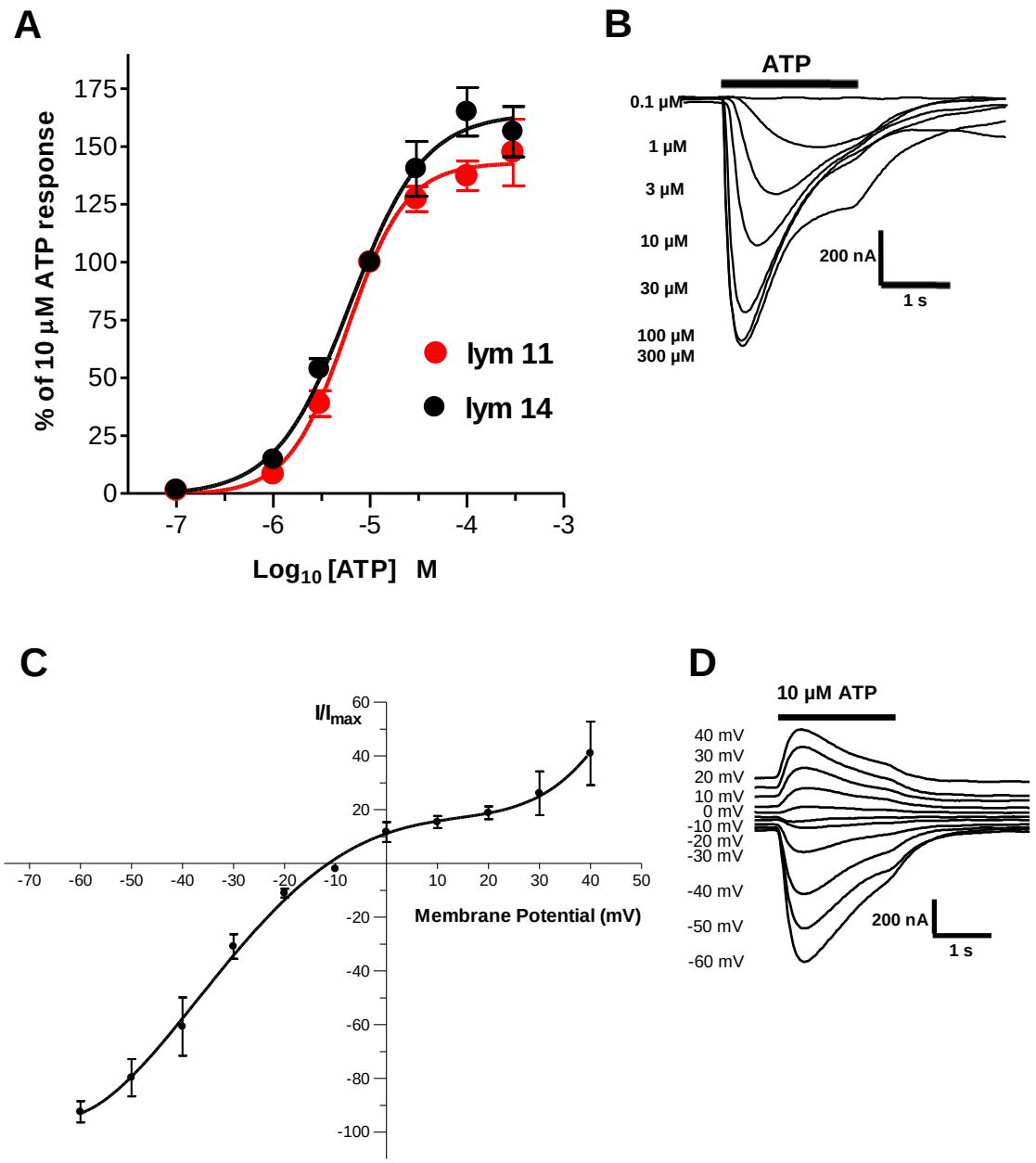

Figure 2.8. A, concentration-response curves for ATP activation at both variants of the *Lym*P2X receptor. B, trace currents from the shorter variant of the *Lym*P2X receptor. C, plot of Current-Voltage curve of *Lym*P2X obtained by recordings of 10 µM ATP-evoked currents under holding membrane potentials between -60 mV to +40 mV, with representative traces of currents in D

away from the mRNA cap site and it therefore seemed unlikely that this start site would be utilised *in vivo*.

2.3.6 Reversal potential

The current-voltage relationship of *Lym*P2X was investigated by looking at 10 µM ATP-evoked currents under a range of holding potentials between -60 mV and +40 mV. The curve was fitted by a fourth-order polynomial (Figure 2.8C). The reversal potential obtained was -11.4 mV (n = 5 - 6).

2.3.7 Other agonists

The ATP analogue, BzATP (2', 3'-O-(4-Benzoylbenzoyl ATP)) has been previously shown to activate P2X receptors from both vertebrate (Evans *et al.*, 1995) and invertebrate species (Agboh *et al.*, 2004). At *Lym*P2X, BzATP also evoked inward currents similar to ATP with an EC_{50} of 2.4 µM (pEC_{50}: -5.6 ± 0.06, n = 5 - 10) and a Hill slope of 1.1 ± 0.2 (Figure 2.9). BzATP was a partial agonist that evoked currents with sub-maximal current amplitudes compared to the full agonist ATP. 100 µM BzATP-evoked a response that was 110.3 ± 7.9 % of that evoked by 10 µM ATP, and significantly smaller than the response evoked by 100 µM ATP ($p < 0.01$). The time courses of the responses evoked by 10 µM BzATP (rise time = 301.2 ± 33.8 ms, T_{50} = 1.0 ± 0.07 s, τ_{desen} = 1.2 ± 0.09 s) were not significantly different ($p > 0.05$ for each parameter) to 10 µM ATP currents (rise time = 272.2 ± 18.8 ms, T_{50} = 1.2 ± 0.1 s, τ_{desen} = 1.2 ± 0.2 s) (Figure 2.9A).

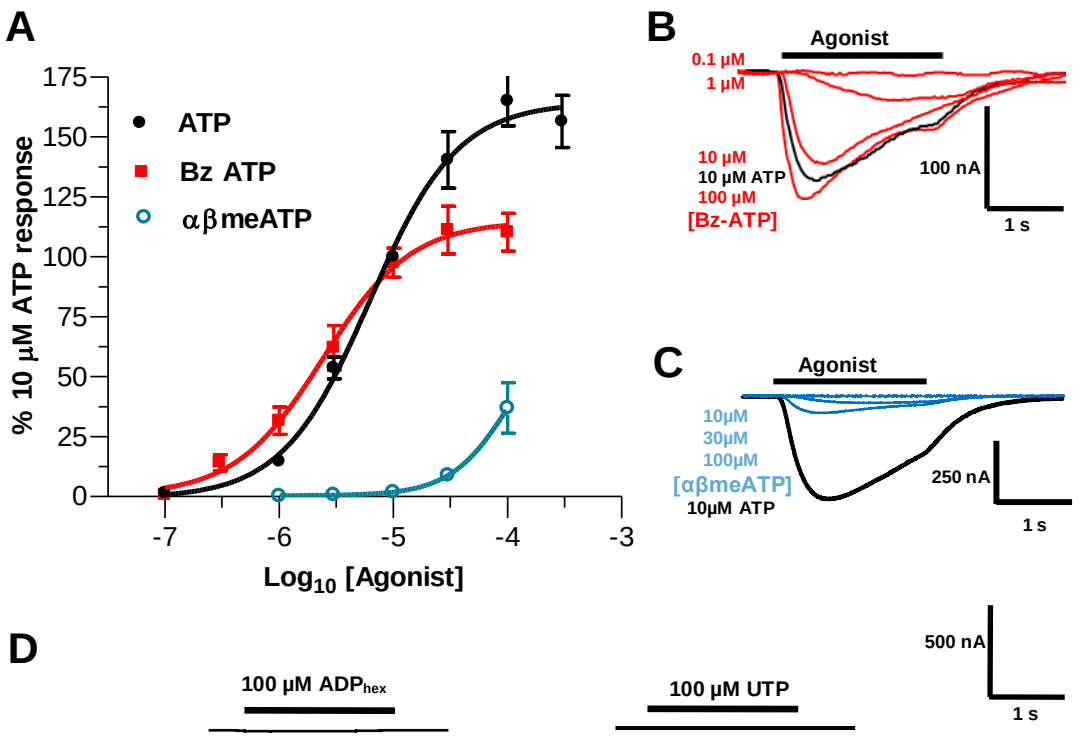

Figure 2.9. A, concentration-response curves for activation of *Lym*P2X receptor by ATP, BzATP and αβmeATP. B and C, representative current traces of *Lym*P2X receptor in response to BzATP and αβmeATP. D, neither 100 µM ADP (hexokinase treated) nor UTP activated *Lym*P2X

Another ATP analogue previously shown to activate P2X receptors, αβmeATP (Valera *et al.*, 1994), was a weak agonist at *Lym*P2X with 100 µM αβmeATP evoking 36.9 ± 10.6 % of the response evoked by 10 µM ATP (n = 6). 100 µM αβmeATP-evoked currents had significantly slower kinetics than 10 µM ATP, with a rise time of 488.7 ± 88.3 ms ($p < 0.01$). The desensitizing curve failed to reduce to less than 50 % of the peak current at the end of agonist application, and had a T_{10} of 557.0 ± 90.5 ms (10 µM ATP T_{10} = 301.3 ± 23.8 ms, $p < 0.01$) (Figure 2.9B).

Hexokinase-treated ADP and UTP are known to be partial agonists at $P2X_5$ homomeric receptors (Wildmann *et al*., 2002), and are also well known P2Y receptor agonists (von Kugelgen, 2006). Both hexokinase treated-ADP and UTP at 100 µM failed to evoke currents at the *Lym*P2X (Figure 2.9D). The ADP utilised in these experiments was hexokinase treated to convert any contaminating ATP to ADP, as commercial stocks of ADP have previously been shown to contain small amounts of ATP contamination (Mahaut-Smith *et al.*, 2000).

2.3.8 Antagonists

The general P2 receptor antagonist PPADS (pyridoxalphosphate-6-azophenyl-2',5'-disulphonic acid) has previously been shown to inhibit both P2X and P2Y receptors (Boyer *et al.*, 1994, Khakh *et al.*, 1994) and also reduced 10 µM ATP-evoked responses at *Lym*P2X in a concentration dependent manner. An IC_{50} of 8.1 µM (pIC_{50}: -5.1 ± 0.1, *n* = 5 - 9) and a Hill slope of -0.7 ± 0.1 (Figure 2.10) was obtained. The highest concentration of PPADS tested (300 µM) reduced the *Lym*P2X currents by ~90 %, with ~10 % of the 10 µM ATP-evoked response remaining. This information will be useful

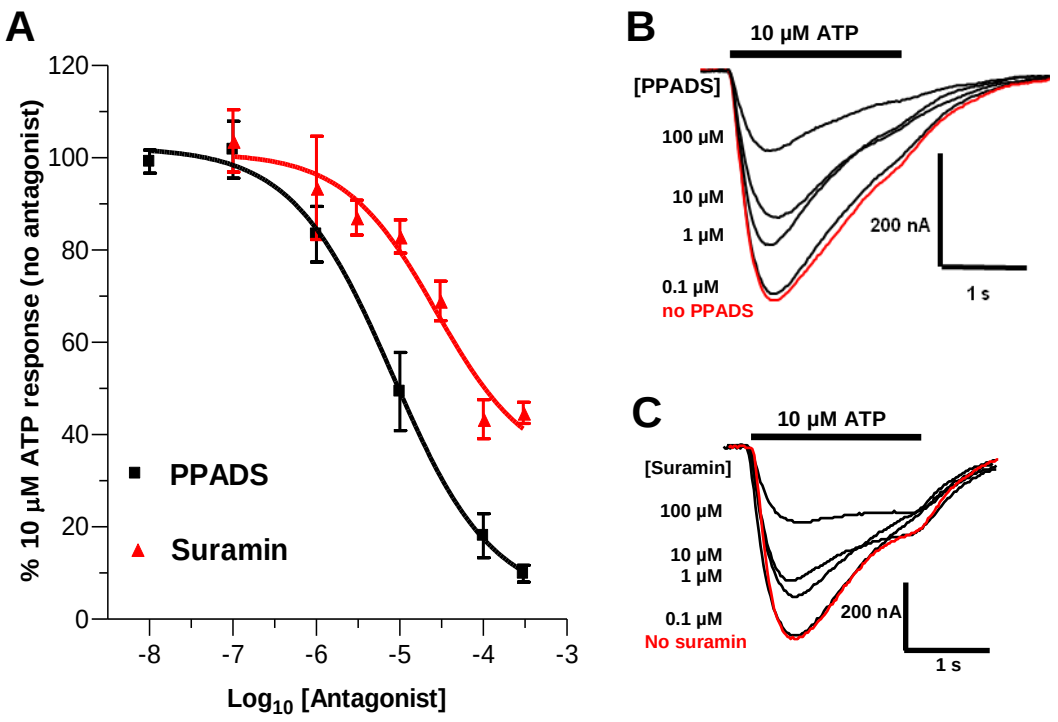

Figure 2.10. A, concentration-response curves showing inhibition of 10 µM ATP responses at *Lym*P2X by PPADS and suramin. B and C, current traces of 10 µM ATP currents in the presence of PPADS and suramin.

for future *in vivo* electrophysiological recordings in *Lymnaea* neurons, as application of PPADS of a particular concentration to modify P2X currents may be informative about the presence and specific roles of *Lym*P2X in the *Lymnaea* central nervous system. The time courses of the responses evoked by 10 µM ATP in the presence of 10 µM PPADS (rise time = 258.5 ± 23.3 ms, T_{50} = 1.2 ± 0.1 s, τ_{desen} = 1.5 ± 0.5 s) were not significantly different to 10 µM ATP currents without PPADS ($p > 0.05$ for each parameter) (Figure 2.10B).

Suramin, another widely used P2 receptor antagonist (Valera *et al.*, 1994) also decreased responses to 10 µM ATP in a concentration dependent manner (Figure 2.10), with an IC_{50} of 27.4 µM (pIC_{50}: -4.6 ± 0.1, n = 5 - 6) and a Hill slope of -0.8 ± 0.1. At the highest concentration of suramin tested (300 µM), complete inhibition was not observed with a ~40 % suramin resistant component of the 10 µM ATP current. 10 µM ATP current kinetics in the presence of 10 µM suramin (rise time = 235.8 ± 15.2 ms, T_{50} = 1.1 ± 0.2 s, τ_{desen} = 1.4 ± 0.2 s) were not significantly different to 10 µM ATP currents in the absence of suramin ($p > 0.05$ for each kinetics parameter) (Figure 2.10C).

2.3.9 Effect of pH

Altering the proton concentration of the recording solution towards more acidic pH or alkaline pH has been previously shown to modify the amplitude of P2X currents (Stoop *et al.*, 1997). To investigate if *Lym*P2X currents are also modulated by extracellular pH, the ND96 recording solution was changed to either pH 6.5 or pH 8.5 and compared to the normal pH 7.5 solution. Increasing proton concentration of the recording solution

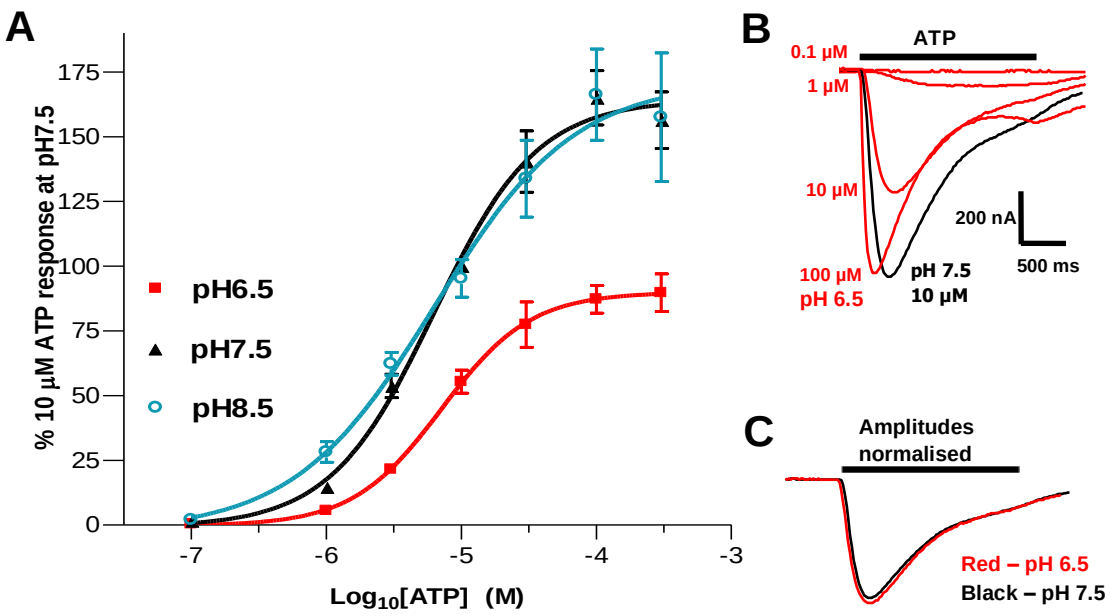

Figure 2.11. A, Concentration-response curves of ATP activation of *Lym*P2X receptor at pH 6.5, 7.5 and 8.5. B, representative current races of the responses at pH6.5. C, normalising the current trace at pH 7.5 to that at pH 6.5. The traces almost overlap in rise time, time of peak and rate of desensitization.

10-fold to decrease the pH to 6.5 decreased the amplitude of the 10 µM ATP-evoked responses (Figure 2.11). At pH 6.5, 10 µM ATP-evoked responses exhibited reduced amplitudes that were 55.4 ± 4.5% of the response evoked by the same concentration at pH 7.5. *Lym*P2X currents evoked by 10, 30, 100 and 300 µM ATP also had significantly reduced amplitudes at pH 6.5 compared to at pH 7.5 recording solution ($p < 0.01$ at 10, 30, 100 and 300 µM ATP). The potency of ATP at pH 6.5 was not significantly different ($p > 0.05$), with an EC_{50} of 7.1 (pEC_{50} -5.2 ± 0.01, $n = 6$) and a Hill slope of 1.3 ± 0.04. At pH 6.5, 10 µM ATP current kinetics (rise time = 180.9 ± 13.1 ms, T_{50} = 0.9 ± 0.1 s, τ_{desen} = 1.3 ± 0.3 s) did not significantly differ to 10 µM ATP in pH 7.5 ($p > 0.05$) (Figure 2.11C).

Decreasing the proton concentration 10-fold from pH 7.5 to the more alkaline pH 8.5 had no significant effect on the amplitude of 10 µM ATP-evoked responses. At pH 8.5, 10 µM ATP-evoked responses were 95.3 ± 7.2 % of the response evoked by the same concentration at pH 7.5, and 100 µM responses under pH 8.5 and pH 7.5 were not significantly different ($p > 0.05$). At pH 8.5, the potency of ATP was not significantly altered ($p > 0.05$), an EC_{50} of 6.2 µM (pEC_{50}: -5.2 ± 0.07, n = 5 - 8) with a Hill slope of 1.1 ± 0.2 obtained.

2.3.10 Ivermectin does not potentiate LymP2X

Ivermectin (IVM) is a semisynthetic macrocyclic lactone under the general class of compounds known as avermectin. Ivermectin is known to potentiate ATP-evoked currents at human $P2X_4$ (Khakh *et al.*, 1999b) and *Schistosoma mansoni* P2X receptors (Agboh *et al.*, 2004). The effects of ivermectin on *Lym*P2X currents were therefore

investigated as this could provide a useful pharmacological tool for future *in vivo* studies in *Lymnaea* CNS. 3 µM ivermectin applied for 5 min in the bath solution and co-applied with 10 µM ATP failed to potentiate the response compared to that of the same concentration of ATP with no ivermectin (n = 6) (Figure 2.12).

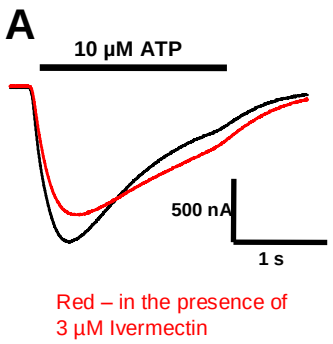

Figure 2.12. 10 µM ATP responses are not potentiated in the presence of 3 µM ivermectin.

	EC_{50}/ IC_{50} (µM)	Rise Time (ms) (10 - 90%)	Desensitization (ms) (T_{10})	Desensitization (ms) (T_{50})	τ_{desen} (1 time constant) (ms)
ATP (shorter clone)	6.2	272.2 ± 18.8	301.3 ± 23.8	1.2 ± 0.1	1.2 ± 0.2
BzATP	2.4	301.2 ± 33.8		1.0 ± 0.07	1.2 ± 0.09
αβmeATP	-	488.7 ± 88.3	557.0 ± 90.5		
ATP + PPADS	8.1	258.5 ± 23.3		1.2 ± 0.1	1.5 ± 0.5
ATP + Suramin	27.4	235.8 ± 15.2		1.1 ± 0.2	1.4 ± 0.2
ATP (pH 6.5)	7.1	180.9 ± 13.1		0.9 ± 0.1	1.3 ± 0.3

Table 1, showing values for rise time and desensitization kinetic parameters at *Lym*P2X. Agonists are at 10 µM, antagonists are at 10 µM.

HdP2X pharmacology

2.3.11 Agonists

ATP-evoked an inward current in *Xenopus* oocytes expressing *Hd*P2X receptors. *Hd*P2X currents had a rapid rise time and fast rate of desensitization. *Hd*P2X currents showed a rapid rise time (71.4 ± 2.5 ms) and a fast rate of desensitization. Current desensitization during the continued presence of agonist showed a T_{50} (time for current to decay to 50% peak amplitude) of 289.9 ± 16.1 ms, and was fitted by a two component exponential (τ_{desen1} = 121.8 ± 26.2 ms and τ_{desen2} = 627.4 ± 147.8 ms). The time course of currents varied slightly between different batches of oocytes with rise times ranging between 30 – 120 ms and T_{50} decay values ranging between 120 – 400 ms.

A 5 min interval between applications of 100 µM ATP was sufficient time for the receptor to recover from desensitization, and produced reproducible responses of almost equal amplitudes (Figure 2.13A).

ATP-evoked responses at *Hd*P2X in a concentration dependent manner, and a range of ATP concentrations up to 1 mM were tested (Figure 2.13B and C). 1 mM ATP gave responses that were 117.9 ± 11.2 % of that evoked by 100 µM ATP. An EC_{50} of 28.5 uM (pEC_{50} -4.6 ± 0.05, n = 6 - 7) with a Hill slope of 1.1 ± 0.1 obtained. The concentration-response curve for ATP and current amplitudes were unaffected by acidic conditions (pH 6.5) (n = 5, data not shown).

Current-voltage relationships of *Hd*P2X currents were obtained by applying 100 µM ATP at a range of holding potentials between -60 mV and +40 mV and observing the

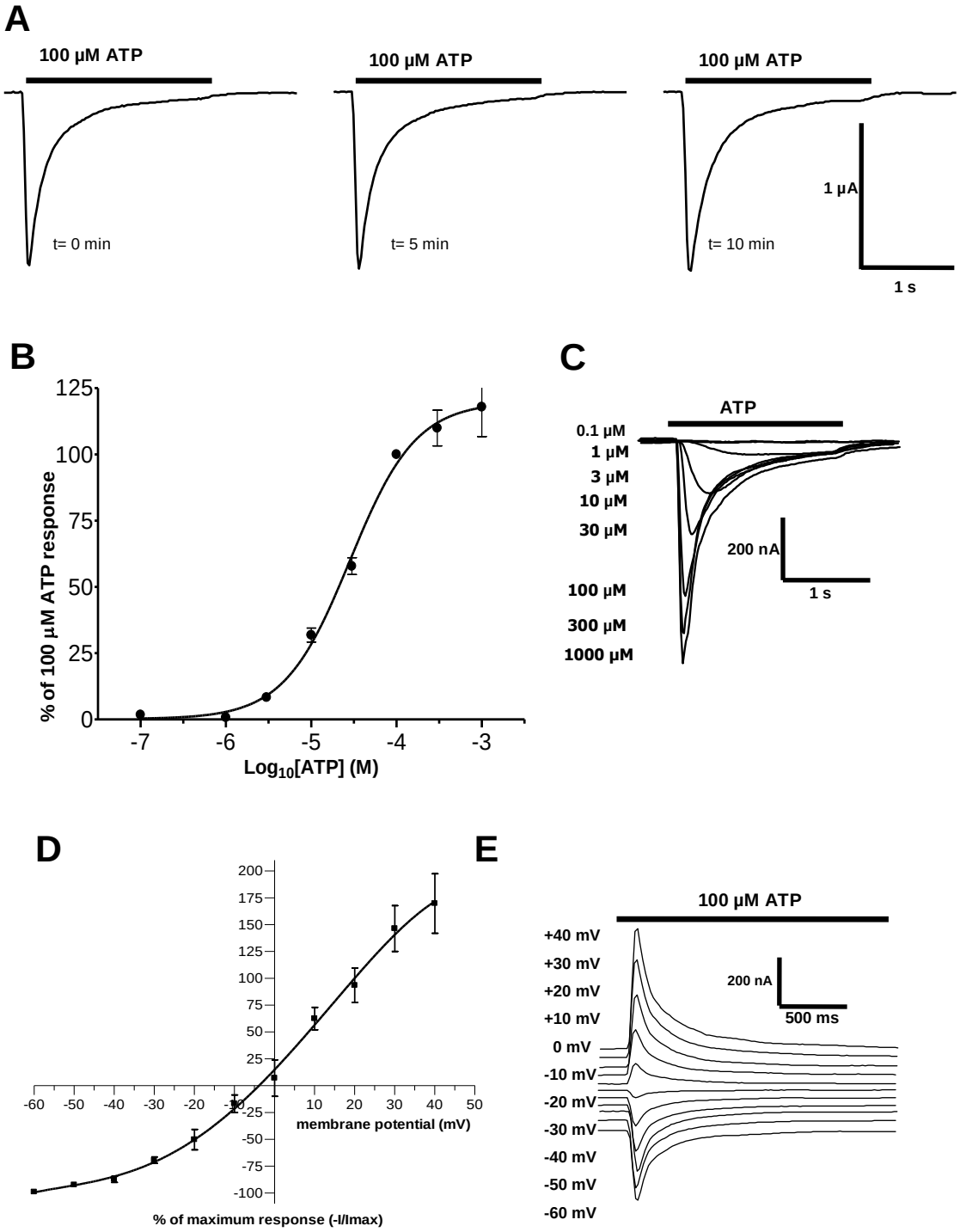

Figure 2.13. A, currents at *Hd*P2X of almost equal amplitudes were seen with 100 µM ATP applications at 5 min intervals. Currents had a fast rise time and rate of desensitization. B, concentration-response curve showing ATP activation of *Hd*P2X receptor, with example currents shown in C. D, plot of Current-Voltage relationship of *Hd*P2X responses evoked by 100 µM ATP at holding membrane potentials between -60 mV to +40 mV, and example traces shown in E.

amplitudes of the currents (Figure 2.13D and E). The curve was fitted by a fourth-order polynomial. The reversal potential obtained was -3.8 mV (*n* = 5 - 6).

BzATP also evoked inward currents at *Hd*P2X with an EC_{50} of 12.2 µM (pEC_{50} -5.9 ± 0.17, n = 5 - 9) and a Hill slope of 0.7 ± 0.2. 100 µM BzATP-evoked currents had significantly slower current kinetics compared to 100 µM ATP, with a rise time of 136.0 ± 13.9 ms ($p < 0.001$) and the desensitizing current with a T_{50} of 495.0 ± 45.4 ms ($p < 0.001$) (Figure 2.14). However the time constants of desensitization were not significantly different to currents evoked by ATP, with τ_{desen1} = 103.3 ± 10.3 ms and τ_{desen2} = 375.8 ± 9.4 ms ($p > 0.05$ for both time constants). This can be explained by the absence of a sharp peak and lower gradient of the desensitizing current from peak to ~90 % amplitude for BzATP current responses (Figure 2.14B). After ~10 % current desensitization, the remainder of the 100 µM BzATP desensitizing current had the same kinetics as 100 µM ATP. BzATP efficacy was significantly lower than for ATP, with 100 µM BzATP giving 76.2 ± 6.7 % of the amplitude response evoked by 100 µM ATP ($p < 0.01$), and was therefore considered a partial agonist at the receptor.

αβmeATP (100 µM) evoked currents that were less than 50 % in amplitude to those evoked by 100 µM ATP. 100 µM αβmeATP currents displayed a significantly slower time course compared to 100 µM ATP with a rise time of 249.7 ± 39.0 ms ($p < 0.001$). The desensitizing current did not always reduce to less than 50 % peak amplitude at the end of 100 µM αβmeATP application, with a T_{10} of 434.7 ± 136.8 ms, significantly slower than 100 µM ATP response (T_{10} = 70.0 ± 3.7 ms, $p < 0.001$) (Figure 2.14C). The concentration-response curve for αβmeATP did not reach plateau at the highest concentration tested (100 µM) and an EC_{50} value could therefore not be obtained.

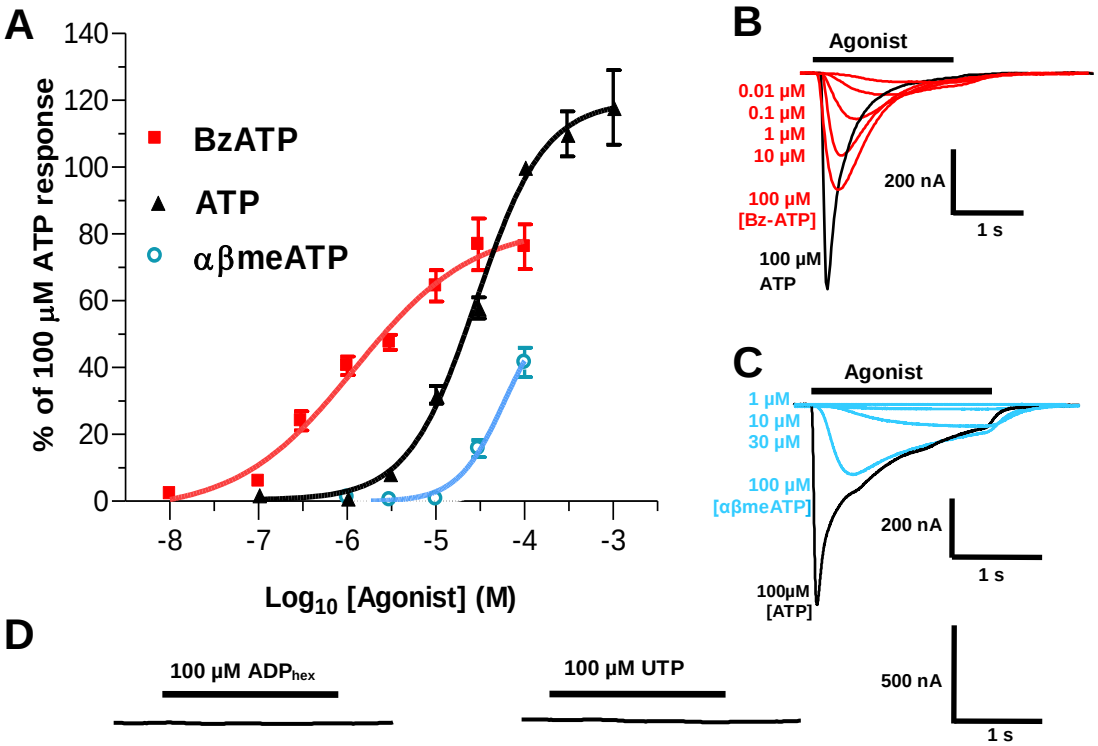

Figure 2.14. A, comparison of BzATP and αβmeATP with ATP concentration-response curves at the *Hd*P2X, with trace currents shown in B and C respectively. D, ADP (hexokinase treated) and UTP failed to evoke currents.

ADP (hexokinase treated) and UTP (100 µM) failed to elicit currents at the *Hd*P2X receptor (Figure 2.14D).

2.3.12 Antagonists

PPADS antagonised 100 µM ATP-evoked currents at *Hd*P2X with an IC_{50} of 8.4 µM (pIC_{50}: -5.1 ± 0.1, *n* = 5 - 8) and a Hill slope of -1.0 ± 0.3 (Figure 2.15). 10 µM PPADS did not significantly alter most parameters of current kinetics of 100 µM ATP-evoked currents (rise time = 41.8 ± 2.8 ms, T_{50} = 249.4 ± 31.5 ms, τ_{desen1} = 145.9 ± 15.2 ms, $p > 0.05$ for each parameter). However, the second time constant of desensitization, τ_{desen2} of 1619.0 ± 407.0 ms was significantly slower than 10 µM ATP currents without PPADS ($p < 0.05$) (Figure 2.15B).

Suramin also decreased *Hd*P2X currents in a concentration dependant manner, though less strongly than PPADS. Suramin inhibited 100 µM ATP responses with an IC_{50} of 22.6 µM (pIC_{50}: -4.7 ± 0.3, *n* = 5 - 7) and a Hill slope of -0.8 ± 0.3. At the highest concentration of suramin tested (300 µM), complete inhibition was not observed with a suramin resistant component of the 100 µM ATP-evoked response being about ~25 %. 10 µM suramin did not significantly alter the current kinetics of 100 µM ATP-evoked currents (rise time = 71.1 ± 10.4 ms, T_{50} = 440.5 ± 87.5 ms, τ_{desen1} = 167.3 ± 55.3 ms, τ_{desen2} of 761.0 ± 269.1 ms, $p > 0.05$ for each parameter) (Figure 2.15C).

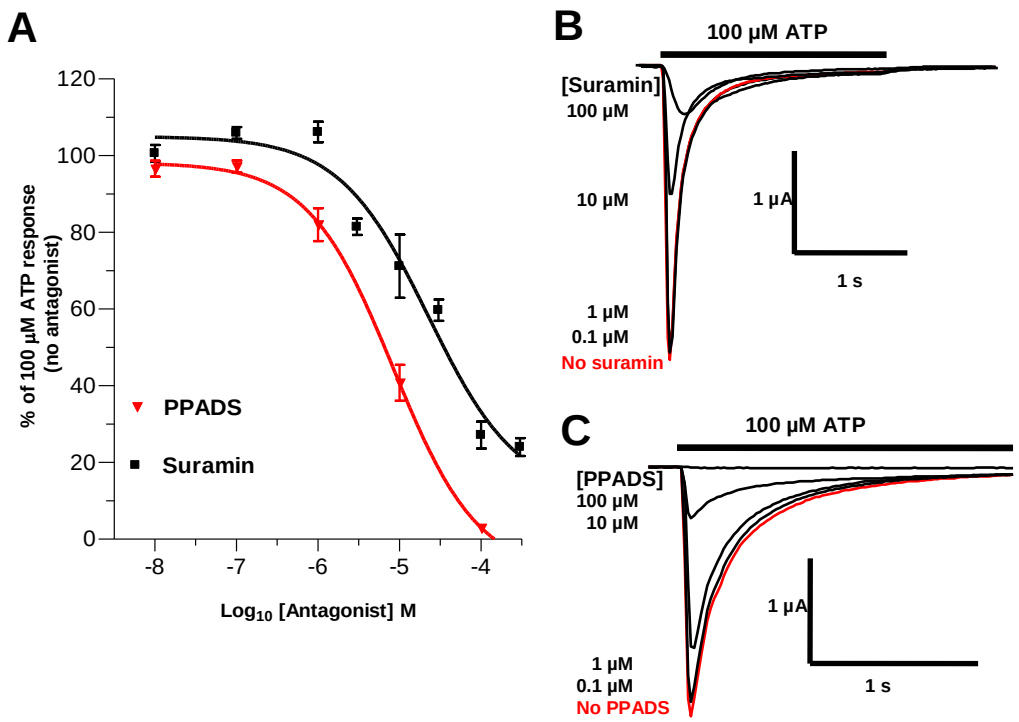

Figure 2.15. A, concentration-response curves showing inhibition of 100 µM ATP-evoked *Hd*P2X responses by PPADS and suramin. B and C, representative current traces of inhibition of 100 µM ATP responses by PPADS and suramin at *Hd*P2X.

2.3.13 HdP2X currents are potentiated by ivermectin

In contrast to the *Lym*P2X receptor, 3 µM ivermectin potentiated 100 µM ATP-evoked current amplitudes in *Hd*P2X by 172.6 ± 5.2 %, and a significant potentiation occurred in the presence of 3 µM ivermectin at all ATP concentration above 1 µM ($p < 0.05$) (Figure 2.16). The concentration-response curve of ATP in the presence of 3 µM ivermectin had an EC_{50} of 32.1 µM (pEC_{50} -4.5 ± 0.1, n = 5-10) with a Hill slope of 0.8 ± 0.2. The maximum response evoked by ATP in the presence of 3µM ivermectin was 223.8 ± 14.1 % of the response to 100 µM ATP (in the absence of ivermectin). 3µM ivermectin did not significantly affect the current kinetics of 100 µM ATP-evoked responses (rise time = 32.2 ± 1.3 ms, T_{50} = 126.5.4 ± 14.7 ms, τ_{desen1} = 75.1 ± 11.9 ms, τ_{desen2} = 394.6 ± 53.0 ms, $p > 0.05$ for each parameter) (Figure 2.16B).

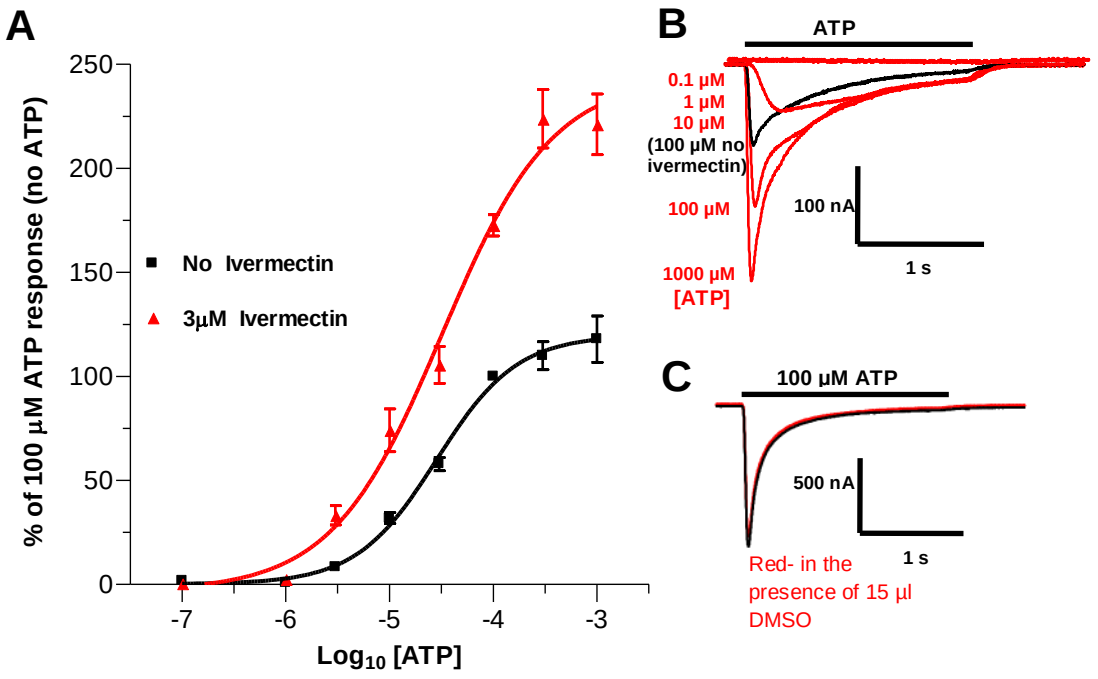

Figure 2.16. A, concentration-response curves of *Hd*P2X activation by ATP in the presence and absence of 3 µM ivermectin. B, example current traces of ATP activation of *Hd*P2X in the presence of 3 µM ivermectin. C, ivermectin is dissolved in DMSO before 15 µl aliquots of ivermectin at 10 mM/µl of DMSO is added to the solutions. Therefore DMSO was tested for having any effects on currents. 15 µl DMSO had no notable effects on ATP-evoked currents.

2.4 DISCUSSION

This chapter describes the identification, cloning and functional characterisation of P2X receptors from *Lymnaea stagnalis* and *Hypsibius dujardini*. Sequence analysis demonstrates that both these lower organism P2X receptors share several highly conserved amino acid sequences that are present in all vertebrate and most other non-vertebrate P2X receptors identified to date. These include ten conserved cysteine residues that have been shown to form five disulphide bonds, lysine residues, FT and NFR motifs thought to be involved in ATP binding (Ennion *et al.*, 2000, Ennion and Evans, 2002a, Kawate *et al.*, 2009). The consensus protein kinase C phosphorylation site in the amino terminus, the only feature to be conserved in all known vertebrate and non-vertebrate P2X receptors, is also present in both *Lymnaea stagnalis* and *Hypsibius dujardini* P2X receptors. The conservation of these residues in tardigrade and mollusc species further highlights the functional importance of these residues since they have been highly conserved during the course of evolution. The protein kinase C site plays a role in desensitization (Boue-Grabot *et al.*, 2000), and therefore can function to limit neurotoxicity.

*Lym*P2X and *Hd*P2X cRNAs both produced functional channels when injected into *Xenopus* oocytes, and gave rise to an inward current upon ATP application. Following the cloning and pharmacological characterisation of P2X receptors from *Schistosoma mansoni* (Agboh *et al.*, 2004), *Dictyostelium discoideum* (Fountain *et al.*, 2007) and the green algae *Ostreococcus tauri* (Fountain *et al.*, 2008), this study on *Lym*P2X and *Hd*P2X provides further evidence that this class of ion channels emerged relatively early in eukaryotic evolution (Burnstock and Verkhratsky, 2009). The lack of P2X receptor sequences in genomes of the invertebrates *Anopheles gambiae*, *Caenorhabditis*

elegans, *Drosophila melanogaster*, and *Apis mellifera*, organisms for which the full genomic sequence is known may have initially suggested that P2X receptors emerged later in evolution following the divergence of vertebrates from non-vertebrates (Burnstock and Verkhratsky, 2009). However the identification and cloning of P2X receptor homologues from the non-vertebrate organisms *Schistosoma mansoni* (Agboh *et al.*, 2004), and subsequently from the slime mould *Dictyostelium discoideum* (Fountain *et al.*, 2007) and the single celled green algae *Ostreococcus tauri* (Fountain *et al.*, 2008) indicates that P2X receptors were present early in the evolution of invertebrate species.

It would be of interest to know if there are more P2X receptor sequences present in the *Lymnaea stagnalis* and *Hypsibius dujardini* genomes that are yet to be identified. Amongst the invertebrates, only in *Dictyostelium discoideum* have multiple P2X subtypes been identified. Interestingly, the family of five P2X receptors in *Dictyostelium* (Ludlow *et al.*, 2008) and indeed all other invertebrate P2X receptors identified to date, including the *Lymnaea stagnalis* and *Hypsibius dujardini* receptors described in this study, do not appear to correspond directly to orthologs of the mammalian $P2X_{1-7}$ family (Figure 2.6). This suggests that the emergence of a family of $P2X_{1-7}$ subtypes in mammals was a later evolutionary event that occurred subsequent to the divergence of vertebrates from invertebrates.

This part of the investigation focused on the pharmacological characterisation of *Lym*P2X and *Hd*P2X receptors in *Xenopus* oocytes, a heterologous expression system, and the pharmacological properties of these receptors obtained can be compared with other P2X receptors. Both *Lym*P2X and *Hd*P2X have similarities and a number of

notable differences in pharmacological properties between each other and with P2X receptors from other organisms, as elaborated below. The pharmacological data of *Lym*P2X in *Xenopus* oocytes gathered in this chapter will be extremely useful in identifying the *in vivo* roles of *Lym*P2X in relation to other unidentified purinergic receptors present in this organism when carrying out intracellular (*in vivo*) electrophysiological recordings in *Lymnaea* neurons.

2.4.1 LymP2X has slow and HdP2X has fast current kinetics

ATP-evoked currents in *Hd*P2X, displayed a fast rise time, rapid rate of desensitization and an EC_{50} of 28.5 µM. The ATP-evoked currents at the *Lym*P2X receptor had a slower rise time and rate of desensitization, with an EC_{50} of 6.2 µM. P2X receptors have been previously classified into groups based on their current kinetics and ATP potency (MacKenzie *et al.*, 1999). The so called group 1 receptors consist of $P2X_1$ and $P2X_3$ and display fast current kinetics that reach peak and desensitize rapidly, have high potency for ATP (EC_{50} < 10 µM), and are αβmeATP-sensitive. Group 2 consists of slowly activating and desensitizing receptors with slightly lower ATP potency (EC_{50} = ~10 µM), insensitivity to αβmeATP (EC_{50} > 100 µM), and include $P2X_2$, $P2X_4$ and $P2X_5$ subtypes. Group 3 features $P2X_7$, a very slow desensitizing receptor with much lower ATP potency, little rectification and increases in pore size during ATP application. While *Lym*P2X can be easily assigned into group 2 by virtue of its slow current kinetics, low sensitivity to αβmeATP and EC_{50} of 6.2 µM, it is difficult to classify *Hd*P2X into any of the existing groups. Therefore the identification of *Hd*P2X opens the possibility of a new group of P2X receptor(s) defined by fast current kinetics and low ATP potency. This feature also further strengthens the theory that a receptor's

current kinetics and EC_{50} are not linked and that ATP binding and gating can be independent processes.

2.4.2 BzATP and αβmeATP are partial agonists at both LymP2X and HdP2X.

BzATP was observed to be a partial agonist with an EC_{50} near to ATP but a significantly lower maximal response compared to ATP at both *Lym*P2X and *Hd*P2X. Similar characteristics are seen at other P2X receptors except for $P2X_7$ where BzATP has a higher efficacy compared to ATP (Surprenant *et al.*, 1996), and the *Dictyostelium discoideum Dd*P2X channel which has low sensitivity to BzATP (Fountain *et al.*, 2007). The residue Lys^{127} was found to be responsible for increased potency of BzATP at rat $P2X_7$, compared to mouse $P2X_7$, which has an alanine residue at the equivalent position (Young *et al.*, 2007). This Lys^{127} residue is proposed to lie in the head region near the ATP binding site and therefore may bind the Bz group of BzATP (Kawate *et al.*, 2009, Young, 2009). Ile^{131} in *Lym*P2X and Ala^{140} in *Hd*P2X are present at equivalent sequence positions of rat $P2X_7$ Lys^{127}, and therefore offer an explanation as to why BzATP has lower efficacy than ATP at these invertebrate P2X receptors.

BzATP currents at *Lym*P2X did not have an altered time course compared to ATP currents, whereas they were slower than ATP currents at *Hd*P2X. This indicates that BzATP has slower binding and unbinding kinetics at *Hd*P2X than ATP, and it would therefore possibly be informative in terms of the mechanism involved to determine which residues are responsible for these properties.

The BzATP sensitivity of *Lym*P2X may also be of use in determining the *in vivo* roles of this receptor in the CNS as this may be the only BzATP sensitive among the

purinergic receptors in the *Lymnaea*, and application of BzATP to *Lymnaea* neurons may inform us more easily about the precise function of *Lym*P2X.

It has been found from crystallographic and electrophysiological studies on AMPA-subtype ionotropic glutamate receptors that binding of the receptor to partial agonists leads to distinctly graded conformational changes of the receptor, resulting in ligand-binding core conformational states and incremental pore openings that differ compared to the binding and activation from full agonists (Jin *et al.*, 2003, Roberts and Evans, 2004). Therefore these partial agonists can determine the open probability of the channel and hence the activation of distinct amplitude currents (Jin, Banke et al. 2003). The binding of Benzo-Benzoyl group of BzATP could incrementally control the movement of a group of residues or domains at or near the ligand binding core of the P2X receptor to give currents of different amplitudes compared to ATP. BzATP therefore appears to preferentially activate the receptor in a less energetically favourable way that leads to lower subconductance levels during activation at both *Lym*P2X and *Hd*P2X and also a slower desensitization rate at *Hd*P2X, relative to the full agonist ATP. With these properties, partial and full agonists can be used together in an approach to distinguish mutations that interfere with ligand binding and those mutations that affect gating (Haines *et al.*, 2001, Roberts and Evans, 2004).

The non-hydrolysable ATP analogue αβmeATP is a weak agonist at both *Lym*P2X and *Hd*P2X receptors. Of the human P2X receptors, $P2X_1$ (Valera *et al.*, 1994) and $P2X_3$ (Chen *et al.*, 1995) are sensitive to αβmeATP and therefore the residues responsible for αβmeATP activation appear to be poorly conserved. As with all other known invertebrate and most vertebrate P2X receptors, ADP did not activate *Lym*P2X or

*Hd*P2X. ADP and UTP are well known P2Y agonists, and hexokinase-treated ADP and UTP are only known to activate $P2X_5$ homomers of the known P2X receptors (Wildmann *et al*., 2005). Confirmation that ADP and UTP do not activate *Lym*P2X will inform us about the presence of P2Y receptors in *Lymnaea* CNS following the application of these agonists to *Lymnaea* neurons.

*2.4.3 Lym*P2X *but not Hd*P2X *currents were potentiated by acidic pH*

ATP-evoked *Lym*P2X currents showed a reduced amplitude and maximal response at pH 6.5 compared to at pH 7.5. $P2X_1$, $P2X_3$ and $P2X_4$ currents are also inhibited by higher proton concentrations (Stoop *et al.*, 1997, Khakh *et al.*, 1999b, Wildman *et al.*, 1999b). Increasing proton concentration is known to inhibit $P2X_7$ receptors (Virginio *et al.*, 1997). There were no significant differences in the EC_{50} and current kinetics for ATP-evoked *Lym*P2X currents at pH 6.5 compared to at pH 7.5, similarly seen in human $P2X_1$, $P2X_3$ and $P2X_4$ (Stoop *et al.*, 1997). This suggests that higher proton concentrations affect the gating of the ion channel and that binding affinity of *Lym*P2X for ATP is not altered under acidic conditions. In contrast, ATP-induced currents at pH 6.5 are increased at $P2X_2$ and *Dictyostelium discoideuim* dP2XB, with a leftward shift in the concentration response curve and no change in maximal response (King *et al.*, 1997, Stoop *et al.*, 1997, Ludlow *et al.*, 2009). The acidic pH is expected to enable an increase in ATP affinity rather than affecting gating at $P2X_2$ (King *et al.*, 1997). At pH 8.5, there was no notable difference in amplitudes and an EC_{50} of 6.3 µM was obtained, which is not significantly different to the EC_{50} under pH 7.5 recording solution ($p > 0.05$). Rat $P2X_1$ and $P2X_3$ have lower ATP potencies at more acidic pH (Wildman *et al.*, 1999b). Of the human and invertebrate P2X receptors, only $P2X_2$ and *Dictyostelium*

dP2XB are affected by increasing the pH from pH 7.5, with reduction in amplitudes observed (Stoop *et al.*, 1997, North and Surprenant, 2000, Roberts *et al.*, 2006, Ludlow *et al.*, 2009), however the underlying mechanisms for this inhibition are not known. *Hd*P2X currents are not affected by decreasing pH to 6.5. These differences in sensitivities to pH are due to the variations in the positioning of histidine residues in the extracellular ligand-binding loop. The number and positioning of the histidine residues on the extracellular ligand-binding loop are not conserved between the P2X subtypes (Stoop *et al.*, 1997). The extracellular domain of *Lym*P2X has only a single histidine residue, His^{81}, mutation of which would be expected prevent the reduction of ATP-evoked currents at acidic pH. Mutating His^{319} at $P2X_2$ reduced pH potentiation (Clyne *et al.*, 2002a), and this extracellular residue is located close to the ATP binding site.

*Hd*P2X was not sensitive to higher proton concentration in the recording solution despite the extracellular domain of *Hd*P2X having histidines at three positions (His^{232}, His^{252} and His^{306}). Therefore it may be hypothesised that histidine residues that are present at extracellular positions near the ATP binding site and transmembrane domains such as His^{81} at *Lym*P2X or His^{319} at rat $P2X_2$, are more likely play roles in modulation of P2X currents in acidic conditions. However, His^{206} has been found to play a role in the dual agonist concentration-dependant effect that low pH has on human $P2X_3$ currents (Gerevich *et al.*, 2007). Acidic pH was found to shift the concentration-response curve to the right and increase maximum response of αβmeATP-evoked responses at human $P2X_3$, and this effect was abolished after the substitution of His^{206} with alanine (Gerevich *et al.*, 2007).

Protons and zinc ions should have different sites of action for *Lym*P2X, as observed for

rat, as mutating His^{319} did not affect zinc potentiation and mutating either His^{120} or His^{213} almost prevented zinc potentiation without changing the modulation by pH (Clyne *et al.*, 2002a). Furthermore, protons and zinc were found to have additive effects on the inhibition of rat $P2X_1$ and $P2X_3$ currents, extending evidence that different binding sites for these modulators exist (Wildman *et al.*, 1999b).

Localised acidosis during tissue injury, ischaemia and inflammation (King *et al.*, 1997) provides a physiological significance for studying the effect of pH on P2X receptor function. Also, during the release of neurotransmitters from pre-synaptic terminally located vesicles, acidic shifts take place at the synaptic cleft (Krishtal *et al.*, 1987, King *et al.*, 1997) that could act to modulate P2X receptor activity.

2.4.4 PPADS and suramin are antagonists at both LymP2X and HdP2X

100 µM PPADS inhibited the large majority of the ATP-evoked currents at both *Lym*P2X and *Hd*P2X. PPADS also slowed down the second component of desensitization of ATP-evoked *Hd*P2X currents. Suramin was a less potent and effective antagonist, inhibiting a lower proportion of the current at 100 µM in comparison to the same concentration of PPADS. These properties differ from those of the *Schistosoma mansoni Sm*P2X, which is inhibited more by suramin in comparison to PPADS at higher concentrations (Agboh *et al.*, 2004), and also to *Ostreococcus tauri Ot*P2X and *Dd*P2X, which are not antagonised by PPADS or suramin (Fountain *et al.*, 2007, Fountain *et al.*, 2008, Ludlow *et al.*, 2009). Among the vertebrate P2X receptors, suramin blocks $P2X_1$ (Valera *et al.*, 1994), $P2X_2$ (Brake *et al.*, 1994), $P2X_3$ (Chen *et al.*, 1995) and $P2X_5$ (Garcia-Guzman *et al.*, 1996), but does not inhibit $P2X_4$ (Bo *et al.*,

1995) and $P2X_7$ channels (Collo *et al.*, 1996, Soto *et al.*, 1997). PPADS also effectively inhibit currents at all human P2X receptors except at $P2X_4$ (Bo *et al.*, 1995) and $P2X_6$ (Collo *et al.*, 1996). This shows the low conservation of residues involved in PPADS and suramin inhibition at P2X receptors.

Mutagenesis studies have shown that ATP and PPADS bind to different amino acid residues of the P2X receptors (Buell *et al.*, 1996). The presence of a lysine residue at position 246 in $P2X_2$ and at equivalent positions in other subunits has been found to be critical in the inhibition of P2X receptors by PPADS, possibly forming a Schiff base with the aldehyde group of PPADS (Buell *et al.*, 1996, Collo *et al.*, 1996). Substitution of Glu^{249} with lysine in $P2X_4$ gave rise to PPADS sensitive channels (Buell *et al.*, 1996). *Hd*P2X has a positively charged arginine near this position, Arg^{246} that may bind PPADS. However *Lym*P2X has no lysine or arginine at or near this equivalent position, suggesting that residues that are not positively charged can take part in binding PPADS, or the PPADS binding site is in a different position in the sequence of *Lym*P2X. Since PPADS is not found endogenously in the cells or tissues of living organisms and PPADS binds at positions away from the ATP binding site to non-competitively inhibit P2X currents, there is no evolutionary basis for PPADS binding residues to be conserved among P2X receptors of different organisms.

Suramin has antinociceptive effects and PPADS has the ability to act as an antihypertensive agent (Lambrecht, 2000). Acidic pH has an effect on increasing potency of antagonism of $P2X_2$ by suramin (King *et al.*, 1997). Lys^{138} in human $P2X_1$ has been found to play roles in suramin inhibition of P2X currents as the K138E mutant had reduced suramin inhibition (Sim *et al.*, 2008). Glutamate at position 138 is present

in mouse $P2X_1$, which has reduced suramin inhibition (Sim *et al.*, 2007), and an E138K substitution at the mouse $P2X_1$ gave rise to channels that are more strongly inhibited by suramin (Sim *et al.*, 2008). The equivalent human $P2X_1$ Lys^{138} residue in zebrafish $P2X_4$ is Asp^{141}, and the crystal structure proposed that this residue is placed within and around the proposed ATP-binding pocket (Kawate *et al.*, 2009). These antagonists are suggested to prevent or slow conformational rearrangements by occupying part or the entire ATP-binding site and prevent shutting of the head, right flipper and dorsal fin domain jaws (Kawate *et al.*, 2009). With suramin binding interfering with ATP binding to the receptor, presence of residues contributing to suramin binding may depend on evolutionary conserved mechanisms of ATP binding. Suramin insensitive $P2X_4$ has ATP-evoked currents that are of slow time course and higher EC_{50} (Bo *et al.*, 1995), suggesting that the absence of suramin binding residues may have interfered with ATP binding.

2.4.5 Ivermectin potentiated HdP2X and not LymP2X currents

Ivermectin had no effect on ATP-evoked currents in *Lym*P2X receptors. This was in marked contrast to *Hd*P2X where ivermectin showed a marked potentiation of ATP-evoked currents. Of the mammalian P2X receptors, only $P2X_4$ is potentiated by ivermectin (Khakh *et al.*, 1999b), as are glycine, and GABA- receptors (Adelsberger *et al.*, 2000, Priel and Silberberg, 2004). Among the invertebrate P2X receptors, the currents at the *Schistosoma mansoni* P2X receptor are also potentiated by ivermectin (Agboh *et al.*, 2004). Ivermectin action at P2X receptors will enhance our understanding of the process of gating and motions of the pore of the channel.

Ivermectin was thought to have an allosteric mode of action by increasing maximum current when binding to a high affinity site on the receptor to stabilise the open state, whereas binding to a low affinity site was proposed to slow the rate of deactivation (Priel and Silberberg, 2004). However the desensitization rate of invertebrate *Hd*P2X and *Sm*P2X (Agboh *et al.*, 2004) currents are not altered by ivermectin. This suggests the absence of the proposed low affinity ivermectin binding site in these invertebrate P2X receptors, implying that this site was not present in the ancestral P2X receptor and its emergence in the vertebrate $P2X_4$ receptor was a relatively recent evolutionary event. Subsequently it was proposed that during the gating of the ion channel, TM1 rotates relative to TM2, and ivermectin is able to access the lipid environment and optimally bind into a hydrophobic crevice created by TM1 and TM2 at the protein-lipid interface (Silberberg *et al.*, 2007). This explains the broad spectrum of action by ivermectin at various ligand-gated channels.

Mutagenesis studies have shown that mutation of the TM1 domain decreases ivermectin affinity and its effects (Silberberg *et al.*, 2007). Furthermore, a cysteine mutagenesis experiment showed that rat $P2X_4$ receptors with a cysteine replacing residues Gln^{36}, Leu^{40}, Val^{43}, Val^{47}, Trp^{50}, Asn^{338}, Gly^{342}, Leu^{346}, Ala^{349}, and Ile^{356} were fully functional but had no currents that were potentiated by ivermectin, while Arg^{33} and Cys^{353} were also suggested to play roles in ivermectin binding (Jelinkova *et al.*, 2008). The arrangement of these residues is consistent with the helical nature of the transmembrane domains. This demonstrates that the ivermectin binding site consists of mainly hydrophobic, non-polar residues located at the plasma membrane-facing side of each of the transmembrane helices, as opposed to facing the pore region (Jelinkova *et al.*, 2008). *Hd*P2X sequence maintains a similar complement of hydrophobic non-polar

residues at the equivalent positions found to be responsible for ivermectin binding at rat $P2X_4$ (Jelinkova *et al.*, 2008). The ivermectin insensitivity of *Lym*P2X is possibly explained by the presence of a smaller side chain Ala^{50} residue, whereas the sequence of *Hd*P2X and has an Ile^{60} and rat $P2X_4$ possesses a Val^{47} residues at the equivalent position.

2.4.6 Evolution of P2X receptors

It was previously considered that P1 and P2Y, which are G-protein-coupled receptors were expressed earlier in evolution and P2X sequences emerged later with the requirement for fast signalling in the nervous system (Burnstock and Verkhratsky, 2009). However following the identification and cloning of receptors from a range of invertebrates including P2X receptors in intracellular membranes of *Dictyostelium* and in the smallest living eukaryote *Ostreococcus tauri*, this work on *Lym*P2X and *Hd*P2X is further evidence that fast purinergic signalling and P2X receptors for ATP emerged early in the evolution of eukaryotes. This work will help us to unearth the true extent of the P2X receptor family, its origins and also associated signalling pathways. It provides a comparative model to enable structure-function studies and leading to the better understanding of P2X receptors in mammals. The absence of P2X receptor sequences in *A. gambiae, C. elegans and D. melanogaster* and the evidence for strong effects of purines in these organisms indicates that purinergic receptors different in sequence, structure, and properties to P2X or P2Y possibly evolved in these species (Burnstock and Verkhratsky, 2009).

Chapter 2 conclusion

The pharmacological data obtained in this chapter for *Lym*P2X will aid in the discovery of the roles played by this receptor in the CNS of *Lymnaea stagnalis*, a convenient model system in which feeding and respiratory systems are well understood. *Lym*P2X and *Hd*P2X sequence and pharmacological data can also facilitate structure-function studies in combination with other P2X receptors. Mutagenesis of unconserved residues may highlight the residues that are responsible for variations in pharmacological profiles that exist between different subtypes.

It can be concluded that neither *Lym*P2X nor *Hd*P2X share all or even majority of pharmacological characteristics with a particular subtype among the mammalian P2X receptors. *Lym*P2X currents do not show the same fast desensitization rate as human $P2X_1$, but similar to human $P2X_1$ has reduced currents under acidic pH. *Hd*P2X currents are potentiated by ivermectin, as seen with human $P2X_4$ but unlike human $P2X_4$ the *Hd*P2X receptor is inhibited by PPADS.

It is of interest to know if there are multiple splice variants of this cloned *Lym*P2X receptor gene, which may affect function like observed in the human $P2X_2$ receptor (Brandle *et al.*, 1997). Further study can look at ion permeability of the P2X ion channel and whether ion pore increases to a size that allows the flow of large molecules, as observed in $P2X_7$.

The *Hd*P2X receptor, which is from a species able to survive extreme temperatures and pressures, is likely to be a more stable receptor complex than other P2X receptors, and therefore possibly represents an attractive candidate for further X-ray crystallographic

studies, potentially to definitively determine the nature of the agonist binding site and the roles of the intracellular domains in P2X function, both features that are missing from the current zebrafish $P2X_4$ crystallographic data.

Chapter 3: Mutagenesis of invertebrate P2X receptors to investigate divalent metal binding sites and mechanisms of desensitization.

3.1 INTRODUCTION

Following the cloning, identification and pharmacological characterisation of the *Hd*P2X receptor, mutagenesis experiments were carried out to further investigate structure-function relationships of P2X receptors. The study of P2X receptors in lower organisms evolutionary remote from human could potentially improve our understanding of general P2X function since only those residues or amino acid motifs that are functionally important will likely to have been conserved over evolution. Differences between lower organism and human receptors may also highlight residues or domains that confer variations in pharmacological properties observed between different P2X receptor subtypes. The study of purinergic signalling in lower organism models may also shed light on novel P2 receptor mediated signalling pathways that can be extrapolated to human P2X receptors. A prime example of this is the recent discovery that *Dictyostelium* P2X receptors have an intracellular function (Fountain *et al.*, 2007). This has led to the reassessment of the possible functional roles of intracellular mammalian $P2X_4$ receptors which have been found by antibody labelling to be expressed on the intracellular membranes of lysosomes in macrophages and endothelial cells (Qureshi *et al.*, 2007).

In this chapter the effects of zinc and copper at *Lym*P2X and *Hd*P2X receptors is investigated and subsequently particular residues are mutated in *Hd*P2X in an attempt to elucidate structural determinants that underlie divalent metal ion activity at P2X receptors. The effects of divalent metal ions on P2X receptors have been previously

investigated (Nakazawa and Ohno, 1997). The action of zinc and copper at P2X receptors is of physiological significance due to the storage of divalent cations within vesicles in presynaptic terminals, which are released into the synaptic cleft after nerve stimulation (Assaf and Chung, 1984, Smart *et al.*, 1994, Frederickson and Bush, 2001, Huidobro-Toro *et al.*, 2008). Charged residues have been previously shown to be important in zinc and copper inhibition of ligand-gated ion channels (Nakazawa and Ohno, 1997, Paoletti *et al.*, 2000). Histidine residues have been shown to play roles in metal binding and co-ordination in zinc-binding proteins such as metaloproteases (Vallee and Auld, 1990), as well as in P2X receptors to allow copper and zinc to influence ATP-evoked responses (Clyne *et al.*, 2002a, Coddou *et al.*, 2003a, Acuna-Castillo *et al.*, 2007). Therefore charged and histidine residues would be suitable candidates for mutagenesis in *Hd*P2X to observe their role of binding divalent cations. The results may give further indications of whether metal binding sites developed independently through evolution or originated from a common ancestor in the different P2X receptor subtypes. This study may also give clues to the nature of divalent metal binding residues in other receptors.

The second part of this chapter uses a chimeric approach to explore particular regions of the P2X receptor that impart current kinetics for the channel. Desensitization is the reduction in agonist-evoked current amplitude during the continued application of agonist, and can function to limit neurotoxicity. *Hd*P2X is the only invertebrate P2X receptor identified to date that displays fast channel kinetics. A P2X receptor from another invertebrate species *Boophilus microplus* (*Bm*P2X), a species of cattle tick, has also recently been cloned and pharmacologically characterised within this laboratory (unpublished data). In marked contrast to *Hd*P2X, this arthropod P2X receptor displays

ATP-evoked currents with exceptionally slow rise and decay times. A continuous application of ATP for 30 seconds at *Bm*P2X results in little desensitization of the current and after ATP washout the current decays with a large time constant. This *Bm*P2X receptor is 414 amino acid residues in length and has 33.5 - 53.5 % sequence identity with human P2X receptor subtypes.

Since *Hd*P2X and *Bm*P2X display markedly contrasting desensitisation characteristics, chimeras of *Hd*P2X and *Bm*P2X were made to further investigate the regions involved in desensitization. The intracellular N- and C-termini have been previously shown to play roles in desensitization in P2X receptors (Werner *et al.*, 1996, Boue-Grabot *et al.*, 2000) and these domains were swapped between the *Hd*P2X and *Bm*P2X receptor sequences. The results may give further clues about possible mechanisms of P2X receptor desensitization, such as whether the cytoplasmic domains take part in pore block or if they take part in interactions with each other to influence current flow. Since *Bm*P2X displays marked run down in current amplitude between repeated 100 µM ATP applications at 5 min intervals, the chimeras were also assessed for the level of run down in current amplitude. This will inform us if desensitization rate has a relationship with current run down.

3.2 METHODS

3.2.1 Site directed mutagenesis

Point mutations in the *Hd*P2X plasmid construct were introduced using the QuikChange™ Mutagenesis Kit (Stratagene, U.S.A.) according to the manufacturer's instructions by my supervisor. In brief, 25 µl PCR reactions consisted of 200 µM dNTPs, 200 nM of forward and reverse primers, PFU Ultra enzyme and buffer, and 50 ng of wild type *Hd*P2X template plasmid. Histidines at positions 232, 252 and 306, glutamic acid residues at positions 110 and 249, an aspartic acid residue at position 183 and lysine residues at positions 130 and 297 were mutated to alanine. Mutations were introduced at the sites of the sequence using the following primers:

H232A:

forward 5’ CAA CAC TTG CCG GTA CGC TCC CGT GTC CGA CCC TTA C 3’

reverse 5’ GTA AGG GTC GGA CAC GGG AGC GTA CCG GCA AGT GTT G 3’

H252A:

forward 5’ CTT GGT GGA GTT GGC AGC TGA AAA CTT CTC CGT CG 3’

reverse 5’ CGA CGG AGA AGT TTT CAG CTG CCA ACT CCA CCA AG 3’

H306A:

forward 5’ GGG CTG GAA CTT TCG TGC TGC TGA CTA TTG GAA TG 3’

reverse 5’ CAT TCC AAT AGT CAG CAG CAC GAA AGT TCC AGC CC 3’

E110A:

forward 5’ GTA ATT CCA TCT GCG GCT AAC GAT GCG GTC TTC 3’

reverse 5’ GAA GAC CGC ATC GTT AGC CGC AGA TGG AAT TAC 3’

K130A:

forward 5’ ACC TAG CCA GCA GAG TGG AGC TTG CCC CGA GGA CAC CAA CAA 3’ reverse 5’ TTG TTG GTG TCC TCG GGG CAA GCT CCA CTC TGC TGG CTA GGT 3’

D183A:

forward 5’ GTC CGG CGG AAG TGG CTG ACA AGC CAG AGC C 3’

reverse 5’ GGC TCT GGC TTG TCA GCC ACT TCC GCC GGA C 3’

E249A:

forward 5’ GCA ACG CTT GGT GGC TTT GGC ACA TGA AAA C 3’

reverse 5’ GTT TTC ATG TGC CAA AGC CAC CAA GCG TTG C 3’

K297A:

forward 5’ GAT TCC GTT GAA GAG GCG ATA GCG AAG GGC TG 3’

reverse 5’ CAG CCC TTC GCT ATC GCC TCT TCA ACG GAA TC 3’

PCR reactions were carried out with an initial hot start at 94 ºC, followed by 16 cycles of 95 ºC for 30 s, 55 ºC for 1 min, 68 ºC for 15 min, followed by holding at 4 ºC. PCR reactions contained 5 ng/µl forward and reverse primer.

Double mutations where two of the three histidines were both mutated to alanine were created by conducting serial rounds of site directed mutagenesis as follows: H252A/H232A, H252A/H306A, H232A/H306A. A triple mutant where all the three histidines were mutated to alanine was produced by introducing a H306A mutation into the H252A/H232A double mutant. DNA sequencing (Automated ABI sequencing service, Leicester University) was used to confirm the introduction of the correct mutation(s) and the absence of spontaneous mutations in all mutant constructs.

Both mutant and wild type plasmids were digested with *NotI* restriction enzyme in order to linearise, and sense strand cRNA was synthesised using the T7 mMessage mMachine™ kit (Ambion, U.S.A.) according to the manufacturer's instructions.

3.2.2 Generation of BmP2X-HdP2X chimeras

Six chimeras were generated where either or both of the amino and carboxy intracellular domains of *Bm*P2X and *Hd*P2X were interchanged, while not manipulating the extracellular or transmembrane domains (Figure 3.1A). These chimeras were generated by my supervisor using the technique of seamless cloning. This technique utilises a restriction enzyme (in this instance EarI) that cleaves outside of its recognition sequence. This allows the design of compatible sticky ends of the desired sequence to facilitate precise ligation of DNA fragments with no disruption of the reading frame or introduction of unwanted extra sequence. PCR primers were designed incorporating EarI restriction sites to allow amplification of the component parts of the chimera which were subsequently ligated together after EarI digestion. For example, to produce Chimera A (Figure 3.1B), the wildtype *Bm*P2X plasmid was first used in a PCR reaction with TICKNtermFOR and TICKTM2REV primers to amplify the sequence from the N-terminus to the end of TM2. The forward primer binds to the beginning of the sequence at the kozak sequence / start metionine and reverse primer binds at the end of TM2. The reverse primer has an incorporated EarI restriction site (red) so that a 5' CAG 3' overhang (blue) remains on the bottom strand after EarI digestion of the PCR product.

Wildtype *Hd*P2X plasmid was then employed as template for a PCR reaction using

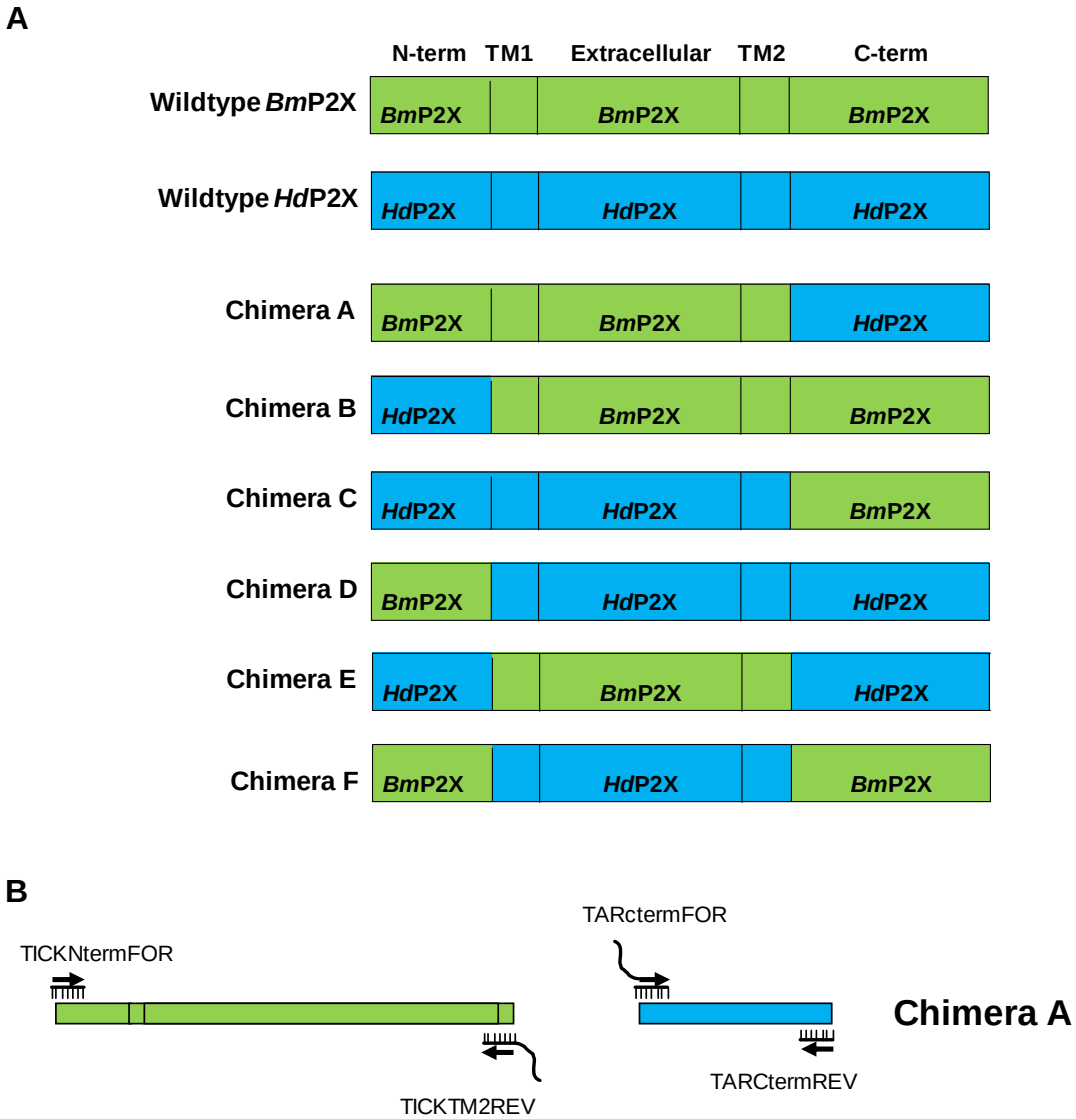

TICKNtermFOR 5' GCCGCCACCATGGGCTTGAAC 3'

TICKTM2REV 5' AA**CTCTTC**A**CAG**CAGGCAGTTAAGAACAACAAG 3'

TARctermFOR 5' AA**CTCTTC**A**CTG**AGAACAGACGCATTTGG 3'

TARCtermREV 5' GGAGTTTTGGTAGCGCACAG 3'

Figure 3.1. A. Schematic representation of *Hd*P2X-*Bm*P2X chimera constructs. B. Example cloning strategy for Chimera A showing positions of PCR primers. In this case TICKTM2REV and TARctermFOR primers contain EarI restriction sites to generate compatible sticky ends after EarI digestion, that they could be subsequently ligated together. *Hd*P2X sequences are represented in blue and *Bm*P2X sequences are indicated in green

TARCtermfor and TARCtermREV primers to obtain the full C-terminus sequence. Reverse primer binds at the end of the sequence (C-terminus). The forward primer consists of an EarI site that is located at the beginning of the C-terminus. Following digestion of the PCR product with EarI a 5' CTG 3' overhang remains on the top strand.

After ligation of EarI digested PCR products, PCR was carried out on the ligated product using TICKNtermFOR and TARCtermREV primers to obtain the full length of chimera A, which was subcloned into SE15'UTR TA cloning vector.

Xenopus oocyte preparation, injection of P2X cRNA and two-electrode voltage clamp were carried out as described in Chapter 2. Copper and zinc were both bath-perfused for 5 min before ATP applcation as well as being present at the same concentration in the U-tube solution along with the agonist. Experiments carried out on *Bm*P2X-*Hd*P2X chimeras to examine current kinetics analysed the responses of the first ATP application to each oocyte expressing the particular chimera. Investigation on current amplitude run-down of the chimeras involved 5 applications of 100 µM ATP at 5 min intervals.

3.2.3 Data analysis

Data are displayed as means ± S.E. Differences between means of data were analysed by either the Student's t-test for simple comparison between two data sets or by ANOVA (analysis of variance) followed by Dunnett's post test when multiple data sets were compared (GraphPad Prism software (La Jolla, USA)). Concentration-response

data were fitted with the Hill equation $Y = ((X)^H \cdot M)/((X)^H + (EC_{50})^H)$, where Y is response, X is agonist concentration, H is the Hill coefficient, M is maximum response, and EC_{50} is the concentration of agonist evoking 50% of the maximum response. pEC_{50} is the $-\log_{10}$ of the EC_{50} value. All concentration-response curves, bar charts, EC_{50} values and Hill coefficients were obtained using GraphPad Prism software.

*Hd*P2X-*Bm*P2X currents were analysed for their current kinetics by fitting curves for decaying currents with the following equations:

Current desensitization were fitted either by a double exponential curve equation:

$(t) = A_1\exp(-t/\tau_{desen1}) + A_2\exp(-t/\tau_{desen2}) + Ss$

or a single exponential curve equation :

$y(t) = A\exp(-t/\tau_{desen}) + Ss$

where :

A_1 and A_2 = relative amplitudes of the first and second exponential

τ_{desen1} and τ_{desen2} = time constant of desensitization for first and second exponential

t = time

Ss = plateau

Current rise times (from 10 – 90 % peak current amplitude), T_{50} (time from peak to 50 % peak current amplitude) and T_{10} (time from peak to 90 % peak current amplitude) were also calculated.

3.3 RESULTS

3.3.1 Biphasic Effect of divalent cations at LymP2X

Divalent metal cations have been previously shown to have effects on ATP-evoked currents at both vertebrate and invertebrate P2X receptors (Nakazawa and Ohno, 1997, Raouf *et al.*, 2005). The effects of divalent cations were therefore investigated on *Lym*P2X and *Hd*P2X receptors. Zinc and copper ions had similar biphasic effects on currents induced by 10 µM ATP at the *Lym*P2X receptor (Figure 3.2). Increasing copper or zinc concentration to 100 µM significantly potentiated responses, with 100 µM zinc enhancing to 146.5 ± 13.9 % ($p < 0.05$) and 100 µM copper giving 159.6 ± 21.8 % ($p < 0.01$) of the responses of 10 µM ATP (no copper or zinc) ($n = 5–8$). In contrast, 10 µM ATP responses were significantly reduced by 1 mM zinc to 34.6 ± 1.8% ($p < 0.05$) and by 1 mM copper to 36.6 ± 4.1% ($p < 0.05$) of control responses. The time courses of the 10 µM ATP-evoked responses were significantly slowed in the presence of both divalent ions at 100 µM, and the desensitizing currents failed to reduce by more than 50 % of the peak amplitude during the two second application of ATP. 100 µM copper slowed 10 µM ATP-evoked current rise times to 960.1 ± 292.2 ms ($p < 0.01$) and desensitization T_{10} to 625.9 ± 120.6 ms ($p < 0.01$). 100 µM zinc slowed 10 µM ATP-evoked current rise times to 438.5 ± 42.2 ms ($p < 0.001$), and T_{10} to 725.7 ± 205.8 ms ($p < 0.01$).

3.3.2 Inhibitory effects of divalent cations at HdP2X

Zinc and copper had similar effects at the *Hd*P2X receptor, but these differed in comparison to their action at *Lym*P2X receptors (Figure 3.3). Zinc and copper both caused concentration dependant inhibition of ATP-evoked currents at *Hd*P2X rather

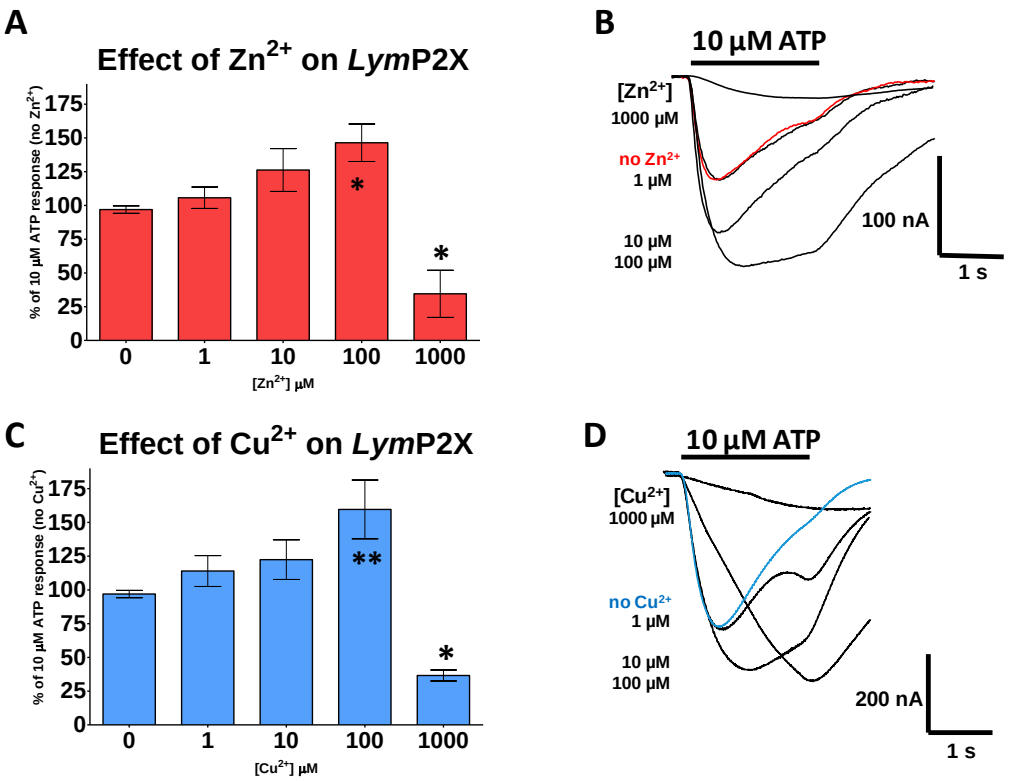

Figure 3.2. A, bar chart showing [Zn^{2+}] effects on 10 µM ATP currents, with representative currents traces shown in B. C, bar chart showing effect of [Cu^{2+}] on 10 µM ATP currents, with example currents shown in D. Significant potentiation of 10 µM ATP currents are shown by stars inside the bars, * for 100 µM Zn^{2+} ($p < 0.05$), ** for 100 µM Cu^{2+} ($p < 0.01$). Significant inhibition of 10 µM ATP currents are shown by a star above the bars ($p < 0.01$ for both Zn^{2+} and Cu^{2+}).

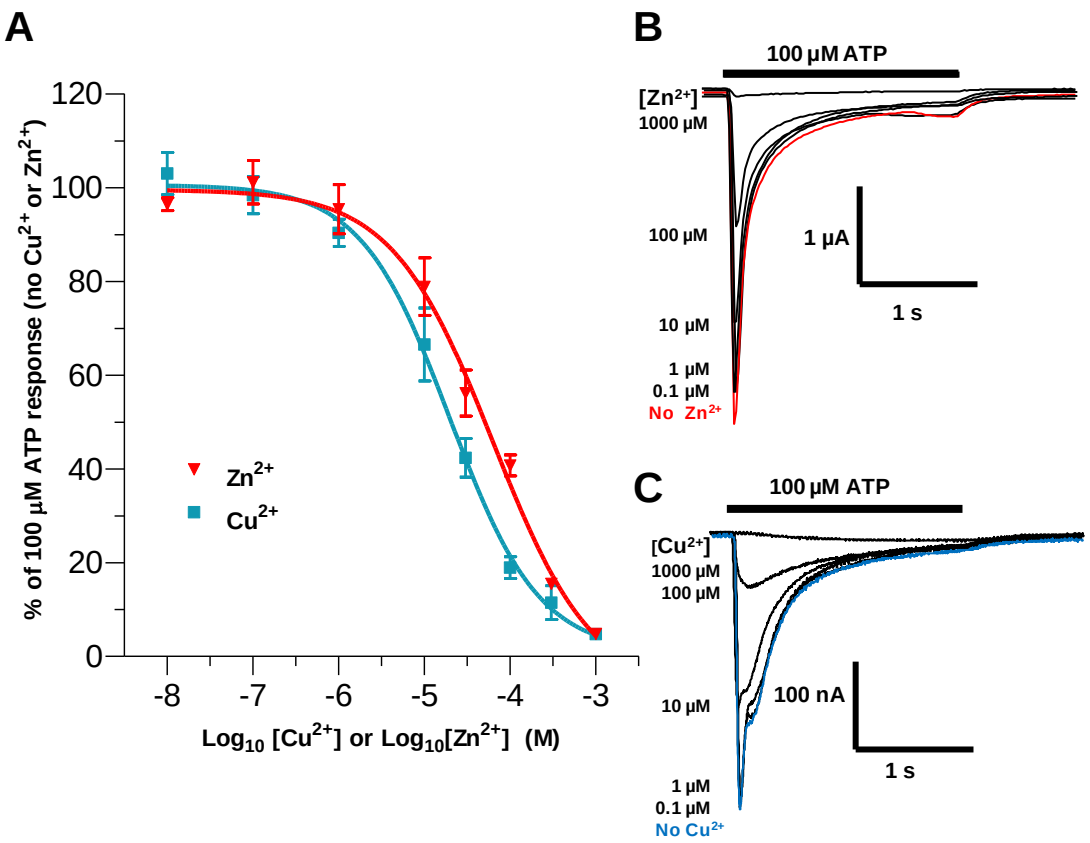

Figure 3.3. A, Concentration-response curves showing inhibition of 100 µM ATP-evoked responses at *Hd*P2X by Zn^{2+} (black) and Cu^{2+} (red). B and C, example traces of inhibition of 100 µM ATP-evoked currents by Zn^{2+} (B) and Cu^{2+} (C).

than the biphasic response observed at *Lym*P2X. Zinc inhibited 100 µM ATP currents, with an IC_{50} of 62.8 µM (pIC_{50} -4.2 ± 0.1, n = 5 -6) and a Hill slope of 0.7 ± 0.1. Copper also acted as an inhibitor of 100 µM ATP currents with an IC_{50} of 19.9 µM (pIC_{50} -4.7 ± 0.1, n = 5 - 6) and a Hill slope of -0.8 ± 0.1. Application of 10 µM divalent cations did not slow the time course of 100 µM ATP-evoked *Hd*P2X currents. 100 µM ATP currents with 10 µM copper had a rise time of 46.7 ± 8.0 ms, T_{50} of 305.4 ± 38.7 ms, τ_{desen1} of 91.6 ± 25.7 ms and a τ_{desen2} of 521.8 ± 128.3 ms, and these were not significantly different to currents in the absence of copper ($p > 0.05$ for all parameters). Similarly 100 µM ATP currents in the presence of 10 µM zinc had a mean rise time of 37.0 ± 1.5 ms, T_{50} of 162.0 ± 13.0 ms, τ_{desen1} = 115.2 ± 7.9 ms, τ_{desen2} = 505.8 ± 32.8 ms, (not significantly different to currents in the absence of zinc ($p > 0.05$) for all parameters).

3.3.3 Effect of mutating histidine residues on copper and zinc action at HdP2X

Histidine residues have been previously shown to play roles in divalent metal ion inhibition of P2X and other ligand-gated receptors. There are three histidine residues present in the extracellular domain of the *Hd*P2X amino acid sequence: His^{232}, His^{252} and His^{306}. Using primer mutagenesis, all these histidines were substituted to alanines individually as well as in combinations to observe their role in zinc and copper inhibition of *Hd*P2X currents. Therefore seven histidine mutants in total were produced: single mutants H232A, H252A, H306A; double mutants H232A / H252A, H232A / H306A, H252A / H306A; triple mutant H232A / H252A / H306A.

ATP-evoked inward currents in all of the *Hd*P2X histidine single and double mutants with similar rise times to the wildtype *Hd*P2X receptor. The triple mutant H232A / H252A / H306A however was non-functional (Figure 3.4). EC_{50} values were unchanged for ATP concentration – response curves for all single and double mutants ($n = 5 - 8$, $p > 0.05$ for all mutants) (Figure 3.4 and Table 1). This indicates that agonist potencies were not altered and that no gross alterations in receptor structure had occurred due to histidine mutation. Therefore any effect these mutations have on divalent metal ion action is unlikely to be due to disruption of ATP binding or gating of the receptors.

The single histidine mutants exhibited currents which desensitised slower than the wildtype *Hd*P2X receptor (T_{50} values in Table 1). The desensitizing current in each of the single histidine mutants were best fit by a single exponential rather than a double exponential for wildtype *Hd*P2X currents evoked by ATP. The time constants of desensitization obtained for 100 µM ATP-evoked currents at the single histidine mutants were $\tau_{desen} = 711.7 \pm 59.2$ ms for H232A ($T_{50} = 562.4 \pm 67.4$ ms, $p < 0.01$), $\tau_{desen} = 602.6 \pm 79.1$ ms for H252A ($T_{50} = 561.8 \pm 91.2$ ms, $p < 0.01$), and $\tau_{desen} = 615.4 \pm 118.3$ ms for H306A ($T_{50} = 509.4 \pm 66.9$, $p < 0.01$) compared to wildtype *Hd*P2X T_{50} of 289.9 ± 16.1 ms.

The double histidine mutant currents also displayed significantly slower desensitization in comparison to the wildtype *Hd*P2X receptor, as observed by their higher T_{50} values (Table 1). The desensitizing current in each of the double histidine mutants were also best fit by a single exponential rather than a double exponential for wildtype *Hd*P2X currents evoked by ATP. The time constants of desensitization gathered for 100 µM

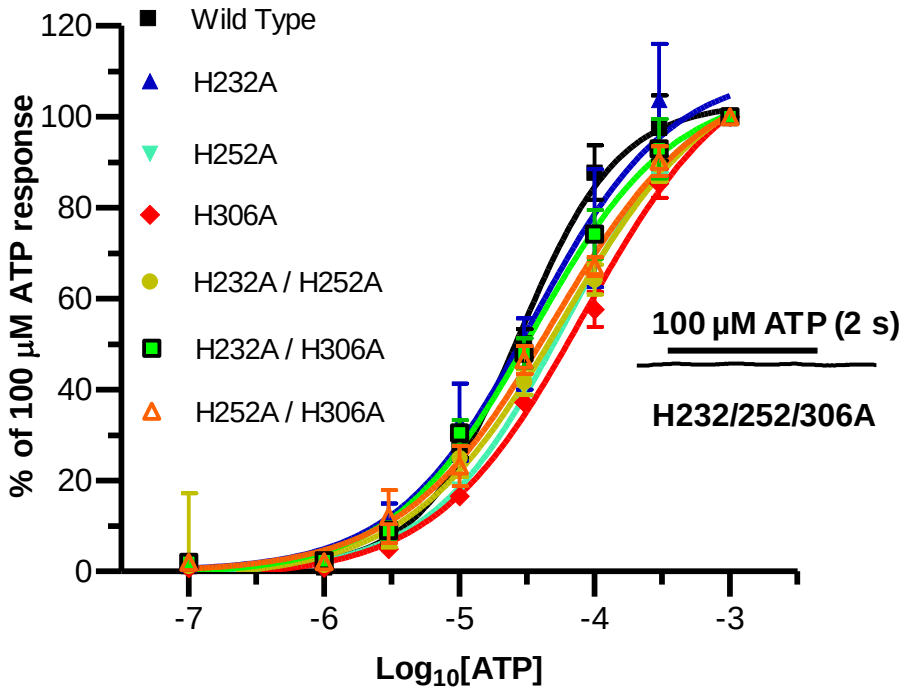

Figure 3.4. ATP concentration response curves for *Hd*P2X wildtype, single and double histidine mutant *Hd*P2X receptors. Responses expressed as a percentage of maximum response. Triple mutant H232A / H252A / H306A was non-functional after no inward currents observed upon 100 µM ATP application (six oocytes).

	EC_{50} (µM)	Rise Time (ms) (10 - 90%)	Desensitization (ms) (T_{50})	τ_{desen} (single time constant) (ms)	τ_{desen1} (double time constant) (ms)	τ_{desen2} (double time constant) (ms)
Wildtype	27.6	71.4 ± 2.5	289.9 ± 16.1	-	121.8 ± 26.2	627.4 ± 147.8
H232A	35.0	65.2 ± 14.3	562.4 ± 67.4 **	711.7 ± 59.2	-	-
H252A	60.3	66.7 ± 4.8	561.8 ± 91.2 **	602.6 ± 79.1	-	-
H306A	83.8	59.0 ± 3.5	509.4 ± 66.9 **	615.4 ± 118.3	-	-
H232A/ H252A	58.5	67.0 ± 2.7	414.7 ± 43.5 **	1206.3 ± 99.2	-	-
H232A/ H306A	35.0	100.9 ± 9.9	564.8 ±78.4 **	739.6 ± 29.3	-	-
H252A/ H306A	49.3	115.7 ± 2.7	617.5 ± 46.6 **	825.6 ± 117.9	-	-

Table 1, showing EC_{50} values, rise time and desensitization current kinetic values for the histidine single and double mutant *Hd*P2X receptors. ** = $p < 0.01$.

ATP-evoked currents at the double histidine mutants were τ_{desen} = 1206.3 ± 99.2 ms for H232A / H252A (T_{50} = 414.7 ± 43.5 ms, $p < 0.01$), τ_{desen} = 739.6 ± 29.3 ms for H232A / H306A (T_{50} = 564.8 ± 78.4 ms, $p < 0.01$), and τ_{desen} = 825.6 ± 117.9 ms for H252A / H306A (T_{50} = 617.5 ± 46.6 ms, $p < 0.01$) compared to wildtype *Hd*P2X T_{50} of 289.9 ± 16.1 ms.

Copper and zinc at concentrations of 100 µM inhibited ATP-evoked responses in all the single and double histidine mutants (Figure 3.5). The level of inhibition as a result of application of these divalent cations was only significantly reduced for H232A / H306A and H252A / H306A double mutants by 100 µM copper. *Hd*P2X H232A / H306A was inhibited by 60.0 ± 5.9 % ($p < 0.05$) and H252A / H306A inhibited by 50.8 ± 10.9 % ($p < 0.05$) of the control current amplitude by 100 µM copper, compared to wildtype *Hd*P2X inhibited by 81.1 ± 5.3 % (Figure 3.5A and C). Therefore His^{306} plays a minor but non-essential role in copper action at the *Hd*P2X, and possibly takes part in metal ion co-ordination with other residues yet to be discovered. In the H232A / H252A mutant the level of inhibition by copper was unchanged, and none of the histidine mutants were reduced in their level of inhibition of ATP-evoked currents by 100 µM zinc (Figure 3.5B and C).

3.3.4 Effect of mutating charged residues on copper and zinc action at HdP2X

As stated earlier, negatively charged and lysine residues have been previously revealed to play roles in divalent metal ion inhibition of P2X receptors and other ligand-gated ion channels (Nakazawa and Ohno, 1997, Paoletti *et al.*, 2000, Liu *et al.*, 2007). Similar

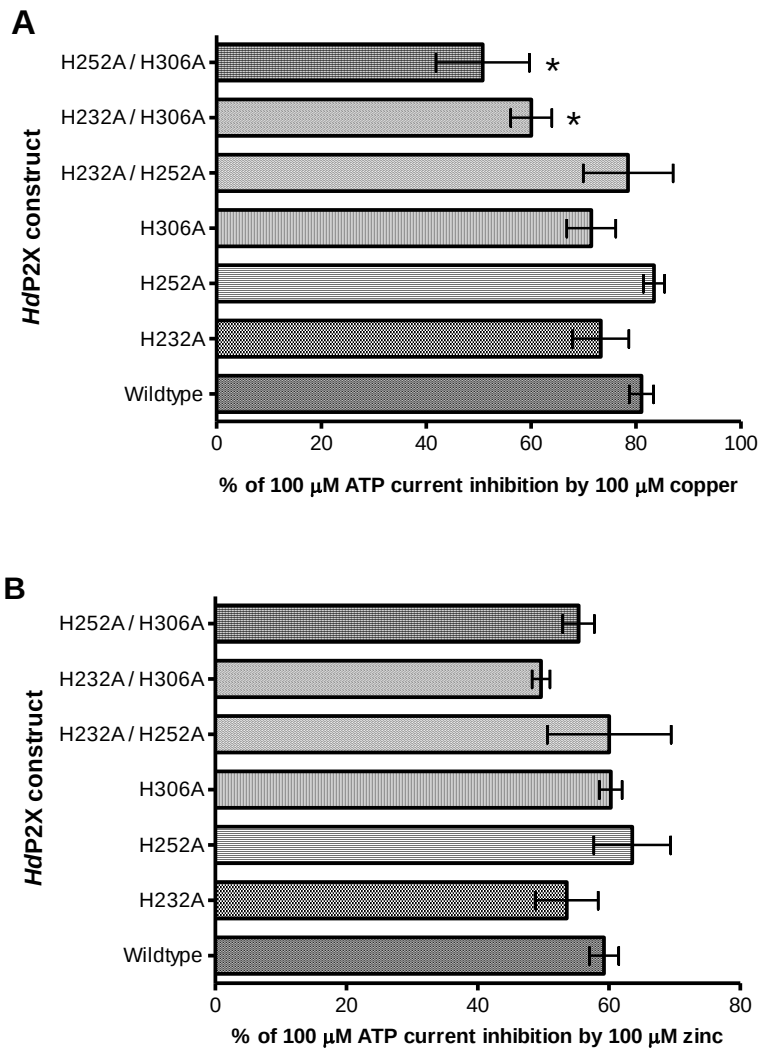

Figure 3.5. A and B, graphical summary to show levels of 100 μM Zn^{2+} (A) and Cu^{2+} (B) inhibition of 100 μM ATP-evoked *Hd*P2X currents (* = $p < 0.05$).

C

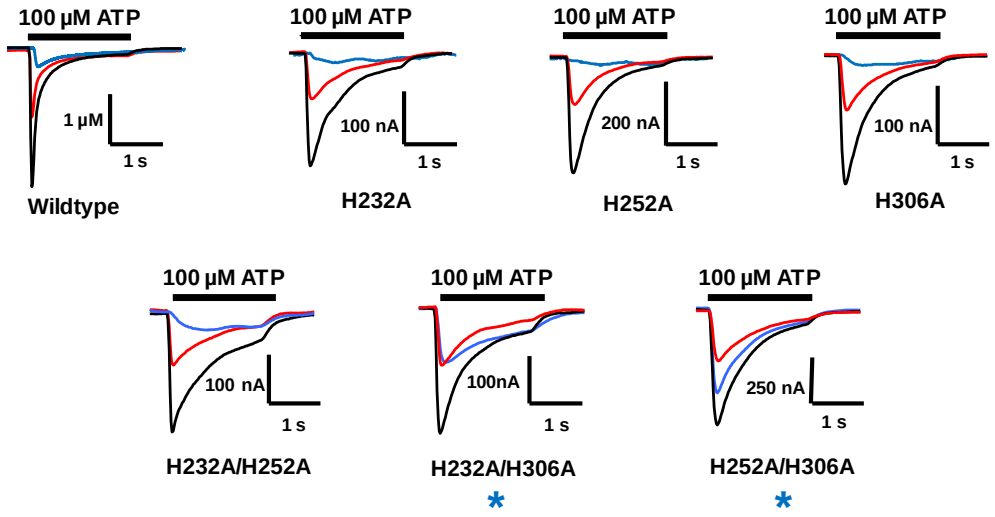

Figure 3.5C, representative current traces of 100 µM Zn^{2+} (red) and Cu^{2+} (blue) inhibition of 100 µM ATP-evoked *Hd*P2X currents in wildtype and His mutant *Hd*P2X receptors. Stars denote *Hd*P2X mutants with significantly reduced 100 µM Cu^{2+} inhibition (* = $p < 0.05$) (n = 5 - 6)

to the *Hd*P2X, *Sm*P2X receptor from *Schistosoma mansoni* is also inhibited by zinc (Raouf *et al.*, 2005).

Therefore an alignment of *Hd*P2X and *Sm*P2X receptor sequences was carried out and lysine and negatively charged residues conserved in the same positions in *Hd*P2X and *Sm*P2X sequences that are not fully conserved in other P2X receptors were investigated for their role in divalent metal ion inhibition of *Hd*P2X receptors. Altogether there were 5 charged residues in *Hd*P2X that were selected and were individually substituted to alanine residues to generate mutants: E110A, K130A, D183A, E249A and K297A.

The charged mutant receptors were all functional, observed by ATP-evoked currents (Figure 3.6). Currents of all charged mutants exhibited significantly slower desensitizing kinetics compared to wildtype *Hd*P2X. E110A had a rise time of 74.1 ± 5.4 ms, and the desensitizing current (T_{50} of 526.7 ± 22.8 ms, $p < 0.01$) was fit by two exponentials (τ_{desen1} = 171.7 ± 31.1 ms and τ_{desen2} = 874.3 ± 124.9 ms). K130A had a rise time of 57.7 ± 7.8 ms, and the desensitizing current (T_{50} of 409.4 ± 46.1ms, $p < 0.01$) was fit by two exponentials (τ_{desen1} = 102.1 ± 16.7 ms and τ_{desen2} = 763.4 ± 100.2 ms). D183A had a rise time of 92.9 ± 3.9 ms, and a desensitizing current best fit by a single exponential with a τ_{desen} of 959.8 ± 78.6 ms (T_{50} = 582.7 ± 36.3 ms, $p < 0.01$). The currents at E249A had a rise time of 52.3 ± 1.5ms, with the desensitizing current (T_{50} of 478.9 ± 76.2 ms, $p < 0.01$) was best fit by two exponentials (τ_{desen1} = 173.5 ± 33.6 ms and τ_{desen2} = 756.6 ± 78.1 ms). A rise time of 128.4 ± 5.3 ms, and a slower desensitizing current that was fitted by a single exponential with a τ_{desen} of 897.8 ± 94.0 ms (T_{50} = 620.2 ± 25.4 ms, $p < 0.01$), was obtained for K297A *Hd*P2X.

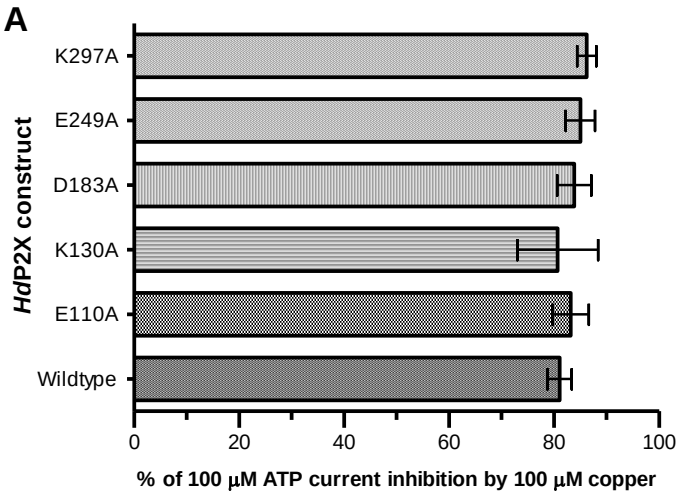

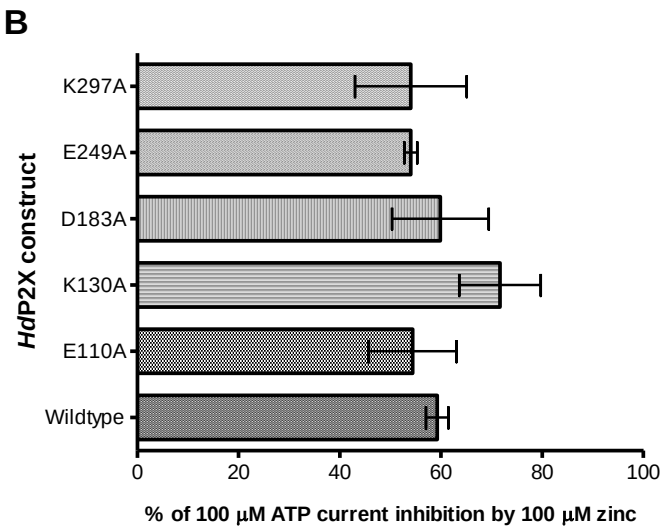

Figure 3.6. A and B, bar charts to show the level of 100 μM zinc (A) and copper (B) inhibition of 100 μM ATP-evoked *Hd*P2X currents.

C

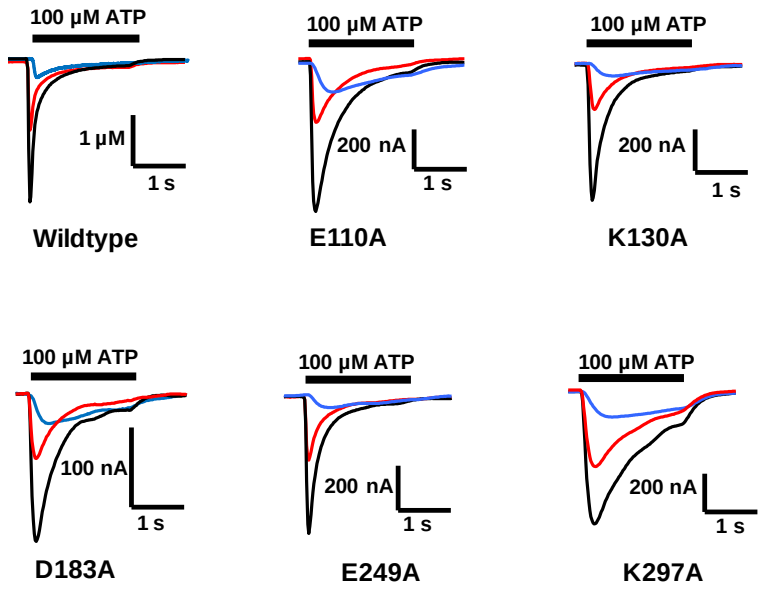

Figure 3.6C, current traces of 100 µM zinc (red) and copper (blue) inhibition of 100 µM ATP-evoked *Hd*P2X currents in wildtype and charged mutant *Hd*P2X receptors (n = 5 - 7).

	Rise Time (ms) (10 - 90%)	Desensitization (ms) (T_{50})	τ_{desen} (single time constant) (ms)	τ_{desen1} (double time constant) (ms)	τ_{desen2} (double time constant) (ms)
Wildtype	71.4 ±2.5	289.9 ± 16.1	-	121.8 ± 26.2	627.4 ± 147.8
E110A	74.1 ± 5.4	526.7 ± 22.8**	-	171.7 ± 31.1	874.3 ± 124.9
K130A	57.7 ± 7.8	409.4 ± 46.1**	-	102.1 ± 16.7	763.4 ± 100.2
D183A	92.9 ± 3.9	582.7 ± 36.3**	959.8 ± 78.6	-	-
E249A	52.3 ± 1.5	478.9 ± 76.2**	-	173.5 ± 33.6	756.6 ± 78.1
K297A	128.4 ± 5.3	620.2 ± 25.4**	897.8 ± 94.0	-	-

Table 2, showing rise time and desensitization current kinetic values for the charged mutant *Hd*P2X receptors. ** = $p < 0.01$.

Copper and zinc inhibited ATP-evoked currents in all the charged *Hd*P2X mutants, and there were no significant differences in the level of inhibition by 100 µM copper or 100 µM zinc in any of the mutants compared to wildtype (Figure 3.6). Due to mutations of these charged residues not having a significant effect on copper and zinc inhibition, no ATP concentration-response curves were investigated.

3.3.5 Role of N- and C- termini in current kinetics

100 µM ATP-evoked currents at wildtype *Hd*P2X have very fast channel kinetics, a property unique among the P2X receptors identified, cloned and characterized from non-vertebrate species to date. *Hd*P2X currents had a rise time of 71.4 ± 2.5 ms (n = 39) and the desensitizing current (T_{50} of 289.9 ± 16.1 ms) was fit by a two exponential curve with τ_{desen1} of 121.8 ± 26.2 ms and τ_{desen2} of 627.4 ± 147.8 ms. This current fully desensitizes within 6 seconds of ATP application.

In contrast, 100 µM ATP-evoked currents at wildtype *Bm*P2X, a receptor previously identified and cloned in the laboratory have very slow kinetics (Figure 3.7), a rise time that reaches peak at 5.0 ± 1.2 s and τ_{onset} of 3.5 ± 0.5 s. The current has a very slow rate of desensitization with a T_{10} of 9.1 ± 1.2 s. The majority of the current remains after 30 seconds of ATP application.

In order to investigate the role of the intracellular domains in determining the markedly contrasting desensitization kinetics of these two invertebrate P2X channels, the N- and C- termini were exchanged between the two receptors. Six chimeras were made by my supervisor by exchanging intracellular N- and C- termini between the *Hd*P2X and

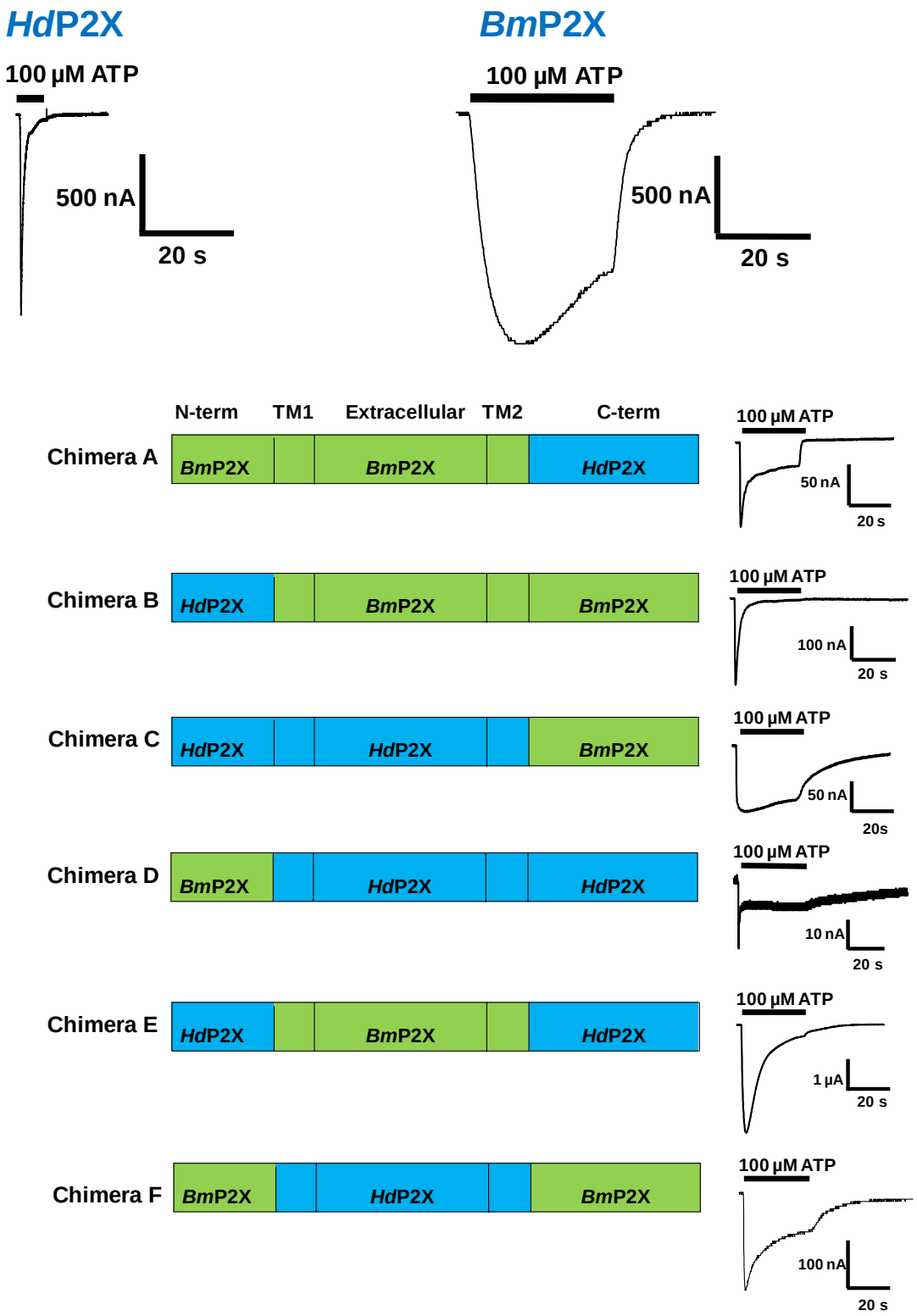

Figure 3.7. Top: Current traces of wildtype *Hd*P2X and *Bm*P2X. Below: a schematic of the sequence content of each of the *Bm*P2X-*Hd*P2X chimeras with representative current traces for each of the chimeras at the right.

*Bm*P2X channels (Figure 3.7). From TMpred (Hofmann, 1993) predictions, wild type *Hd*P2X has N- and C-termini of 46 and 114 amino acids residues respectively whilst wildtype *Bm*P2X has N- and C-termini lengths of 31 and 40 amino acids.

The sequences of the extracellular and transmembrane domains were unaltered in these chimeric channels. After injection of cRNA for these chimeras into *Xenopus* oocytes, application of 100 µM ATP-evoked inward currents in each receptor showing that all *Hd*P2X-*Bm*P2X chimeras formed functional channels. The current kinetics in these chimeras were analysed as follows.

HdP2X-BmP2X chimeras with C-terminal exchanged:

Chimera A, consisting of the slow *Bm*P2X channel sequence with the C-terminus replaced with that of the fast *Hd*P2X channel sequence had a fast rise time of 443.4 ± 64.8 ms (n = 9). The current desensitized with a T_{10} of 847.8 ± 160.6 ms, and the desensitizing current was best fit by two exponentials. This chimera's first component of desensitization was quite fast with a τ_{desen1} of 2.4 ± 0.6 s, and second component desensitized slowly and not completely during the ATP application (τ_{desen2} > 30 s). Upon removal of agonist after the 30 seconds of ATP application the currents returned rapidly to baseline values.

Chimera C, which consisted of fast *Hd*P2X channel sequence with the C-terminus replaced with that of the slow *Bm*P2X channel had a very slow rise time of 4.8 ± 3.1 s (n = 9). The current did not desensitize during application of ATP with a T_{10} of 10.4 ± 3.1 s and in the majority of recordings the current did not reduce to less than 50 % of

the peak current amplitude by the end of the 30 second ATP application. Currents returned to baseline values very slowly after removal of agonist. These current kinetics were similar to *Bm*P2X wildtype receptor.

HdP2X-BmP2X chimeras with N-terminal exchanged:

Chimera B had a fast rise time of 332.0 ± 44.1 ms (n = 9). The current fully desensitized during the application of ATP with a T_{10} of 296.9 ± 32.5 ms. The desensitizing current had a τ_{desen1} of 0.9 ± 0.1 s and a τ_{desen2} of 4.7 ± 0.7 s. This chimera has fast *Hd*P2X sequence forming the N-terminus with slow *Bm*P2X forming the rest of the receptor sequence, however had a current phenotype that resembled the wildtype *Hd*P2X current.

100 µM ATP application to Chimera D gave rise to currents with a very rapid rise time of 142.3 ± 11.6 ms (n = 8). The current exhibited an initial rapid desensitization (T_{10} = 95.7 ± 5.9 ms), with a τ_{desen1} of 204.1 ± 15.9 ms. However the second phase of desensitization did not desensitize in the duration of ATP application (τ_{desen2} > 30 sec), and following 30 seconds of ATP application the current deactivated very slowly to baseline. Chimera D had very low amplitude currents that were often less than 50 nA upon 100 µM ATP applications, suggesting reduced functionality or membrane expression following the swapping of *Bm*P2X for *Hd*P2X sequence at the N-terminal.

HdP2X-BmP2X chimeras with N- and C- termini exchanged:

Chimera E, containing fast *Hd*P2X sequence at the intracellular domains had a rather slow rise time of 1.7 ± 0.1 s (n = 7). The current desensitized slowly but almost fully

within the 30 second ATP application, best fit with a single exponential, a τ_{desen} of 9.3 ± 0.9 s with a T_{10} of 2.4 ± 0.06 s. After the ATP application had stopped, the small remainder current soon deactivated to baseline.

Chimera F, consisting of slow *Bm*P2X sequence at the N- and C- termini exhibited a fast rise time of 615.3 ± 81.3 ms (n = 11). The current desensitized slowly (T_{10} of 2.8 ± 0.7 s), with a τ_{desen1} of 2.5 ± 0.3 s, and the second component of desensitization did not fully desensitize during the application of ATP (τ_{desen2} > 30 s). Current still remained after ATP application stopped, which deactivated slowly afterwards.

	Rise Time (s) (10 – 90 %)	Desensitization (s) (T_{10})	τ_{desen} (single time constant) (s)	τ_{desen1} (double time constant) (s)	τ_{desen2} (double time constant) (s)
Wildtype *Hd*P2X	0.07 ± 0.003	0.07 ± 0.03	-	0.1 ± 0.03	0.6 ± 0.1
Wildtype *Bm*P2X	5.0 ± 1.2	9.1 ± 1.2	-	-	-
Chimera A	0.4 ± 0.06	0.8 ± 0.2	-	2.4 ± 0.6	> 30
Chimera B	0.3 ± 0.04	0.3 ± 0.03	-	0.9 ± 0.1	4.7 ± 0.7
Chimera C	4.8 ± 3.1	10.4 ± 3.1	-	-	-
Chimera D	0.1 ± 0.01	0.1 ± 0.006	-	0.2 ± 0.02	> 30
Chimera E	1.7 ± 0.1	2.4 ± 0.2	9.3 ± 0.9	-	-
Chimera F	0.6 ± 0.08	2.8 ± 0.7	-	2.5 ± 0.3	> 30

Table 3, showing rise time and desensitization current kinetic values for wildtype *Hd*P2X, wildtype *Bm*P2X and *Hd*P2X-*Bm*P2X chimeras.

3.3.6 Run-down of current amplitudes of HdP2X-BmP2X chimeras

Repeated 100 µM ATP applications to *Bm*P2X leads to run down of current amplitudes after subsequent ATP applications (Figure 3.8). The 2nd ATP application gave 63.7 ± 10.1 % of the current amplitude of the 1st ATP application, and this was significantly greater than the responses of 5th ATP application that gave 16.3 ± 1.3 % of the 1st response ($p < 0.01$). Following repeated applications of 100 µM ATP to *Bm*P2X, there is also a noticeable displacement in the time of peak current, shifting to later times after more ATP applications. Repeated 100 µM ATP applications to *Hd*P2X did not lead to run down of current amplitudes. The chimeras were investigated for the rundown of current amplitudes to observe any relationship between current kinetics and rundown of current amplitudes.

Five consecutive 100 µM ATP applications at 5 min intervals were carried out at each of the six chimeras (Figure 3.9). Following the first ATP application, subsequent ATP applications did not show significant run down in each of the chimeras (Figure 3.9 and 3.10). The 2nd ATP application did not have a significantly different current amplitude to the 5th ATP application in any of the six chimeras ($p > 0.05$ for all chimeras). This suggests that the N- and C- termini are possibly able to influence the rate of internalisation and trafficking of these P2X receptors, and that the presence of *Hd*P2X sequence at the N- or C- termini of *Bm*P2X sequence background is able to prevent the strong run down of current amplitude of the *Bm*P2X receptor. However, *Bm*P2X sequence at the N- or C- termini of *Hd*P2X did not result in strong run down in current amplitude suggesting that the intracellular domains are not the sole determinants of current rundown and that residues within the extracellular and transmembrane domain also play a role.

*Bm*P2X

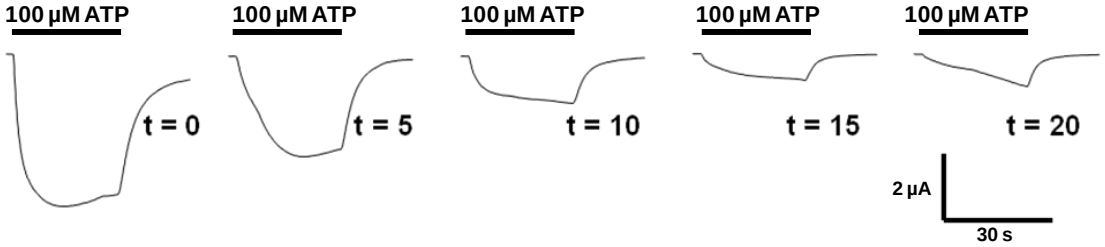

*Hd*P2X

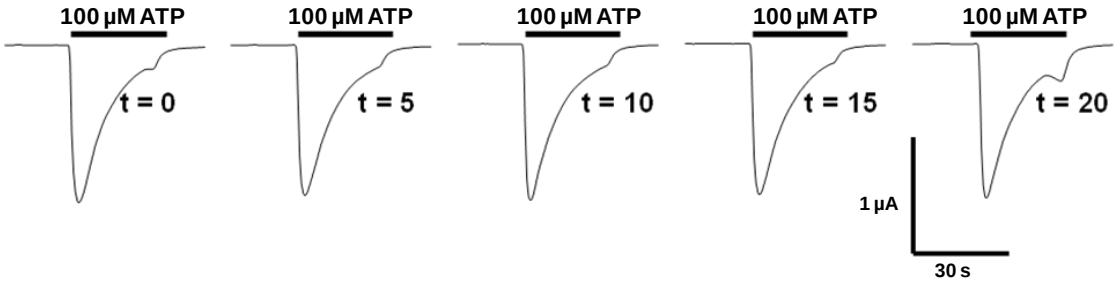

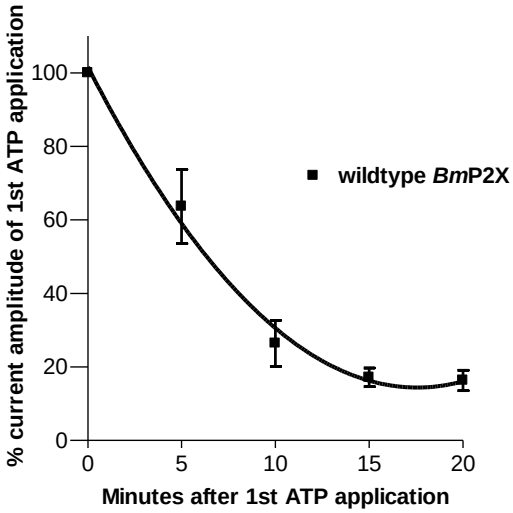

Figure 3.8. *Bm*P2X run down of current amplitude after 100 µM ATP applications at 5 min intervals. This differs from the effect of 100 µM ATP applications at *Hd*P2X. Graphical representation below of relative current amplitudes at each ATP application for *Bm*P2X (n = 6).

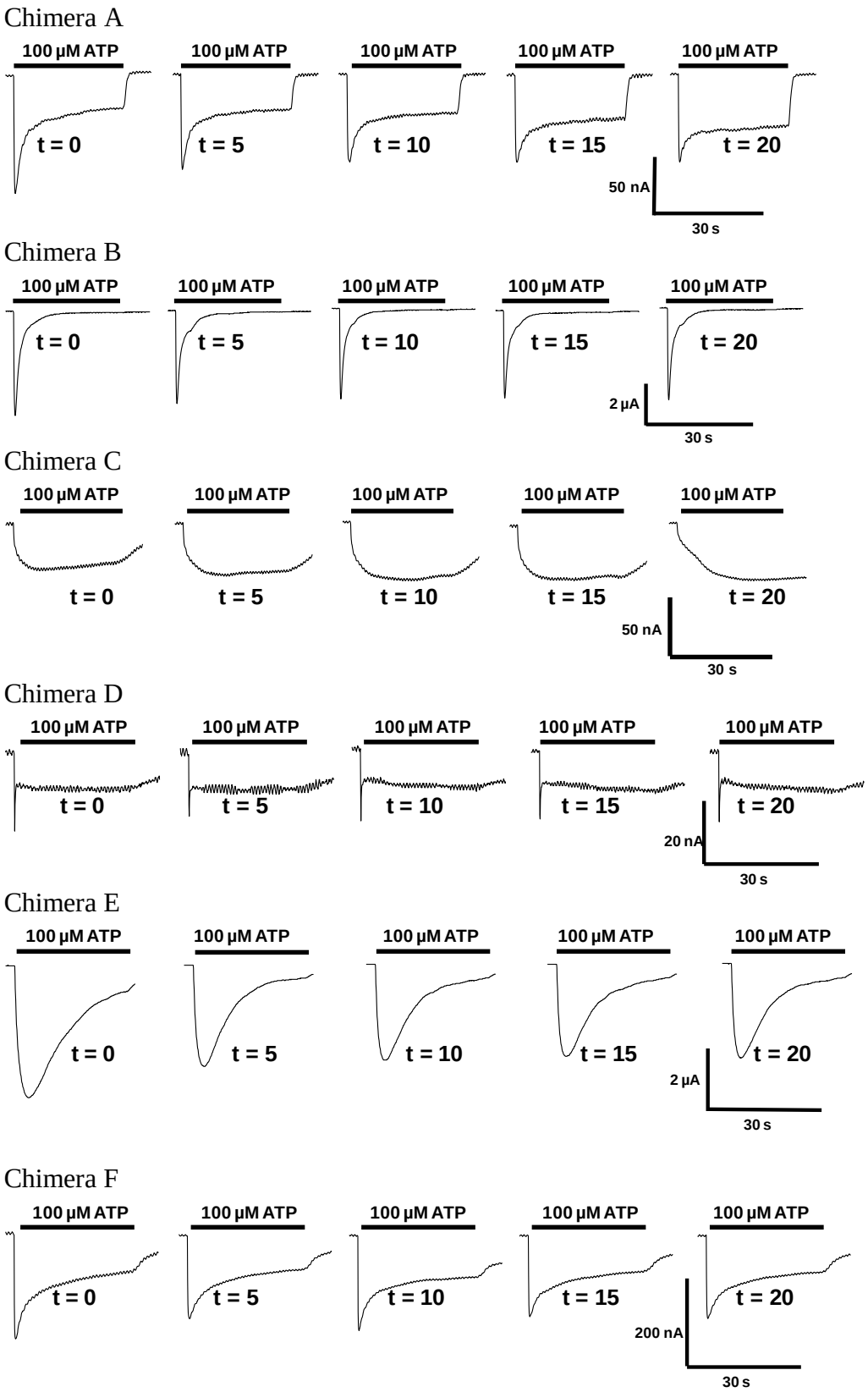

Figure 3.9. Effect of 100 µM ATP applications at 5 min intervals in each of the chimeras, with current traces.

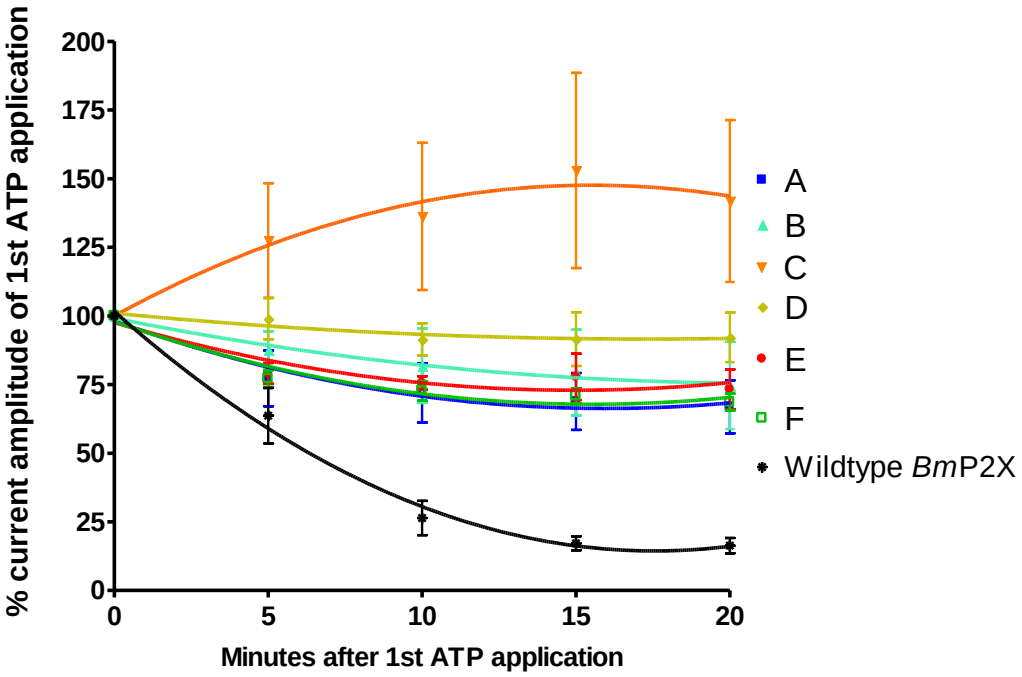

Figure 3.10. Graphical representation of relative current amplitudes at each ATP application for each *Bm*P2X-*Hd*P2X chimera and wildtype *Bm*P2X (n = 5 - 7).

3.4 DISCUSSION

3.4.1 Divalent cations inhibit HdP2X and have a bi-phasic effect at LymP2X

When zinc or copper ions at concentrations up to 100 µM were applied to *Lym*P2X, there was potentiation of 10 µM ATP-evoked responses. However, at higher [Zn^{2+}] or [Cu^{2+}] an inhibition of currents was observed. For the *Hd*P2X receptor, zinc or copper ions inhibited currents in a concentration dependent manner. Similarly at the *Schistosoma mansoni Sm*P2X, zinc acts as an antagonist of the receptor (Raouf *et al.*, 2005), and the *Dictyostelium discoideum* dP2XA receptor is sensitive to block by nanomolar concentrations of Cu^{2+} (Fountain *et al.*, 2007), however dP2XB and E are insensitive to copper (Ludlow *et al.*, 2009).

Similar to the action of divalent cations at *Lym*P2X, altering [Zn^{2+}] has the same biphasic effect on human $P2X_2$, $P2X_3$ and $P2X_4$ currents, whereas $P2X_1$ and $P2X_7$ are inhibited by zinc (Nakazawa and Ohno, 1996, Nakazawa *et al.*, 1997, Nakazawa and Ohno, 1997, Virginio *et al.*, 1997, Wildman *et al.*, 1998, Wildman *et al.*, 1999a, Wildman *et al.*, 1999b). Copper ions have potentiating effects on $P2X_2$ but inhibitory effects at $P2X_4$ and $P2X_7$ receptors (Virginio *et al.*, 1997, Xiong *et al.*, 1999).

The effects of divalent cations at P2X receptors are of physiological significance since storage of zinc occurs in presynaptic vesicles which are released into the synaptic cleft subsequent to nerve stimulation (Assaf and Chung, 1984, Smart *et al.*, 1994, Frederickson and Bush, 2001). There is also co-localization of zinc and P2X receptors in the hippocampus and cerebral cortex (Clyne *et al.*, 2002a), implying possible *in vivo* roles. Following synaptic stimulation, copper is released from cortical and hypothalamic neurons and has been found to markedly potentiate ATP responses in rat

nodose ganglia dissociated neurons (Li *et al.*, 1996).

Biphasic effects of zinc have also been described *in vivo* in P2X expressing hypothalamic tuberomamillary neurons of the rat (Vorobjev *et al.*, 2003), and both zinc and copper also had similar biphasic effects on the dorsal motor nucleus of the rat vagus nerve (Ueno *et al.*, 2001). In rat sympathetic neurons, zinc causes potentiation of ATP-evoked currents (Cloues *et al.*, 1993), but gives rise to inhibition of currents in bullfrog dorsal root ganglion neurons (Li *et al.*, 1997).

This biphasic action by zinc and copper implies that the *Lym*P2X receptor has two distinct sites of modulation by divalent cations. A high affinity site leading to potentiation, and following the saturation of these high affinity sites zinc or copper bind to a lower affinity site, leading to inhibition (Ueno *et al.*, 2001). Potentiation of the ATP-induced currents at $P2X_2$ by these divalent cations occurs by acting as an allosteric modulator to increase the affinity of the receptor for ATP (Coddou *et al.*, 2003b) in addition to the slowing of the dissociation of ATP from the receptor (Coddou *et al.*, 2003b, Vorobjev *et al.*, 2003). Cu^{2+} caused a leftward shift in the concentration-response curve at $P2X_2$ in a parallel manner, while decreasing EC_{50} (Xiong *et al.*, 1999).

3.4.2 Divalent metal ion binding site in HdP2X

Mutation of all histidine residues in the extracellular domain of *Hd*P2X demonstrated that histidine residues do not play an essential role in zinc or copper inhibition of *Hd*P2X. This is surprising considering the fact that histidine residues have been

previously shown to play important roles in zinc and copper modulation of mammalian P2X and other ion channels. His^{306} however appears to play a minor role in copper but not zinc modulation, further suggesting that copper and zinc may have different binding sites in P2X receptors, as previously it was shown that zinc can potentiate while copper only inhibits $P2X_4$ currents (Xiong *et al.*, 1999). His^{140} was found to be responsible for this copper inhibition at $P2X_4$ receptors (Coddou *et al.*, 2003a).

The zinc binding site at rat $P2X_2$ receptors is formed by residues His^{120} and His^{213} (Clyne *et al.*, 2002a), which was subsequently proposed to be at the interface of two adjacent subunits (Nagaya *et al.*, 2005). This zinc binding site is also suggested to have a flexible but not parallel or anti-parallel arrangement of residues around the zinc-binding histidine residues His^{120} and His^{213}, elucidated after a histidine scan of residues around positions 120 and 213 (Tittle *et al.*, 2007). The zebrafish $zP2X_4$ crystal structure indicates that Pro^{125} and His^{219} of $zP2X_4$, which are at equivalent positions to rat $P2X_2$ His^{120} and His^{213} are positioned in the head and dorsal fin regions of the extracellular body and also close to the ATP binding site (Kawate *et al.*, 2009, Young, 2009).

Other ligand-gated channels such as GABA ρ1 are also inhibited by zinc in a pH-dependant and voltage-independent manner, and mutation of a single histidine residue (His^{156}) in the putative extracellular domain to tyrosine renders the receptor insensitive to zinc inhibition (Wang *et al.*, 1995).

Charged residues have also been previously found to play roles in zinc and copper action at P2X receptors and other ligand activated ion channels. At $P2X_4$, Asp^{221} was found to play roles in zinc potentiation at $P2X_4$, as substitution of this residue to

histidine and prevented this potentiation (Nakazawa and Ohno, 1997). The equivalent position of this $P2X_4$ Asp^{221} residue in the *Hd*$P2X_4$ sequence was His^{232}, which was found to not have a role in divalent metal action at the receptor.

In rat $P2X_7$, Asp^{197} in addition to His^{62} play roles in copper and zinc inhibition as their individual substitution to alanine reduces inhibition by divalent metal cations and mutation of both residues prevents inhibition (Liu *et al.*, 2007). *Lym*P2X Lys^{208}, at the equivalent position of Asp^{197} in rat $P2X_7$ may possibly be part of the low-affinity zinc or copper binding site leading to inhibition of ATP currents.

Positively charged Lys^{233}, negatively charged Glu^{266}, two histidine residues (His^{44} and His^{128}) and Asp^{102} have been shown to play roles in reducing zinc affinity to the ligand-gated NMDA receptor (Paoletti *et al.*, 2000). Mutation of these residues does not affect agonist binding or Ni^{2+} action at the receptor (Paoletti *et al.*, 2000). Residues His^{44}, His^{128}, Lys^{233} and Glu^{266} are proposed to contribute to a specific zinc binding site on the extracellular LIVBP-like domain of the N2A NMDA receptor (Paoletti *et al.*, 2000). This LIVBP-like domain has been modelled to consist of two lobes separated by a hinge and subsequent to zinc binding the two lobes close tightly around the metal ion (Paoletti *et al.*, 2000).

In the light of these previous findings, the role of lysine and negatively charged residues in inhibition of *Hd*P2X currents by zinc and copper was further investigated. Certain charged residues in *Hd*P2X were selected as candidates for mutagenesis to see their effect on divalent metal ion modulation. These charged residues were conserved at the same positions in another invertebrate P2X receptor from *Schistosoma mansoni* that

is also inhibited by zinc (Raouf *et al.*, 2005), and not fully conserved in other P2X receptors. However all of these mutations failed to prevent or even decrease the extent of divalent metal ion inhibition of ATP-evoked currents at *Hd*P2X. Therefore additional analysis is required to select other charged residues as suitable candidates for playing roles in divalent metal ion inhibition at *Hd*P2X. Possibly charged residues near to the equivalent position of human $P2X_7$ Asp^{197}, such as Glu^{211} or Asp^{213} in *Hd*P2X may have potential roles in zinc or copper inhibition. At *Lym*P2X, Asp^{125} and Asp^{225} may form an intersubunit site for zinc to cause potentiation of ATP-evoked currents similarly observed at near equivalent positions with His^{120} and His^{213} in rat $P2X_2$ (Clyne *et al.*, 2002a, Nagaya *et al.*, 2005). These negatively charged aspartate residues may possibly have electrostatic interactions with Zn^{2+}, forming a zinc binding site by the head and dorsal fin regions of the extracellular body as indicated for the zinc binding site in rat $P2X_2$.

This work shows that while residues of binding sites for divalent metal ions are common across ligand-gated ion channels of different families, these residues and mechanism of inhibition can also differ among the various subtypes within the same receptor family. With regards to P2X, it is hard to predict what may be the earliest evolutionary mechanism of divalent metal ion modulation for ion channels and the particular residues involved. Among the invertebrate P2X receptors, zinc and copper have biphasic effects at *Lym*P2X currents, while at *Hd*P2X, *Sm*P2X (Raouf *et al.*, 2005) and *d*P2X (Fountain *et al.*, 2007) zinc or copper have been only found to inhibit the receptor.

Further investigation can find out whether the decrease in *Hd*P2X currents by divalent cations are due to changes in agonist binding, decrease in the channel open frequency, changes in unitary conductance, or in mean burst duration. The lack of function of the triple H232A / H252A / H306A mutant is also surprising as the $P2X_4$ receptor also has three extracellular histidines, and mutation of all these histidines still gives rise to functional receptors with currents evoked upon ATP application (Coddou *et al.*, 2003a).

The sequence of *Hd*P2X can be further used for structure-function studies to look for residues playing a role in other pharmacological or physiological properties, similarly used for the green algae *Ostreococcus tauri* P2X. *Ot*P2X has low calcium permeability and alignment of the second transmembrane domain of *Ot*P2X with other P2X receptors shows conservation of an aspartate residue in the other P2X receptor sequences, whereas *Ot*P2X has an asparagine in this position (Fountain *et al.*, 2008). Substitution of this Asn^{353} residue to aspartate had significantly increased calcium permeability and the reversal potential for *Ot*P2X (Fountain *et al.*, 2008), demonstrating the potential of using the sequence and properties of invertebrate receptors for mapping functionally important residues.

3.4.3 Current kinetics of HdP2X-BmP2X chimeras

Chimeras produced by swapping N- and C- termini domains between *Hd*P2X and *Bm*P2X receptor sequences were used to further investigate roles of the intracellular domains in current kinetics and run-down. These domains of the receptor have been previously shown to affect current desensitization in P2X and other receptors.

Desensitization rates of P2X receptors are of physiological importance as it can function to limit neurotoxicity (Werner *et al.*, 1996).

Mutation of the threonine residue of the highly conserved protein kinase C site T*X*(K/R)N-found in the N- terminal domain of all known P2X receptors was shown to significantly speed up the desensitization kinetics of rat $P2X_2$ expressed in both *Xenopus* oocytes and HEK293A cells (Boue-Grabot, Archambault et.., 2000). N- and C-termini were suggested to interact with each other through studies on C-terminal truncations of rat $P2X_2$ (Boue-Grabot *et al.*, 2000). Substitution of the human $P2X_4$ C-terminal residues Lys^{373} to alanine or arginine, or Tyr^{374} to alanine also results in faster desensitization kinetics (Fountain and North, 2006).

By using chimeras of $P2X_1$ and $P2X_2$, it was determined that regions containing amino acids residues 14 – 47 corresponding to TM1 with part of the N-terminal, and amino acids 332 - 365 corresponding to TM2 with part of the C-terminal of $P2X_2$ were responsible for fast rate of desensitization at $P2X_1$ through possible interactions between these hydrophobic regions (Werner *et al.*, 1996). The role of the extracellular ligand binding loop in desensitization needs to be investigated further, however in this chapter the mutation of extracellular histidines, Glu^{110}, Lys^{130}, Asp^{183}, Glu^{249} or Lys^{297} had significantly slowed the desensitization rate of *Hd*P2X. In human $P2X_2$, alternate splicing was found to affect the rate of desensitization (Brandle *et al.*, 1997).

The N-termini showed an ability to determine the rise time and desensitization rate in chimera B, and the desensitization rate in chimera D. Chimera B, which has an N-terminal fast kinetics *Hd*P2X sequence with the rest of the sequence being slow kinetics

*Bm*P2X sequence exhibited fast rise time and desensitization rate that was more similar to wildtype *Hd*P2X than wildtype *Bm*P2X. Chimera D, which has an N-terminal slow kinetics *Bm*P2X sequence with fast *Hd*P2X forming the remainder of the sequence had a second component of desensitization that was very slow, with a current that continued to slowly decay after 30 seconds of ATP application.

The C-termini also displayed the potential to influence current kinetics in chimeras A and C. Chimera A, which has a C-terminal fast kinetics *Hd*P2X sequence in a slow kinetics *Bm*P2X sequence background had fast rise time, initial desensitization rate and the current amplitude returned to baseline soon following agonist withdrawal. Many of the current characteristics of chimera A are more similar to wildtype *Hd*P2X than wildtype *Bm*P2X. Similarly chimera C had very slow rise time, desensitization rate and slow decay after ATP application had stopped. The current phenotype for chimera C was much more similar to wildtype *Bm*P2X than wildtype *Hd*P2X, despite chimera C being same in sequence to wildtype *Hd*P2X except for the presence of slow kinetics *Bm*P2X sequence at the C-terminus.

Chimera E had an interesting current phenotype, as the current kinetics was slower than chimera B, despite chimera E being same in sequence as chimera B except for the presence of fast kinetics *Hd*P2X sequence in the N-terminus. This is possibly due to increased interactions between the *Hd*P2X sequences in the N- and C- terminus, which in future studies could possibly be measured by fluorescence resonance energy transfer (FRET) (Stryer, 1978). The increased interactions between the N- and C- termini possibly cause the TM domains to play a more dominant role in determine desensitization kinetics. This may subsequently lead to the TM domains in chimera E

which are of slow *Bm*P2X sequence to greater determine the slower current kinetics of this chimera compared to chimera B, possibly by being brought closer together. The intracellular domains would still play a role in current kinetics in chimera E, since chimera E has faster current kinetics than wildtype *Bm*P2X. A similar pattern is seen in chimera F, which has faster current kinetics than chimera C, despite having the same sequence except for chimera F having slow *Bm*P2X sequence in the N-terminus.

Chimeras that have one intracellular domain from *Hd*P2X and another from *Bm*P2X sequence may not interact with each other as strongly and therefore the TM domains of that chimera have less influence over determining desensitization rate, possibly as a consequence of particular conformational changes of the TM domains (Figure 3.11). FRET has shown that P2X receptors with longer C-terminals have less inter-fluorophore distance with other intracellular domains (Young *et al.*, 2008). Therefore *Hd*P2X, which has longer intracellular domains than *Bm*P2X, can be predicted to have large interactions between intracellular domains.

N- and C- termini sequence and changes in conformation can give us an understanding of ATP-evoked physiological responses that are less easy to unravel, for example why ATP application causes internalisation of some P2X receptor subtypes but not others (Bobanovic *et al.*, 2002). Further studies could also indicate how invertebrate P2X receptors interact with intracellular proteins and signalling pathways, for example interactions of $P2X_7$ with heat shock proteins, α-actinin, β-actin and supervilin were detected with MALDI-TOF mass spectrometry and Western blotting (Kim *et al.*, 2001). Interactions of $P2X_7$ receptor with intracellular proteins was discovered to be dependent on phosphorylation of the Tyr^{343} residue, as mutation of this residue prevented coupling

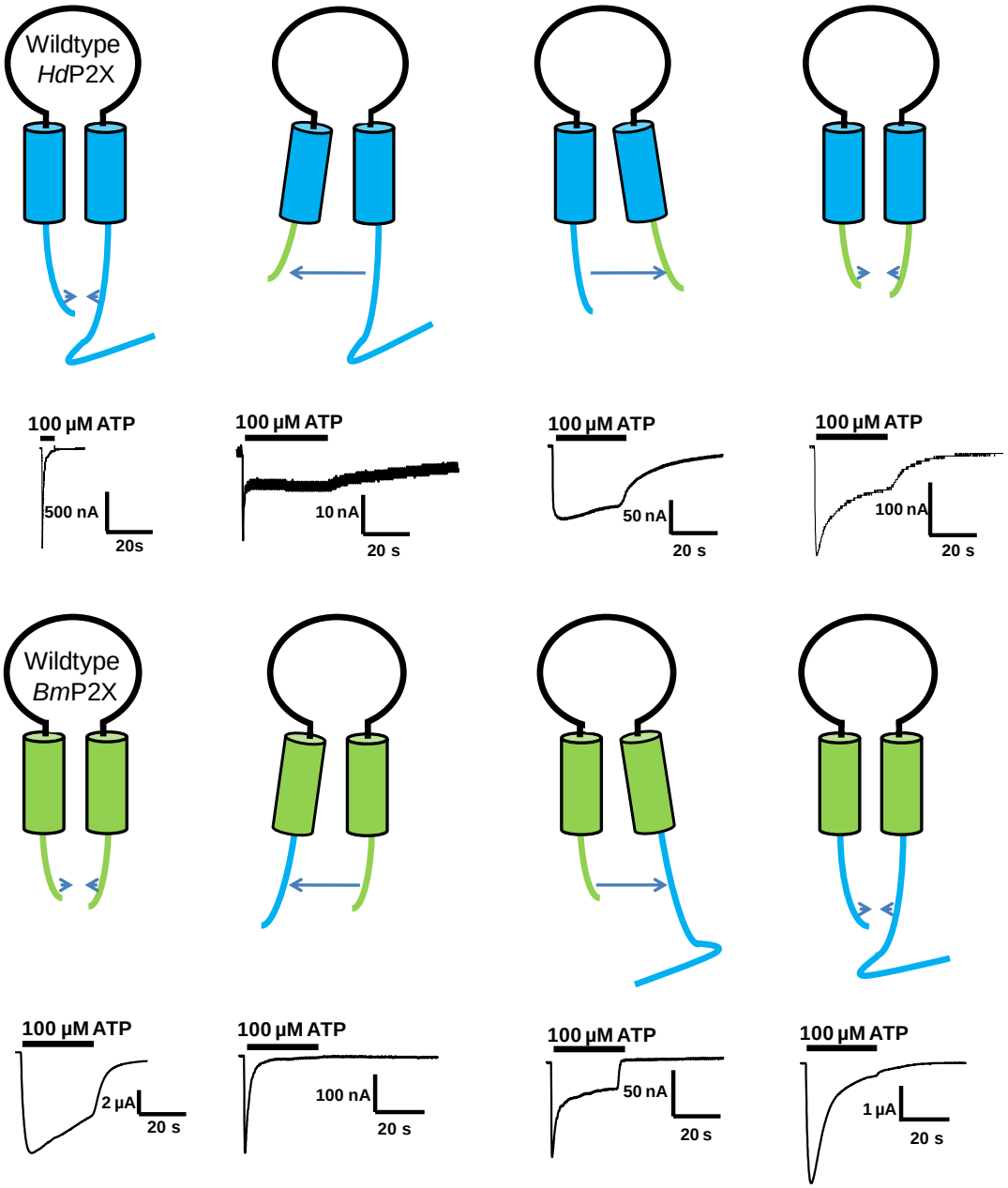

Figure 3.11. *Bm*P2X-*Hd*P2X chimeras that have intracellular termini sequence from the same wildtype receptor converge at the tips of their intracellular domains, possibly interacting to allow the TM domains to more determine the current kinetics of the receptor. Chimeras that have N- and C- termini from different wildtype receptors may repel each other, and conformational changes that are transduced to the TM domains possibly prevent the TM domains from playing a dominant role in desensitization characteristics. To represent the differences in lengths of the intracellular termini between *Bm*P2X and *Hd*P2X, *Bm*P2X intracellular termini are indicated by shorter green lines, *Hd*P2X intracellular termini are indicated by longer blue lines.

to cytoskeletal elements and blebbing formation (Kim *et al.*, 2001). Mutation of Tyr^{343} to phenylalanine also prevents run-down of current amplitude after repeated stimulation with BzATP (Kim *et al.*, 2001). The mechanism underlying permeability increases in $P2X_2$ were indicated by studies monitoring the movements of N- and C-termini by patch clamp-co-ordinated FlAsH (fluorescein arsenical hairpin) spectroscopy, and this experiment ruled out roles of Pannexin-1 channels for the I_2 conduction state (Chaumont and Khakh, 2008).

A cytoplasmic loop region known as the HA stretch situated between M3 and M4 transmembrane domains of 5-HT_3 receptors has been found to influence single channel conductance (Kelley *et al.*, 2003). Arginine residues of the HA stretch were discovered to be responsible for channel conductance, as their mutation increases channel conductance as measured by fluctuation analysis with voltage-clamp (Kelley *et al.*, 2003). Charged residues of cytosolic domains of *Bm*P2X or *Hd*P2X may possibly interfere with ionic movements and concentration of ions within the channel vestibule, and certain charged residues can form an unfavourable charge distribution to restrict ion flow (Kelley *et al.*, 2003).

3.4.4 Run Down of current amplitude of the HdP2X-BmP2X chimeras

Strong run down of wildtype *Bm*P2X receptor currents after consecutive 100 µM ATP applications at 5 min intervals suggests *Bm*P2X has either a faster rate of internalisation or slower rate of receptor recycling to the membrane surface compared to *Hd*P2X.

Internalisation of P2X receptors was first shown in $P2X_1$-GFP infected ganglion cells,

and a decrease in flourescence was measured by confocal microscopy following agonist exposure (Li *et al.*, 2000). $P2X_1$ was then shown by using surface biotinylation and Western blotting methods to be internalised in the rat *vas deferens* during continued agonist application (Ennion and Evans, 2001). However 10 min following agonist stimulation, 80 % of the receptors had re-appeared on the cell surface, but only 40 % of the contractile response was recovered suggesting transitions to and from the inactive state is another factor and possibly the rate determining step affecting desensitization and run down of P2X currents after agonist stimulation (Ennion and Evans, 2001).

$P2X_4$ receptors were found to undergo rapid constitutive internalization and subsequent reinsertion into the plasma membrane, whereas surface $P2X_2$ receptors are more stable at the membrane surface (Bobanovic *et al.*, 2002). Internalisation of the $P2X_4$ channel occurs by the process of endocytosis, and is dependant on a GTPase called dynamin (Bobanovic *et al.*, 2002).

C-termini domains have previously been shown to play roles in the internalisation of other receptor types. Mutations and truncations of the intracellular C-terminus of β_2-adrenergic receptor (Krasel *et al.*, 2008) and the $P2Y_1$ receptor (Reiner *et al.*, 2009) result in reduced receptor internalization. Trafficking of the receptor to the membrane, which is important for recovery from run down and rate of desensitization of the receptor have been previously shown to be linked in intracellular C-terminal truncated AMPA ion channels modulated by stargazin (Bedoukian *et al.*, 2006).

Substitution of either or both *Bm*P2X N- and C- termini with those from *Hd*P2X prevented the strong current run down observed with the wild type *Bm*P2X channel.

However, the converse experiments where *Bm*P2X N- or C- termini were placed in the *Hd*P2X receptor background interestingly did not induce strong current run down. This shows that current run down and receptor internalization is a multifactorial process involving the co-operation of a number of domains.

Chapter 3 conclusion

Histidine residues do not play essential roles in inhibition of *Hd*P2X currents, however His^{306} plays a minor role in copper but not zinc inhibition. This further suggests that zinc and copper have separate binding sites in P2X receptors. Extracellular histidines also play roles in receptor desensitization, as critical positioning of these residues were found to influence the length of time the channel is open for in the duration of ATP being bound to the receptor.

Intracellular N- and C- termini can determine current kinetics and also have interactions that may influence the ability of the transmembrane domains to affect gating transitions, thereby influencing the desensitization characteristics of ATP-evoked currents. FRET may prove to be a useful technique in future studies to analyze interactions between intracellular domains with respect to the mechanisms of P2X desensitization. Run down of current amplitude and receptor internalization is a multifactorial process that is determined by the co-operation of a number of domains, with the intracellular domains playing an important role. The only crystal structure determined to date for a P2X receptor (zebrafish $P2X_4$) is missing information of the N- and C- termini. The studies described in this chapter on *Hd*P2X-*Bm*P2X chimeric channels emphasize the importance of the intracellular domains in determining P2X receptor function.

Chapter 4: Localization of *Lym*P2X mRNA by RT-PCR and *in situ* hybridization

4.1 INTRODUCTION

P2X receptors are amongst the most widely distributed membrane proteins in vertebrates. A variety of methods have shown P2X receptors to be located in the brain (Bo *et al.*, 1995, Seguela *et al.*, 1996), spinal cord (Valera *et al.*, 1994), sensory neurons (Chen *et al.*, 1995), platelets (MacKenzie *et al.*, 1996), smooth muscle (Vial and Evans, 2000), and in many other cells and tissues. P2X receptors from *Dictyostelium* have also been shown to be present on intracellular membranes (Fountain *et al.*, 2007). Determining the location of P2X receptors provides some insight into their functions in a particular cellular or physiological pathway.

Following the cloning and pharmacological characterisation of a P2X receptor from the snail *Lymnaea stagnalis* (*Lym*P2X) described in previous chapters, this chapter's work focuses on the localization of *Lym*P2X in the *Lymnaea* central nervous system (CNS). The detection of *Lym*P2X expression in CNS ganglia and subsequently in specific neurons together with the *Lym*P2X pharmacological profile obtained in *Xenopus* oocytes will aid *in vivo* studies to elucidate the physiological roles of *Lym*P2X in the CNS. *Lymnaea* CNS has sensory, modulatory and motor neurons playing distinct roles in various functions, and localization of expression will give clues as to which neuronal networks *Lym*P2X has a function in.

There are several possible strategies to locate P2X receptor expression such as *in situ* hybridization, reverse transcription-PCR (RT-PCR) and immunocytochemistry. *In situ*

hybridization and RT-PCR detect mRNA expression, whereas immunocytochemistry detects protein expression and therefore the actual location where P2X carries out its function. *In situ* hybridization and RT-PCR are widely used techniques for the study of ion channel localization in situations where a specific antibody to the protein is not available. To map the distribution of *Lym*P2X in *Lymnaea* CNS, RT-PCR and *in situ* hybridization were carried out with the aim of localizing P2X mRNA expression within ganglia, and then to specific neurons of *Lymnaea* CNS. Immunoreactivity for P2X receptor protein has been previously shown to correspond well to mRNA localization (Brake *et al.*, 1994, Collo *et al.*, 1996, Seguela *et al.*, 1996, North and Barnard, 1997), demonstrating the reliability of elucidating P2X expression by detection of mRNA.

RT–PCR has been used previously in *Lymnaea Stagnalis* to identify pseudo nitric oxide synthase (NOS) and functional neuronal NOS transcripts (Korneev *et al.*, 1999). The procedure of *in situ* hybridization has been previously used in *Lymnaea Stagnalis* for the detection of nicotinic acetylcholine receptors (van Nierop *et al.*, 2006), glutamate receptors (Stuhmer *et al.*, 1996) and the neuropeptide myomodulin (Kellett *et al.*, 1996, Perry *et al.*, 1998).

Two different methods of *in situ* hybridisation were utilised in this chapter. Firstly, whole mount *in situ* on CNS preparations was utilised with oligonucleotide probes. cRNA probes were also utilised on both cryo- and paraffin-embedded sections of *Lymnaea* CNS. Oligonucleotide probes are advantageous as they are resistant to RNAses, conferring greater stability and their small size allows good tissue penetration. The use of cRNA probes is beneficial due to the high thermal stability of cRNA-mRNA bonds and also their larger size offers the ability to incorporate a greater number of

labelled nucleotides in comparison to oligonucleotide probes thereby offering a greater sensitivity.

4.2 METHODS

4.2.1 Reverse Transcription – PCR

Lymnaea Stagnalis CNS were dissected using forceps in 0.1 % diethyl-pyrocarbonate (DEPC) treated-Phosphate buffered saline (PBS) solution (Sigma, Poole, U.K.) into the seven ganglia components: buccal, cerebral, pedal, pleural, left parietal, right parietal and visceral ganglia. RNA was isolated from each ganglia using the RNeasy Fibrous Tissue Mini Kit (Qiagen, West Sussex, U.K.) in a procedure that involved removing genomic DNA contaminants by DNAse digestion. RNA concentration was quantified using a Nanodrop spectrophotometer and ganglia samples were diluted to a concentration of 1 ng/µl. The RNA of each ganglia was reverse transcribed to first strand cDNA using Bioscript reverse transcriptase (Bioline, London, UK). Negative control included a non reverse transcriptase control (nonRT) where exactly the same procedures were followed with the omission of the reverse transcriptase enzyme in order to control for genomic DNA contamination.

cDNA transcribed from 300 pg of RNA from each CNS ganglia were run in 25 µl PCR reactions with 1 x SYBR Green mix (Heat-activated Taq DNA polymerase, Reaction Buffer, dNTPs, 3 mM $MgCl_2$, internal reference dye, stabilisers and SYBR Green I) (SYBR Green Jump Start Taq ReadyMix for High Throughput qPCR (Sigma, Poole, U.K.)) and 75 nM primers (either *Lym*P2X or β-tubulin) as follows:

*Lym*P2X forward- 5' GGGATCGTCTTCGTGGTGA 3'

*Lym*P2X reverse- 5' TGT CT GAGGCGACTCTTCTT 3'

β-tubulin forward- 5' GAAATAGCACCGCCATCC 3'

β-tubulin reverse- 5' CGCCTCTGTGAACTCCATCT 3'

β-tubulin has been previously used to normalise qRT-PCR experiments in *Lymnaea stagnalis* since this gene is expressed at almost equal levels in different *Lymnaea* tissues (Korneev *et al.*, 2002, van Nierop *et al.*, 2006). Quantitative RT-PCR (qRT-PCR) uses SYBR green as a double stranded DNA-binding dye that intercalates in the double helix of DNA to emit fluorescence. The ratio of fluorescence by SYBR green when bound to double-stranded DNA to the fluorescence when bound to single-stranded DNA is much higher than the equivalent ratio for ethidium bromide. The expected PCR product amplicon sizes were 229 bp for the *Lym*P2X primer pair and 128 bp for the β-tubulin primer pair.

qRT-PCR thermal cycling (MJ-Research Thermocycler RT-PCR machine) consisted of: 94 ºC for 2 min followed by 35 cycles of 94 ºC for 15 s, 55 ºC for 1 min and 72 ºC for 30 s. Reactions were then incubated at 72ºC for 10 min followed by a hold at 4ºC. C_t values were taken at a threshold of 0.01 units of fluorescence.

*Lym*P2X expression in each ganglia was quantified as followed:

C_t(*Lym*P2X) = number of PCR cycles for *Lym*P2X primers to reach 0.01 threshold

C_t(β-tubulin) = number of PCR cycles for β-tubulin primers to reach 0.01 threshold

$\Delta C_t = C_t(Lym\text{P2X}) - C_t(\beta\text{-tubulin})$

$\Delta\Delta C_t = \Delta C_{t(X)} - \Delta C_{t(Z)}$

where $\Delta C_{t(X)}$ = ganglia sample ΔC_t

$\Delta C_{t(Z)}$ = ganglia sample with the highest ΔC_t and lowest relative expression

The relative quantity of *Lym*P2X in ganglia sample is expressed as a multiple of ganglia sample Z:

$Lym\text{P2X}^{N} = 2^{-\Delta\Delta Ct}$

Melting curves carried out at 1 degree intervals between 50 - 95 degrees were used to check the purity of the PCR product. Completed PCR reactions were also separated on a 1.75 % agarose gel containing ethidium bromide in order to verify the correct size product (~230 bp for *Lym*P2X and ~130 bp for β-tubulin).

4.2.2 Whole mount in situ hybridisation with digoxigenin-labelled oligonucleotide probes

Dissection of *Lymnaea Stagnalis* in PBST (Phospho Buffered Saline in 0.1 % Tween (0.1 % DEPC treated)) (Sigma, Poole, U.K.) was carried out to isolate the CNS and remove connective tissue sheaths. This was followed by fixation of the CNS tissue for 2 hours with 4 % paraformaldehyde (PFA) in PBST. Proteinase K was added at a concentration of 10 µg/ml in PBST for 40 min to permeabilise the CNS tissue to enable penetration of probes, followed by addition of glycine in PBST at 2 mg/ml for 2 min to quench the reaction. Samples were then washed twice in PBST for 5 min each, re-fixed at room temperature with addition of ice-cold 4% PFA (in PBST) for 30 min and washed twice in PBST for 5 min each. Samples were then washed twice in 0.1M triethanolamine hydrochloride (TEA HCl), pH8.0 and then acetylated by the addition of acetic anhydride (2.5µl of acetic anhydride per 1mL of TEA HCl solution) for 5 min at room temperature with stirring. The same amount of acetic anhydride was then added again and incubated for a further 5 min at room temperature before washing twice in

PBST (5 min each wash). *Lymnaea* CNS were then incubated in pre-hybridization buffer (3 x SSC, pH7.0 ; 25 % formamide; 500 µg/ml sonicated salmon sperm DNA; 500 µg/ml yeast tRNA; 1 x Denhardt's solution) with no probe at the hybridization temperature of 57.2 ºC for 1 hour in a volume sufficient to cover the CNS. Pre-hybridization buffer was replaced by hybridization buffer containing DIG-labelled oligonucleotide probes (synthesised using a DIG-DNA Labelling and Detection Kit (Roche, West Sussex, UK) according to the manufacturer's instructions) at a concentration of 10 pmoles/ml and hybridized overnight at 57.2 ºC. Digoxigenin (DIG) was selected as the labelling molecule as other labelling molecules such as biotin are also endogenous in many tissues, and so there could be a likely chance to encounter false positive signals.

DIG-labelled antisense and complementary sense probes were synthesised corresponding to a region 1004 – 1048 bp in the *Lym*P2X cDNA sequence (extracellular domain proximal to TM2).

*Lym*P2X antisense:

5' AAC TTC CCA GCC TTC CCT TGG ACA GTC ACC ACG AAG ACG ATC CCT 3'

*Lym*P2X sense:

5' AGG GAT CGT CTT CGT GGT GAC TGT CCA AGG GAA GGC TGG GAA GTT 3'

Myomodulin antisense:

5’ CGC TTG GTC CTC GAC TGG GCG GGC TCT GTC TTG TCA TTA CTT G – 3’

Myomodulin sense:

5’ CAA GTA ATG ACA AGA CAG AGC CCG CCC AGT CGA GGA CCA AGC 3’

Probes were selected on the basis of similar GC content and melting temperatures.

Post hybridisation washes were carried out first in hybridization buffer (no probe), twice at 57.2 °C for 30 min each, then washes in serial dilutions (4:1, 3:2, 2:3, 1:4) of hybridization solution: PBST for l0 min each wash at room temperature. Samples were rinsed briefly in washing buffer, followed by incubation for 30 min in blocking solution **(**blocking reagent in maleic acid buffer (Roche, West Sussex, UK)). This was followed by incubation of CNS in 150 mU/ml primary anti-DIG antibody (Roche, West Sussex, UK) at room temperature for 1 hour followed by overnight incubation at 4 ºC. The following day there were two 15 min washes with washing buffer. The CNS samples were then equilibrated for 2 - 5 min in detection buffer, followed by the replacement of this solution with the substrate for alkaline phosphatase (NBT/BCPIP) in detection buffer (Roche, West Sussex, UK) for the detection of oligonucleotide probe-mRNA hybridised signals. Substrate reactions were stopped by washes in water.

4.2.3 In situ hybridization with DIG-labelled cRNA probes on Lymnaea CNS cryosections

Digoxigenin-labelled sense and antisense cRNA probes were synthesised from PCR templates using a DIG RNA Labelling Kit (Roche, West Sussex, UK) according to the manufacturer's instructions. PCR templates for cRNA synthesis were prepared with the following primer pairs.

PCR primer pair to make the sense strand template:

LymT7FORWinsit:

5' GAAAT**TAATACGACTCACTATAGGG**ACTATAATGCCAGGAGG 3'

LyminsituREV: 5' CCTTCAACAGATAGAGCACGATG 3'

Primer pair to make anti sense strand template:

LyminsituFOR: 5' GGGACTATAATGCCAGGAGG 3'

LymT7REVinsit:

5' GAAAT**TAATACGACTCACTATAGGG**CCTTCAACAGATAGAGCACG 3'

KEY:

Red sequence = 5 additional bases added so the T7 promoter sequence is not at the very end of the product. Bold underline sequence = Minimal T7 promoter sequence. Purple G = first base incorporated into resulting cRNA probe. The 21 bases from the 3' end of the T7 containing LymT7FORWinsit primer and 22 bases from the 3' end of the T7 containing LymT7FORWinsit primer anneal to the *Lym*P2X plasmid template.

The above 2 primer pairs generated PCR products of 728 bp. Transcription of either sense or antisense cRNA from these PCR product templates gave cRNA transcripts of 706 bp corresponding to nucleotide positions 430 – 1135 in the *Lym*P2X sequence.

Dissected *Lymnaea* CNS preparations were fixed in 4 % PFA for 2 hours, incubated in 30% sucrose in PBS overnight and then embedded in Tissuetek (Sakura Finetek, Netherlands), frozen in isopentane cooled in liquid nitrogen. Cryosections (20 µm) were adhered onto plus™ slides (VWR, Leighton Buzzard, UK) and postfixed for 20 min in 4 % paraformaldehyde in DEPC-treated PBS followed by washing twice for 15 min in PBS with 0.1 % DEPC at room temperature. Slides were then equilibrated in 5 X SSC before prehybridization in 50 % formamide, 5 X SSC, 40 µg/ml salmon sperm DNA at 58 °C for 2 hours. Hybridization was carried out in 50 % formamide, 5 X SSC, 40 µg/ml salmon sperm DNA and 400ng/ml of DIG-labelled cRNA probe at 58°C for 20 hours. Posthybridization washes consisted of a 30 min wash in 2 X SSC at room temperature, 1 hour wash in 2 X SSC at 65 °C, and a 1 hour wash in 0.1 X SSC at 65 °C. This was followed by a 30 min equilibration in blocking buffer, and 2 hour incubation with alkaline phosphatase conjugated anti-DIG antibody (1:2000) diluted in blocking buffer. Two 15 min washes were then carried out with washing buffer (Roche, West Sussex, UK). Slides were equilibrated in detection buffer for 5 min before addition of the substrate solution (45 µl NBT and 35 µl BCIP per 10 ml of detection buffer) for an overnight staining reaction. The following day the reactions were stopped in distilled water, followed by one hour in 95 % ethanol. The slides were then washed twice in distilled water for 15 min, followed by dehydration steps before mounting in DPX for photomicroscopy.

4.2.4 In situ hybridization with DIG-labelled cRNA probes on Lymnaea CNS paraffin embedded sections.

The same protocol for *in situ* hybridization on *Lymnaea* CNS cryosections was followed, except 4 % PFA-treated whole *Lymnaea* CNS were dehydrated in 25 % ethanol for 10 min, 40 % ethanol for 10 min, 60 % ethanol for 10 min, and 70 % ethanol for 10 min. Paraffin-embedded sections were then cut at 5µm. Slices were dewaxed in xylene three times for 5 min each, washed in 100 % ethanol twice for 5 min each, 90 % ethanol for 2 min, 70% ethanol for 2 min, 40 % ethanol for 2 min and PBS for 5 min.

4.3 RESULTS

4.3.1 Reverse Transcription – PCR

Conventional RT-PCR

Conventional non quantitative RT-PCR experiments demonstrated *Lym*P2X gene expression in each of the CNS ganglia analysed. Amplification of β-tubulin served as a positive control and ganglia RNA samples that were not reverse transcribed (non RT) served as negative controls (Figure 4.1).

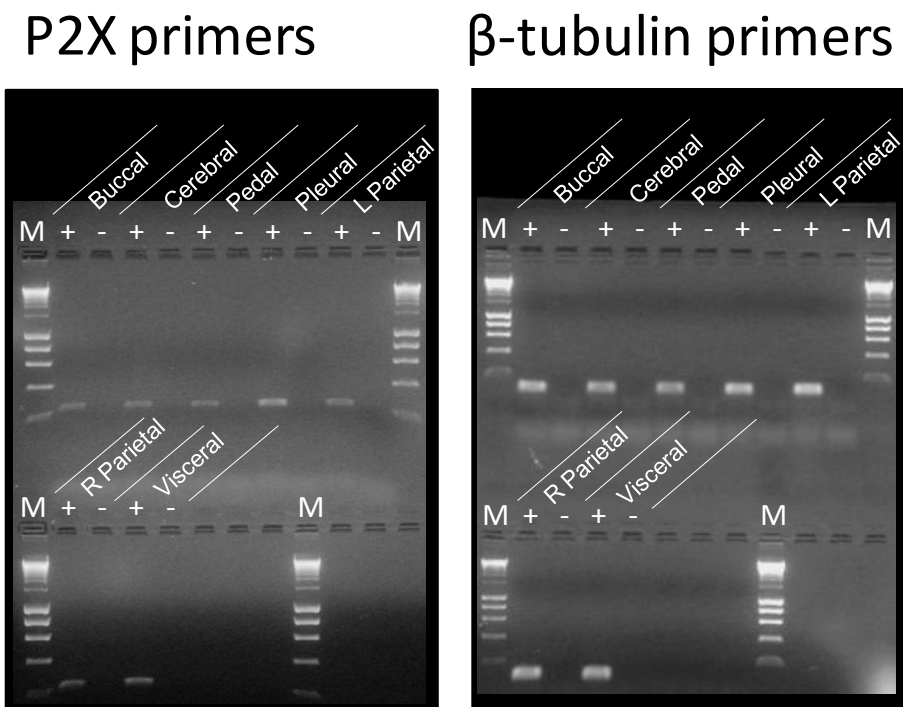

Figure 2.1. Conventional (non-quantitative) RT-PCR of *Lymnaea* CNS ganglia samples demonstrates the presence of *Lym*P2X mRNA in each ganglia. *Lym*P2X primers amplified a 229 bp fragment of the *Lym*P2X gene, and β-tubulin primers amplified a 128 bp fragment of β-tubulin gene. + = ganglia cDNA sample, - = no reverse transcriptase negative control, M = Hyper ladder I (Bioline) molecular mass marker

Quantitative RT-PCR

Since the ΔΔCt method was used to quantify the relative expression of *Lym*P2X in the different ganglia of the *Lymnaea* CNS, it was important to show that β-tubulin and *Lym*P2X PCR products were amplified with a similar efficiency.

To test the similarity in amplification efficiency of the *Lym*P2X and β-tubulin primers, dilutions of the cDNA samples were carried out at five different concentrations (cDNA transcribed from 1 ng, 0.3 ng, 0.1 ng, 0.03 ng, 0.01 ng, referred to as input RNA). As the amount of input RNA decreases, the C_t value should increase correspondingly in proportion (0.1 ng RNA should have a 3-4 C_t values higher than 1 ng cRNA as it takes ~3.3 replication cycles to amplify DNA tenfold). *Lym*P2X and β-tubulin primers were observed to amplify their respective sequences with almost equal amplification efficiencies at input RNA quantities of 0.03 – 1 ng (Figure 4.2). *Lym*P2X primers had an amplification efficiency of 105.4 % and β-tubulin primers had an efficiency of 93.4 % (Figure 2A). PCR of 0.01 ng input RNA using *Lym*P2X primers did not enter the exponential phase and pass the 0.01 threshold, therefore no C_t value was obtained for this amount (Figure 4.2C). These primer efficiency values demonstrate that the primers amplify sequences with approximately equal efficiency. This can be substantiated by the relative efficiency plot that shows a graph of ΔC_t (C_t(*Lym*P2X) - C_t(*Lym* β-tubulin)) versus log cRNA to have a slope of -0.004 ± 0.08, which is within the -0.1 and +0.1 range of values that is considered acceptable for using primers for qRT-PCR (Figure 4.2D).

Once equal efficiencies between reference (β-tubulin) and experimental (*Lym*P2X) primers had been verified, CNS ganglia were quantified for *Lym*P2X expression.

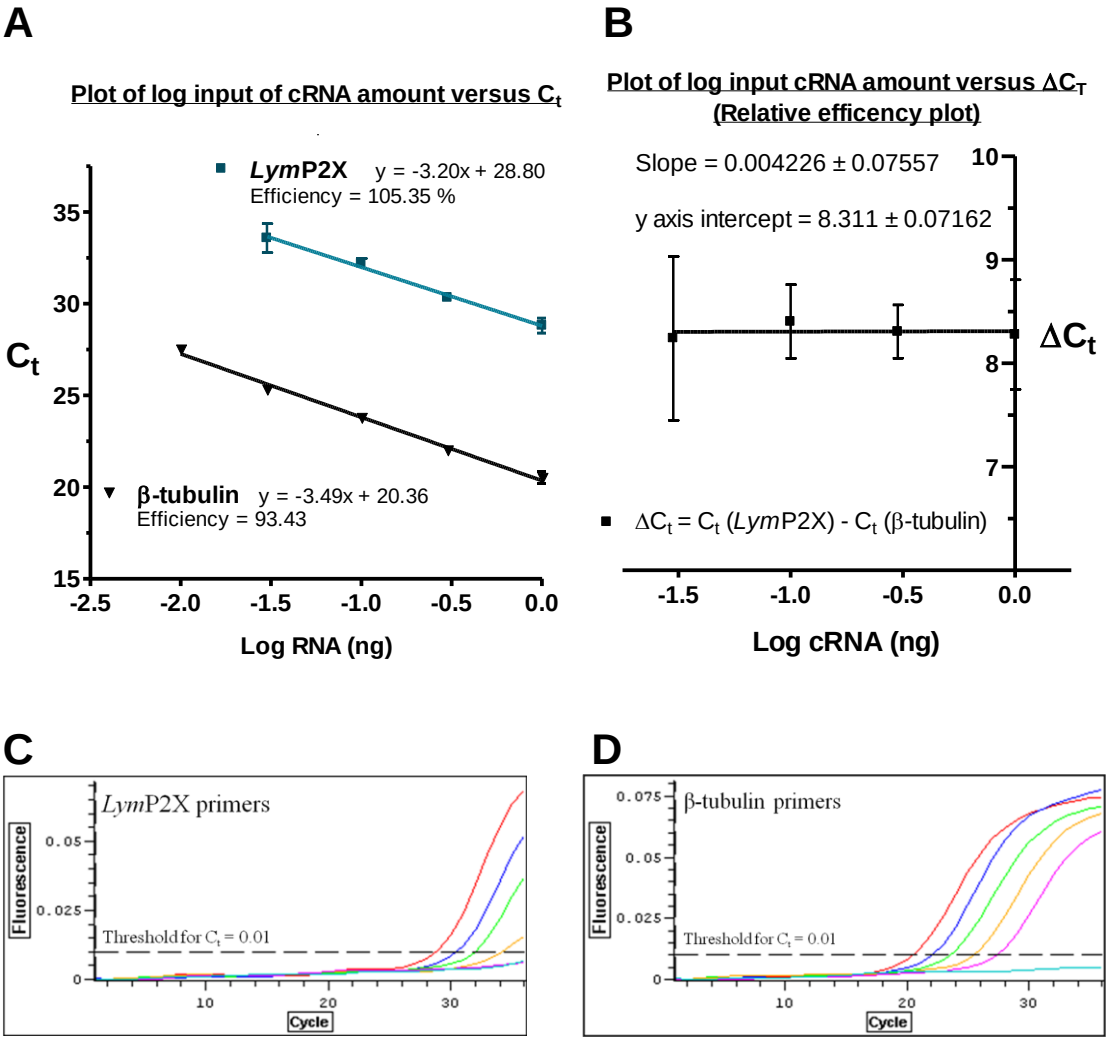

Figure 4.2 A. Efficiency graphs for *Lym*P2X and β-tubulin primers displaying the number of PCR cycles required to reach threshold of the exponential phase (C_t) at different dilutions of input cRNA (10 pg to 1 ng). B. Graph of ΔCt (different in C_t of *Lym*P2X and β-tubulin) versus dilutions of cRNA input (10 pg to 1 ng) shows a gradient of between 0.1 to -0.1, thereby demonstrating equal efficiencies of the primers and suitability for use in qRT-PCR. C and D, traces showing the PCR amplification of fragments from *Lym*P2X (left) and β-tubulin (right) genes measured in real time at different input cRNA quantities (1 ng – red, 300 pg – dark blue, 100 pg – green, 30 pg – orange, 10 pg – pink, and 1 ng non-reverse transcribed RNA – light blue). Threshold for the measuring the number of cycles to reach the exponential phase was set at 0.01. Amplification of all nonRT samples and *Lym*P2X amplified from 10 pg did not pass the threshold of the amplification phase, and therefore no C_t value obtained.

*Lym*P2X was found to be present in all CNS ganglia, as demonstrated by the presence of an amplicon of the expected size (229 bp) (Figure 4.3D). No PCR bands or C_t cycles were observed for the non-RT controls, illustrating that there are no significant quantities of genomic DNA or other contamination present in the samples.

Pleural ganglia was found to have the least amount of *Lym*P2X expression per ng of input RNA from CNS tissue of all the ganglia. This was evident from the highest ΔC_t value, demonstrating that more PCR cycles are required to reach the threshold of the exponential phase relative to β-tubulin (Table 1). Therefore the ΔC_t of pleural ganglia was selected as the ΔC_{tZ}, the value to be subtracted from ΔC_t values of other CNS ganglia samples in order to give a $\Delta\Delta C_t$ value. Thus *Lym*P2X expression for each ganglia sample was expressed relative to pleural ganglia.

Pedal ganglia showed the highest amount of *Lym*P2X expression, with 2.60 times (range 1.71 – 3.97 times) the amount of *Lym*P2X present in pleural ganglia per ng of input RNA (Figure 4.3A, Table 1). Cerebral and visceral ganglia also have over twice the quantity of *Lym*P2X mRNA than pleural ganglia. Buccal ganglia has 1.69 times, right parietal has 1.55 times and left parietal has 1.30 times the amount of pleural ganglia *Lym*P2X.

Having determined *Lym*P2X expression in each ganglia of the *Lymnaea* CNS, it would be of interest to determine which specific neurons in these ganglia are expressing *Lym*P2X in order to facilitate electrophysiological analysis of *Lym*P2X functions at the level of *Lym*P2X-expressing identified neurons.

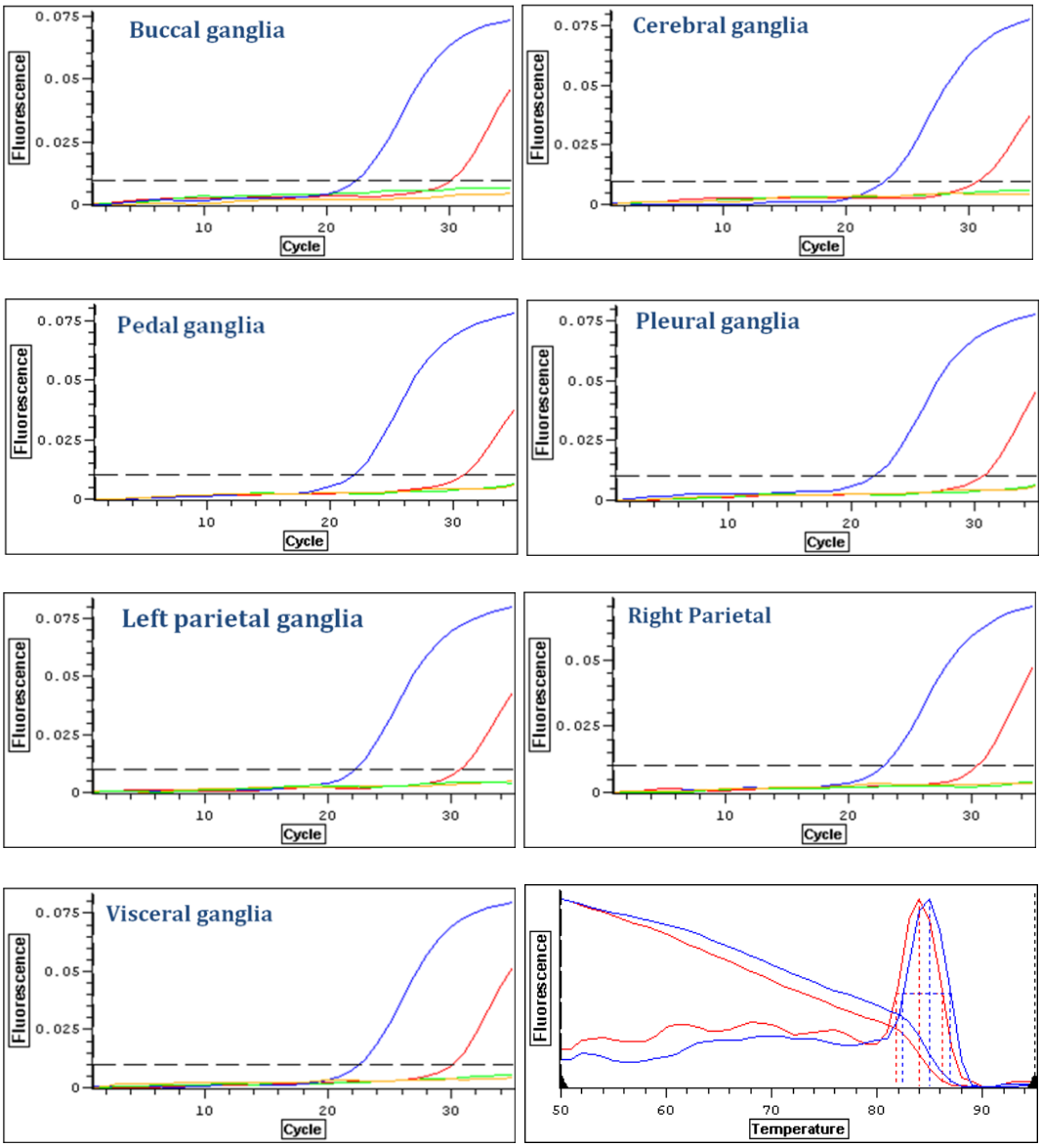

Figure 4.3. A, traces showing the amplification of *Lym*P2X (red) and β-tubulin (blue) cDNAs reverse transcribed from 0.3 ng RNA from each ganglia. Non-reverse transcribed (nonRT) negative control samples contained 0.3 ng RNA, with *Lym*P2X (yellow) and β-tubulin (green) primers. The threshold for PCR reactions entering amplification phase was set at 0.01 units of fluorescence. nonRT samples did not pass C_t threshold. Bottom right panel shows melting curves for *Lym*P2X (red) and β-tubulin amplified PCR products, a single peak for both amplicons indicates the purity of the products.

C

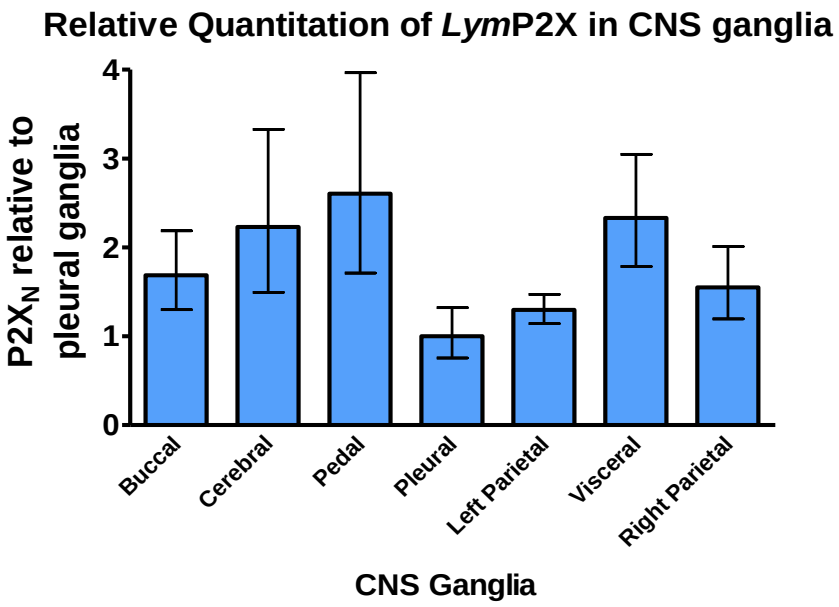

D

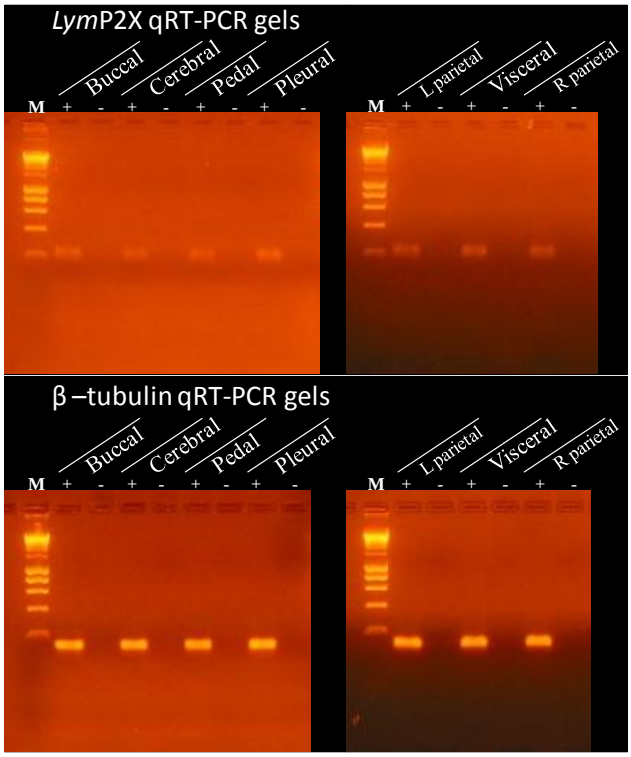

Figure 4.3. C, relative quantity of *Lym*P2X expression in each ganglia relative to expression in pleural ganglia, representative of three experiments, showing results from a triplicate qRT-PCR run that is representative of three separate experiments. D, gels from qRT-PCR products showing the presence of 229 bps *Lym*P2X bands and 128 bps β-tubulin bands in each CNS ganglia sample. Gels also show absence of PCR products in non-RT ganglia samples (negative controls = -) in lanes next to their corresponding positive RT-samples (+). M = Hyperladder I marker.

		CNS Ganglia						
C_t values		Buccal	Cerebral	Pedal	Pleural	Left Parietal	Visceral	Right Parietal
*Lym*P2X	C_t	30.48	30.76	31.03	30.71	30.54	29.97	30.85
	S.D	0.37	0.56	0.59	0.15	0.15	0.14	0.36
	S.E.	0.21	0.32	0.34	0.08	0.08	0.08	0.21
β-tubulin	C_t	22.55	23.23	23.72	22.02	22.23	22.51	22.79
	S.D	0.06	0.15	0.15	0.38	0.11	0.36	0.09
	S.E.	0.04	0.08	0.09	0.22	0.06	0.21	0.05
ΔC_t = (*Lym*P2X C_t –β-tubulin)		**7.93**	**7.53**	**7.31**	**8.69**	**8.31**	**7.47**	**8.06**
	S.D.	0.38	0.58	0.61	0.40	0.18	0.39	0.37
$\Delta\Delta C_t$ = **ΔC_t - ΔC_{tZ}** (pleural)		**-0.75**	**-1.16**	**-1.38**	**0.00**	**-0.37**	**-1.22**	**-0.63**
	S.D.	0.38	0.58	0.61	0.40	0.18	0.39	0.37
*Lym*P2X_N		**1.69**	**2.23**	**2.60**	**1.00**	**1.30**	**2.33**	**1.55**
(Relative to pleural)								
Range	min	1.30	1.49	1.71	0.76	1.14	1.78	1.20
	max	2.19	3.33	3.97	1.32	1.47	3.05	2.01

Table 1, showing C_t, ΔC_t and relative quantities of *Lym*P2X expression in each ganglia sample.

4.3.2 Whole mount in situ with DIG-labelled oligonucleotide probes

DIG-labelled oligonucleotide probes were used to try to localize *Lym*P2X expression by hybridization to specific neurons containing *Lym*P2X mRNA transcripts. An antisense oligonucleotide probe corresponding to the myomodulin mRNA was also used as a positive control, since the myomodulin gene has previously been found to be present at high abundance in specific cells in the CNS of *Lymnaea* by *in situ* hybridization and immunocytochemistry (Kellett *et al.*, 1996, Perry *et al.*, 1998). Myomodulin is a neuropeptide known to modulate neuromuscular transmission, and it has been found to be located in many parts of the *Lymnaea* CNS by *in situ* hybridization and antibody staining.

The positive control antisense myomodulin probe hybridized with target mRNA sequences in the *Lymnaea* CNS, identifying specific neurons expressing the myomodulin gene (Figure 4.4A). Areas of hybridization include medium intensity staining of B1 and B2 neurons of the buccal ganglia, intense staining in cerebral ganglion neurons, strong signals in pedal ganglion cells (at and near LPeD7 and 8 cells), abundant staining in pleural and left parietal pleural ganglion cells (strong D gp cells), visceral ganglion was widely stained (strong H I, J, K cells, strong G gp cells, E gp cells are faint) and medium staining of right parietal ganglia (A gp cells). Neuronal staining appeared as black circular ring shapes, indicating that the cell bodies of the neurons were stained. The sense myomodulin probe did not hybridise, thereby demonstrating the specificity of the antisense hybridization signals (Figure 4.4B).

Antisense *Lym*P2X and sense *Lym*P2X probes failed to show a specific hybridization signal (Figure 4.4C and D). The lack of hybridization signal with the sense probe

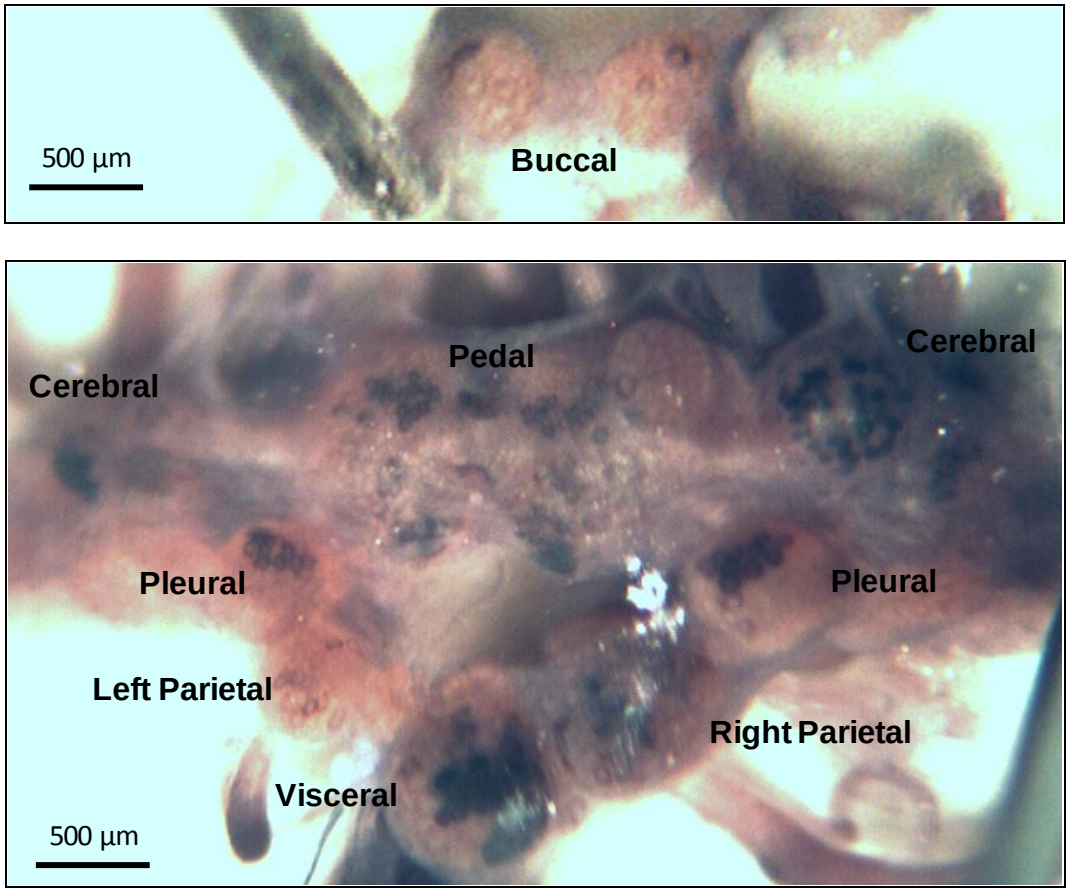

Figure 4.4. A, representative image of whole mount *in situ* hybridization of myomodulin mRNA sequences with corresponding antisense myomodulin oligonucleotide probe. Upper panel shows buccal ganglia staining and lower panel show cerebral, pedal, pleural, parietal and visceral ganglia. Hybridization signals (black circular staining) was seen in a subset of neurons in all *Lymnaea* CNS ganglia. The different ganglia (buccal, pedal, cerebral, pleural, left parietal, right parietal, and visceral) are labelled.

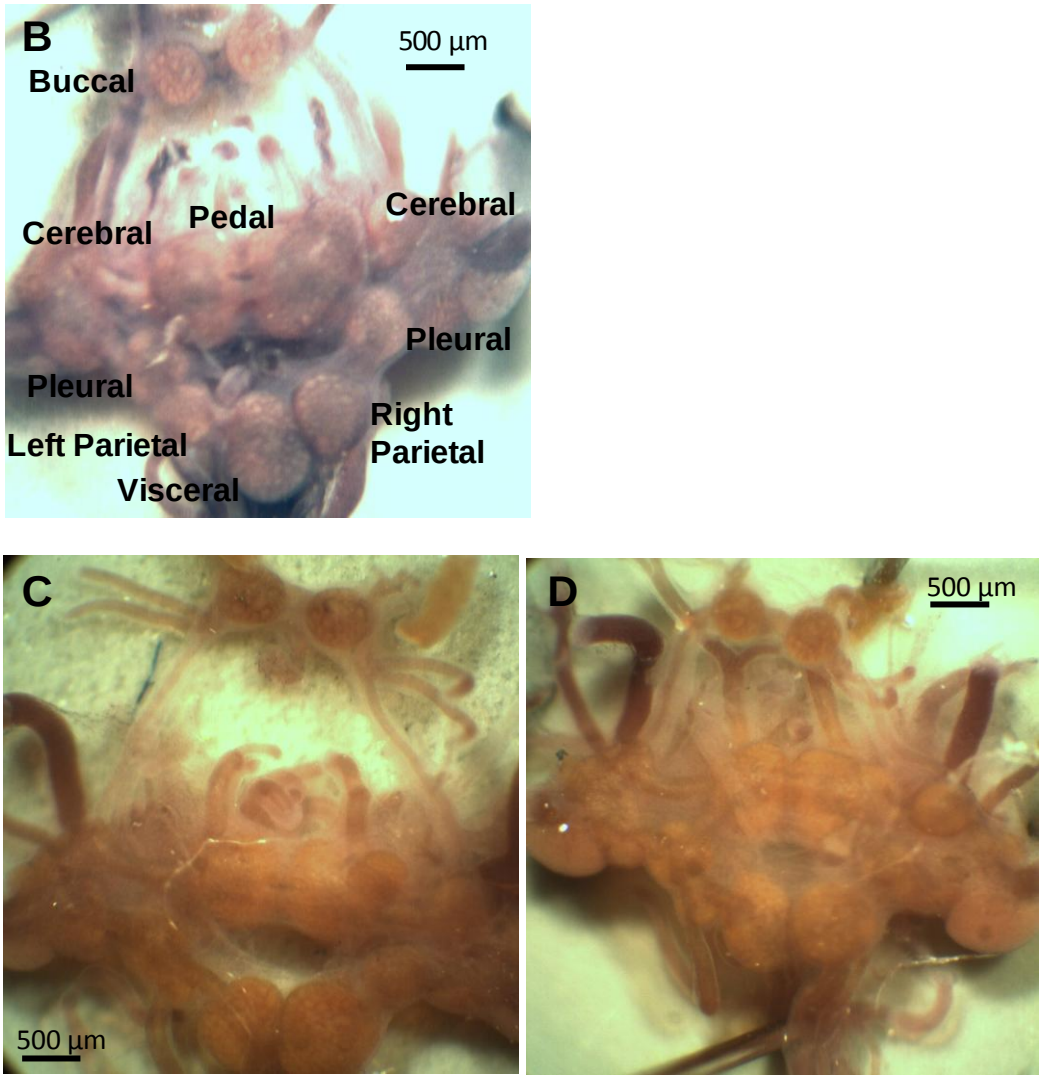

Figure 4.4. B, Absence of hybridization signals for the myomodulin sense probe, demonstrating a lack of unspecific binding. 4. C and D, *Lym*P2X antisense (C) and sense (D) probes did not bind to sequences to give signals.

demonstrates a lack of unspecific binding. The inability of the antisense *Lym*P2X probe to produce a signal implies that *Lym*P2X mRNA is absent or has low abundance or alternatively that certain properties of the probe do not allow efficient hybridization to take place. Three different sets of *Lym*P2X antisense and sense oligonucleotide probes were subsequently used simultaneously in an attempt to increase signal strength. However, this strategy also failed to produce detectable hybridization (data not shown). In order to try to amplify low abundance mRNA sequences, the Tyramide Signal Amplification (TSA) protocol was also utilised. This system allows amplification of mRNA signals without increasing background or reducing resolution and works on the principle of the addition of a horse radish peroxidise-conjugated anti-DNP secondary antibody that binds to an anti-DIG conjugated dinitrophenol (DNP) primary antibody. The horse radish-peroxidase activates multiple copies of biotinylated tyramide that covalently attaches to nucleophilic residues in the vicinity of the target. This leads to amplification of signals that are localized to the sites of hybridization.

However, when the tyramide amplification system was used, all probes including the myomodulin antisense positive control probe (Figure 4.5), failed to produce a detectable signal. This suggests that the antibody or amplification reagent used in the TSA method may have problems in penetrating the tissue. Tyramide Signal Amplification has not been established for use in whole mount *in situ* hybridization protocols, and it is possible that *Lymnaea* CNS components may be involved in inactivating the tyramide or peroxidase enzymes.

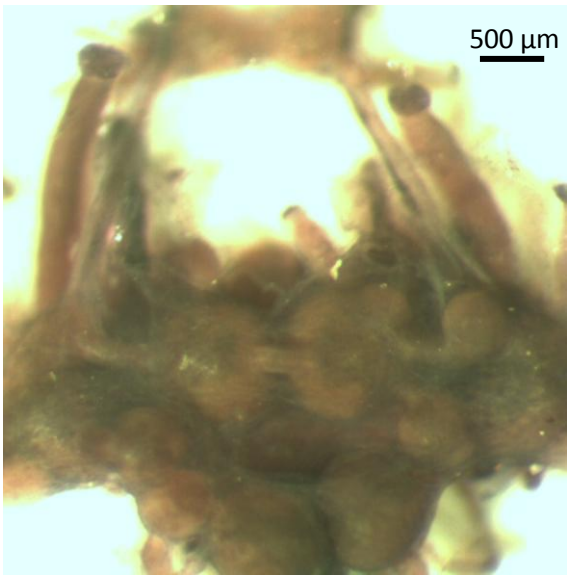

Figure 4.5, lack of hybridization signals in neurons with the myomodulin antisense strand with tyramide labelling, showing that the tyramide labelling procedure was not successful in the detection of myomodulin gene. Sense myomodulin, *Lym*P2X antisense and *Lym*P2X sense also did not give hybridization signals.

4.3.3 In situ hybridization with DIG-labelled cRNA probes on cryosections

Digoxigenin-labelled cRNA probes were utilized in a strategy to try to map *Lym*P2X distribution by hybridizing to specific neurons in 20 µm cryosections of *Lymnea* CNS. *Lym*P2X hybridization signals were present in neurons of all ganglia, however freezing damage was evident in many cryosections (Figure 4.6). An additional problem experienced with cryosections was that the tissue slices often detached from the surface of either plus™ or poly-L-lysine coated slides. To overcome these problems wax embedded sections were therefore used in subsequent studies.

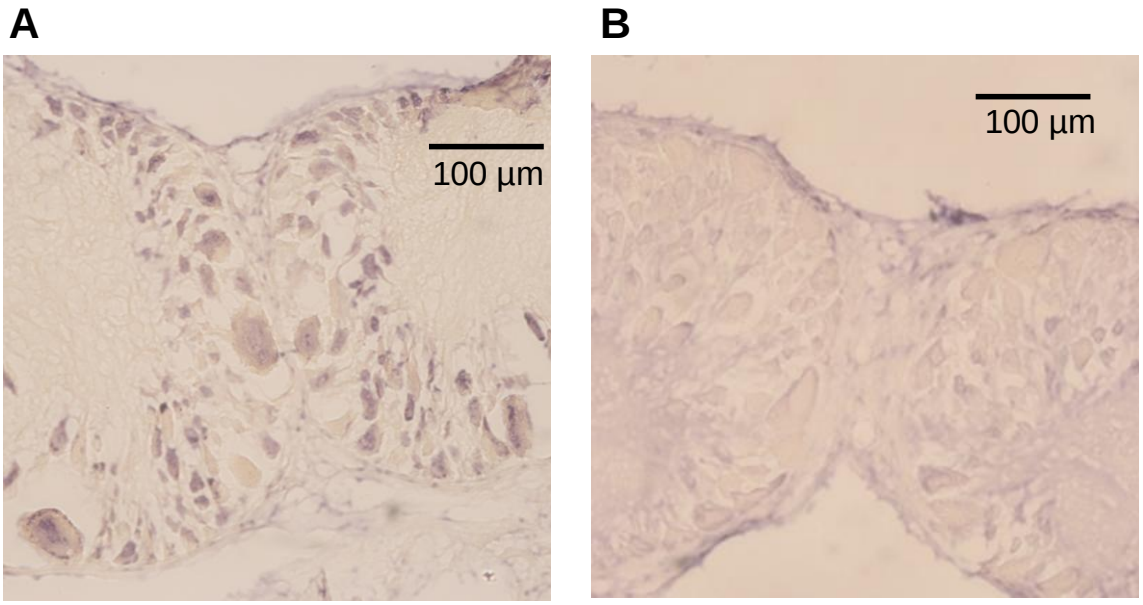

Figure 4.6. *In situ* hybridization using antisense (A) and sense (B) DIG-labelled cRNA on cryosections. Morphological damage caused by freezing artefacts was present in the *Lymnaea* CNS tissue (pedal ganglia shown as example).

4.3.4 In situ hybridization with DIG-labelled cRNA probes on paraffin-embedded sections

Digoxigenin-labelled cRNA probes were used to try to localize *Lym*P2X expression in paraffin-embedded 5 µm sections by hybridizing to specific neurons containing *Lym*P2X mRNA transcripts. The *Lym*P2X antisense probe produced a strong punctate

nuclear signal, with a weaker diffuse staining present in the cytoplasm. This staining pattern was observed in the vast majority of the neurons in each ganglia (Figure 4.7), with smaller neurons showing a slightly more dense punctate nuclear staining than that of the larger neurons (Figure 4.7 and 4.8). This staining pattern of the *Lym*P2X antisense probe was in marked contrast to the control sense probe which gave a much weaker diffuse background pattern of staining. These results suggests that *Lym*P2X mRNA is localised primarily in the nucleus in the majority of *Lymnaea* CNS neurons.

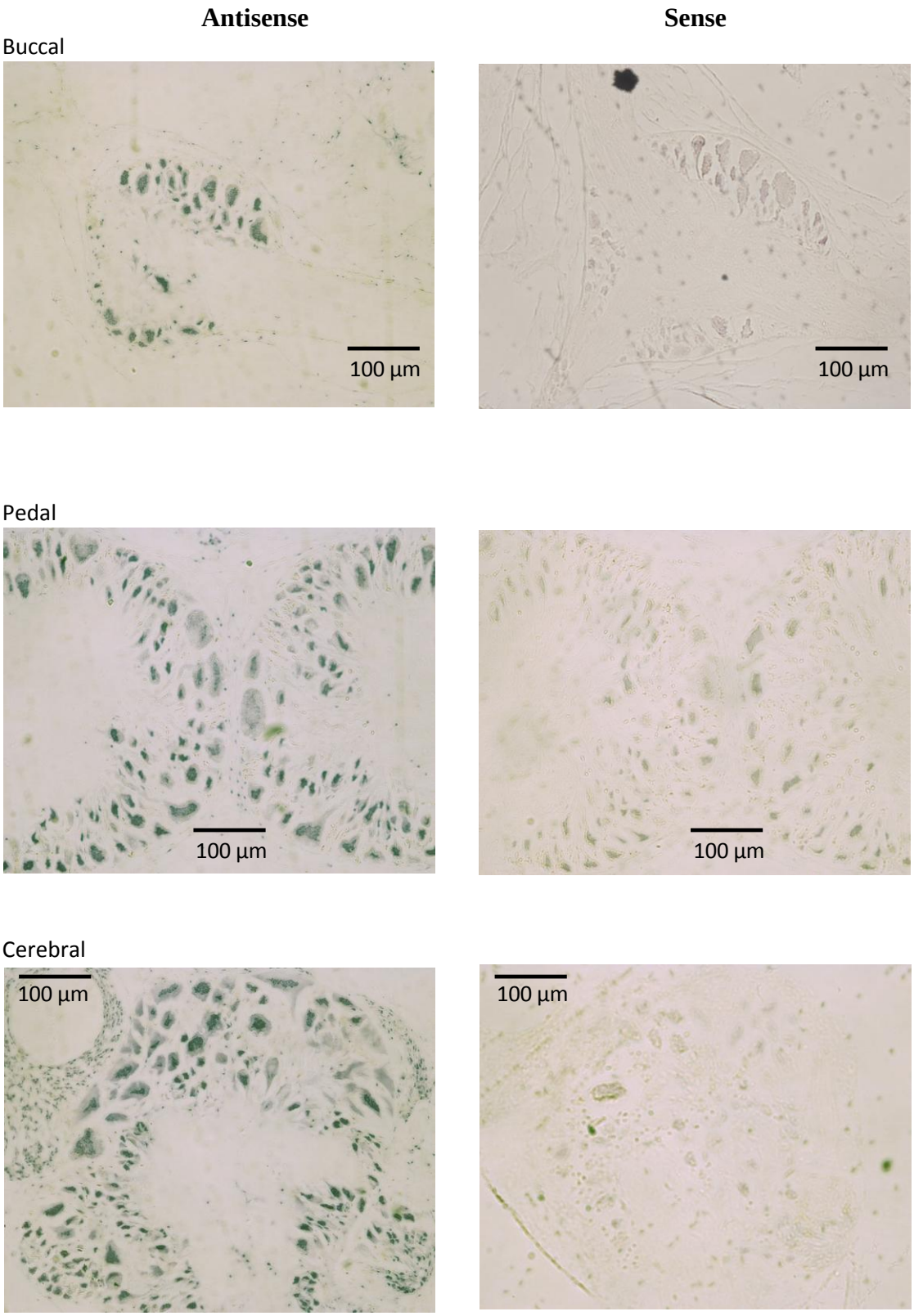

Figure 4.7. *In situ* hybridization with DIG-labelled cRNA probes on paraffin-embedded sections of *Lymnaea* CNS buccal, pedal and cerebral ganglia. The *Lym*P2X antisense probe produced a dense punctate staining in the nucleus and weaker diffuse cytoplasmic staining in the majority of neurons of each ganglia.

Pleural

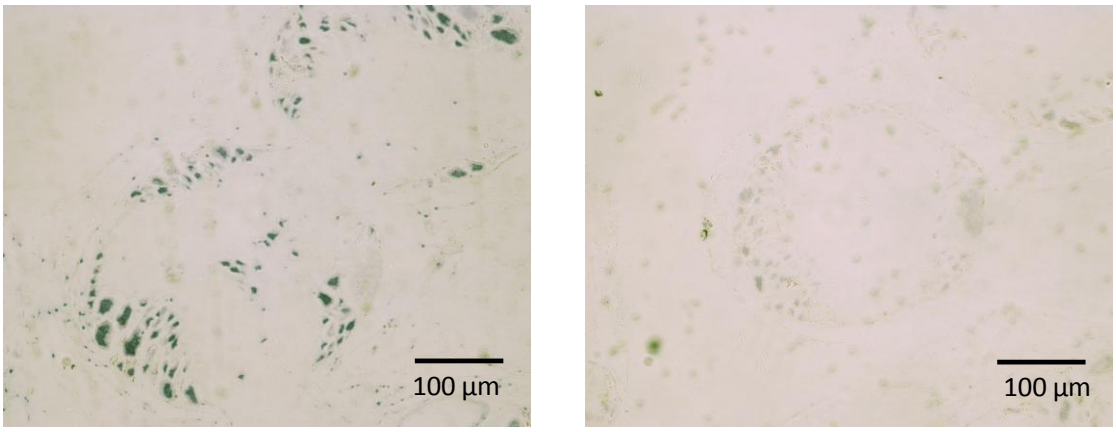

Left parietal

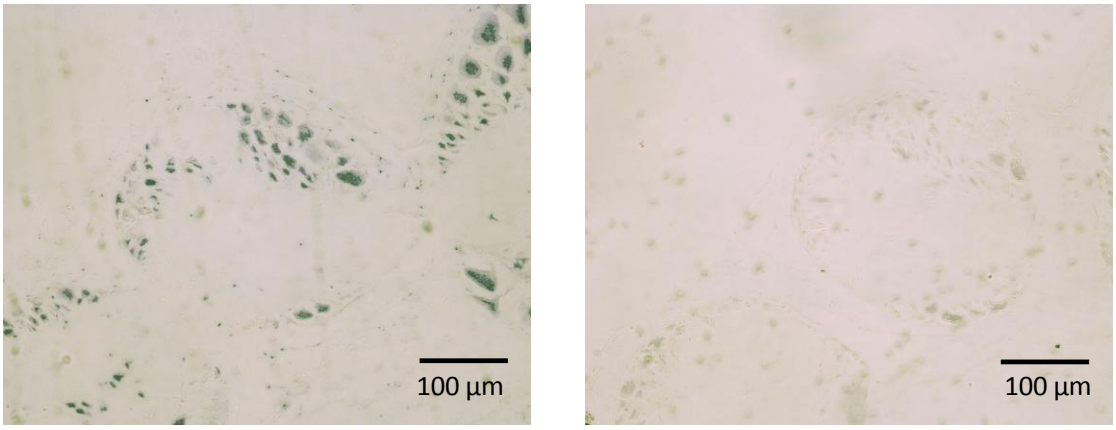

Visceral

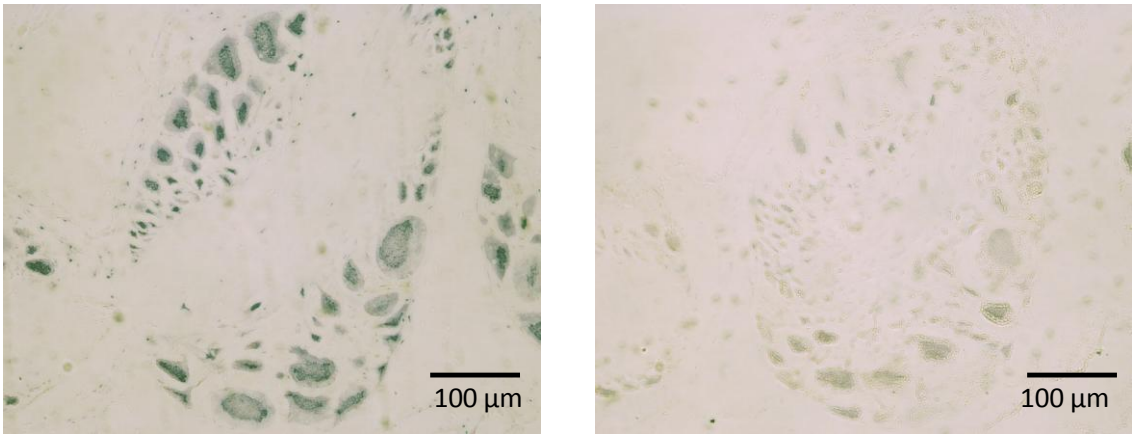

Figure 4.7. *In situ* hybridization with DIG-labelled cRNA probes on paraffin-embedded sections of *Lymnaea* CNS pleural, left parietal and visceral ganglia. The *Lym*P2X antisense probe produced a dense punctate staining in the nucleus and weaker diffuse cytoplasmic staining in the majority of neurons of each ganglia.

Right parietal

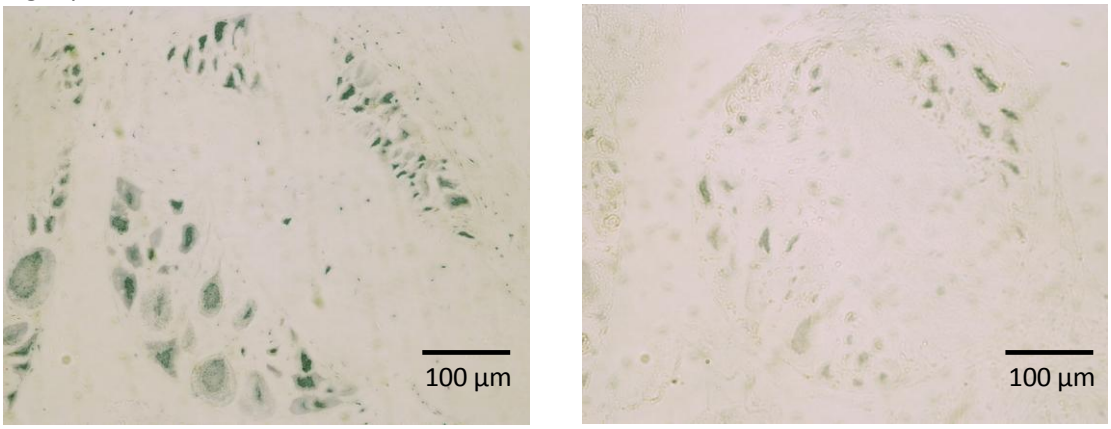

Figure 4.7. *In situ* hybridization with DIG-labelled cRNA probes on paraffin-embedded sections of *Lymnaea* CNS right parietal ganglia. The *Lym*P2X antisense probe produced a dense punctate staining in the nucleus and weaker diffuse cytoplasmic staining in the majority of neurons of each ganglia.

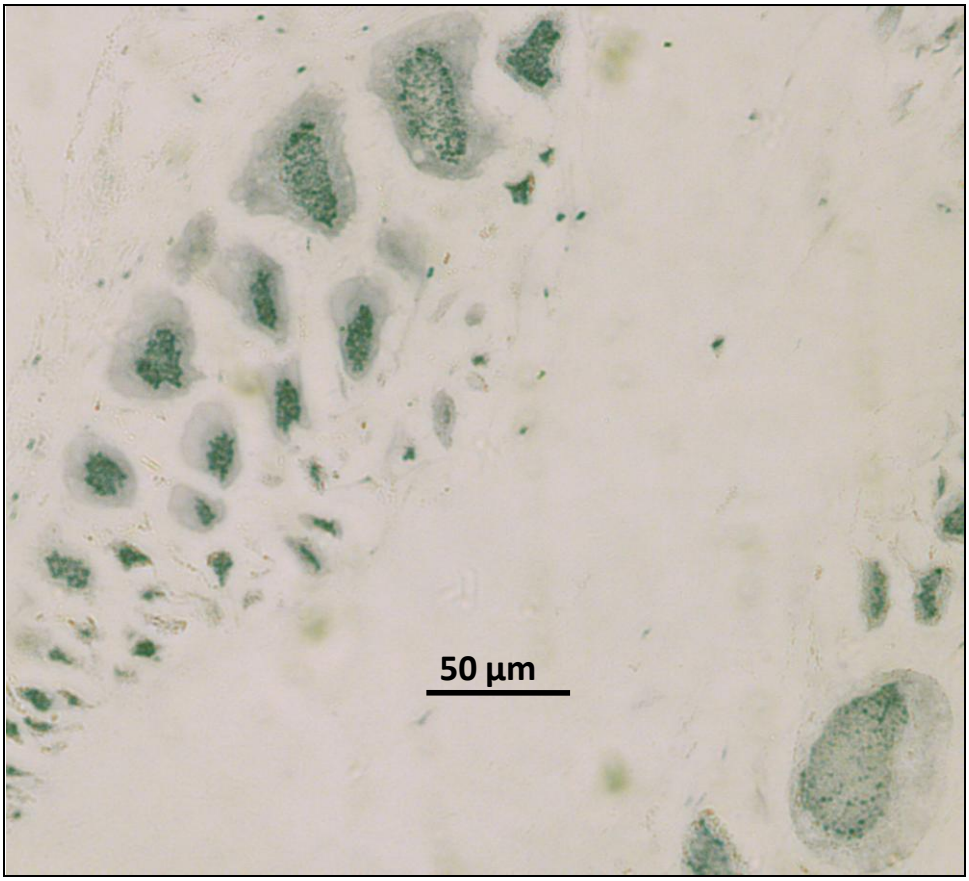

Figure 4.8. Zoom in image of visceral ganglia section treated with antisense P2X probe. A denser punctate staining pattern is observed in the smaller neurons than the larger neurons, with cytoplasm having only diffuse staining.

4.4 DISCUSSION

Knowledge of the CNS distribution of *Lym*P2X is of importance in giving clues as to which neuronal pathways this receptor may feature in. Localization of *Lym*P2X receptors to specific CNS ganglia and neurons that are known to control a physiological process such as feeding or respiration would imply a role for *Lym*P2X function in that particular system. Immunohistochemistry with a receptor specific antibody is the method of choice for protein localization studies. However, most of the currently available P2X receptor antibodies, being raised against specific epitopes within the carboxy terminal domain, are vertebrate P2X subtype, and in some cases species specific making them unsuitable for the detection of *Lym*P2X. In the absence of a "general P2X" or *Lym*P2X specific antibody, this chapter focused on localization of *Lym*P2X CNS gene expression by detecting mRNA by both RT-PCR and *in situ* hybridisation.

4.4.1 RT-PCR

*Lym*P2X expression was found to be expressed in all ganglia in the *Lymnaea* CNS by both conventional RT-PCR and quantitative RT-PCR. *Lym*P2X was found to be most abundantly expressed in the pedal ganglia, where *Lym*P2X expression was between 1.7 and 4 times the quantities found in the pleural ganglia, the area with the least amount of *Lym*P2X expression detected. The presence of *Lym*P2X in each CNS ganglia and the small variation in expression pattern of *Lym*P2X implies that P2X receptor is likely to function in many neuronal pathways in the CNS of *Lymnaea*. qRT-PCR analysis of ganglia in *Lymnaea* CNS is limited in that it is not able to differentiate between *Lym*P2X expression in neurons, glial cells, or connective tissue. P2X expression has

been previously reported in astrocytes (Lalo *et al.*, 2008) and oligodendrocytes (Matute *et al.*, 2007), so another technique to detect *Lym*P2X expression was required to confirm its presence in neurons of the CNS. Therefore *in situ* hybridization was carried out on *Lymnaea* CNS in an attempt to identify specific neurons that express *Lym*P2X mRNA.

4.4.2 In situ hybridization

The first attempt of locating *Lym*P2X mRNA expression using *in situ* hybridization used the whole mount method with oligonucleotide probes. However *Lym*P2X hybridization signals were not observed, indicating that either *Lym*P2X expression is of a very low abundance that is below the detection limit of the experimental procedure or that the oligonucleotide *Lym*P2X probe was not able to penetrate through the *Lymnaea* tissue to the target mRNA.

Myomodulin was used as a positive control to verify the hybridization protocol. This oligonucleotide probe produced hybridization signals in the soma of a subset of neurons in all ganglia of the *Lymnaea* CNS, with some ganglia having more stained neurons than others. This result is in agreement with previous studies that have also demonstrated myomodulin expressing neurons in all CNS ganglia (Kellett *et al.*, 1996, Perry *et al.*, 1998). However, the pattern of specific myomodulin positive neurons within each ganglia did not correspond exactly to previous studies in that the LPeD4 and I cl cells of pedal ganglia, F gp cells of the visceral ganglia and B gp cells of the right parietal ganglia, which were all positive for myomodulin mRNA in previous

studies (Kellett *et al.*, 1996, Perry *et al.*, 1998), did not show hybridisation in this current study.

Myomodulin has previously been shown to be located in the B1 and B2 cells of the buccal ganglia and in the cerebral giant cell (CGC) of the cerebral ganglia by both *in situ* hybridisation and antibody staining (Perry *et al.*, 1998). The presence of myomodulin peptides in B2 neurons has also been confirmed by MALDI-TOF mass spectrometry (Perry *et al.*, 1998). Buccal ganglia B3 neurons have previously been shown to stain faintly positive with a myomodulin antibody (Santama *et al.*, 1994). However, *in situ* hybridizations carried out in the same study failed to detect myomodulin mRNA in B3 neurons. This was also the case in a subsequent study (Perry *et al.*, 1998) and the whole mount *in situ* hybridisations performed in this thesis suggesting that the faint antibody staining described by Santama and co-workers was possibly an artefact and that B3 buccal neurons do not express myomodulin.

Whilst the pattern of myomodulin hybridisation observed in this study was broadly in line with previous studies (Kellett *et al.*, 1996, Perry *et al.*, 1998), specific neurons that were seen to be myomodulin negative in these previous investigations were positive in this study. Similarly, these previous investigations localized myomodulin expression in specific neurons that were not detected in this study. This suggests that myomodulin gene expression may be transient or show some plasticity between individual neurons.

In situ hybridization using DIG-labelled cRNA probes on paraffin-embedded *Lymnaea* CNS sections revealed *Lym*P2X mRNA in the majority of neurons in all of the CNS ganglia. This staining pattern is consistent with the qRT-PCR studies that also showed

*Lym*P2X expression in every ganglia with little variation in expression level between ganglia. The *Lym*P2X antisense cRNA probe hybridised predominantly to the nucleus of neurons, displaying a strong punctate staining pattern. This nuclear binding is unlikely to be due to hybridisation to genomic DNA as the control sense probe did not show this strong punctuate staining pattern and each nucleus contained multiple puncta. Furthermore, if the cRNA probe was hybridising to genomic DNA then a pattern of multiple puncta would not be expected since each nucleus contains only two copies of the *Lym*P2X gene, one on each chromosome. A less intense more diffuse pattern of *Lym*P2X antisense cRNA staining was also observed in the cytoplasm of positive cells suggesting that *Lym*P2X mRNA is located predominantly within the nucleus. However, the presence of more abundant *Lym*P2X transcripts in the cytoplasm can not be ruled out, as it is possible that the antisense DIG-labelled cRNA probe has reduced binding ability to cytoplasmic mRNA compared to nuclear RNA due to preferential loss of cytoplasmic RNA during tissue preparation. This possibility could be substantiated by using a positive control for cytoplasmic mRNA signals, for example using myomodulin antisense DIG-labelled cRNA probe on paraffin-embedded sections, since myomodulin mRNA has been previously localised to the cytoplasm (Kellett *et al.*, 1996).

Nuclear localization of mRNA has been previously reported in other cell types. For example, *in situ* hybridization using cRNA probes for Cytochrome P450 1B1 (CYP1B1) demonstrates that the mRNA for this gene is present only in the nucleus of human brain neurons and astrocytes (Muskhelishvili *et al.*, 2001). An mRNA encoding for a transcription factor implicated in tumorigenesis, human Wilms' tumor gene WT1 has also been found to display nuclear localization by *in situ* hybridization (Mundlos *et al.*, 1993).

Further research can investigate whether different environmental conditions, experimenter-applied stimuli or modifying expression of other receptors or neuronal components is able to up- or down-regulate P2X expression in the various ganglia. This would give further indications of *Lym*P2X roles in the *Lymnaea* CNS.

The presence of *Lym*P2X in the buccal ganglia suggests a role in the feeding network, as the major components of the feeding pathway are located in the buccal ganglia (Benjamin and Rose, 1979). The feeding network is a neuronal pathway well characterised in *Lymnaea* (Benjamin and Rose, 1979, Elliott and Benjamin, 1985b). Widespread localization of *Lym*P2X also indicates a possible role in the respiratory network, another well studied neuronal pathway in *Lymnaea* (Syed *et al.*, 1990).

Chapter 4 conclusion

*Lym*P2X expression was observed in all ganglia by qRT-PCR, with highest relative expression in the pedal ganglia. Expression of *Lym*P2X in the buccal ganglia is of interest as it is where the major components of the *Lymnaea* feeding network are located, therefore implying possible roles of *Lym*P2X in the feeding network. *In situ* hybridization with DIG-labelled cRNA probes targeting *Lym*P2X transcripts on paraffin-embedded sections displayed staining in the majority of neurons, however there was a darker punctuate staining in the nucleus with a less diffuse signal in the cytoplasm.

Chapter 5: Assessing the potential function of *Lym*P2X in the feeding network of *Lymnaea stagnalis*

5.1 INTRODUCTION

Previous chapters focussed on the identification of a *Lymnaea* P2X receptor, its pharmacological characterization in *Xenopus* oocytes and localizing its expression in the *Lymnaea* central nervous system. This information can now guide studies to elucidate the physiological roles of *Lym*P2X in the *Lymnaea stagnalis* CNS, a simple model system that may prove useful in probing fundamental aspects of purinergic signalling in neuronal networks. P2X receptors have been previously found to play roles in synaptic transmission (Khakh and Henderson, 1998, Sim *et al.*, 2006), long term potentiation (Pankratov *et al.*, 2002), and pain sensation (Hamilton *et al.*, 2000).

Intracellular recordings of neurons located in ganglia where *Lym*P2X expression has been identified will provide further information that may suggest the physiological roles of *Lym*P2X. *Lymnaea* neurons are on average much larger than mammalian neurons (Moroz, 2000), making electrophysiological recordings and functional analysis easier and more accessible. *Lymnaea stagnalis* has a simple CNS, further facilitating the study of cyclical patterns of electrical burst activity in neurons, where the firing of neuronal components occurs in a defined temporal relationship (Benjamin and Rose, 1979). These rhythmic patterns in identified neurons (for example buccal motoneurons) in response to stimuli can be directly correlated to specific behavioural activity such as feeding.

*Lym*P2X expression was observed in all ganglia of the *Lymnaea* CNS, implying that *Lym*P2X is a component of many neuronal pathways and therefore potentially has a wide range of functions. One of the most studied and well characterized neuronal pathways in *Lymnaea* is the feeding network, which has its central pattern generator located in the buccal ganglia (Benjamin and Rose, 1979, Benjamin *et al.*, 2000). The movement of feeding muscles during ingestion activity of *Lymnaea* has been correlated to the phase-dependant activity of interneurons and motoneurons of the CNS buccal ganglia (Benjamin *et al*., 2000). The presence of *Lym*P2X expression in the buccal ganglia suggests a role of *Lym*P2X in the feeding network. Further indication of an important purinergic component of the feeding pathway was also recently shown by preliminary experiments in our laboratory that demonstrated inhibition of sucrose-induced feeding activity by injection of the P2 receptor antagonist PPADS into the *Lymnaea* body cavity (Waheeda Nasreen and Volko Straub personal communication).

The feeding central pattern generator (CPG) is an interconnected network of higher order interneurons (Elliott and Benjamin, 1985a) with the property of imposing rhythm on the motoneurons (Rose, 1981). The feeding CPG is composed of N1 type interneurons that are active during the protraction phase of feeding, the N2 type interneurons active during the rasp phase, and the N3 type interneurons active during the swallow phase of feeding (Figure 5.1). The CPG receives sensory information in response to chemical or tactile stimuli from the lips, and subsequently the CPG processes this information to specify feeding activity via motoneurons. Fictive feeding is the electrophysiological recording of phasic inputs from N1, N2 and N3 interneurons

of the CPG–driven rhythmic activity in the feeding network in the absence of feeding muscles (Kemenes and Elliott, 1994). These CPG interneurons have connections amongst each other and with motoneurons present in the buccal ganglia (Figure 5.1), and these motoneurons in turn have connections to the buccal mass. The buccal mass contains muscles to trigger movements of the radula (toothed tongue of a mollusc) for feeding.

The buccal ganglia motoneurons are classified as B1 – B10, based on their location and firing pattern (Benjamin and Rose, 1979). B1 motoneurons become excited during the protraction phase following N1 interneuron activation through cholinergic synapses, but do not receive inputs during the rasp and swallow phases (Elliott and Kemenes, 1992, Kemenes *et al.*, 1997, Vehovszky and Elliott, 2001) (Figure 5.1). The rasp phase is characterized by the activation of the N2 interneuron that excites the B3 motoneuron. The N3 interneuron is activated in the final swallow phase. B4 and B4Cl motoneurons are inhibited in the protraction phase and first part of the rasp phase (Kemenes *et al.*, 1997). However, they are excited through the second part of the rasp phase and during the swallow phase (Kemenes *et al.*, 1997) (Figure 5.1). The electrical activity of these feeding motoneurons have also been correlated to the sequential activity of muscles in the buccal mass involved in feeding movements (Rose and Benjamin, 1979). The discovery of motoneuron to interneuron electrotonic connections demonstrates that these feeding motoneurons in the buccal ganglia also play a small role in the maintenance of feeding rhythm generation (Staras *et al.*, 1998).

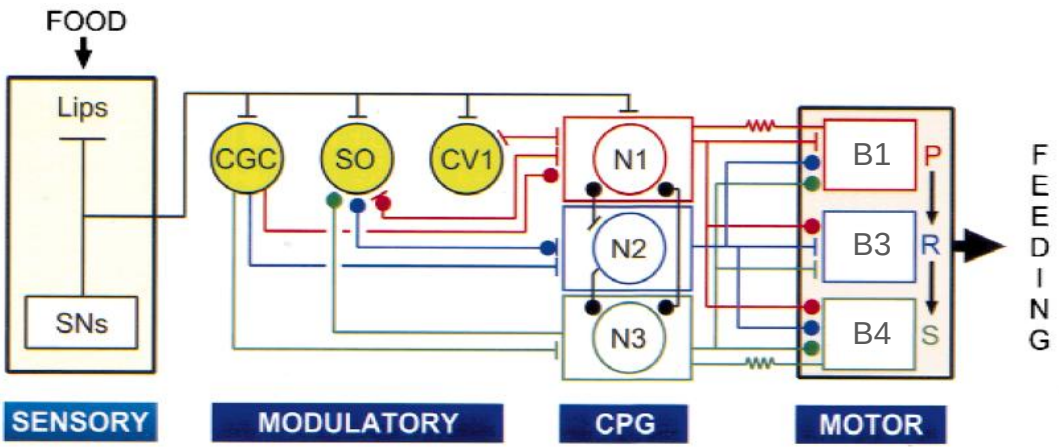

Figure 5.1. A schematic diagram displaying the connections between sensory and modulatory neurons with the feeding CPG, and CPG to motoneuron connections responsible for imposing the feeding rhythm. Inhibitory chemical (circles), excitatory chemical (vertical and diagonal bars) and electrotonic connections (crooked lines) between CPG N1, N2, and N3 interneurons, and between CPG interneurons to B1, B3 and B4 motoneuron connections are responsible for phasic activation of the motoneurons required for generation of feeding, following the sensory detection of food at the lips. Other buccal ganglia motoneurons (B2, B5 - 10), direct SO to motoneuron, and most motoneuron to interneuron connections are omitted for simplicity. Figure modified from Benjamin *et al.*, (2000).

In this chapter, the potential roles of *Lym*P2X in the feeding network will be assessed by making intracellular recordings of buccal ganglia motoneurons following purinergic receptor activation of neurons of isolated buccal ganglia preparations. This will provide a read-out of feeding activity induced by synaptic inputs received from CPG interneurons. Detection of fictive feeding cycles upon ATP application will demonstrate the direct influence purinergic signalling in the buccal ganglia has in the feeding network, and subsequent pharmacological characterisation may narrow the purinergic component responsible for rhythm generation to P2X or P2Y receptors. The effects of modulating *Lym*P2X expression on the feeding network will also be investigated using RNA interference in an attempt to silence *Lym*P2X expression.

5.2 METHODS

5.2.1 Sample preparation

Lymnaea CNS were dissected as described in Chapter 4 followed by cutting of the cerebrobuccal connective nerves to isolate the buccal ganglia. Isolated buccal ganglia were used rather than whole CNS preparations in order to prevent applied agonists from activating receptors in other ganglia and producing indirect effects (Yeoman *et al.*, 1994a, Yeoman *et al.*, 1994b, Wheelan H.A., 1996, Yeoman *et al.*, 1996). All essential neuronal components of the feeding network are located within the buccal ganglia. Snails were starved for 24 hours before dissection in order to increase spontaneous feeding activity (Kemenes and Elliott, 1994). This is due to reduction of tonic activity in the N3t interneuron of starved *Lymnaea* to a level not sufficient to suppress feeding CPG activity (Staras *et al.*, 2003).

5.2.2 Electrophysiological recordings

The feeding process of *Lymnaea stagnalis* consists of a sequence of three phases known as the protraction, rasp and swallow phases which constitute one feeding cycle (Figure 5.2) and results in movements of a toothed radula in response to chemical or tactile stimuli. These feeding cycle components can be detected by electrophysiological recordings from the large and easily identifiable B1 and B4 buccal ganglia motor neurons (Figure 5.2) that receive phasic inputs from CPG interneurons by chemical synapses (Elliott and Kemenes, 1992, Elliott *et al.*, 1992). Recording from the CPG interneurons N1 and N2 to directly monitor feeding activity is possible but difficult due

to their small size (10 – 25 µm) (Rose, 1981), and the fact that it is difficult to distinguish these interneurons from surrounding cells in the buccal ganglia. Therefore it was decided to record the large, easily identifiable motoneurons to monitor feeding activity in the buccal ganglia.

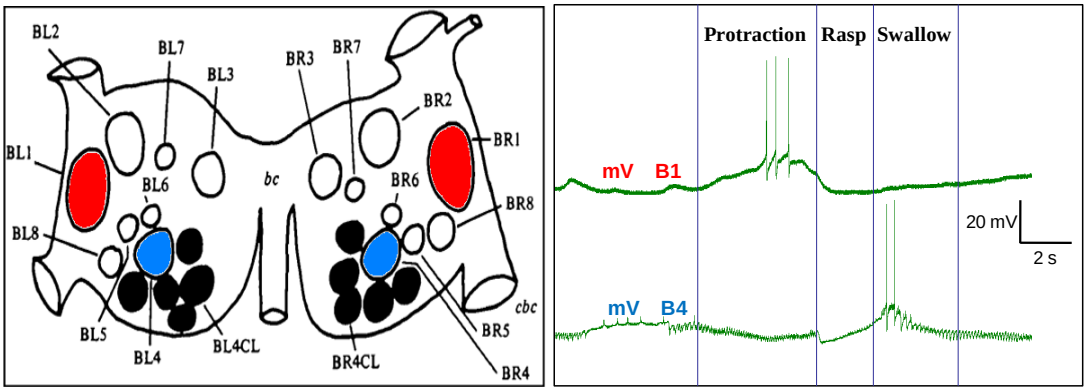

Figure 5.2. *Left*, Schematic of buccal ganglia motoneurons and their positions. Neurons from which recordings were made are highlighted in red (B1) and blue (B4). L = left, R = right. Figure modified from Benjamin and Rose, (1979). *Right*, recording of B1 and B4 motoneurons receiving inputs from CPG during a fictive feeding cycle. B1 is excited, sometimes with action potentials during the protraction phase. B4 receives inhibitory inputs during the protraction and rasp phases, and is excited in the swallow phase, occasionally with action potentials.

Intracellular recordings were made simultaneously from B1 and B4 motoneurons of the isolated buccal ganglia pinned out on a Sylgard-coated dish in the recording chamber. These motoneurons were visually identified based on their size and respective positions (Figure 2) using a microscope. Recording electrodes were pulled from 1.5 mm glass capillaries (GC150TF-10; Harvard apparatus, Kent, UK), dipped in ink for visualization and filled with 4 M potassium acetate to give a resistance of 20 - 30 MΩ. Recordings were made using a custom-built intracellular amplifier with a Digidata 1200 analogue

to digital converter (Axon Instruments U.S.A.) and Axoscope (version 8.0, Axon Instruments) acquisition software. Recordings were analysed using Spike2 software (Cambridge Electronics Design). Isolated buccal ganglia were treated with protease powder (Sigma, Poole, UK) for 1 min, to facilitate penetration of electrodes into the motoneurons. Protease digestion was stopped by thoroughly washing the buccal ganglia preparation with saline (composition: 50 mM NaCl, 1.6 mM KCl, 2 mM $MgCl_2$, 3.5 mM $CaCl_2$, 10 mM HEPES, pH 7.5).

Agonists (ATP (0.1 mM and 1 mM), ADP (1 mM), adenosine (1 mM), UTP (1 mM) and BzATP (400 µM)) were dissolved in saline and applied for 30 seconds to allow sufficient time for penetration. Antagonist studies were carried out with antagonist in the bathing solution (saline) as well as in the applied agonist solution. Bathing solution (with or without antagonist) and agonist solutions were superfused at a flow rate of 1 - 2 ml/min in the recording chamber. Solution exchange was facilitated by a voltage-operated valve system to allow flow of only agonist or bath solution through one superfusion outlet positioned ~1 cm away from the buccal preparation. Bathing volume was maintained at ~2 ml by removing excess bathing volume by suction pump.

Preparations were perfused in saline for 30 min before the first agonist application. Subsequent applications were made at 15 min intervals with each CNS preparation receiving a total of four agonist applications each for a continuous duration of 30 s. A 15 min interval between agonist applications was chosen after consideration of the desensitization characteristics of *Lym*P2X expressed in *Xenopus* oocytes (Chapter 2) where the 2nd - 4th applications of 100 µM ATP produced similar amplitude responses.

5.2.3 Data analysis

Integrals of the membrane potential recordings were determined relative to the membrane potential baseline using Spike 2 software (Version 6.03) for two min before agonist application, one min during agonist application, and one min after agonist application. The baseline was defined as the average membrane potential for the 2 min before agonist application without consideration of large depolarizing or hyperpolarizing shifts in this time period. The activity before agonist application was determined as the integral between the curve and the baseline during the two min period before the start of agonist application (expressed as mV.s). This activity before agonist application was compared to the integral between the depolarizing / hyperpolarizing curve and baseline for the min during and for the min after agonist application using one way analysis of variance (ANOVA) with Dunnett's test. B1 and B4 motoneuron depolarization was represented for the average 1st, 2nd, 3rd and 4th agonist applications as well as the average overall agonist applications (average depolarization of 1st – 4th application) to each buccal ganglia preparation. The net response was calculated as the difference between the depolarization during the min of agonist application and the integral relative to the baseline for the period before agonist application (difference between the orange and blue bars in Figures 5.3 – 5.9).

Feeding cycles during the min of agonist application were similarly compared to the feeding rate two min before agonist application using paired student's t-test. Feeding cycles in the recording were defined as shown in figure 5.2. The presence of a feeding cycle in a time frame was decided by occurrence of a notable B1 depolarisation concurrent with a simultaneous hyperpolarisation of the B4 motoneuron followed by a

hyperpolarizing hook of the B4 motoneuron recording at the end of protraction and start of rasp phase (Figure 5.2). Feeding activity is represented by the average number of feeding cycles per min at the 1st, 2nd, 3rd and 4th agonist application.

Depolarization / hyperpolarization and feeding cycles in response to agonist or antagonist was analysed by blind analysis. The recorded files were renamed by another person before analysing, to prevent bias of the effects by certain agonists or antagonist.

5.2.4 RNA interference with double stranded RNA

Lymnaea were deshelled, washed in 20 % listerine in saline for 10 min and transferred to antibiotic saline (ABS) (sterile normal saline + 20 µg/ml gentamicin). CNS were dissected as in chapter 4 in ABS, and washed 5 times for 5 min in ABS before being individually placed in 1.5 ml eppendorf tubes in 0.5 ml ABS containing double stranded RNA (dsRNA), also known as short interfering RNA (siRNA) at 400 nM and 2 µM concentration. siRNA sequences designed to target the *Lym*P2X receptor gene (offset = 1st nucleotide of sequence region targeted) for gene silencing were purchased from Qiagen and had the following sequences:

P2X-1-1 Target ACA GCT TGT TAT TAT TTC TTA

Offset : 126

Sense r(AGC UUG UUA UUA UUU CUU A)dTdT

Antisense r(UAA GAA AUA AUA ACA AGC U)dGdT

P2X-1-2 Target AAG AGG ATT CAA TTT CAG ATA

Offest 915

Sense r(GAG GAU UCA AUU UCA GAU A)dTdT

Antisense r(UAU CUG AAA UUG AAU CCU C)dTdT

Tubes containing siRNA and *Lymnaea* CNS were incubated at 22 ºC for 22 - 24 hours. Soaking worms in dsRNA without use of a transfecting agent or injection into cells has been previously shown to specifically silence the target mRNA by crossing cellular boundaries from outside the cell (Tabara *et al*., 1998). Similarly, injection of dsRNA constructs into the body cavity of *Lymnaea* has also been shown to result in gene silencing (Korneev *et al*., 2002). Control samples contained *Lymnaea* CNS preparations without any siRNA. RNA was extracted by RNeasy Fibrous Tissue Mini Kit and qRT-PCR was carried out on 0.3 ng of input cRNA as previously described in Chapter 4. Samples were quantified for *Lym*P2X mRNA relative to non-treated control (CNS not treated with siRNA) and normalised to β-tubulin.

5.3 RESULTS

5.3.1 Responses evoked by 100 µM ATP application

Intracellular recordings of B1 and B4 buccal ganglia motoneurons were carried out to investigate how membrane potential and feeding activity are affected upon the application of various purinergic agonists and antagonists. Since the results from Chapter 2 showed that 100 µM ATP application evokes a maximal activation of *Lym*P2X, this concentration of ATP was used as a starting point to assess the role of *Lym*P2X on buccal ganglia activity. 100 µM ATP applications to isolated buccal ganglia evoked depolarization of the B1 and B4 motoneurons (Figure 5.3A). The increase in membrane potential of B1 and B4 exhibited a slow onset. After averaging the recordings of four ATP applications to each preparation, the B1 motoneurons had a depolarization of 142.5 ± 44.1 mV.s during ATP application, compared to the integral relative to the curve of 67.3 ± 35.0 mV.s before agonist application ($p < 0.05$, $n = 5$; Figure 5.3C). The area between the depolarizing curve and baseline in the min during 100 µM ATP application for B4 motoneuron was 80.3 ± 26.5 mV.s, which was significantly greater than the integral of the curve relative to the baseline before ATP application (13.0 ± 17.3 mV.s) ($p < 0.05$, $n = 7$; Figure 5.3D). However, responses to each of the four individual 100 µM applications to each buccal ganglia were not always significantly higher than the baseline, demonstrating that depolarization was variable. The depolarization of the B1 and B4 motoneuron during the min after 100 µM ATP application was not significantly different from the integral relative to the baseline before 100 µM ATP application ($p > 0.05$ for B1 and B4).

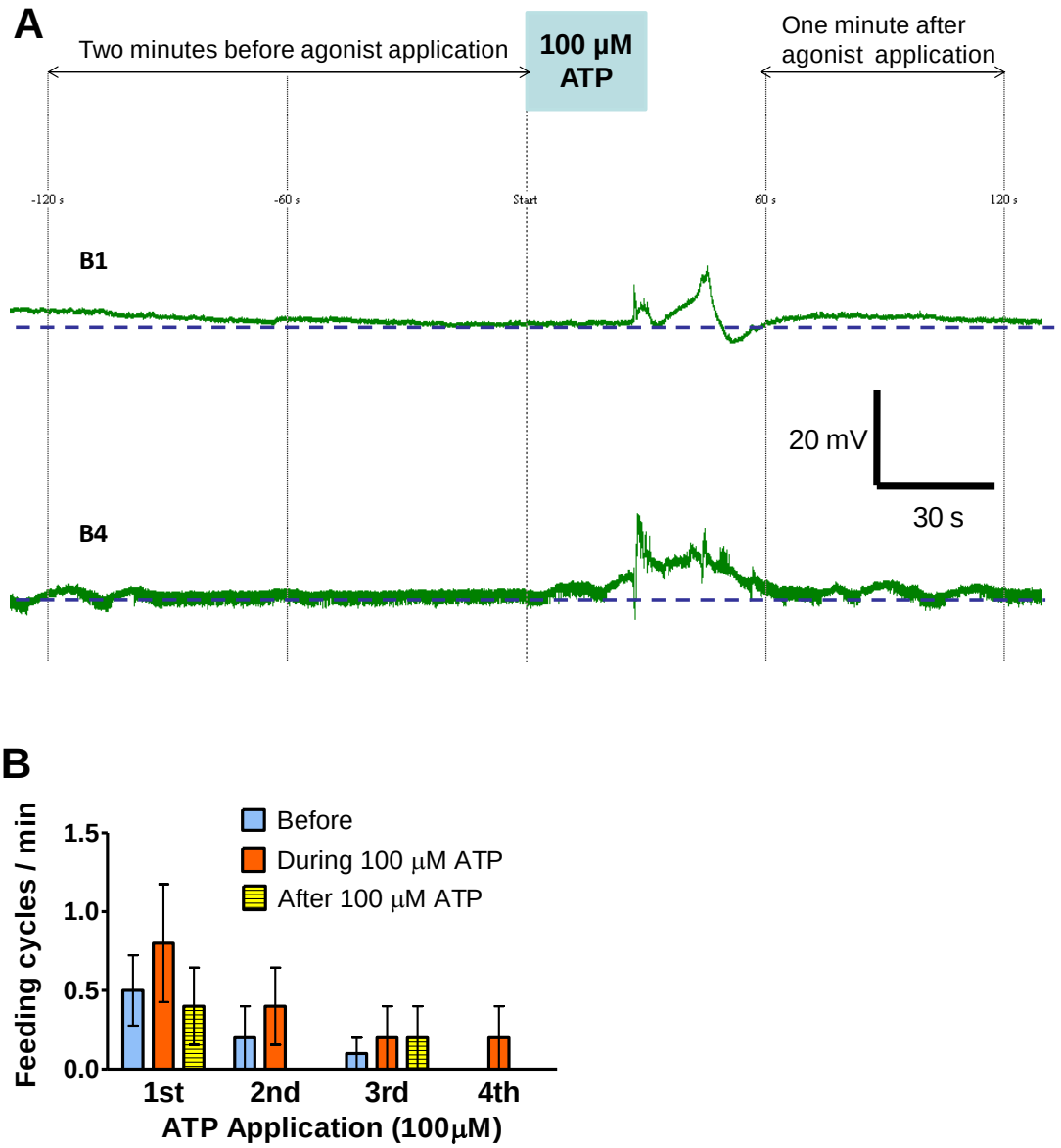

Figure 5.3. A, representative trace of intracellular recording of B1 and B4 buccal motoneurons. 100 µM ATP application caused small depolarization of the B1 and B4 motoneurons, but did not increase fictive feeding rate. The resting membrane potential (baseline) for the B1 and B4 motoneurons is highlighted by a blue line. B, bar graph showing the average fictive feeding rate at the 1st, 2nd, 3rd and 4th 100 µM ATP applications, compared to the feeding rate before and 1 min after the corresponding ATP application (n = 5).

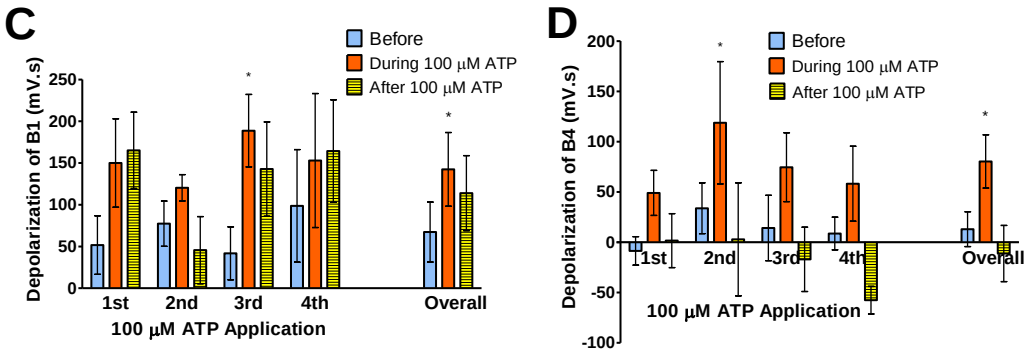

Figure 5.3C and D, bar graphs showing depolarization of B1 and B4 at the 1st, 2nd, 3rd and 4th 100 μM ATP applications and average depolarization for all recorded preparations, compared to before and 1 min after ATP application.

Whilst 100 µM had clear effects on motoneuron activity, it did not increase fictive feeding compared to the spontaneous feeding rate prior to ATP applications (Figure 5.3B). For example, during the 1st 100 µM ATP application the feeding rate was 0.84 ± 0.37 feeding cycles/min, whereas before 100 µM ATP application the spontaneous feeding rate was 0.50 ± 0.22 feeding cycles/min, ($n = 5$, $p > 0.05$) (Figure 5.3B). The feeding rate for the min after 100 µM ATP application also did not appear to increase.

5.3.2 Effects of increasing ATP concentration to 1 mM on fictive feeding rate

The lack of effect on feeding activity could be due to the low level of penetration of the applied 100 µM ATP through the connective tissue and other barriers, leading to reduced ATP concentrations at the sites of purinergic receptors on *Lymnaea* sensory or modulatory neurons. Since PPADS was found to inhibit sucrose-induce feeding in the laboratory, it was of interest to look further at the possibility of ATP-evoked fictive feeding. Therefore to increase the likelihood of obtaining a maximum response-evoking ATP concentration at the *Lym*P2X sites in buccal ganglia neurons, 1 mM ATP was applied to the buccal ganglia.

The first 1 mM ATP application significantly increased the fictive feeding rate to 1.29 ± 0.52 feeding cycles/min from the spontaneous feeding rate of 0.29 ± 0.15 feeding cycles/min ($p < 0.05$, $n = 7$) (Figure 5.4A and B). Feeding cycles occurred after an average latency of 11.3 ± 2.4 s after the start of ATP application. Subsequent 1 mM ATP applications did not increase the rate of fictive feeding ($p > 0.05$) (Figure 5.4 B).

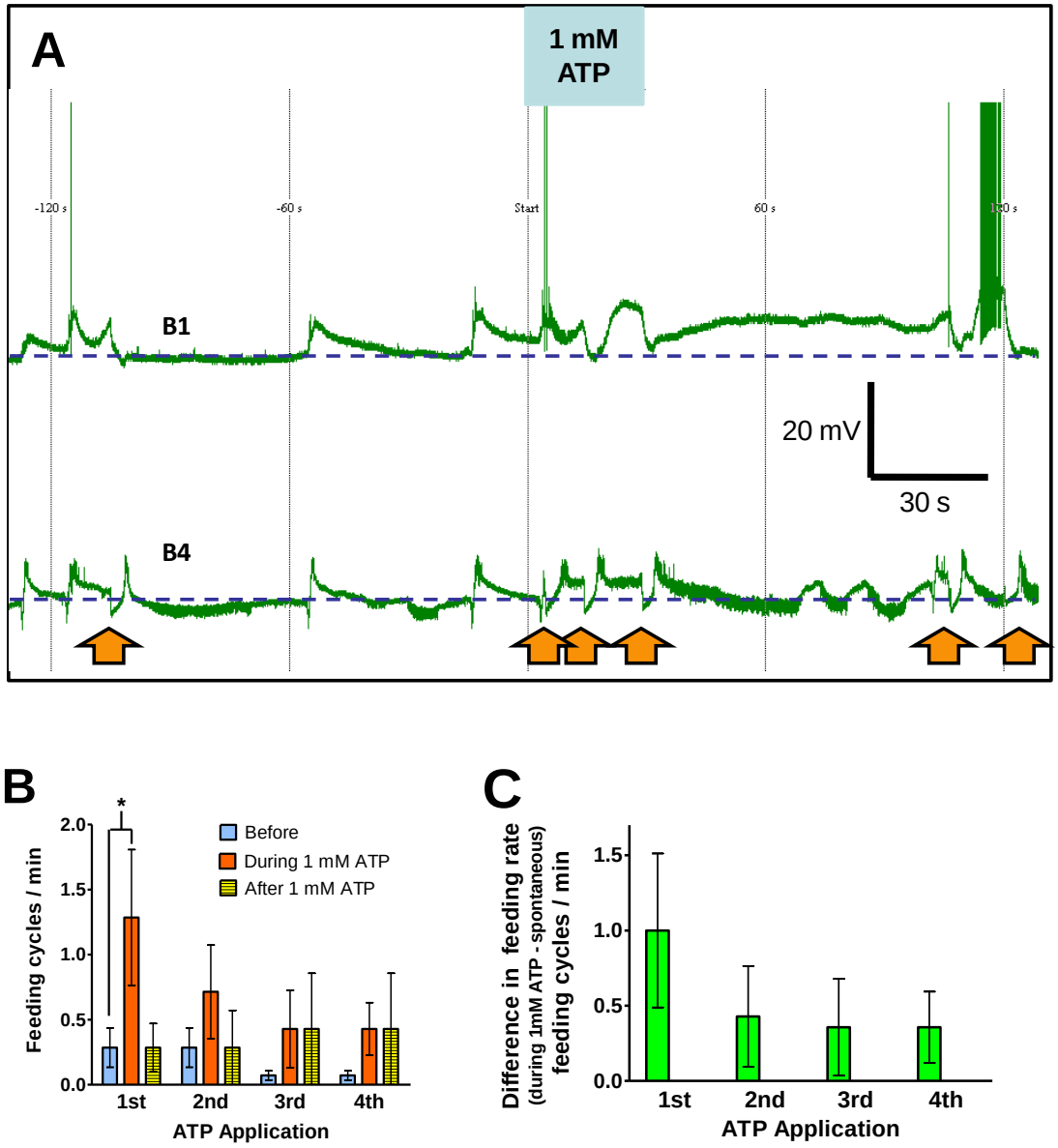

Figure 5.4. A, Representative trace showing 1 mM ATP-evoked depolarization of B1 and B4, and higher rate of fictive feeding. Feeding cycles are highlighted by orange arrows beneath the start of the rasp phase. B, bar graph showing the average fictive feeding rate at the 1st, 2nd, 3rd and 4th 1 mM ATP applications, compared to the rate before and 1min after the corresponding ATP application (n = 7). C, difference between 1 mM ATP-evoked feeding rate and spontaneous rate at each ATP application, which appeared to decrease at each application.

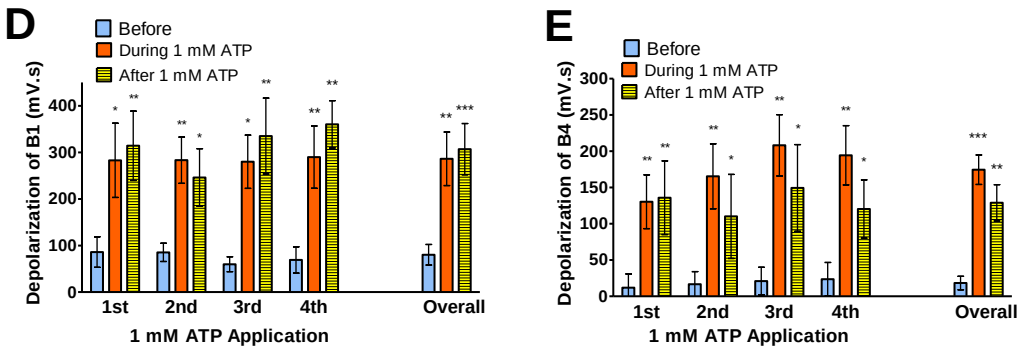

5.4D and E, bar graph showing depolarization of B1 and B4 at the 1st, 2nd, 3rd and 4th 1 mM ATP applications, compared to before and 1 min after 1 mM ATP application. * = $p < 0.05$, ** = $p < 0.01$, *** = $p < 0.001$.

The net change in feeding rate appeared to decrease with subsequent ATP applications (Figure 5.4C).

1 mM ATP applications also evoked significant levels of depolarization at the motoneurons, and this depolarization was maintained a min after ATP application at both B1 and B4 (Figure 5.4D and E). The B4 motoneuron had an average depolarization during 1 mM ATP application of 174.6 ± 33.2 mV.s, significantly higher than the integral relative to the baseline before agonist application of 18.3 ± 9.3 mV.s ($p < 0.001$, $n = 7$). One min after ATP application, the B4 motoneuron depolarization was 129.0 ± 42.3 mV.s, also significantly greater than the integral relative to the baseline before agonist application ($p < 0.01$). 1 mM ATP-evoked depolarization of B1 motoneuron had an area under the depolarizing curve of 286.6 ± 30.5 mV.s, significantly greater than the integral of the curve relative to the baseline of 76.1 ± 12.1 mV.s ($p < 0.01$). One min after ATP application the B1 motoneuron depolarization was 306.9 ± 54.9 mV.s, also significantly greater than the integral before agonist application ($p < 0.01$). This effect was very consistent as indicated by the fact that each of the 1st, 2nd, 3rd and 4th 1 mM ATP applications to the buccal ganglia preparations evoked significantly higher depolarization both during and 1 min after ATP application compared to the activity before agonist application at both B1 and B4 (Figure 5.4D and E). The depolarization of B1 and B4 across the 4 ATP applications did not significantly change ($p > 0.05$). The net depolarizing effect of 1 mM ATP on B1 and B4 was significantly greater than the depolarizing effect by 100 µM ATP ($p < 0.05$ for both B1 and B4) (Table 1).

5.3.3 PPADS effects on 1 mM ATP-evoked fictive feeding

100 µM PPADS reduced *Lym*P2X current amplitudes by over 80 % in *Xenopus* oocytes (Chapter 2). In order to study whether the 1 mM ATP-evoked increase in fictive feeding involves activation of PPADS sensitive receptors, preparations were exposed to this antagonist to see if ATP-induced feeding activity and motoneuron responses could be blocked. This would implicate activation of particular P2X and P2Y receptors in rhythm generation. 100 µM PPADS when present in both bathing and agonist solutions abolished the 1 mM ATP-evoked increase in fictive feeding at the first ATP application (before: 0.71 ± 0.39 feeding cycles/min, during 1 mM ATP application with 100 µM PPADS: 0.57 ± 0.43 feeding cycles/min, $n = 7$, $p > 0.05$), in addition to not having significant effects on feeding activity upon subsequent ATP applications ($p > 0.05$). However, PPADS during ATP application did not significantly alter the fictive feeding rate compared to spontaneous rate (no agonist or antagonist). There was also inhibition of the ATP-evoked depolarization of the B4 motoneuron. The integral of the curve relative to the baseline before ATP application of the B4 motoneuron was 8.3 ± 10.1 mV.s, compared to 43.6 ± 8.3 mV.s depolarization during 1 mM ATP with 100 µM PPADS ($p > 0.05$), and 13.6 ± 27.0 mV.s depolarization for the min after agonist application ($p > 0.05$) (Figure 5.5D). The net depolarization of B4 during 1 mM ATP with 100 µM PPADS application was 35.3 ± 22.0 mV.s, which was significantly lower ($p < 0.01$) than the net depolarization of B4 by 1 mM ATP (no PPADS) of 156.3 ± 27.3 mV.s (Table 1). However B1 motoneuron depolarization by 1 mM ATP was neither prevented both during or 1 min after ATP application in 100 µM PPADS (Figure 5.5C). Depolarization during 1 mM ATP application in 100 µM PPADS was 251.5 ± 59.8 mV.s ($p < 0.05$), for the 1 min after ATP application was 262.8 ± 53.1 mV.s ($p < 0.05$), compared to the integral of B1 before agonist application of 85.9 ±

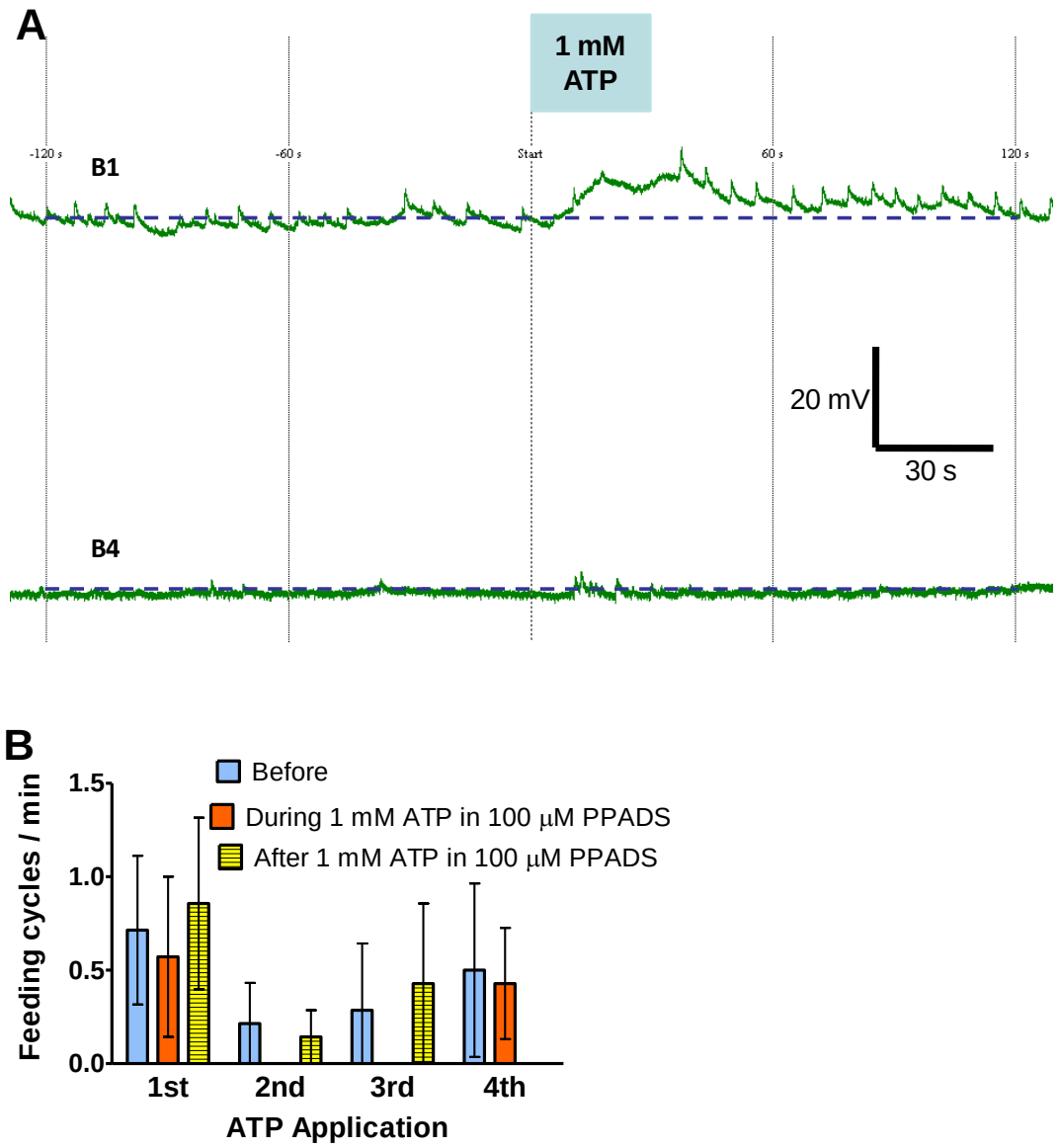

Figure 5.5. A, Representative trace showing 1 mM ATP-evoked fictive feeding is prevented in the presence of 100 μM PPADS. B, bar graph showing the average fictive feeding rate at the 1st, 2nd, 3rd and 4th 1 mM ATP applications in PPADS, compared to the feeding rate before and 1 min after the corresponding ATP application (n = 5).

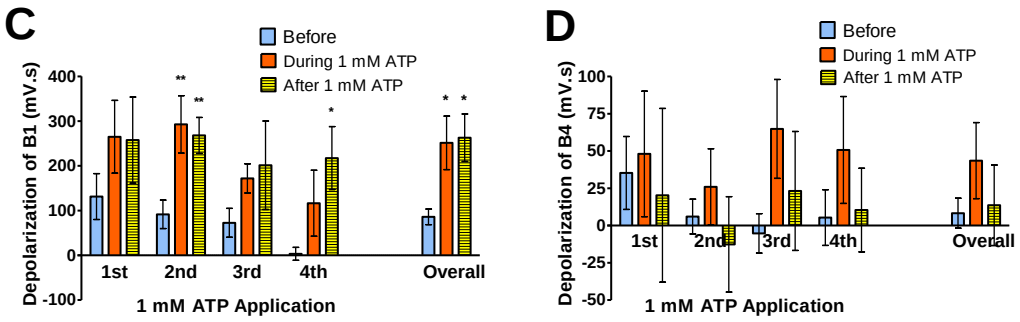

5.5C and D, bar graph showing depolarization of B1 and B4 at the 1st, 2nd, 3rd and 4th 1 mM ATP applications in PPADS, compared to before and 1 min after 1 mM application (* = $p < 0.05$, ** = $p < 0.01$).

17.4 mV.s (Figure 5.5C). The net depolarization of B1 during 1 mM ATP with 100 µM PPADS exposure was 165.5 ± 68.6 mV.s, and this value was not significantly different ($p > 0.05$) to the net depolarization of B1 by 1 mM ATP without PPADS (206.3 ± 64.3 mV.s). Therefore 100 µM PPADS had an inhibitory effect on B4 depolarization and prevented the increase in fictive feeding rate upon the 1st 1 mM ATP application, while having no significant effect on B1 depolarization.

5.3.4 Effects of ADP and adenosine

The effects of the 1st 1 mM ATP application on increasing fictive feeding rate and depolarization of motoneuron could possibly be a consequence of ATP breakdown products, due to the presence of endogenous ectonucleotidases near the receptor sites that cleave off phosphates from ATP, before binding to purinergic receptors (Zimmermann, 1996). These breakdown products could be ADP, which can act on P2Y receptors, or adenosine that can evoke responses at P1 receptors.

ADP was therefore tested for its effects on buccal ganglia activity. ADP was previously shown in Chapter 2 to not evoke currents at *Lym*P2X, consistent with P2X receptors in other species that are also not activated by ADP (Mahaut-Smith *et al*., 2000), with the exception of $P2X_5$ homomers (Wildmann *et al*., 2002). ADP application to *Lymnaea* neurons will therefore inform us about the existence of ADP-sensitive P2Y receptor component in buccal ganglia activity.

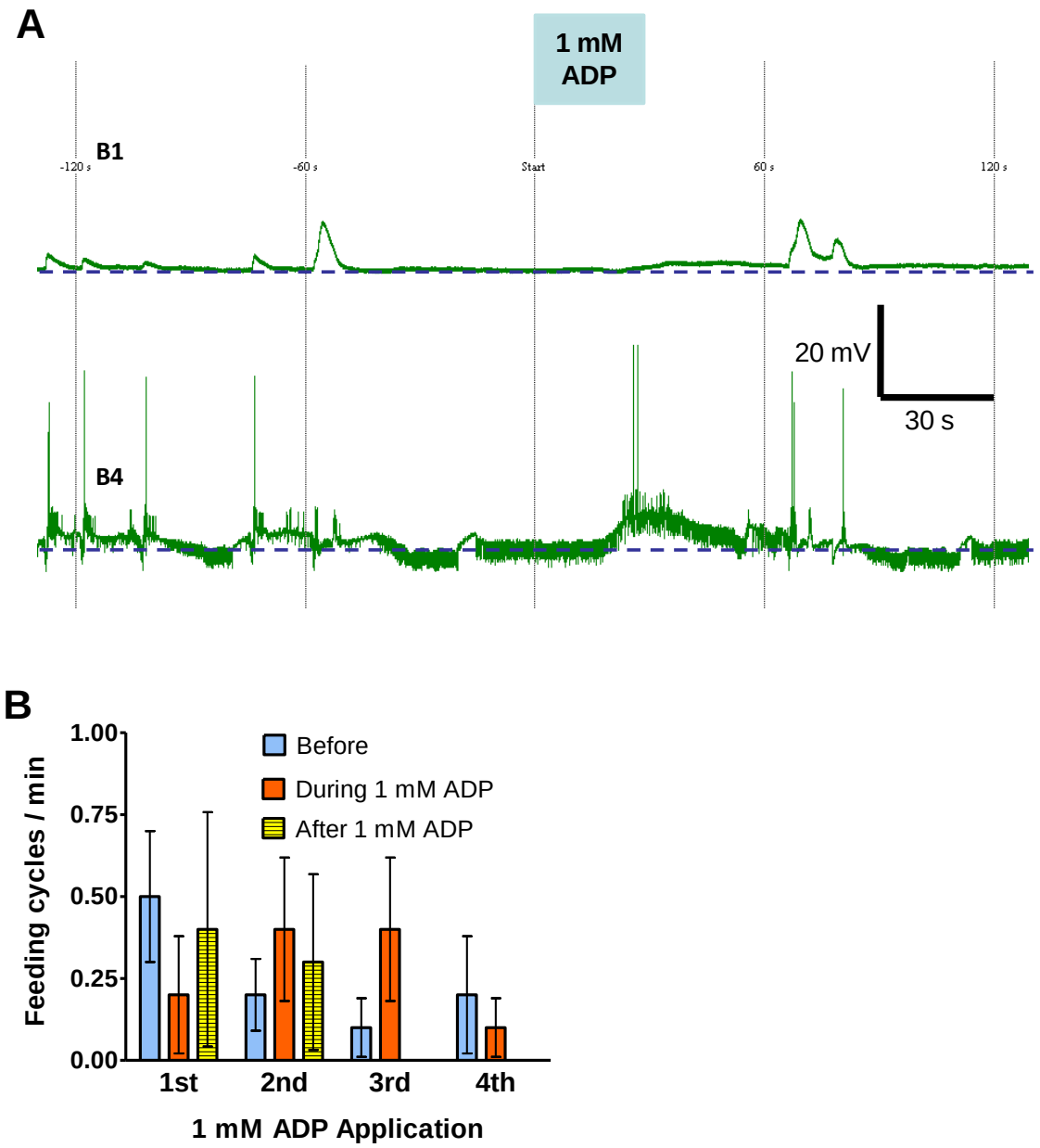

Figure 5.6. A, representative trace showing 1 mM ADP does not trigger fictive feeding. B, bar graph showing the average fictive feeding rate at the 1st, 2nd, 3rd and 4th 1mM ADP applications, compared to the feeding rate before and 1 min after the corresponding ADP application (n = 5).

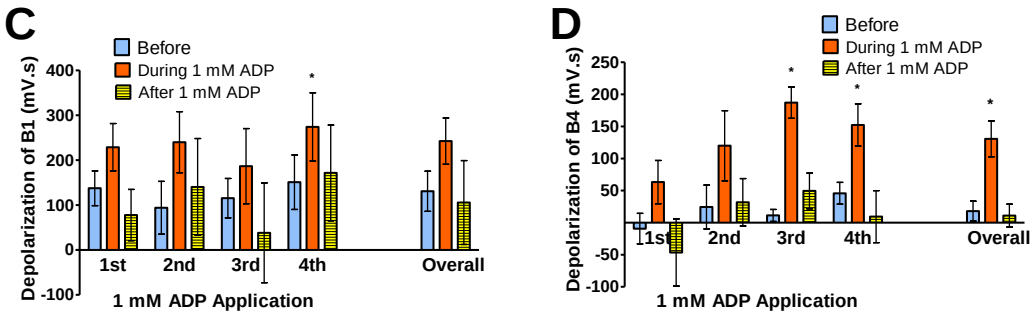

5.6C and D, bar graph showing depolarization of the B1 and B4 motoneurons at the 1st, 2nd, 3rd and 4th 1 mM ADP applications, compared to before and 1 min after ADP application. (* = $p < 0.05$).

The feeding rate for the first ADP application was 0.4 ± 0.3 cycles/min, which was not significantly different to the spontaneous activity of 0.2 ± 0.2 cycles/min ($p > 0.05$). Similarly, subsequent ADP applications also did not alter feeding rate ($p > 0.05$, $n = 5$) (Figure 5.6B). ADP application was only observed to significantly depolarize B4 motoneuron during the min of the agonist application without altering B1 motoneuron depolarization significantly (Figure 5.6), however a small net depolarization of B1 was seen to be evoked by ADP in all the recorded buccal preparations. The depolarization of the B4 motoneuron during the min of 1 mM ADP application (130.6 ± 27.9 mV.s) was significantly greater ($p < 0.01$) than the integral of the curve relative to the baseline before ADP application (18.0 ± 15.5 mV.s) for overall recordings. However, for each ADP application there was not a significant depolarization due to the variability in the responses (Figure 5.6C and D). ADP application did not have significant depolarizing effects one min after ADP application at the B4 motoneuron (11.0 ± 17.8 mV.s) ($p > 0.05$).

Adenosine is also another possible breakdown product of ATP, and its effects at the buccal ganglia were tested to see if non-P2 purinergic receptors such as adenosine-sensitive P1 receptors mediate any significant effects. 1 mM adenosine application did not cause significant depolarization of the B1 and B4 motoneurons, compared to the baseline before agonist application ($p > 0.05$ for both B1 and B4, during and 1 min after adenosine application). The feeding rate also did not significantly alter upon 1 mM adenosine application (eg. fictive feeding rate before the first adenosine application: 0.83 ± 0.71 feeding cycles/min, during 1 mM adenosine: 0.5 ± 0.43 feeding cycles/min, $p > 0.05$, $n = 6$) (Figure 5.7). 1 mM adenosine applications also did not evoke significant depolarization of the B1 or B4 motoneurons compared to the effects before

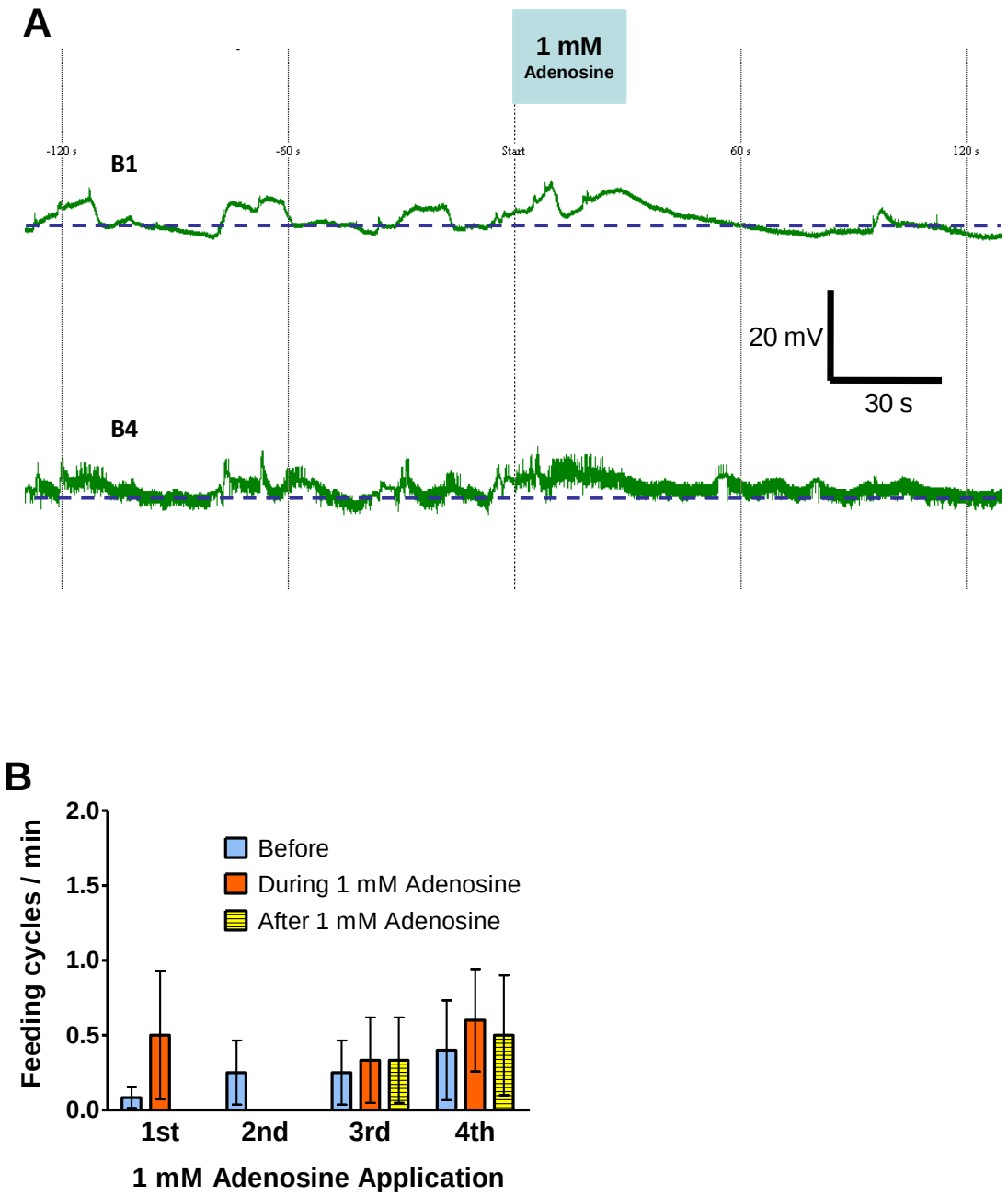

Figure 5.7. A, representative trace showing 1 mM adenosine did not trigger fictive feeding or depolarization of B1 or B4. B, bar graph showing the average fictive feeding rate at the 1st, 2nd, 3rd and 4th 1 mM adenosine applications, compared to the feeding rate before and after the corresponding adenosine application (n = 5).

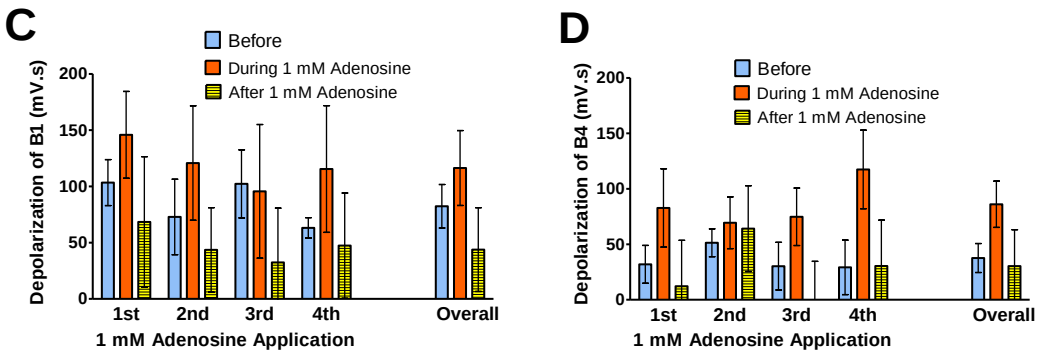

5.7C and D, bar graph showing depolarization of B1 and B4 motoneurons at the 1st, 2nd, 3rd and 4th 1 mM adenosine application, compared to before and 1 min after adenosine application.

agonist application (Figure 5.7C and D). These effects of adenosine are different to the responses upon application of the P2Y agonist ADP, which evoked a significantly greater net depolarization of both B1 and B4 motoneuron than adenosine (ADP = 111.7 ± 19.2 mV.s and 112.6 ± 16.6 mV.s, adenosine = 34.0 ± 18.3 mV.s and 48.5 ± 13.3 mV.s, $p < 0.01$ for both B1 and B4 respectively).

5.3.5 UTP evoked strong depolarizing effects on motoneurons

Since the effects of ADP on depolarization of buccal motoneurons were stronger than adenosine, and *Lym*P2X being found to be insensitive to ADP, the P2Y component of the feeding network was investigated further. Another nucleotide, UTP, has been previously found to activate some vertebrate P2Y receptor subtypes (Lustig *et al.*, 1993), and only activate $P2X_5$ of the P2X subtypes (Wildmann et al., 2002). To determine the presence of UTP-sensitive P2Y receptors and analyse if their activation can increase fictive feeding rate, 1 mM UTP was applied to buccal ganglia preparations. UTP was found to significantly depolarize both B1 and B4 neurons at the time periods during and 1 min after agonist application (Figure 5.8C and D). Before UTP application, B1 motoneuron had an integral relative to the baseline of 46.4 ± 45.0 mV.s, compared to depolarization of 284.3 ± 77.6 mV.s during 1 mM UTP application ($p < 0.05$), and 326.8 ± 59.3 mV.s for the min after UTP application ($p < 0.01$). Prior to UTP exposure, B4 motoneuron had an integral relative to the baseline of 42.2 ± 22.9 mV.s before UTP application, compared to 137.4 ± 45.9 mV.s during 1 mM UTP application ($p < 0.01$), and 159.6 ± 34.4 mV.s depolarization for the min after UTP application ($p < 0.01$).

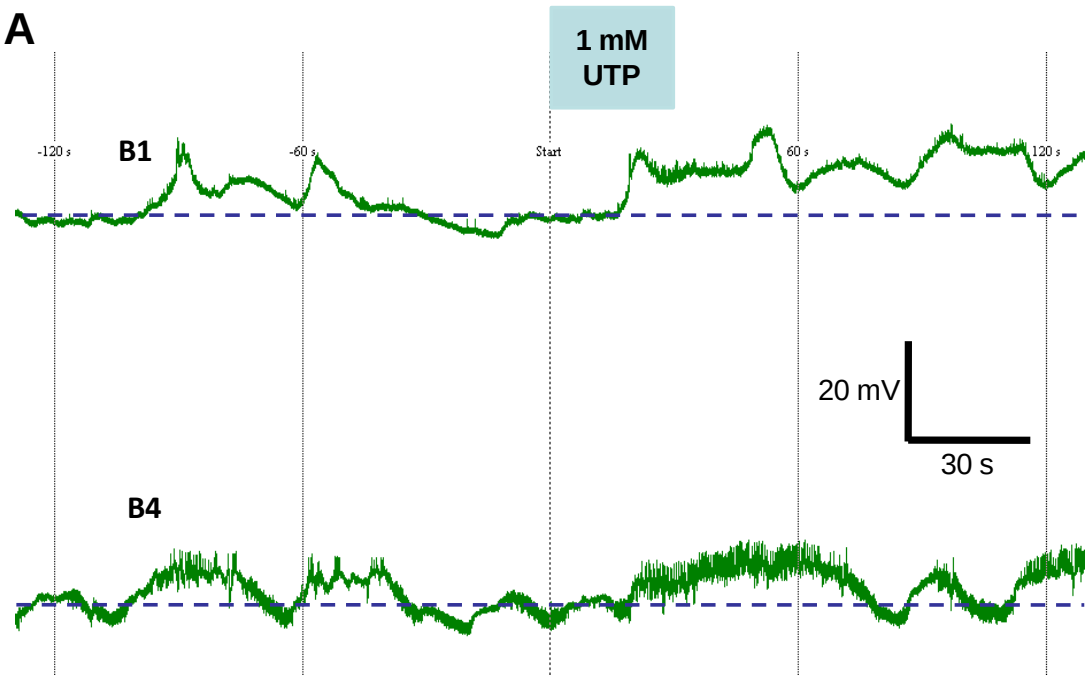

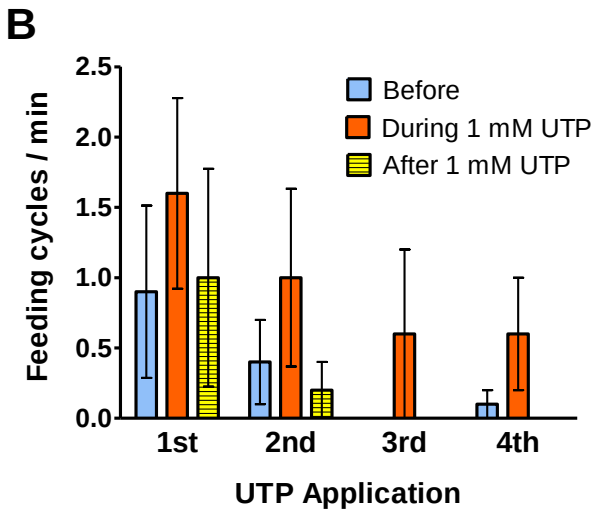

Figure 5.8. A, representative trace showing 1 mM UTP depolarizes B1 and B4, but does not trigger fictive feeding. B, bar graph showing the average fictive feeding rate at the 1st, 2nd, 3rd and 4th 1 mM UTP applications, compared to the feeding rate before and 1 min after the corresponding UTP application (n = 5).

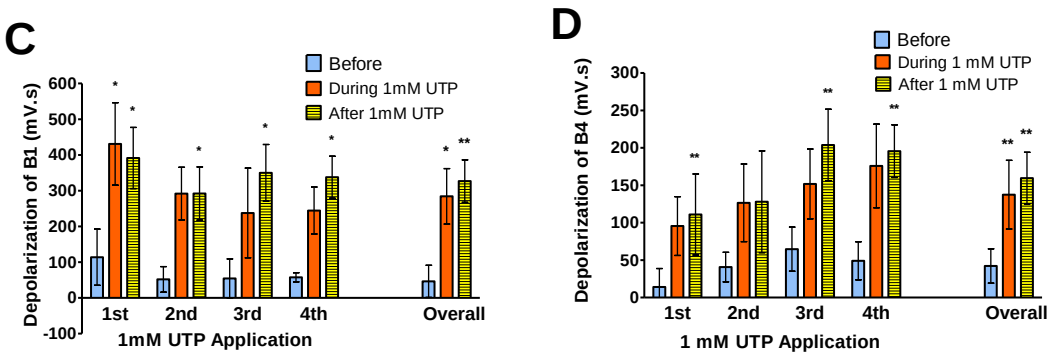

5.8C, bar graph showing depolarization of B1 and B4 motoneurons at the 1st, 2nd, 3rd and 4th 1 mM UTP applications, compared to before and 1 min after UTP application. (* = $p < 0.05$, ** = $p < 0.01$).

There appeared to be a net increase of fictive feeding of ~0.7 cycles/min across the four applications of UTP (Figure 5.8B). 2 of the 5 preparations recorded showed increased feeding activity relative to the spontaneous feeding rate. However the perceived increase in fictive feeding rate was not statistically significant at either of the four 1 mM UTP applications. For example, the feeding rate during the first 1 mM UTP application was 1.6 ± 0.7 feeding cycles/min, compared to the spontaneous feeding rate of 0.9 ± 0.6 cycles/min ($p > 0.05$, $n = 5$), with subsequent UTP applications not having a statistically significant effect on fictive feeding rate either (Figure 5.8B). The net effects of UTP on B1 motoneuron net depolarization were significantly stronger than ADP ($p < 0.05$) (Table 1). This is in agreement with previous findings that UTP is a more potent agonist than ADP at the majority of P2Y subtypes (von Kugelgen, 2006). However net depolarization evoked by UTP at B4 was not significantly different to that evoked by 1 mM ADP ($p > 0.05$). The net depolarizing effect by 1 mM UTP at B1 and B4 were not significantly different to the level of net depolarization evoked by 1 mM ATP at these motoneurons ($p > 0.05$ for both) (Table 1).

5.3.6 Application of BzATP in attempt to selectively activate P2X receptors

To further examine if the depolarization and increased feeding rate upon 1 mM ATP application is due to *Lym*P2X or to unidentified P2Y receptors, the ATP analogue BzATP was also analysed. BzATP is a partial agonist at the cloned *Lym*P2X receptor with an EC_{50} of 2.4µM and maximal currents ~80% of maximum ATP currents (Chapter 2). BzATP does not activate the large majority of P2Y receptors (von Kugelgen, 2006). Of the eight human P2Y receptors only $P2Y_{11}$ is activated by BzATP

where it is more potent than ATP (Communi *et al.*, 1999). BzATP is also reported to be an antagonist at $P2Y_1$ receptors from some but not all species (Vigne *et al.*, 1999). Therefore BzATP can be applied almost as a selective agonist for P2X, on the condition that *Lymnaea* P2Y receptors are also largely not activated by BzATP. This would allow closer determination and analysis of P2X roles in feeding. 400 µM BzATP was applied in order to increase the likelihood of obtaining a maximum-response evoking BzATP concentration at the receptor sites. BzATP injection into the body cavity of intact *Lymnaea* in the preliminary study was interestingly found to reduce the rate of sucrose-induced feeding (Waheeda Nasreen and Volko Straub personal communication). However in this study, 400 µM BzATP did not significantly alter the feeding rate compared to the spontaneous feeding rate at the first application (before: 0.4 ± 0.27 feeding cycles/min, during 400 µM BzATP: 0.6 ± 0.4 feeding cycles/min, $n = 5$, $p > 0.05$), or for subsequent applications ($p > 0.05$) (Figure 5.9 and B). BzATP however did trigger a significant depolarization of B1 neurons compared to the integral of the curve relative to the baseline before agonist application. This depolarization however was transient and was not maintained a min after BzATP application (Figure 5.9C). B1 motoneuron exhibited an integral relative to the baseline of 37.6 ± 7.3 mV.s before BzATP application, compared to 105.0 ± 18.1 mV.s ($p < 0.05$) during BzATP application and 2.0 ± 47.2 mV.s depolarization for the min after BzATP application ($p > 0.05$). Interestingly, BzATP (400µM) triggered significant hyperpolarization of B4 motoneuron, both during application (-86.2 ± 22.1 mV.s ($p < 0.05$)) and for the min after BzATP application, where the hyperpolarisation was stronger (-260.5 ± 30.0 mV.s ($p < 0.01$)) compared to the integral relative to the baseline before BzATP application of 2.2 ± 10.4 mV.s (Figure 5.9D). This demonstrates that while BzATP effects at B1 motoneuron occur during the min of agonist application, the effects at B4 motoneuron

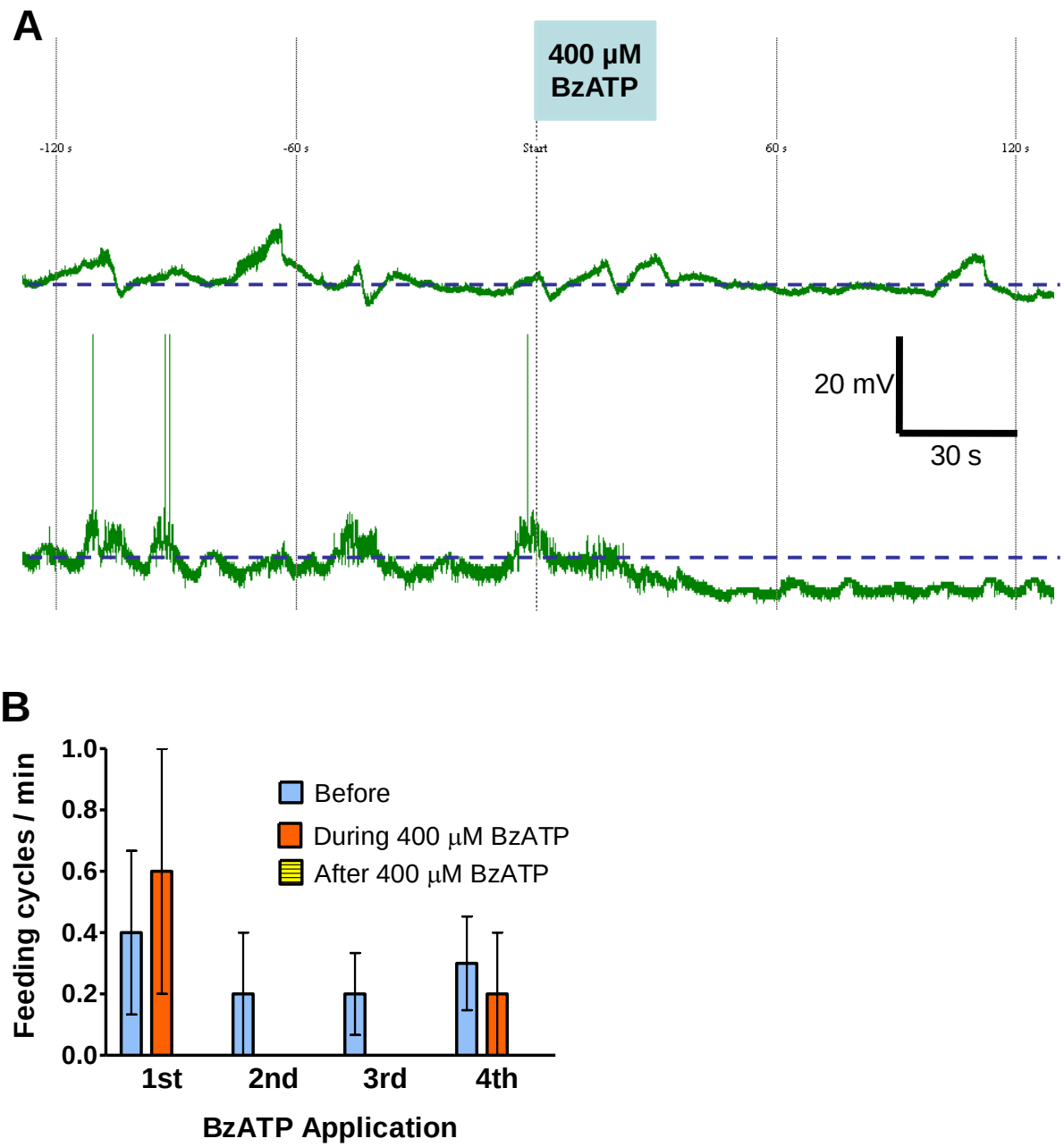

Figure 5.9. A, representative trace showing 400 µM BzATP caused hyperpolarization of B4, depolarization of B1, and did not trigger fictive feeding. B, bar graph showing the average fictive feeding rate at the 1st, 2nd, 3rd and 4th BzATP applications, compared to the feeding rate before and 1 min after the corresponding BzATP application (n = 5).

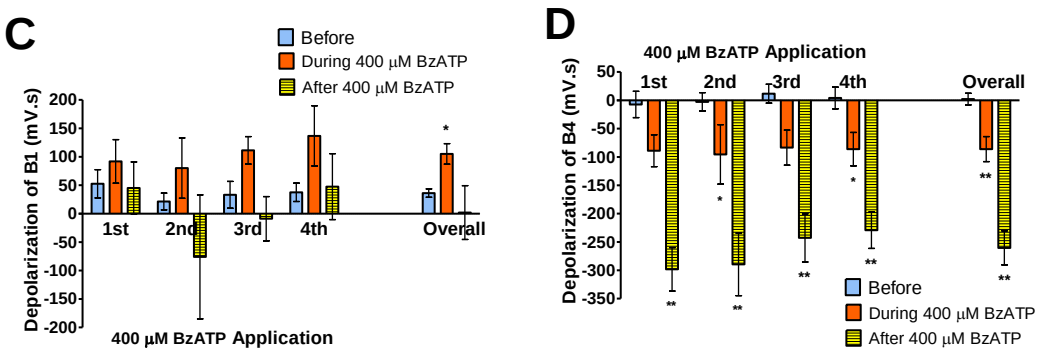

5.9C and D, bar graph showing depolarization of B1 and B4 motoneurons at the 1st, 2nd, 3rd and 4th BzATP, compared to before and 1 min after BzATP application.

are maintained for a longer time period. The net depolarization of B1 motoneuron evoked by 400 µM BzATP was significantly less than that triggered by 1 mM ATP ($p < 0.05$).

	B1 (ΔmV.s)	**B4 (ΔmV.s)**	**Δ feeding rate (1st application)**
100 µM ATP	75.1 ± 10.5 *	67.3 ± 13.3 *	0.3 ± 0.2
1 mM ATP	206.3 ± 64.3 **	156.3 ± 27.3 **	1.0 ± 0.5 *
1 mM ATP + 100 µM PPADS	165.5 ± 68.6 *	35.3 ± 22.0	-0.1 ± 0.5
1 mM ADP	111.7 ± 19.2	112.6 ± 16.6 *	-0.2 ± 0.2
1 mM Adenosine	34.0 ± 18.3	48.5 ± 13.3	0.4 ± 0.4
1 mM UTP	237.9 ± 51.5 **	95.3 ± 33.8 *	0.7 ± 0.7
400 µM BzATP	68.8 ± 21.5 *	-88.3 ± 21.7 *	0.2 ± 0.2

Table 1. Effect of agonists and antagonists on net depolarization (depolarization during agonist application – integral relative to the baseline before agonist application) and Δ fictive feeding rate (feeding rate during agonist application – feeding rate before agonist application). * = $p < 0.05$, ** = $p < 0.01$ for significant depolarization /hyperpolarization or increased fictive feeding rate.

5.3.7 Silencing LymP2X by RNA interference

Classical gene knock-out technologies have not been developed for molluscs. Therefore, in order to directly evaluate the importance of *Lym*P2X receptors in the feeding network of *Lymnaea*, an attempt to selectively reduce *Lym*P2X expression was carried out using the method of RNA interference. This technique disrupts expression of specific genes by application of a short RNA molecule corresponding to the gene of

interest and was first used in silencing the expression of *unc-22* gene in *C. elegans* (Fire *et al*., 1998). RNA interference has subsequently been successfully applied to a range of organisms including *Lymnaea* (Korneev *et al*., 2002).

In this study RNA interference was utilised in an effort to correlate expression levels of *Lym*P2X with altered behavioural or electrophysiological properties such as feeding behaviour. Isolated *Lymnaea* CNS were incubated with siRNA (at 400 nM or 2 µM) targeting different regions of the *Lym*P2X nucleotide sequence (start positions 126 and 915), followed by qRT-PCR to assess gene knock-down. Both siRNA molecules investigated did not produce a significant change in the relative quantity of *Lym*P2X mRNA at either of the concentrations tested ($p > 0.05$, $n = 4$ CNS preparations for each siRNA at each concentration) (Figure 5.10) demonstrating an inability of these siRNAs to silence *Lym*P2X expression.

A

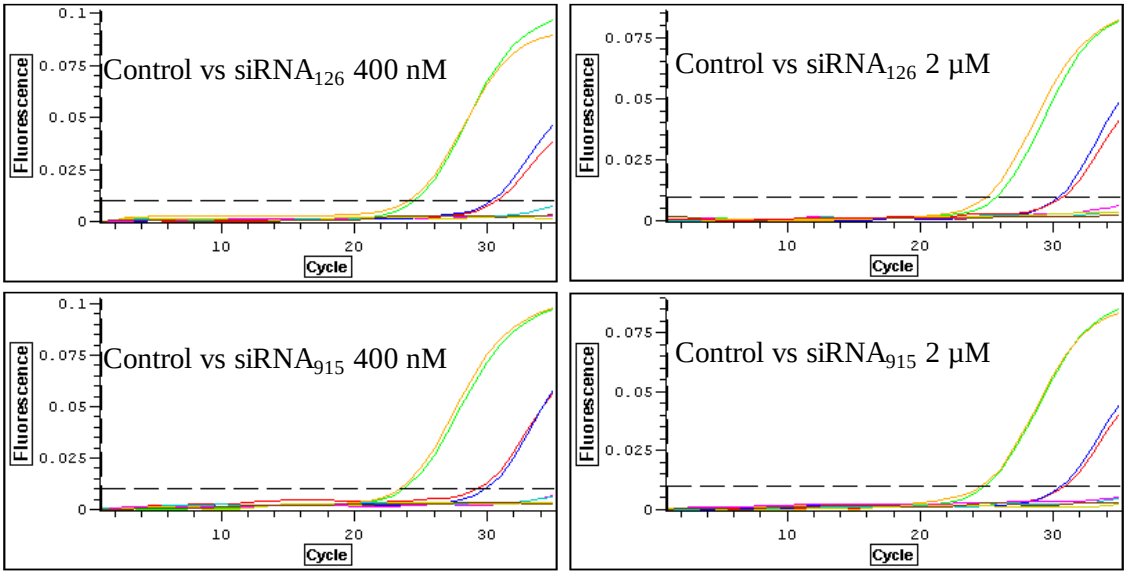

B

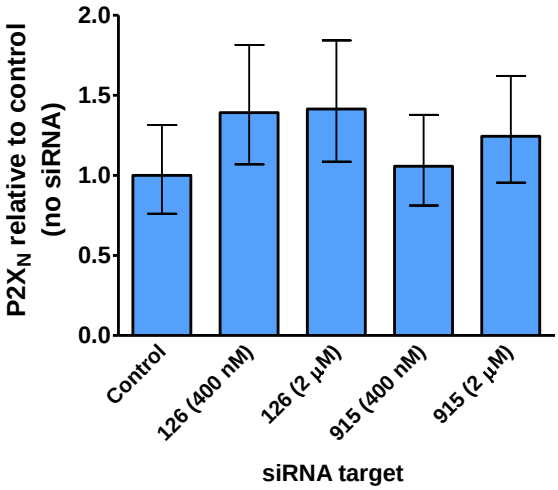

Figure 5.10. Representative qRT-PCR traces (A) and bar chart of mean values (B) for *Lym*P2X mRNA quantification. Neither of the siRNAs tested (at either 400 nM or 2 µM) altered *Lym*P2X mRNA levels relative to controls (no siRNA) (n = 4).

C

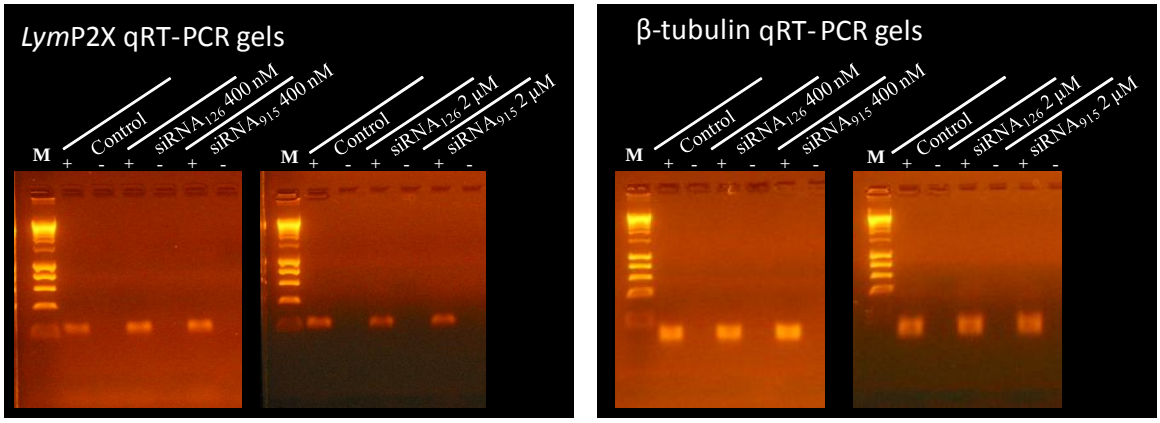

5.10C, example agarose gels from qRT-PCR experiments showing *Lym*P2X and β-tubulin amplification products for control and siRNA treated samples. No reverse transcriptase (RT) (-) negative control samples did not show any amplification products demonstrating the absence of contaminating genomic DNA.

5.4 DISCUSSION

*Lym*P2X has been shown to be located in all ganglia of the *Lymnaea* CNS, indicating its role in a variety of neuronal pathways. The buccal ganglia contain the CPG and motoneurons of the feeding network, and preliminary data in the laboratory demonstrated the reduced sucrose-induced feeding after injection of PPADS into the body cavity. This put forward a potential role for *Lym*P2X in the feeding network, which was further investigated in this chapter's work. Without the availability of a specific *Lym*P2X agonist or antagonist and the inability to knock down *Lym*P2X expression, knowledge of the probable function of *Lym*P2X in *Lymnaea* CNS was gathered by the use of commonly-used P2X agonists and antagonists that may influence activity of purinergic receptors other than *Lym*P2X. The feeding system is a well characterized neural network in *Lymnaea*, and work in this chapter concentrated to see effects of *Lym*P2X in feeding activity. In this part of the investigation, P2X receptor activation in combination with P2Y activation was found to be required for ATP-evoked fictive feeding.

5.4.1 Both P2X and P2Y activation is required for ATP-evoked increase in fictive feeding

The first application of 1 mM ATP increased the rate of fictive feeding implying that activation of purinergic receptors can generate a feeding rhythm. The 11 - 12 second latency in fictive feeding upon 1 mM ATP application to the buccal ganglia is much faster than the responses observed in motoneurons (25 - 35s) following sucrose

application to the lips of semi-intact *Lymnaea* preparations (Kemenes, 1986). The lack of increased fictive feeding upon subsequent ATP applications may be possibly due to: the slightly reduced current amplitudes of *Lym*P2X receptors observed on the second ATP application due to desensitization, or / and; by a negative feedback mechanism affecting CPG components in a manner to prevent expression of fictive feeding after earlier ATP-evoked feeding activity. The second possibility is highly likely as continuous sucrose application to *Lymnaea* lip—tentacle—buccal mass preparations caused a gradual reduction in feeding activity over time (Kemenes, 1986). Also the spontaneous fictive feeding rate appeared to decrease after the first application of ATP (Figure 5.4B). The ATP concentrations used in this study to trigger an enhanced fictive feeding rate are many times above the nanomolar range ATP concentrations discovered in *Lymnaea* CNS (Gruenhagen *et al*., 2004). One may therefore question the physiological relevance of the ATP concentration required to evoke a feeding response in this study. However, innovative nucleotide-sensing assays have provided independent lines of evidence that the majority of the released ATP is preserved in the pericellular space with no notable significant convection into the bulk milieu and these cell-surrounding ATP concentrations are sufficient for triggering purinergic responses (Yegutkin, 2008). The findings in the preliminary study that the purinergic antagonist PPADS (at 100 µM) was able to abolish sucrose-induced feeding indicates further that ATP concentrations at the synapses are likely to be much greater than 50 nM, and are expected to be nearer to the EC_{50} concentrations (in the µM range) of purinergic receptors.

The inability of 1 mM UTP, ADP or adenosine to alter feeding activity further suggests the requirement of *Lym*P2X activation for ATP-evoked fictive feeding. However, it

cannot be ruled out that the activation of an ATP-selective P2Y receptor and not P2X receptors is the determining factor for the generation of fictive feeding upon ATP exposure.

1 mM ATP application would stimulate both P2X and P2Y receptor components of the feeding pathway. UTP, ADP and adenosine application would not activate *Lym*P2X as previously shown in *Xenopus* oocytes. Therefore buccal motoneuron responses to the P2Y agonists UTP and ADP and the P1 receptor agonist adenosine informs us of the non-P2X purinergic component of *Lymnaea* buccal neuronal networks.

All purinergic agonists with the exception of adenosine affected the membrane potential of the buccal motoneurons, indicating the high expression levels of functional P2X and P2Y receptors, and suggesting the low abundance of adenosine-sensitive P1 receptors. Changes in membrane potential of buccal motoneurons following agonist application could be due to three factors:

1) direct effect through agonist binding to purinergic receptors located on the recorded motoneurons, leading to receptor activation, ion flow and depolarization.

2) purinergic receptor activation on sensory and modulatory neurons distinct from the recorded motoneurons to affect feeding CPG interneuron activity, which then imposes rhythm and / or influences activity of the recorded motoneurons.

3) purinergic receptor activation modifying other physiological processes that does not interfere with feeding CPG activity, however influencing activity of feeding motoneuron connections.

The first possibility appears unlikely as the time courses of the membrane potential changes upon agonist application and the 11 - 12 s latency in the generation of the initial fictive feeding cycle upon the first 1 mM ATP application is too slow compared to the current kinetics of heterologously-expressed P2X or P2Y receptor responses. The second and third possibilities are more likely to account for the delayed alterations in membrane potential following exposure to purinergic agonists, therefore it appears unlikely that the purinergic receptors are expressed in significant quantities on the recorded motoneurons.

Application of purinergic agonists caused variable responses in membrane potential of the *Lymnaea* motoneurons between buccal preparations. This variability is mainly due to spontaneous physiological processes in the feeding CPG and other neural components of the buccal ganglia, leading to pattern of activity at the motoneurons that may only be partially influenced by purinergic agonist application.

5.4.2 P2X activation is likely to result in excitation of the N3 interneuron

The lack of increased feeding activity upon BzATP application rules out the specific activation of *Lym*P2X in initiating CPG activity to cause feeding cycles. However *Lym*P2X may still have a role in increased feeding activity evoked by ATP. The observed long lasting hyperpolarizing shift of the B4 motoneuron upon BzATP application suggests that there is activation of P2X receptors in N3 interneurons, or possibly activation of P2X receptors expressed in sensory or modulatory neurons that

are connected to N3 interneurons. This will lead to increased excitability of N3 interneurons, causing chemical inhibitory inputs from the N3 interneurons into the B4 cell, resulting in the observed hyperpolarization of B4 during BzATP application (Rose, 1981). Preliminary data in the laboratory that showed a reduced sucrose-induced feeding rate of intact *Lymnaea* upon BzATP injection gives further evidence that P2X receptors are associated with N3 interneuron activation. N3 interneuron has inhibitory chemical connections with N1 interneuron, and therefore N3 excitation functions to prevent generation of the feeding rhythm (Elliott and Benjamin, 1985a). Recordings of the CPG interneurons upon BzATP application can confirm excitation of N3 or other interneurons following P2X activation.

It is unlikely for P2X receptors to be highly expressed on N1 interneurons or on neurons leading to N1, as only a small depolarization of B1 was observed upon BzATP application. Excitation of N1 interneuron would be expected to lead to a larger depolarization of the B1 motoneuron and increase the likelihood of fictive feeding upon BzATP application if there was a large abundance of P2X receptors on N1 or on neurons leading to N1. P2X activation leading to N2 interneuron excitation is possible since the N2 interneuron also has chemical inhibitory connections with the B4 motoneuron and no excitatory connections with B1 (Benjamin *et al*., 2000). P2X expression on N2 or on neurons leading to N2 can be substantiated by recordings to show depolarization of both N2 interneuron and B3 motoneuron upon BzATP application, characteristics that are not seen when only N3 interneuron is activated (Benjamin *et al*., 2000).

The N3 interneurons are divided into phasic (N3p) and tonic (N3t) neurons, with N3p firing for a short duration earlier in the feeding rhythm, and N3t firing later towards the end of the feeding cycle (Elliott and Benjamin, 1985a, Yeoman *et al.*, 1995). It is difficult to distinguish or suggest from the results analysis whether BzATP application and P2X activation causes excitation of either the N3p, N3t, or both N3 interneurons to cause hyperpolarization of the B4 cell. N3 interneurons also have an excitatory electrotonic connection with B4 to cause increased excitability of this motoneuron, and these connections are responsible for the depolarization of B4 motoneuron in the swallow phase during ATP-evoked fictive feeding (Benjamin *et al*., 2000).

A possible explanation for lack of feeding from BzATP application is the insufficient excitation of N1 interneurons. However the small B1 motoneuron depolarization by BzATP application may be due to small level of activation of N1 interneuron. This excitation of N1 by P2X activation may have a small contribution to increasing the N1 interneuron excitation above the threshold to generate a feeding rhythm upon ATP application. N1L and N1M are the two types of N1 CPG interneurons in the buccal ganglia, through which BzATP activation may exert small effects on the motoneurons. Strong N1L interneuron activation can fully drive the fictive feeding rhythm through its connections with other interneurons and motoneurons (Yeoman *et al*., 1995). N1M has endogenous plateauing properties to contribute to the feeding rhythm, illustrated by plateau potentials occurring both spontaneously and upon brief current injections into isolated N1M cells (Straub *et al*., 2002). Activation of N1M interneuron is essential for generating the feeding rhythm. This was demonstrated by the complete inhibition in feeding activity upon a photoinactivation protocol where N1M interneuron loaded with fluorescent dye was irradiated with laser light (Kemenes and Elliott, 1994). N1M has

widespread connections with many motoneurons whereas N1L has connections with only B1 (excitatory) and B4 (inhibitory) (Yeoman *et al.*, 1995). Likewise SO interneuron, current injection into which can generate a feeding rhythm has direct connections with B1 (excitatory) and B4 (inhibitory) motoneurons (Rose, 1981, Yeoman *et al.*, 1993). Therefore activation of N1L and N1M is required for rhythm generation for fictive feeding by ATP application.

BzATP application may possibly cause changes in membrane potential of B1 through very small activation of either N1 interneuron or affect SO interneurons. Alternatively, the small depolarization of B1 motoneuron by BzATP could be caused by activation of other neuronal pathways not associated with feeding that subsequently influence the membrane potential of this feeding motoneuron. It is likely that P2X receptor activation causes excitation of N3 interneurons and therefore increasing the threshold for N1 interneuron activation to trigger the feeding rhythm. This theory is supported by preliminary data in the laboratory that displayed a reduced feeding rate upon BzATP application. The results of this chapter did not suggest that BzATP causes reduction in feeding rate, however the spontaneous feeding rate was very low.

*Lym*P2X activation may also be partially responsible for generation of the feeding rhythm by hyperpolarization of B4 preventing N3 tonic (N3t) -> N1M interneuron inhibition, as B4 hyperpolarization has been found to inhibit the N3t interneuron by electrotonic synapses (Staras *et al.*, 1998). The relief of inhibitory inputs by chemical synapses from N3t-> N1M (Elliott and Benjamin, 1985a), followed by further

excitation of N1 interneurons by activation of P2Y receptors in *Lymnaea* may help generate the feeding rhythm.

BzATP effect on increasing membrane potential of B1 motoneuron was smaller than 1 mM ATP and UTP, suggesting P2Y activation is responsible for strengthening B1 excitation through activation of N1 interneuron. As stated previously, the slow time course of increase in B1 motoneuron membrane potential indicates that it is unlikely that functional P2Y receptors are located on B1 motoneuron, and therefore P2Y-containing neurons are more likely located upstream of the pathway, such as on N1 interneurons. Therefore by P2Y activation may be largely contribute to the first phase (protaction phase) of the feeding cycle by 1 mM ATP through excitation of the N1 interneuron.

Unlike BzATP, P2Y agonists did not cause hyperpolarization of B4, indicating that P2Y activation causes activation of other neuronal pathways that eventually leads to depolarization of B4 motoneuron. It is unknown whether these connections from P2Y sensitization to B4 are excitatory, or whether P2Y activation leads to inhibition of the inhibitory inputs into B4. ADP, UTP or adenosine were not able to increase feeding rate when applied alone because their activation of N1 interneurons may also not be sufficient for rhythm generation. An alternate possibility is that there is sufficient expression of ADP and UTP sensitive-P2Y receptors on N1 interneurons or on neurons leading to N1 that once activated cause generation of a feeding rhythm, however a subset of P2Y-expressing neurons are simultaneously responsible for preventing fictive feeding. In the second case, P2X activation may possibly be responsible for preventing

these particular inhibitory inputs from P2Y-containing neurons to suppress feeding, allowing P2Y activation that excites N1 interneurons alone to trigger fictive feeding.

Since the hyperpolarizing effects of BzATP on B4 are different to the depolarizing effects caused by P2Y receptor agonists, it is likely that none or very few of the *Lymnaea* P2Y receptors are BzATP sensitive. This is in agreement with the findings that only one mammalian P2Y subtype has so far been identified to be sensitive to BzATP (Communi *et al.*, 1999, von Kugelgen, 2006). BzATP was found to concentration-dependantly inhibit ADP-evoked currents at rat and human $P2Y_1$ receptors (Vigne *et al.*, 1999), and therefore the application of BzATP may have a small effect on the endogenous P2Y signalling component of *Lymnaea* feeding pathway that is mediated by ADP.

The discovery that PPADS inhibits the 1 mM ATP-evoked increase in fictive feeding with a reduction of B4 motoneuron depolarization rather than an increase shows that some P2Y receptors in *Lymnaea* are also PPADS sensitive. This is further substantiated by findings that the P2Y agonist ADP elicited significant depolarization of B4 motoneuron, the opposite effect of BzATP-triggered B4 depolarization. However, the lack of significant effect of ADP on B1 motoneuron depolarization and the inability of PPADS to inhibit B1 depolarization by ATP also suggests the presence of PPADS-insensitive ATP-gated purinergic receptors in *Lymnaea*. These receptors would be expected to cause B1 motoneuron depolarization in the presence of PPADS. An alternate explanation is that the small PPADS-resistant component of the current flowing through PPADS sensitive receptors is sufficient to cause significant

depolarization of B1, but not the B4 motoneuron. PPADS when applied with ATP was unable to significantly reduce the fictive feeding rate below the spontaneous rate, and may suggest that purinergic receptor activation does not play a major role in generation of a feeding rhythm. This data can still be correlated to the finding in the preliminary study that showed a reduced feeding rate stimulated by sucrose application to intact *Lymnaea* that were injected with PPADS into the body cavity. This is because sucrose-induced fictive feeding may have a different level of purinergic component compared to spontaneous fictive feeding.

The lack of significant effects of ADP on B1 motoneuron depolarization suggests that ADP binds to different purinergic receptors to ATP and UTP, and activate a separate set of neurons to cause differential activation of motoneurons downstream of the pathway. ADP has been previously shown to activate P2Y receptor subtypes that are not sensitive or less sensitive to ATP or UTP (von Kugelgen, 2006). It is likely that ADP exert its depolarizing effects on the B4 cell through neuronal pathway components distinct to the feeding CPG interneurons.

Whether *Lym*P2X receptor containing neurons are sensory, modulatory, interneurons and which interneurons they have more influence over remains to be determined. Fictive feeding of isolated buccal ganglia was investigated, and exclusion of other parts of *Lymnaea* CNS had also removed some of the modulatory components of the feeding pathway that are not essential for feeding to occur. These include the serotonergic cerebral giant cell that can modulate the strength and frequency of the feeding rhythm after its initiation by their connections with N1M and SO interneurons, but not trigger

feeding in a quiescent preparation (Yeoman *et al.*, 1994a, Yeoman *et al.*, 1994b, Yeoman *et al.*, 1996). This was found by serotonergic agonist and antagonist application, and by photoinactivation of these neurons (Yeoman *et al.*, 1994a, Yeoman *et al.*, 1994b). Future studies can investigate if ATP application in the cerebral ganglia can activate cerebral giant cells there to affect feeding rhythm through SO or N1M interneurons (Yeoman *et al*., 1996), or depolarizing buccal motoneurons by their direct excitatory connections (McCrohan and Benjamin, 1980).

5.4.3 UTP sensitive receptors in Lymnaea. Equipotent as ATP?

UTP application was found to significantly depolarize both B1 and B4 motoneurons, and increase fictive feeding in some of the preparations to suggest that activation of UTP-sensitive P2Y neurons activates N1 interneurons close to the threshold for rhythm generation, and only a slight amount of further excitation is likely to generate more consistent fictive feeding. The level of B4 depolarization by 1 mM UTP appeared to be less than triggered by 1 mM ATP, though not significantly, and this perceived difference in values could be explained by the excitation of the B4 motoneuron through post-inhibitory rebound (Benjamin and Rose, 1979) upon ATP application and P2X activation. Taking into consideration that few P2Y receptors have equal potency for ATP and UTP (von Kugelgen, 2006), 1 mM ATP application to preparations that are effectively silenced for *Lym*P2X expression may give the same pattern of results as UTP. Increased fictive feeding rate upon co-application of UTP and BzATP can give further evidence if *Lymnaea* P2Y receptors are equipotent for ATP and UTP, as well as show that P2X activation is required for ATP-evoked fictive feeding. However, $P2Y_6$ is

sensitive to UTP and not ATP (von Kugelgen, 2006), and therefore *Lymnaea* P2Y receptors may have differential sensitivity to UTP and ATP. UTP, like hexokinase-treated ADP has also been reported to activate $P2X_5$ receptors (Wildmann et al., 2005), and there is a small posibilty that there may be unidentified UTP- or ADP-sensitive P2X receptors in *Lymnaea* that influence the responses.

Another interesting feature of UTP-evoked responses is the net increase in fictive feeding is similar across the four UTP applications, suggesting that the first UTP application does not prevent the generation of a feeding rhythm upon subsequent exposure to UTP. This shows that UTP and ATP may activate the feeding rhythm through different mechanisms.

5.4.4 Adenosine receptors in Lymnaea CNS

Adenosine did not change the membrane potential of the B1 and B4 motoneurons, which is a different effect observed by adenosine application to *Lymnaea* whole CNS preparations with electrophysiological recordings from pedal ganglia RPeDG or LPeDG neurons (Malik and Buck, 2010). Adenosine application was found to cause hyperpolarization of membrane potential of these pedal ganglia neurons (Malik and Buck, 2010). This suggests that adenosine-sensitive P1 receptors are expressed in the *Lymnaea* CNS, however the expression pattern and neuronal connections of these adenosine-sensitive receptors in the buccal ganglia may not cause significant change in the membrane potential of B1 or B4 cells after application of adenosine.

Unlike other purinergic agonists, adenosine application did not appear to reduce the spontaneous feeding rate at later stages of the recording (Figure 5.7B). This suggests that only agonists that cause significant change in membrane potential of motoneurons or affect feeding rate are likely to affect the spontaneous fictive feeding rate at later time points of the recording, and ATP, ADP, UTP, and BzATP-treated bucccal preparations do not reduce in fictive feeding rate due to time.

5.4.5 Attempt to directly elucidate LymP2X function by RNA interference using siRNA

The attempted silencing of *Lym*P2X expression using double stranded RNA was not successful. Double stranded RNA is able to reduce gene expression by a sequence-specific degradation of the target mRNA by forming a complex with a ribonucleotide complex (RISC) (Tinoco *et al.* 2010). RISC unwinds the duplex to produce single stranded siRNA, that leads to activation of the RISC, which subsequently search for homologous mRNA transcripts by a base-pairing mechanism, directing the degradation of mRNA (Tinoco *et al.* 2010). Inability of the siRNA strands to cause complete knock down or significant reduction in *Lym*P2X expression levels indicates that either the siRNA strands are not able to penetrate *Lymnaea* tissue barriers and access *Lym*P2X mRNA sequences to carry out its knock down function, or the siRNA is able to reach the target *Lym*P2X mRNA sequence but not able to function in silencing the target mRNA expression. Injection of longer dsRNA strands can cross cellular boundaries to knock down expression in non-injected surrounding cells (Fire *et al.*, 1998), and

therefore injection of *Lym*P2X siRNA in neurons or the body cavity can be used in future strategies to silence *Lym*P2X. Simply soaking worms in dsRNA without use of transfecting agents for knocking down genes has been found to be less effective than microinjection (Tabara *et al*., 1998). Neuronal cells have been stated as being more resistant to RNA interference (Tinoco *et al.* 2010).

Double stranded RNA mediated silencing in *Lymnaea stagnalis* has been used previously to successfully decrease gene expression of neuronal nitric oxide synthase (nNOS) (Korneev *et al*., 2002), and was found to be more effective than single stranded RNA (ssRNA) in reducing nNOS expression. That investigation involved the use of double stranded RNA molecules ~600 bp in length that were injected into the buccal cavity (Korneev *et al*., 2002), and this methodology may have allowed successful silencing of the target gene in comparison to the attempted knockdown of *Lym*P2X. The study revealed that nitric oxide is essential for the function of fictive feeding as CNS preparations exposed to the dsRNA targeting nNOS exhibited reduced expression of nNOS (Korneev *et al*., 2002). DsRNA targeted to nNOS had also suppressed the rate of fictive feeding in response to sucrose application to the lips of semi-intact preparations compared to ssRNA for the same target (Korneev *et al*., 2002). Using dsRNA strands in attempts to silence genes in human cells have been shown to be ineffective (Lin *et al*., 2001), however mRNA-cDNA hybrids larger than 500 bases were successful in reducing expression of bcl-2 gene in human prostrate cancer LNCaP cells with corresponding phenotypic changes (Lin *et al*., 2001).

Chapter 5 conclusion

Activation of both P2X and P2Y is required to trigger an increase in fictive feeding rate by ATP, with the differential effects of P2X and P2Y receptor excitation suggesting that these receptors are involved in separate phases of the feeding cycle. P2X receptors would appear to play key role in the swallow phase by excitation of the N3 interneuron leading to chemical inhibitory inputs into B4, as demonstrated by the hyperpolarization of B4 that occur upon BzATP application. Application of P2Y agonists, but not Bz-ATP, caused depolarization of the B1 interneuron, possibly due to the activation of P2Y receptors located on N1, and possibly N2 interneurons indicating that P2Y activation is responsible for the first and possibly second phase of fictive feeding. This activation of feeding CPG interneuron components and their integration upon the first ATP application leads to phasic activation and inhibition pattern of B1 and B4 motoneurons, displaying fictive feeding activity. Subsequent ATP applications at 15 min intervals did not cause increased fictive feeding, and this can be explained by the possible presence of a negative feedback mechanism in the CPG or due to the desensitization of *Lym*P2X.

Chapter 6: Final discussion

6.1 LymP2X and HdP2X correspond to ATP-gated ion channels

ATP-evoked currents in *Xenopus* oocytes expressing either *Lym*P2X or *Hd*P2X cDNAs provides definitive molecular evidence that these two invertebrate P2X-like genes encode ATP-gated ion channels and can therefore now be considered as members of the expanding family of P2X ion channels. Both sequences display 25 – 50 % sequence identity with mammalian P2X subtypes and like the P2X receptor from *Schistosoma mansoni* (Agboh *et al.*, 2004), have closest similarity to mammalian $P2X_4$ (*Lym*P2X: 45.9 % and *Hd*P2X: 38.4 % amino acid sequence identity with $hP2X_4$). This suggests that $P2X_4$ is the oldest member of the family of seven mammalian P2X receptors, being most similar to the evolutionary ancestral P2X sequence and this is also suggested in the dendogram presented in Chapter 2 (Figure 2.6). *Lym*P2X shares many characteristics with the so-called group 2 P2X receptors ($P2X_2$, $P2X_4$ and $P2X_5$), exhibiting an EC_{50} of ~10 µM, αβmeATP insensitivity, and slow rise time and desensitizing current. *Hd*P2X possesses fast current kinetics upon ATP application, a unique property among the invertebrate P2X receptors identified to date. The low ATP potency (EC_{50} = 28.5 µM) of *Hd*P2X allows classification of this receptor into a P2X group distinct from those previously proposed (MacKenzie *et al.*, 1999). *Lym*P2X and *Hd*P2X have common pharmacological properties such as sensitivity to BzATP as a partial agonist, and have currents that are inhibited in a concentration dependent manner by PPADS and suramin. The gathering of a pharmacological profile for *Lym*P2X allowed a closer analysis of the likely function of this receptor in the *Lymnaea* CNS by intracellular recordings from specific motoneurons.

The identification of these invertebrate P2X sequences adds to the hypothesis that P2X sequences emerged during evolution prior to the divergence of vertebrates from non-vertebrates. The conservation of amino acids such as those involved in ATP binding, ten extracellular cysteines and an N-terminal protein kinase C site between *Lym*- and *Hd*P2X and mammalian P2X receptors suggests that vertebrate and invertebrate P2X receptors evolved from the same primitive ancestral P2X receptor and that there has been strong evolutionary pressure for the conservation of these functionally important residues. The $P2X_{1-7}$ subtypes have greater homology amongst each other than with any of the invertebrate P2X receptor sequences. This adds to the hypothesis that the emergence of seven P2X subtypes in mammals is a later evolutionary event subsequent to the separation of vertebrates and invertebrates. Similarly, the family of five P2X subtypes in *Dictyostelium discoideum* are more similar to each other than to any other known P2X receptor indicating that expansion of P2X gene families were independent events in different evolutionary lineages.

Future studies to further elucidate the properties of *Lym*P2X and *Hd*P2X include single channel recordings to asses how open probability, ion channel gating and conductance of agonist-evoked currents are altered by protons, divalent cations and ivermectin. Permeability studies in HEK293 cells transfected with *Lym*P2X and *Hd*P2X, where reversal potentials are determined under a range of extracellular cationic solutions could also be conducted to elucidate ion selectivity. Surface biotinylation experiments could also be used to ascertain whether some of the mutants generated in this study, such as *Hd*P2X charged or histidine mutants and some of the *Hd*P2X-*Bm*P2X chimeras, have reduced cell surface expression.

6.2 Invertebrate P2X receptors as models for structure-function studies

Invertebrate receptors have a high scope for use in structure-function studies, as exemplified by research on *Ostreococcus tauri* P2X (Fountain *et al.*, 2008). The finding that Asn^{353} in this channel conferred reduced calcium permeability was aided by sequence alignments of P2X receptors from a range of different phyla. A similar future comparative approach could potentially be used to further define P2X residues involved in ivermectin sensitivity for example by generating mutants that remove ivermectin sensitivity in *Hd*P2X, or introduce ivermectin sensitivity in *Lym*P2X. Using information about the helical nature of residues responsible for ivermectin binding and potentiation of P2X currents (Jelinkova *et al.*, 2008), mutation of Ala^{60} in *Lym*P2X to a bulkier amino acid may confer ivermectin sensitivity to this channel. Conversely the substitution of Ile^{60} in *Hd*P2X to a smaller residue may abolish the ivermectin sensitivity of this receptor.

An interesting feature of the *Lym*P2X sequence is the absence of a lysine or arginine residue at or near position 249, as Lys^{249} in $P2X_4$ has been found to play role in PPADS inhibition (Buell *et al.*, 1996). This opens up the possibility of lysine residues positioned further away from position 249 or unidentified mechanisms existing for PPADS inhibition of P2X receptors.

The divalent metal binding site in *Hd*P2X has proved difficult to elucidate due to different P2X subtypes having different mechanisms of modulation by zinc and copper. Residues important for zinc and copper co-ordination may not align well among P2X sequences, and instead positioned at a common location in certain structures such as the

head and dorsal fin regions of P2X, similarly observed for rat $P2X_2$ His^{120} and His^{213} residues (Clyne *et al.*, 2002a, Kawate *et al.*, 2009, Young, 2009).

6.3 Interactions between N- and C- termini to determine current kinetics

Future studies using fluorescence resonance energy transfer (FRET) could investigate how the N- and C-termini move and alter conformation relative to each other to influence gating of the channel and ion permeability. Such studies may give clues to the mechanisms underlying the changes in current kinetics observed in the chimeras described in Chapter 3. FRET using the green fluorescent protein derivatives cyan and yellow fluorescent protein (CFP and YFP) has been used previously to study P2X receptors (Fisher *et al.*, 2004). GFP tagged to $P2X_2$ receptors did not significantly alter EC_{50}, Hill Slope, peak current, desensitization kinetics or inhibition by suramin (Khakh *et al.*, 2001). YFP- and CFP-tagging to $P2X_4$ receptors also does not alter EC_{50}, peak currents or current kinetics of the receptor (Young *et al.*, 2008).

If CFP and YFP are within ~70 Å (~7 nm) proximity of each other they give rise to FRET (Fisher *et al.*, 2004). FRET has been used to show that the cytosolic domains of $P2X_2$ receptors narrow from their origins at the plasma membranes to their tips by 10 Å, and also showed that the T18A mutant that alters desensitization rate and lacks I_2 current state also has no movement of cytosolic domains relative to each other and lacks changes in ATP-evoked FRET (*F*Y/*F*C) (Fisher *et al.*, 2004). FRET also showed that the longer the length of the cytoplasmic domains of a P2X receptor subtype, the larger the FRET efficiency (FRET *e*) between the intracellular domains, further confirming that the tips of intracellular domains converge from its origins at the plasma

membrane (Young *et al.*, 2008). *Hd*P2X, which has a comparatively longer intracellular C-terminal domain than most P2X receptors may have greater interactions with the N-termini and therefore more likely to influence pore regions within the membrane to determine current flow and desensitization rate. Limitations of using FRET are that changes in relative orientation and interflourophore distance can not be distinguished (Fisher *et al.*, 2004). Also there is the possibility that some P2X receptors will not express functional channels following the fusion of CFP and YFP with the N- and C-intracellular termini.

It is possible to assess the changes in movement or orientation of specific individual amino acid residues of the cytosolic or other domains by making use of cysteine-reactive flourophores such as Tetramethylrhodamine, used previously used to look at the movement of voltage sensing S4 segment during gating in Shaker K_ channels (Sonnleitner *et al.*, 2002). Hydrophobic photoactive probes that are derivatives of 3-trifluoromethyl-3-*m*-iodophenyl diazirine or Benzophenone can be used to measure interactions of the cytosolic domains with the plasma membrane. This particular method was previously used to investigate conformational changes of N-terminal and M3-M4 intracellular loop domains of the nicotinic acetylcholine receptors (Leite *et al.*, 2003).

The above strategies can be used in used in combination with other methodologies to give high-resolution structural information and state dependant information about the conformational shifts of the intracellular domains of P2X, and how they affect the ion conduction pathway.

6.4 ATP-evoked fictive feeding and role of P2X receptors

The ATP concentrations required to elicit higher fictive feeding is many times greater than the endogenous nanomolar ATP concentrations previously measured in *Lymnaea* CNS (Gruenhagen et al., 2004). This may imply that ATP has only a minor contribution through purinergic receptor activation to excite N1 interneurons past the threshold to specify feeding rhythm generation. Inhibition of sucrose-induced feeding by PPADS injection into the body cavity in preliminary experiments in the laboratory indicates that ATP concentrations at the synapse and purinergic receptor sites are much higher than found previously in the CNS (Gruenhagen et al., 2004). This suggests that future experiments to effectively silence P2X receptor expression by RNA interference are likely to be informative regarding the role of P2X receptors in feeding activity.

The intracellular recordings on motoneurons in this investigation were carried out on isolated buccal ganglia preparations, and therefore do not account for the effects of purinergic receptor activation at upstream components of the feeding pathway. Further studies can investigate if application of ATP to other ganglia in the CNS such as cerebral ganglia or pedal ganglia can modulate fictive feeding, or affect motoneurons, similarly seen by serotonin bath application to activate CGCs, causing depolarisation and increase in B4 and B8 cell bursting activity (Straub and Benjamin, 2001).

Also the roles of P2X receptors in sucrose induced feeding can be further investigated. Sucrose has been previously shown to increase the feeding rate in *Lymnaea* semi-intact preparations (Kemenes, 1986), and an experiment can be devised to see if ATP application to the buccal ganglia can prevent feeding cycles triggered by delivering sucrose to the lips of semi-intact *Lymnaea* preparations. If ATP is able to do this it puts

forward a role for ATP and purinergic receptors in appetite control by triggering fictive feeding cycles, which may then desensitize the feeding pathway from being activated by food. BzATP, which from this investigation was proposed to activate N3 interneurons and increase the threshold for feeding activity can be applied to buccal ganglia of semi-intact preparations. If BzATP application is also able to reduce or prevent sucrose-induced feeding, it will further strengthen the theory that P2X activation is responsible for N3 interneuron activation, as this interneuron inhibits the N1 interneuron that is responsible for rhythm generation. Another approach to identify if P2X activation results in increased N3 interneuron activity is through intracellular recordings to show excitation of N3 interneuron or B3 motoneuron that receives inputs from the N3 interneuron (Benjamin *et al.*, 2000) following BzATP application. Measurement of ATP release by luciferase-catalyzed ATP chemiluminescence signals following sucrose treatments, to observe if changes in ATP release corresponds to increase in feeding rates would also be of interest as it would further indicate if purinergic signalling is required for rhythm generation.

The attempts to selectively activate P2X or P2Y receptors may not be successful, for example BzATP application may activate or inhibit *Lymnaea* P2Y receptors, or ADP and UTP application may activate unidentified P2X receptors in *Lymnaea*. Therefore, to gain a comprehensive understanding of *Lym*P2X functions in the feeding network, it is imperative to silence gene expression or knock-out the gene to observe whether the level of functional maintenance is correlated with reduced *Lym*P2X expression levels. Knock-out strategies for deleting genes have not been developed so far for *Lymnaea*, and therefore RNA interference by injection of double strand RNA corresponding to *Lym*P2X sequence in neurons or buccal cavity, or selection of an efficient transfection

agent is likely to improve the chances of siRNA access and silencing *Lym*P2X expression.

6.5 Other possible roles for Lymnaea P2X : respiratory network

The network of neurons that generate respiratory behaviour in *Lymnaea stagnalis* has been previously elucidated (Syed *et al.*, 1990, Syed and Winlow, 1991, Benjamin *et al.*, 2000). Once sensory neurons of the pneumostome osphradial area are activated through for example hypoxia, the respiratory CPG composed of right pedal dorsal 1 (RPeD1), visceral dorsal 4 (VD4) and input 3 (IP3) interneurons of the pedal ganglia in turn becomes activated (Benjamin et al., 2000). Activity in K MN and I/J MN motoneurons are driven by synaptic inputs from VD4 and IP3, and this is responsible for pneumostome closing (inspiration) and pneumostome opening (expiration) respectively (Syed *et al.*, 1990, Syed and Winlow, 1991, Benjamin *et al.*, 2000). Since *Lym*P2X mRNA has been localised in all ganglia of the *Lymnaea* CNS, the role of purinergic receptors in the respiratory network can be investigated. ATP has been previously shown to play a role in respiratory control in rats (Erlichman *et al.*, Gourine *et al.*, 2005). Immediate increases in ATP release from ventral medullary surface chemosensitive regions in rats was reported following a rise in arterial PCO_2 (Gourine *et al.*, 2005). This released ATP operate on distal dendrites of the ventral respiratory column neurons that have projections close to the ventral medullary surface to trigger adaptive enhancements in breathing activity (Gourine *et al.*, 2005). Blockade of purinergic receptors by application of suramin or PPADS at these sites reduced the effect of CO_2 on respiratory activity, further implying that P2X receptors may have a role in the respiratory circuitry (Gourine *et al.*, 2005). Respiratory neurons of the rostral

ventrolateral medulla have been previously shown to express $P2X_2$ receptors (Gourine *et al.*, 2003).

6.6 Does LymP2X mRNA expression correlate with LymP2X protein expression?

Recordings from isolated neurons in response to ATP or BzATP application can be used to give greater confirmation of *in situ* hybridization findings and to further demonstrate if *Lym*P2X receptors are expressed on the surface of the majority of neurons. The predominantly nuclear localization of *Lym*P2X mRNA suggests the presence of a mechanism preventing export of *Lym*P2X transcripts to the cytoplasm and this could control which neurons express functional *Lym*P2X protein. Immunocytochemistry using a *Lym*P2X specific antibody can be utilised to observe if *Lym*P2X protein is expressed in the majority of neurons or if there is in fact a translational control mechanism to prevent formation of *Lym*P2X protein, or whether the receptor protein is retained in the cell cytoplasm.

6.7 Identification of Lymnaea P2Y receptors

Future studies could also be conducted to identify the P2Y receptors proposed to underlie the majority of the N1 interneuron activation for feeding rhythm generation. Genes encoding P2Y receptors are more difficult to identify than P2X receptors due to the large number of closely related seven transmembrane receptors present in the genome, hindering the distinction of P2Y receptors from other G protein-coupled receptors. 7TM GPCR odorant receptor family members have been identified in *Drosophila melanogaster* using computer algorithms to search the Drosophila genome

for candidate open reading frames (ORFs) of odor receptor genes by their physicochemical profile, followed by RT-PCR of transcripts of these ORFs (Clyne *et al.*, 1999). The OR83b odorant invertebrate receptor from *Drosophila* was found to exhibit an inverted topology compared to the canonical N_{out}-C_{in} 7TM GPCR topology, further demonstrating the use of invertebrates to provide novel insights into receptor properties and function (Lundin *et al.*, 2007). Future studies to identify *Lymnaea* P2Y receptor genes could employ a similar bioinformatics approach to that used for the identification of *Drosophila* odor receptors, or alternatively an expression cloning strategy similar to that used in the identification of $P2X_1$ from rat *vas deferens* (Valera *et al.*, 1994) could be utilised.

6.8 Final Conclusion

Extracellular ATP signalling through P2X receptors plays a role in the modulation of a large variety of physiological functions and it is likely that many of these modulatory roles remain to be discovered. Using a simple and accessible model system such as *Lymnaea stagnalis* with well defined physiological pathways provides an ideal test bed to determine P2X function in the CNS allowing correlation to similar roles in mammals. The identification and cloning of *Lym*P2X allowed pharmacological characterization of the receptor in a heterolgous system, and this in turn allowed a closer analysis of the function of P2X receptors in the feeding pathway. *Lym*P2X expressed in *Xenopus* oocytes shared many properties of vertebrate P2X subtypes such as sensitivity to BzATP, PPADS, zinc, copper and pH. This demonstrates the conservation of functionally important residues in the course of evolution, despite *Lym*P2X exhibiting only 31.0 – 45.9 % sequence identity with human P2X subtypes.

P2X receptors were subsequently judged by intracellular recordings of buccal motoneurons to play a role in the third phase of the feeding cycle, the swallow phase through activation of the N3 interneuron. It is likely that both P2X and P2Y receptor activation is required for ATP-evoked fictive feeding, since P2Y agonists UTP and ADP did not enhance the feeding rate. In order to gain a more detailed understanding of P2X function, it is important to either silence or knock out P2X expression, or use agonists or antagonists that are specific for that P2X subtype. The widespread CNS localization of *Lym*P2X indicates that this P2X receptor may play more novel physiological roles that could be correlated to their function in vertebrates.

References

ACUNA-CASTILLO, C., CODDOU, C., BULL, P., BRITO, J. & HUIDOBRO-TORO, J. P. (2007) Differential role of extracellular histidines in copper, zinc, magnesium and proton modulation of the P2X7 purinergic receptor. *J Neurochem,* 101**,** 17-26.

ADELSBERGER, H., LEPIER, A. & DUDEL, J. (2000) Activation of rat recombinant alpha(1)beta(2)gamma(2S) GABA(A) receptor by the insecticide ivermectin. *Eur J Pharmacol,* 394**,** 163-70.

ADOUTTE, A., BALAVOINE, G., LARTILLOT, N., LESPINET, O., PRUD'HOMME, B. & DE ROSA, R. (2000) The new animal phylogeny: reliability and implications. *Proc Natl Acad Sci U S A,* 97**,** 4453-6.

AGBOH, K. C., WEBB, T. E., EVANS, R. J. & ENNION, S. J. (2004) Functional characterization of a P2X receptor from Schistosoma mansoni. *J Biol Chem,* 279**,** 41650-7.

AGUINALDO, A. M., TURBEVILLE, J. M., LINFORD, L. S., RIVERA, M. C., GAREY, J. R., RAFF, R. A. & LAKE, J. A. (1997) Evidence for a clade of nematodes, arthropods and other moulting animals. *Nature,* 387**,** 489-93.

ASCHRAFI, A., SADTLER, S., NICULESCU, C., RETTINGER, J. & SCHMALZING, G. (2004) Trimeric architecture of homomeric P2X2 and heteromeric P2X1+2 receptor subtypes. *J Mol Biol,* 342**,** 333-43.

ASSAF, S. Y. & CHUNG, S. H. (1984) Release of endogenous Zn2+ from brain tissue during activity. *Nature,* 308**,** 734-6.

BARRERA, N. P., ORMOND, S. J., HENDERSON, R. M., MURRELL-LAGNADO, R. D. & EDWARDSON, J. M. (2005) Atomic force microscopy imaging demonstrates that P2X2 receptors are trimers but that P2X6 receptor subunits do not oligomerize. *J Biol Chem,* 280**,** 10759-65.

BEDOUKIAN, M. A., WEEKS, A. M. & PARTIN, K. M. (2006) Different domains of the AMPA receptor direct stargazin-mediated trafficking and stargazin-mediated modulation of kinetics. *J Biol Chem,* 281**,** 23908-21.

BENJAMIN, P. R. & ROSE, R. M. (1979) Central generation of bursting in the feeding system of the snail, Lymnaea stagnalis. *J Exp Biol,* 80**,** 93-118.

BENJAMIN, P. R., STARAS, K. & KEMENES, G. (2000) A systems approach to the cellular analysis of associative learning in the pond snail Lymnaea. *Learn Mem,* 7**,** 124-31.

BERG J. M., T. J. L., STRYER L. (2007) Biochemistry. IN H., F. W. (Ed.). New York.

BIANCHI, L. & DRISCOLL, M. (2006) Heterologous expression of C. elegans ion channels in Xenopus oocytes. *WormBook***,** 1-16.

BLAND-WARD, P. A. & HUMPHREY, P. P. (1997) Acute nociception mediated by hindpaw P2X receptor activation in the rat. *Br J Pharmacol,* 122**,** 365-71.

BO, X., ZHANG, Y., NASSAR, M., BURNSTOCK, G. & SCHOEPFER, R. (1995) A P2X purinoceptor cDNA conferring a novel pharmacological profile. *FEBS Lett,* 375**,** 129-33.

BOBANOVIC, L. K., ROYLE, S. J. & MURRELL-LAGNADO, R. D. (2002) P2X receptor trafficking in neurons is subunit specific. *J Neurosci,* 22**,** 4814-24.

BOUE-GRABOT, E., ARCHAMBAULT, V. & SEGUELA, P. (2000) A protein kinase C site highly conserved in P2X subunits controls the desensitization kinetics of P2X(2) ATP-gated channels. *J Biol Chem,* 275**,** 10190-5.

BOUMECHACHE, M., MASIN, M., EDWARDSON, J. M., GORECKI, D. C. & MURRELL-LAGNADO, R. (2009) Analysis of assembly and trafficking of native P2X4 and P2X7 receptor complexes in rodent immune cells. *J Biol Chem,* 284**,** 13446-54.

BOYER, J. L., ZOHN, I. E., JACOBSON, K. A. & HARDEN, T. K. (1994) Differential effects of P2-purinoceptor antagonists on phospholipase C- and adenylyl cyclase-coupled P2Y-purinoceptors. *Br J Pharmacol,* 113**,** 614-20.

BRAKE, A. J., WAGENBACH, M. J. & JULIUS, D. (1994) New structural motif for ligand-gated ion channels defined by an ionotropic ATP receptor. *Nature,* 371**,** 519-23.

BRANDLE, U., SPIELMANNS, P., OSTEROTH, R., SIM, J., SURPRENANT, A., BUELL, G., RUPPERSBERG, J. P., PLINKERT, P. K., ZENNER, H. P. & GLOWATZKI, E. (1997) Desensitization of the P2X(2) receptor controlled by alternative splicing. *FEBS Lett,* 404**,** 294-8.

BROWN, S. G., TOWNSEND-NICHOLSON, A., JACOBSON, K. A., BURNSTOCK, G. & KING, B. F. (2002) Heteromultimeric P2X(1/2) receptors show a novel sensitivity to extracellular pH. *J Pharmacol Exp Ther,* 300**,** 673-80.

BUELL, G., LEWIS, C., COLLO, G., NORTH, R. A. & SURPRENANT, A. (1996) An antagonist-insensitive P2X receptor expressed in epithelia and brain. *Embo J,* 15**,** 55-62.

BURNSTOCK, G. (1972) Purinergic nerves. *Pharmacol Rev,* 24**,** 509-81.

BURNSTOCK, G. (1996) P2 purinoceptors: historical perspective and classification. *Ciba Found Symp,* 198**,** 1-28; discussion 29-34.

BURNSTOCK, G., CAMPBELL, G., SATCHELL, D. & SMYTHE, A. (1970) Evidence that adenosine triphosphate or a related nucleotide is the transmitter substance released by non-adrenergic inhibitory nerves in the gut. *Br J Pharmacol,* 40**,** 668-88.

BURNSTOCK, G. & VERKHRATSKY, A. (2009) Evolutionary origins of the purinergic signalling system. *Acta Physiol (Oxf),* 195**,** 415-47.

BURNSTOCK, G. & WOOD, J. N. (1996) Purinergic receptors: their role in nociception and primary afferent neurotransmission. *Curr Opin Neurobiol,* 6**,** 526-32.

CAO, L., BROOMHEAD, H. E., YOUNG, M. T. & NORTH, R. A. (2009) Polar residues in the second transmembrane domain of the rat P2X2 receptor that affect spontaneous gating, unitary conductance, and rectification. *J Neurosci,* 29**,** 14257-64.

CAO, L., YOUNG, M. T., BROOMHEAD, H. E., FOUNTAIN, S. J. & NORTH, R. A. (2007) Thr339-to-serine substitution in rat P2X2 receptor second transmembrane domain causes constitutive opening and indicates a gating role for Lys308. *J Neurosci,* 27**,** 12916-23.

CHAUMONT, S., JIANG, L. H., PENNA, A., NORTH, R. A. & RASSENDREN, F. (2004) Identification of a trafficking motif involved in the stabilization and polarization of P2X receptors. *J Biol Chem,* 279**,** 29628-38.

CHAUMONT, S. & KHAKH, B. S. (2008) Patch-clamp coordinated spectroscopy shows P2X2 receptor permeability dynamics require cytosolic domain

rearrangements but not Panx-1 channels. *Proc Natl Acad Sci U S A,* 105**,** 12063-8.

CHEN, C. C., AKOPIAN, A. N., SIVILOTTI, L., COLQUHOUN, D., BURNSTOCK, G. & WOOD, J. N. (1995) A P2X purinoceptor expressed by a subset of sensory neurons. *Nature,* 377**,** 428-31.

CHEN, Y., ZHANG, X., WANG, C., LI, G., GU, Y. & HUANG, L. Y. (2008) Activation of P2X7 receptors in glial satellite cells reduces pain through downregulation of P2X3 receptors in nociceptive neurons. *Proc Natl Acad Sci U S A,* 105**,** 16773-8.

CHESSELL, I. P., SIMON, J., HIBELL, A. D., MICHEL, A. D., BARNARD, E. A. & HUMPHREY, P. P. (1998) Cloning and functional characterisation of the mouse P2X7 receptor. *FEBS Lett,* 439**,** 26-30.

CLOUES, R., JONES, S. & BROWN, D. A. (1993) Zn2+ potentiates ATP-activated currents in rat sympathetic neurons. *Pflugers Arch,* 424**,** 152-8.

CLYNE, J. D., LAPOINTE, L. D. & HUME, R. I. (2002a) The role of histidine residues in modulation of the rat P2X(2) purinoceptor by zinc and pH. *J Physiol,* 539**,** 347-59.

CLYNE, J. D., WANG, L. F. & HUME, R. I. (2002b) Mutational analysis of the conserved cysteines of the rat P2X2 purinoceptor. *J Neurosci,* 22**,** 3873-80.

CLYNE, P. J., WARR, C. G., FREEMAN, M. R., LESSING, D., KIM, J. & CARLSON, J. R. (1999) A novel family of divergent seven-transmembrane proteins: candidate odorant receptors in Drosophila. *Neuron,* 22**,** 327-38.

COCKAYNE, D. A., HAMILTON, S. G., ZHU, Q. M., DUNN, P. M., ZHONG, Y., NOVAKOVIC, S., MALMBERG, A. B., CAIN, G., BERSON, A., KASSOTAKIS, L., HEDLEY, L., LACHNIT, W. G., BURNSTOCK, G., MCMAHON, S. B. & FORD, A. P. (2000) Urinary bladder hyporeflexia and reduced pain-related behaviour in P2X3-deficient mice. *Nature,* 407**,** 1011-5.

CODDOU, C., CODOCEDO, J. F., LI, S., LILLO, J. G., ACUNA-CASTILLO, C., BULL, P., STOJILKOVIC, S. S. & HUIDOBRO-TORO, J. P. (2009) Reactive oxygen species potentiate the P2X2 receptor activity through intracellular Cys430. *J Neurosci,* 29**,** 12284-91.

CODDOU, C., MORALES, B., GONZALEZ, J., GRAUSO, M., GORDILLO, F., BULL, P., RASSENDREN, F. & HUIDOBRO-TORO, J. P. (2003a) Histidine 140 plays a key role in the inhibitory modulation of the P2X4 nucleotide receptor by copper but not zinc. *J Biol Chem,* 278**,** 36777-85.

CODDOU, C., MORALES, B. & HUIDOBRO-TORO, J. P. (2003b) Neuromodulator role of zinc and copper during prolonged ATP applications to P2X4 purinoceptors. *Eur J Pharmacol,* 472**,** 49-56.

COLLO, G., NEIDHART, S., KAWASHIMA, E., KOSCO-VILBOIS, M., NORTH, R. A. & BUELL, G. (1997) Tissue distribution of the P2X7 receptor. *Neuropharmacology,* 36**,** 1277-83.

COLLO, G., NORTH, R. A., KAWASHIMA, E., MERLO-PICH, E., NEIDHART, S., SURPRENANT, A. & BUELL, G. (1996) Cloning OF P2X5 and P2X6 receptors and the distribution and properties of an extended family of ATP-gated ion channels. *J Neurosci,* 16**,** 2495-507.

COMMUNI, D., ROBAYE, B. & BOEYNAEMS, J. M. (1999) Pharmacological characterization of the human P2Y11 receptor. *Br J Pharmacol,* 128**,** 1199-206.

COOK, S. P., VULCHANOVA, L., HARGREAVES, K. M., ELDE, R. & MCCLESKEY, E. W. (1997) Distinct ATP receptors on pain-sensing and stretch-sensing neurons. *Nature,* 387**,** 505-8.

COULL, J. A., BEGGS, S., BOUDREAU, D., BOIVIN, D., TSUDA, M., INOUE, K., GRAVEL, C., SALTER, M. W. & DE KONINCK, Y. (2005) BDNF from microglia causes the shift in neuronal anion gradient underlying neuropathic pain. *Nature,* 438**,** 1017-21.

COX, K. J., TENSEN, C. P., VAN DER SCHORS, R. C., LI, K. W., VAN HEERIKHUIZEN, H., VREUGDENHIL, E., GERAERTS, W. P. & BURKE, J. F. (1997) Cloning, characterization, and expression of a G-protein-coupled receptor from Lymnaea stagnalis and identification of a leucokinin-like peptide, PSFHSWSamide, as its endogenous ligand. *J Neurosci,* 17**,** 1197-205.

D'ARCO, M., GINIATULLIN, R., LEONE, V., CARLONI, P., BIRSA, N., NAIR, A., NISTRI, A. & FABBRETTI, E. (2009) The C-terminal Src Inhibitory Kinase (Csk)-mediated Tyrosine Phosphorylation Is a Novel Molecular Mechanism to Limit P2X3 Receptor Function in Mouse Sensory Neurons. *J Biol Chem,* 284**,** 21393-401.

DERELLE, E., FERRAZ, C., ROMBAUTS, S., ROUZE, P., WORDEN, A. Z., ROBBENS, S., PARTENSKY, F., DEGROEVE, S., ECHEYNIE, S., COOKE, R., SAEYS, Y., WUYTS, J., JABBARI, K., BOWLER, C., PANAUD, O., PIEGU, B., BALL, S. G., RAL, J. P., BOUGET, F. Y., PIGANEAU, G., DE BAETS, B., PICARD, A., DELSENY, M., DEMAILLE, J., VAN DE PEER, Y. & MOREAU, H. (2006) Genome analysis of the smallest free-living eukaryote Ostreococcus tauri unveils many unique features. *Proc Natl Acad Sci U S A,* 103**,** 11647-52.

DOPAZO, H. & DOPAZO, J. (2005) Genome-scale evidence of the nematode-arthropod clade. *Genome Biol,* 6**,** R41.

DOUPNIK, C. A., DAVIDSON, N. & LESTER, H. A. (1995) The inward rectifier potassium channel family. *Curr Opin Neurobiol,* 5**,** 268-77.

DOYLE, D. A. (2004) Structural changes during ion channel gating. *Trends Neurosci,* 27**,** 298-302.

DUCKWITZ, W., HAUSMANN, R., ASCHRAFI, A. & SCHMALZING, G. (2006) P2X5 subunit assembly requires scaffolding by the second transmembrane domain and a conserved aspartate. *J Biol Chem,* 281**,** 39561-72.

EDWARDS, F. A., GIBB, A. J. & COLQUHOUN, D. (1992) ATP receptor-mediated synaptic currents in the central nervous system. *Nature,* 359**,** 144-7.

EGAN, T. M., HAINES, W. R. & VOIGT, M. M. (1998) A domain contributing to the ion channel of ATP-gated P2X2 receptors identified by the substituted cysteine accessibility method. *J Neurosci,* 18**,** 2350-9.

ELLIOTT, C. J. & BENJAMIN, P. R. (1985a) Interactions of pattern-generating interneurons controlling feeding in Lymnaea stagnalis. *J Neurophysiol,* 54**,** 1396-411.

ELLIOTT, C. J. & BENJAMIN, P. R. (1985b) Interactions of the slow oscillator interneuron with feeding pattern-generating interneurons in Lymnaea stagnalis. *J Neurophysiol,* 54**,** 1412-21.

ELLIOTT, C. J. & KEMENES, G. (1992) Cholinergic interneurons in the feeding system of the pond snail Lymnaea stagnalis. II. N1 interneurons make cholinergic synapses with feeding motoneurons. *Philos Trans R Soc Lond B Biol Sci,* 336**,** 167-80.

ELLIOTT, C. J., STOW, R. A. & HASTWELL, C. (1992) Cholinergic interneurons in the feeding system of the pond snail Lymnaea stagnalis. I. Cholinergic receptors on feeding neurons. *Philos Trans R Soc Lond B Biol Sci,* 336**,** 157-66.

ENNION, S., HAGAN, S. & EVANS, R. J. (2000) The role of positively charged amino acids in ATP recognition by human P2X(1) receptors. *J Biol Chem,* 275**,** 29361-7.

ENNION, S. J. & EVANS, R. J. (2001) Agonist-stimulated internalisation of the ligand-gated ion channel P2X(1) in rat vas deferens. *FEBS Lett,* 489**,** 154-8.

ENNION, S. J. & EVANS, R. J. (2002a) Conserved cysteine residues in the extracellular loop of the human P2X(1) receptor form disulfide bonds and are involved in receptor trafficking to the cell surface. *Mol Pharmacol,* 61**,** 303-11.

ENNION, S. J. & EVANS, R. J. (2002b) P2X(1) receptor subunit contribution to gating revealed by a dominant negative PKC mutant. *Biochem Biophys Res Commun,* 291**,** 611-6.

ERLICHMAN, J. S., LEITER, J. C. & GOURINE, A. V. ATP, glia and central respiratory control. *Respir Physiol Neurobiol*.

EVANS, R. J., LEWIS, C., BUELL, G., VALERA, S., NORTH, R. A. & SURPRENANT, A. (1995) Pharmacological characterization of heterologously expressed ATP-gated cation channels (P2x purinoceptors). *Mol Pharmacol,* 48**,** 178-83.

FINGER, T. E., DANILOVA, V., BARROWS, J., BARTEL, D. L., VIGERS, A. J., STONE, L., HELLEKANT, G. & KINNAMON, S. C. (2005) ATP signaling is crucial for communication from taste buds to gustatory nerves. *Science,* 310**,** 1495-9.

FIRE, A., XU, S., MONTGOMERY, M. K., KOSTAS, S. A., DRIVER, S. E. & MELLO, C. C. (1998) Potent and specific genetic interference by double-stranded RNA in Caenorhabditis elegans. *Nature,* 391**,** 806-11.

FISHER, J. A., GIRDLER, G. & KHAKH, B. S. (2004) Time-resolved measurement of state-specific P2X2 ion channel cytosolic gating motions. *J Neurosci,* 24**,** 10475-87.

FOUNTAIN, S. J. & BURNSTOCK, G. (2009) An evolutionary history of P2X receptors. *Purinergic Signal,* 5**,** 269-72.

FOUNTAIN, S. J., CAO, L., YOUNG, M. T. & NORTH, R. A. (2008) Permeation properties of a P2X receptor in the green algae Ostreococcus tauri. *J Biol Chem,* 283**,** 15122-6.

FOUNTAIN, S. J. & NORTH, R. A. (2006) A C-terminal lysine that controls human P2X4 receptor desensitization. *J Biol Chem,* 281**,** 15044-9.

FOUNTAIN, S. J., PARKINSON, K., YOUNG, M. T., CAO, L., THOMPSON, C. R. & NORTH, R. A. (2007) An intracellular P2X receptor required for osmoregulation in Dictyostelium discoideum. *Nature,* 448**,** 200-3.

FREDERICKSON, C. J. & BUSH, A. I. (2001) Synaptically released zinc: physiological functions and pathological effects. *Biometals,* 14**,** 353-66.

FREDHOLM, B. B., AP, I. J., JACOBSON, K. A., KLOTZ, K. N. & LINDEN, J. (2001) International Union of Pharmacology. XXV. Nomenclature and classification of adenosine receptors. *Pharmacol Rev,* 53**,** 527-52.

FREIST, W., VERHEY, J. F., STUHMER, W. & GAUSS, D. H. (1998) ATP binding site of P2X channel proteins: structural similarities with class II aminoacyl-tRNA synthetases. *FEBS Lett,* 434**,** 61-5.

GABRIEL, W. N., MCNUFF, R., PATEL, S. K., GREGORY, T. R., JECK, W. R., JONES, C. D. & GOLDSTEIN, B. (2007) The tardigrade Hypsibius dujardini, a new model for studying the evolution of development. *Dev Biol,* 312**,** 545-59.

GARCIA-GUZMAN, M., SOTO, F., LAUBE, B. & STUHMER, W. (1996) Molecular cloning and functional expression of a novel rat heart P2X purinoceptor. *FEBS Lett,* 388**,** 123-7.

GARCIA-GUZMAN, M., STUHMER, W. & SOTO, F. (1997) Molecular characterization and pharmacological properties of the human P2X3 purinoceptor. *Brain Res Mol Brain Res,* 47**,** 59-66.

GEREVICH, Z., ZADORI, Z. S., KOLES, L., KOPP, L., MILIUS, D., WIRKNER, K., GYIRES, K. & ILLES, P. (2007) Dual effect of acid pH on purinergic P2X3 receptors depends on the histidine 206 residue. *J Biol Chem,* 282**,** 33949-57.

GEVER, J. R., COCKAYNE, D. A., DILLON, M. P., BURNSTOCK, G. & FORD, A. P. (2006) Pharmacology of P2X channels. *Pflugers Arch,* 452**,** 513-37.

GONZALES, E. B., KAWATE, T. & GOUAUX, E. (2009) Pore architecture and ion sites in acid-sensing ion channels and P2X receptors. *Nature,* 460**,** 599-604.

GOURINE, A. V., ATKINSON, L., DEUCHARS, J. & SPYER, K. M. (2003) Purinergic signalling in the medullary mechanisms of respiratory control in the rat: respiratory neurones express the P2X2 receptor subunit. *J Physiol,* 552**,** 197-211.

GOURINE, A. V., LLAUDET, E., DALE, N. & SPYER, K. M. (2005) ATP is a mediator of chemosensory transduction in the central nervous system. *Nature,* 436**,** 108-11.

GRAHAM, A., HOPKINS, B., POWELL, S. J., DANKS, P. & BRIGGS, I. (1991) Isolation and characterisation of the human lung NK-2 receptor gene using rapid amplification of cDNA ends. *Biochem Biophys Res Commun,* 177**,** 8-16.

GRUENHAGEN, J. A., LOVELL, P., MOROZ, L. L. & YEUNG, E. S. (2004) Monitoring real-time release of ATP from the molluscan central nervous system. *J Neurosci Methods,* 139**,** 145-52.

GU, J. G. & MACDERMOTT, A. B. (1997) Activation of ATP P2X receptors elicits glutamate release from sensory neuron synapses. *Nature,* 389**,** 749-53.

GUO, C., MASIN, M., QURESHI, O. S. & MURRELL-LAGNADO, R. D. (2007) Evidence for functional P2X4/P2X7 heteromeric receptors. *Mol Pharmacol,* 72**,** 1447-56.

HAINES, W. R., MIGITA, K., COX, J. A., EGAN, T. M. & VOIGT, M. M. (2001) The first transmembrane domain of the P2X receptor subunit participates in the agonist-induced gating of the channel. *J Biol Chem,* 276**,** 32793-8.

HAINES, W. R., TORRES, G. E., VOIGT, M. M. & EGAN, T. M. (1999) Properties of the novel ATP-gated ionotropic receptor composed of the P2X(1) and P2X(5) isoforms. *Mol Pharmacol,* 56**,** 720-7.

HAMILTON, S. G., WARBURTON, J., BHATTACHARJEE, A., WARD, J. & MCMAHON, S. B. (2000) ATP in human skin elicits a dose-related pain response which is potentiated under conditions of hyperalgesia. *Brain,* 123 (Pt 6)**,** 1238-46.

HANSEN, M. A., BARDEN, J. A., BALCAR, V. J., KEAY, K. A. & BENNETT, M. R. (1997) Structural motif and characteristics of the extracellular domain of P2X receptors. *Biochem Biophys Res Commun,* 236**,** 670-5.

HAYATO, R., OHTUBO, Y. & YOSHII, K. (2007) Functional expression of ionotropic purinergic receptors on mouse taste bud cells. *J Physiol,* 584**,** 473-88.

HECHLER, B., LENAIN, N., MARCHESE, P., VIAL, C., HEIM, V., FREUND, M., CAZENAVE, J. P., CATTANEO, M., RUGGERI, Z. M., EVANS, R. & GACHET, C. (2003) A role of the fast ATP-gated P2X1 cation channel in thrombosis of small arteries in vivo. *J Exp Med,* 198**,** 661-7.

HEGG, C. C., GREENWOOD, D., HUANG, W., HAN, P. & LUCERO, M. T. (2003) Activation of purinergic receptor subtypes modulates odor sensitivity. *J Neurosci,* 23**,** 8291-301.

HIBELL, A. D., THOMPSON, K. M., XING, M., HUMPHREY, P. P. & MICHEL, A. D. (2001) Complexities of measuring antagonist potency at P2X(7) receptor orthologs. *J Pharmacol Exp Ther,* 296**,** 947-57.

HOFMANN, K. A. W. S. (1993) TMbase - A database of membrane spanning proteins segments. *Biol. Chem. Hoppe-Seyler,* 374**,** 166

HOLTON, F. A. & HOLTON, P. (1954) The capillary dilator substances in dry powders of spinal roots; a possible role of adenosine triphosphate in chemical transmission from nerve endings. *J Physiol,* 126**,** 124-40.

HOLTON, P. (1959) The liberation of adenosine triphosphate on antidromic stimulation of sensory nerves. *J Physiol,* 145**,** 494-504.

HORVATH, R. J. & DELEO, J. A. (2009) Morphine enhances microglial migration through modulation of P2X4 receptor signaling. *J Neurosci,* 29**,** 998-1005.

HU, B., SENKLER, C., YANG, A., SOTO, F. & LIANG, B. T. (2002) P2X4 receptor is a glycosylated cardiac receptor mediating a positive inotropic response to ATP. *J Biol Chem,* 277**,** 15752-7.

HUIDOBRO-TORO, J. P., LORCA, R. A. & CODDOU, C. (2008) Trace metals in the brain: allosteric modulators of ligand-gated receptor channels, the case of ATP-gated P2X receptors. *Eur Biophys J,* 37**,** 301-14.

HUXTABLE, A. G., ZWICKER, J. D., POON, B. Y., PAGLIARDINI, S., VROUWE, S. Q., GREER, J. J. & FUNK, G. D. (2009) Tripartite purinergic modulation of central respiratory networks during perinatal development: the influence of ATP, ectonucleotidases, and ATP metabolites. *J Neurosci,* 29**,** 14713-25.

JELINKOVA, I., VAVRA, V., JINDRICHOVA, M., OBSIL, T., ZEMKOVA, H. W., ZEMKOVA, H. & STOJILKOVIC, S. S. (2008) Identification of P2X(4) receptor transmembrane residues contributing to channel gating and interaction with ivermectin. *Pflugers Arch,* 456**,** 939-50.

JIANG, L. H., KIM, M., SPELTA, V., BO, X., SURPRENANT, A. & NORTH, R. A. (2003) Subunit arrangement in P2X receptors. *J Neurosci,* 23**,** 8903-10.

JIANG, L. H., MACKENZIE, A. B., NORTH, R. A. & SURPRENANT, A. (2000a) Brilliant blue G selectively blocks ATP-gated rat P2X(7) receptors. *Mol Pharmacol,* 58**,** 82-8.

JIANG, L. H., RASSENDREN, F., SPELTA, V., SURPRENANT, A. & NORTH, R. A. (2001) Amino acid residues involved in gating identified in the first membrane-spanning domain of the rat P2X(2) receptor. *J Biol Chem,* 276**,** 14902-8.

JIANG, L. H., RASSENDREN, F., SURPRENANT, A. & NORTH, R. A. (2000b) Identification of amino acid residues contributing to the ATP-binding site of a purinergic P2X receptor. *J Biol Chem,* 275**,** 34190-6.

JIN, R., BANKE, T. G., MAYER, M. L., TRAYNELIS, S. F. & GOUAUX, E. (2003) Structural basis for partial agonist action at ionotropic glutamate receptors. *Nat Neurosci,* 6**,** 803-10.

KAAN, T. K., YIP, P. K., GRIST, J., CEFALU, J. S., NUNN, P. A., FORD, A. P., ZHONG, Y. & MCMAHON, S. B. Endogenous purinergic control of bladder activity via presynaptic P2X3 and P2X2/3 receptors in the spinal cord. *J Neurosci,* 30**,** 4503-7.

KAWATE, T. & GOUAUX, E. (2006) Fluorescence-detection size-exclusion chromatography for precrystallization screening of integral membrane proteins. *Structure,* 14**,** 673-81.

KAWATE, T., MICHEL, J. C., BIRDSONG, W. T. & GOUAUX, E. (2009) Crystal structure of the ATP-gated P2X(4) ion channel in the closed state. *Nature,* 460**,** 592-8.

KELLENBERGER, S. & SCHILD, L. (2002) Epithelial sodium channel/degenerin family of ion channels: a variety of functions for a shared structure. *Physiol Rev,* 82**,** 735-67.

KELLETT, E., PERRY, S. J., SANTAMA, N., WORSTER, B. M., BENJAMIN, P. R. & BURKE, J. F. (1996) Myomodulin gene of Lymnaea: structure, expression, and analysis of neuropeptides. *J Neurosci,* 16**,** 4949-57.

KELLEY, S. P., DUNLOP, J. I., KIRKNESS, E. F., LAMBERT, J. J. & PETERS, J. A. (2003) A cytoplasmic region determines single-channel conductance in 5-HT3 receptors. *Nature,* 424**,** 321-4.

KEMENES, G., C. J. ELLIOT, ET AL (1986) Chemical and Tactile Inputs to the Lymnaea Feeding System: Effects on Behaviour and Neural Circuitry. *Journal of Experimental Biology,* 122**,** 113-137.

KEMENES, G. & ELLIOTT, C. J. (1994) Analysis of the feeding motor pattern in the pond snail, Lymnaea stagnalis: photoinactivation of axonally stained pattern-generating interneurons. *J Neurosci,* 14**,** 153-66.

KEMENES, G., STARAS, K. & BENJAMIN, P. R. (1997) In vitro appetitive classical conditioning of the feeding response in the pond snail Lymnaea stagnalis. *J Neurophysiol,* 78**,** 2351-62.

KHAIRA, S. K., POUTON, C. W. & HAYNES, J. M. (2009) P2X2, P2X4 and P2Y1 receptors elevate intracellular Ca2+ in mouse embryonic stem cell-derived GABAergic neurons. *Br J Pharmacol,* 158**,** 1922-31.

KHAKH, B. S., BAO, X. R., LABARCA, C. & LESTER, H. A. (1999a) Neuronal P2X transmitter-gated cation channels change their ion selectivity in seconds. *Nat Neurosci,* 2**,** 322-30.

KHAKH, B. S. & HENDERSON, G. (1998) ATP receptor-mediated enhancement of fast excitatory neurotransmitter release in the brain. *Mol Pharmacol,* 54**,** 372-8.

KHAKH, B. S., MICHEL, A. & HUMPHREY, P. P. (1994) Estimates of antagonist affinities at P2X purinoceptors in rat vas deferens. *Eur J Pharmacol,* 263**,** 301-9.

KHAKH, B. S. & NORTH, R. A. (2006) P2X receptors as cell-surface ATP sensors in health and disease. *Nature,* 442**,** 527-32.

KHAKH, B. S., PROCTOR, W. R., DUNWIDDIE, T. V., LABARCA, C. & LESTER, H. A. (1999b) Allosteric control of gating and kinetics at P2X(4) receptor channels. *J Neurosci,* 19**,** 7289-99.

KHAKH, B. S., SMITH, W. B., CHIU, C. S., JU, D., DAVIDSON, N. & LESTER, H. A. (2001) Activation-dependent changes in receptor distribution and dendritic

morphology in hippocampal neurons expressing P2X2-green fluorescent protein receptors. *Proc Natl Acad Sci U S A,* 98**,** 5288-93.
KICHIN (1994) *The Biology of Tardigrades,* London, Portland Press.
KIM, M., JIANG, L. H., WILSON, H. L., NORTH, R. A. & SURPRENANT, A. (2001) Proteomic and functional evidence for a P2X7 receptor signalling complex. *EMBO J,* 20**,** 6347-58.
KING, B. F., TOWNSEND-NICHOLSON, A., WILDMAN, S. S., THOMAS, T., SPYER, K. M. & BURNSTOCK, G. (2000) Coexpression of rat P2X2 and P2X6 subunits in Xenopus oocytes. *J Neurosci,* 20**,** 4871-7.
KING, B. F., WILDMAN, S. S., ZIGANSHINA, L. E., PINTOR, J. & BURNSTOCK, G. (1997) Effects of extracellular pH on agonism and antagonism at a recombinant P2X2 receptor. *Br J Pharmacol,* 121**,** 1445-53.
KNOFEL, T. & STRATER, N. (2001) Mechanism of hydrolysis of phosphate esters by the dimetal center of 5'-nucleotidase based on crystal structures. *J Mol Biol,* 309**,** 239-54.
KORNEEV, S. A., KEMENES, I., STRAUB, V., STARAS, K., KORNEEVA, E. I., KEMENES, G., BENJAMIN, P. R. & O'SHEA, M. (2002) Suppression of nitric oxide (NO)-dependent behavior by double-stranded RNA-mediated silencing of a neuronal NO synthase gene. *J Neurosci,* 22**,** RC227.
KORNEEV, S. A., PARK, J. H. & O'SHEA, M. (1999) Neuronal expression of neural nitric oxide synthase (nNOS) protein is suppressed by an antisense RNA transcribed from an NOS pseudogene. *J Neurosci,* 19**,** 7711-20.
KORNGREEN, A., MA, W., PRIEL, Z. & SILBERBERG, S. D. (1998) Extracellular ATP directly gates a cation-selective channel in rabbit airway ciliated epithelial cells. *J Physiol,* 508 (Pt 3)**,** 703-20.
KOSHIMIZU, T., KOSHIMIZU, M. & STOJILKOVIC, S. S. (1999) Contributions of the C-terminal domain to the control of P2X receptor desensitization. *J Biol Chem,* 274**,** 37651-7.
KOZAK, M. (1987) An analysis of 5'-noncoding sequences from 699 vertebrate messenger RNAs. *Nucleic Acids Res,* 15**,** 8125-48.
KRACUN, S., CHAPTAL, V., ABRAMSON, J. & KHAKH, B. S. Gated access to the pore of a P2X receptor: structural implications for closed-open transitions. *J Biol Chem,* 285**,** 10110-21.
KRASEL, C., ZABEL, U., LORENZ, K., REINER, S., AL-SABAH, S. & LOHSE, M. J. (2008) Dual role of the beta2-adrenergic receptor C terminus for the binding of beta-arrestin and receptor internalization. *J Biol Chem,* 283**,** 31840-8.
KRISHTAL, O. A., OSIPCHUK, Y. V., SHELEST, T. N. & SMIRNOFF, S. V. (1987) Rapid extracellular pH transients related to synaptic transmission in rat hippocampal slices. *Brain Res,* 436**,** 352-6.
KUBO, Y., BALDWIN, T. J., JAN, Y. N. & JAN, L. Y. (1993) Primary structure and functional expression of a mouse inward rectifier potassium channel. *Nature,* 362**,** 127-33.
LALO, U., PANKRATOV, Y., WICHERT, S. P., ROSSNER, M. J., NORTH, R. A., KIRCHHOFF, F. & VERKHRATSKY, A. (2008) P2X1 and P2X5 subunits form the functional P2X receptor in mouse cortical astrocytes. *J Neurosci,* 28**,** 5473-80.
LAMBRECHT, G. (2000) Agonists and antagonists acting at P2X receptors: selectivity profiles and functional implications. *Naunyn Schmiedebergs Arch Pharmacol,* 362**,** 340-50.

LE, K. T., BABINSKI, K. & SEGUELA, P. (1998) Central P2X4 and P2X6 channel subunits coassemble into a novel heteromeric ATP receptor. *J Neurosci,* 18**,** 7152-9.

LECUT, C., FREDERIX, K., JOHNSON, D. M., DEROANNE, C., THIRY, M., FACCINETTO, C., MAREE, R., EVANS, R. J., VOLDERS, P. G., BOURS, V. & OURY, C. (2009) P2X1 ion channels promote neutrophil chemotaxis through Rho kinase activation. *J Immunol,* 183**,** 2801-9.

LEITE, J. F., BLANTON, M. P., SHAHGHOLI, M., DOUGHERTY, D. A. & LESTER, H. A. (2003) Conformation-dependent hydrophobic photolabeling of the nicotinic receptor: electrophysiology-coordinated photochemistry and mass spectrometry. *Proc Natl Acad Sci U S A,* 100**,** 13054-9.

LEWIS, C., NEIDHART, S., HOLY, C., NORTH, R. A., BUELL, G. & SURPRENANT, A. (1995) Coexpression of P2X2 and P2X3 receptor subunits can account for ATP-gated currents in sensory neurons. *Nature,* 377**,** 432-5.

LI, C., PEOPLES, R. W. & WEIGHT, F. F. (1996) Cu2+ potently enhances ATP-activated current in rat nodose ganglion neurons. *Neurosci Lett,* 219**,** 45-8.

LI, C., PEOPLES, R. W. & WEIGHT, F. F. (1997) Inhibition of ATP-activated current by zinc in dorsal root ganglion neurones of bullfrog. *J Physiol,* 505 (Pt 3)**,** 641-53.

LI, G. H., LEE, E. M., BLAIR, D., HOLDING, C., PORONNIK, P., COOK, D. I., BARDEN, J. A. & BENNETT, M. R. (2000) The distribution of P2X receptor clusters on individual neurons in sympathetic ganglia and their redistribution on agonist activation. *J Biol Chem,* 275**,** 29107-12.

LI, M., CHANG, T. H., SILBERBERG, S. D. & SWARTZ, K. J. (2008) Gating the pore of P2X receptor channels. *Nat Neurosci,* 11**,** 883-7.

LI, Z., MIGITA, K., SAMWAYS, D. S., VOIGT, M. M. & EGAN, T. M. (2004) Gain and loss of channel function by alanine substitutions in the transmembrane segments of the rat ATP-gated P2X2 receptor. *J Neurosci,* 24**,** 7378-86.

LIN, S. L., CHUONG, C. M. & YING, S. Y. (2001) A Novel mRNA-cDNA interference phenomenon for silencing bcl-2 expression in human LNCaP cells. *Biochem Biophys Res Commun,* 281**,** 639-44.

LIU, M., KING, B. F., DUNN, P. M., RONG, W., TOWNSEND-NICHOLSON, A. & BURNSTOCK, G. (2001) Coexpression of P2X(3) and P2X(2) receptor subunits in varying amounts generates heterogeneous populations of P2X receptors that evoke a spectrum of agonist responses comparable to that seen in sensory neurons. *J Pharmacol Exp Ther,* 296**,** 1043-50.

LIU, X., SURPRENANT, A., MAO, H. J., ROGER, S., XIA, R., BRADLEY, H. & JIANG, L. H. (2007) Identification of key residues coordinating functional inhibition of P2X7 receptors by zinc and copper. *Mol Pharmacol*.

LOESCH, A. & BURNSTOCK, G. (1998) Electron-immunocytochemical localization of P2X1 receptors in the rat cerebellum. *Cell Tissue Res,* 294**,** 253-60.

LUDLOW, M. J., DURAI, L. & ENNION, S. J. (2009) Functional characterisation of intracellular Dictyostelium discoideum P2X receptors. *J Biol Chem*.

LUDLOW, M. J., TRAYNOR, D., FISHER, P. R. & ENNION, S. J. (2008) Purinergic-mediated Ca2+ influx in Dictyostelium discoideum. *Cell Calcium,* 44**,** 567-79.

LUNDIN, C., KALL, L., KREHER, S. A., KAPP, K., SONNHAMMER, E. L., CARLSON, J. R., HEIJNE, G. & NILSSON, I. (2007) Membrane topology of the Drosophila OR83b odorant receptor. *FEBS Lett,* 581**,** 5601-4.

LUSTIG, K. D., SHIAU, A. K., BRAKE, A. J. & JULIUS, D. (1993) Expression cloning of an ATP receptor from mouse neuroblastoma cells. *Proc Natl Acad Sci U S A,* 90**,** 5113-7.

MACKENZIE, A., WILSON, H. L., KISS-TOTH, E., DOWER, S. K., NORTH, R. A. & SURPRENANT, A. (2001) Rapid secretion of interleukin-1beta by microvesicle shedding. *Immunity,* 15**,** 825-35.

MACKENZIE, A. B., MAHAUT-SMITH, M. P. & SAGE, S. O. (1996) Activation of receptor-operated cation channels via P2X1 not P2T purinoceptors in human platelets. *J Biol Chem,* 271**,** 2879-81.

MACKENZIE, A. B., SURPRENANT, A. & NORTH, R. A. (1999) Functional and molecular diversity of purinergic ion channel receptors. *Ann N Y Acad Sci,* 868**,** 716-29.

MAHAUT-SMITH, M. P., ENNION, S. J., ROLF, M. G. & EVANS, R. J. (2000) ADP is not an agonist at P2X(1) receptors: evidence for separate receptors stimulated by ATP and ADP on human platelets. *Br J Pharmacol,* 131**,** 108-14.

MALIK, A. & BUCK, L. T. Adenosinergic modulation of neuronal activity in the pond snail Lymnaea stagnalis. *J Exp Biol,* 213**,** 1126-32.

MARQUEZ-KLAKA, B., RETTINGER, J., BHARGAVA, Y., EISELE, T. & NICKE, A. (2007) Identification of an intersubunit cross-link between substituted cysteine residues located in the putative ATP binding site of the P2X1 receptor. *J Neurosci,* 27**,** 1456-66.

MATUTE, C., TORRE, I., PEREZ-CERDA, F., PEREZ-SAMARTIN, A., ALBERDI, E., ETXEBARRIA, E., ARRANZ, A. M., RAVID, R., RODRIGUEZ-ANTIGUEDAD, A., SANCHEZ-GOMEZ, M. & DOMERCQ, M. (2007) P2X(7) receptor blockade prevents ATP excitotoxicity in oligodendrocytes and ameliorates experimental autoimmune encephalomyelitis. *J Neurosci,* 27**,** 9525-33.

MCCROHAN, C. R. & BENJAMIN, P. R. (1980) Synaptic relationships of the cerebral giant cells with motoneurones in the feeding system of Lymnaea stagnalis. *J Exp Biol,* 85**,** 169-86.

MEYER, M. P., GROSCHEL-STEWART, U., ROBSON, T. & BURNSTOCK, G. (1999) Expression of two ATP-gated ion channels, P2X5 and P2X6, in developing chick skeletal muscle. *Dev Dyn,* 216**,** 442-9.

MIO, K., OGURA, T., YAMAMOTO, T., HIROAKI, Y., FUJIYOSHI, Y., KUBO, Y. & SATO, C. (2009) Reconstruction of the P2X(2) receptor reveals a vase-shaped structure with lateral tunnels above the membrane. *Structure,* 17**,** 266-75.

MONIF, M., REID, C. A., POWELL, K. L., SMART, M. L. & WILLIAMS, D. A. (2009) The P2X7 receptor drives microglial activation and proliferation: a trophic role for P2X7R pore. *J Neurosci,* 29**,** 3781-91.

MOROZ, L. L. (2000) Giant identified NO-releasing neurons and comparative histochemistry of putative nitrergic systems in gastropod molluscs. *Microsc Res Tech,* 49**,** 557-69.

MUNDLOS, S., PELLETIER, J., DARVEAU, A., BACHMANN, M., WINTERPACHT, A. & ZABEL, B. (1993) Nuclear localization of the protein encoded by the Wilms' tumor gene WT1 in embryonic and adult tissues. *Development,* 119**,** 1329-41.

MUNNO, D. W., PRINCE, D. J. & SYED, N. I. (2003) Synapse number and synaptic efficacy are regulated by presynaptic cAMP and protein kinase A. *J Neurosci,* 23**,** 4146-55.

MUSKHELISHVILI, L., THOMPSON, P. A., KUSEWITT, D. F., WANG, C. & KADLUBAR, F. F. (2001) In situ hybridization and immunohistochemical analysis of cytochrome P450 1B1 expression in human normal tissues. *J Histochem Cytochem,* 49**,** 229-36.

NAGAYA, N., TITTLE, R. K., SAAR, N., DELLAL, S. S. & HUME, R. I. (2005) An intersubunit zinc binding site in rat P2X2 receptors. *J Biol Chem,* 280**,** 25982-93.

NAKAZAWA, K., FUJIMORI, K., TAKANAKA, A. & INOUE, K. (1990) An ATP-activated conductance in pheochromocytoma cells and its suppression by extracellular calcium. *J Physiol,* 428**,** 257-72.

NAKAZAWA, K., LIU, M., INOUE, K. & OHNO, Y. (1997) pH dependence of facilitation by neurotransmitters and divalent cations of P2X2 purinoceptor/channels. *Eur J Pharmacol,* 337**,** 309-14.

NAKAZAWA, K. & OHNO, Y. (1996) Dopamine and 5-hydroxytryptamine selectively potentiate neuronal type ATP receptor channels. *Eur J Pharmacol,* 296**,** 119-22.

NAKAZAWA, K. & OHNO, Y. (1997) Effects of neuroamines and divalent cations on cloned and mutated ATP-gated channels. *Eur J Pharmacol,* 325**,** 101-8.

NELSON DR, H. R. (1990) *Tardigrada. In,* New York, John Wiley & Sons.

NEWBOLT, A., STOOP, R., VIRGINIO, C., SURPRENANT, A., NORTH, R. A., BUELL, G. & RASSENDREN, F. (1998) Membrane topology of an ATP-gated ion channel (P2X receptor). *J Biol Chem,* 273**,** 15177-82.

NICKE, A. (2008) Homotrimeric complexes are the dominant assembly state of native P2X7 subunits. *Biochem Biophys Res Commun,* 377**,** 803-8.

NICKE, A., BAUMERT, H. G., RETTINGER, J., EICHELE, A., LAMBRECHT, G., MUTSCHLER, E. & SCHMALZING, G. (1998) P2X1 and P2X3 receptors form stable trimers: a novel structural motif of ligand-gated ion channels. *Embo J,* 17**,** 3016-28.

NICKE, A., KERSCHENSTEINER, D. & SOTO, F. (2005) Biochemical and functional evidence for heteromeric assembly of P2X1 and P2X4 subunits. *J Neurochem,* 92**,** 925-33.

NORTH, R. A. (2002) Molecular physiology of P2X receptors. *Physiol Rev,* 82**,** 1013-67.

NORTH, R. A. & BARNARD, E. A. (1997) Nucleotide receptors. *Curr Opin Neurobiol,* 7**,** 346-57.

NORTH, R. A. & SURPRENANT, A. (2000) Pharmacology of cloned P2X receptors. *Annu Rev Pharmacol Toxicol,* 40**,** 563-80.

NOVAK, I., JANS, I. M. & WOHLFAHRT, L. Effect of P2X(7) receptor knockout on exocrine secretion of pancreas, salivary glands and lacrimal glands. *J Physiol,* 588**,** 3615-27.

OSTERMEIER, C. & MICHEL, H. (1997) Crystallization of membrane proteins. *Curr Opin Struct Biol,* 7**,** 697-701.

PANKRATOV, Y., LALO, U., VERKHRATSKY, A. & NORTH, R. A. (2006) Vesicular release of ATP at central synapses. *Pflugers Arch,* 452**,** 589-97.

PANKRATOV, Y., LALO, U., VERKHRATSKY, A. & NORTH, R. A. (2007) Quantal release of ATP in mouse cortex. *J Gen Physiol,* 129**,** 257-65.

PANKRATOV, Y. V., LALO, U. V. & KRISHTAL, O. A. (2002) Role for P2X receptors in long-term potentiation. *J Neurosci,* 22**,** 8363-9.

PANNICKE, T., FISCHER, W., BIEDERMANN, B., SCHADLICH, H., GROSCHE, J., FAUDE, F., WIEDEMANN, P., ALLGAIER, C., ILLES, P., BURNSTOCK, G. & REICHENBACH, A. (2000) P2X7 receptors in Muller glial cells from the human retina. *J Neurosci,* 20**,** 5965-72.

PAOLETTI, P., PERIN-DUREAU, F., FAYYAZUDDIN, A., LE GOFF, A., CALLEBAUT, I. & NEYTON, J. (2000) Molecular organization of a zinc binding n-terminal modulatory domain in a NMDA receptor subunit. *Neuron,* 28**,** 911-25.

PERRY, S. J., STRAUB, V. A., KEMENES, G., SANTAMA, N., WORSTER, B. M., BURKE, J. F. & BENJAMIN, P. R. (1998) Neural modulation of gut motility by myomodulin peptides and acetylcholine in the snail Lymnaea. *J Neurophysiol,* 79**,** 2460-74.

PRIEL, A. & SILBERBERG, S. D. (2004) Mechanism of ivermectin facilitation of human P2X4 receptor channels. *J Gen Physiol,* 123**,** 281-93.

QURESHI, O. S., PARAMASIVAM, A., YU, J. C. & MURRELL-LAGNADO, R. D. (2007) Regulation of P2X4 receptors by lysosomal targeting, glycan protection and exocytosis. *J Cell Sci,* 120**,** 3838-49.

RADFORD, K. M., VIRGINIO, C., SURPRENANT, A., NORTH, R. A. & KAWASHIMA, E. (1997) Baculovirus expression provides direct evidence for heteromeric assembly of P2X2 and P2X3 receptors. *J Neurosci,* 17**,** 6529-33.

RAOUF, R., BLAIS, D. & SEGUELA, P. (2005) High zinc sensitivity and pore formation in an invertebrate P2X receptor. *Biochim Biophys Acta,* 1669**,** 135-41.

RASSENDREN, F., BUELL, G., NEWBOLT, A., NORTH, R. A. & SURPRENANT, A. (1997a) Identification of amino acid residues contributing to the pore of a P2X receptor. *EMBO J,* 16**,** 3446-54.

RASSENDREN, F., BUELL, G. N., VIRGINIO, C., COLLO, G., NORTH, R. A. & SURPRENANT, A. (1997b) The permeabilizing ATP receptor, P2X7. Cloning and expression of a human cDNA. *J Biol Chem,* 272**,** 5482-6.

REINER, S., ZIEGLER, N., LEON, C., LORENZ, K., VON HAYN, K., GACHET, C., LOHSE, M. J. & HOFFMANN, C. (2009) {beta}-ARRESTIN-2 INTERACTION AND INTERNALIZATION OF THE HUMAN P2Y1-RECEPTOR ARE DEPENDENT ON C-TERMINAL PHOSPHORLAYTION SITES. *Mol Pharmacol.*

ROBERTS, J. A. & EVANS, R. J. (2004) ATP binding at human P2X1 receptors. Contribution of aromatic and basic amino acids revealed using mutagenesis and partial agonists. *J Biol Chem,* 279**,** 9043-55.

ROBERTS, J. A. & EVANS, R. J. (2005) Mutagenesis studies of conserved proline residues of human P2X receptors for ATP indicate that proline 272 contributes to channel function. *J Neurochem,* 92**,** 1256-64.

ROBERTS, J. A., VIAL, C., DIGBY, H. R., AGBOH, K. C., WEN, H., ATTERBURY-THOMAS, A. & EVANS, R. J. (2006) Molecular properties of P2X receptors. *Pflugers Arch,* 452**,** 486-500.

ROSE, R. M. & BENJAMIN, P. R. (1979) The relationship of the central motor pattern to the feeding cycle of Lymnaea stagnalis. *J Exp Biol,* 80**,** 137-63.

ROSE, R. M., BENJAMIN, P. R. (1981) Interneuronal Control of Feeding in the Pond Snail Lymnaea Stagnalis : II. The Interneuronal Mechanism Generating Feeding Cycles *Journal of Experimental Biology,* 92**,** 203-228

ROSE, T. M., HENIKOFF, J. G. & HENIKOFF, S. (2003) CODEHOP (COnsensus-DEgenerate Hybrid Oligonucleotide Primer) PCR primer design. *Nucleic Acids Res,* 31**,** 3763-6.

RUBIO, M. E. & SOTO, F. (2001) Distinct Localization of P2X receptors at excitatory postsynaptic specializations. *J Neurosci,* 21**,** 641-53.

RYTEN, M., KOSHI, R., KNIGHT, G. E., TURMAINE, M., DUNN, P., COCKAYNE, D. A., FORD, A. P. & BURNSTOCK, G. (2007) Abnormalities in neuromuscular junction structure and skeletal muscle function in mice lacking the P2X2 nucleotide receptor. *Neuroscience,* 148**,** 700-11.

SANTAMA, N., BRIERLEY, M., BURKE, J. F. & BENJAMIN, P. R. (1994) Neural network controlling feeding in Lymnaea stagnalis: immunocytochemical localization of myomodulin, small cardioactive peptide, buccalin, and FMRFamide-related peptides. *J Comp Neurol,* 342**,** 352-65.

SEGUELA, P., HAGHIGHI, A., SOGHOMONIAN, J. J. & COOPER, E. (1996) A novel neuronal P2x ATP receptor ion channel with widespread distribution in the brain. *J Neurosci,* 16**,** 448-55.

SENATORE, A. & SPAFFORD, J. D. Transient and big are key features of an invertebrate T-type channel (LCav3) from the central nervous system of Lymnaea stagnalis. *J Biol Chem,* 285**,** 7447-58.

SILBERBERG, S. D., CHANG, T. H. & SWARTZ, K. J. (2005) Secondary structure and gating rearrangements of transmembrane segments in rat P2X4 receptor channels. *J Gen Physiol,* 125**,** 347-59.

SILBERBERG, S. D., LI, M. & SWARTZ, K. J. (2007) Ivermectin Interaction with transmembrane helices reveals widespread rearrangements during opening of P2X receptor channels. *Neuron,* 54**,** 263-74.

SIM, J. A., BROOMHEAD, H. E. & NORTH, R. A. (2008) Ectodomain lysines and suramin block of P2X1 receptors. *J Biol Chem,* 283**,** 29841-6.

SIM, J. A., CHAUMONT, S., JO, J., ULMANN, L., YOUNG, M. T., CHO, K., BUELL, G., NORTH, R. A. & RASSENDREN, F. (2006) Altered hippocampal synaptic potentiation in P2X4 knock-out mice. *J Neurosci,* 26**,** 9006-9.

SIM, J. A., PARK, C. K., OH, S. B., EVANS, R. J. & NORTH, R. A. (2007) P2X1 and P2X4 receptor currents in mouse macrophages. *Br J Pharmacol,* 152**,** 1283-90.

SLUYTER, R., BARDEN, J. A. & WILEY, J. S. (2001) Detection of P2X purinergic receptors on human B lymphocytes. *Cell Tissue Res,* 304**,** 231-6.

SMART, T. G., XIE, X. & KRISHEK, B. J. (1994) Modulation of inhibitory and excitatory amino acid receptor ion channels by zinc. *Prog Neurobiol,* 42**,** 393-441.

SONNLEITNER, A., MANNUZZU, L. M., TERAKAWA, S. & ISACOFF, E. Y. (2002) Structural rearrangements in single ion channels detected optically in living cells. *Proc Natl Acad Sci U S A,* 99**,** 12759-64.

SOTO, F., GARCIA-GUZMAN, M., KARSCHIN, C. & STUHMER, W. (1996) Cloning and tissue distribution of a novel P2X receptor from rat brain. *Biochem Biophys Res Commun,* 223**,** 456-60.

SOTO, F., GARCIA-GUZMAN, M. & STUHMER, W. (1997) Cloned ligand-gated channels activated by extracellular ATP (P2X receptors). *J Membr Biol,* 160**,** 91-100.

SOTO, F., LAMBRECHT, G., NICKEL, P., STUHMER, W. & BUSCH, A. E. (1999) Antagonistic properties of the suramin analogue NF023 at heterologously expressed P2X receptors. *Neuropharmacology,* 38**,** 141-9.

STAIKOPOULOS, V., SESSLE, B. J., FURNESS, J. B. & JENNINGS, E. A. (2007) Localization of P2X2 and P2X3 receptors in rat trigeminal ganglion neurons. *Neuroscience,* 144**,** 208-16.

STARAS, K., KEMENES, G. & BENJAMIN, P. R. (1998) Pattern-generating role for motoneurons in a rhythmically active neuronal network. *J Neurosci,* 18**,** 3669-88.

STARAS, K., KEMENES, I., BENJAMIN, P. R. & KEMENES, G. (2003) Loss of self-inhibition is a cellular mechanism for episodic rhythmic behavior. *Curr Biol,* 13**,** 116-24.

STOOP, R., SURPRENANT, A. & NORTH, R. A. (1997) Different sensitivities to pH of ATP-induced currents at four cloned P2X receptors. *J Neurophysiol,* 78**,** 1837-40.

STRAUB, V. A. & BENJAMIN, P. R. (2001) Extrinsic modulation and motor pattern generation in a feeding network: a cellular study. *J Neurosci,* 21**,** 1767-78.

STRAUB, V. A., STARAS, K., KEMENES, G. & BENJAMIN, P. R. (2002) Endogenous and network properties of Lymnaea feeding central pattern generator interneurons. *J Neurophysiol,* 88**,** 1569-83.

STRYER, L. (1978) Fluorescence energy transfer as a spectroscopic ruler. *Annu Rev Biochem,* 47**,** 819-46.

STUHMER, T., AMAR, M., HARVEY, R. J., BERMUDEZ, I., VAN MINNEN, J. & DARLISON, M. G. (1996) Structure and pharmacological properties of a molluscan glutamate-gated cation channel and its likely role in feeding behavior. *J Neurosci,* 16**,** 2869-80.

SUN, B., LI, J., OKAHARA, K. & KAMBAYASHI, J. (1998) P2X1 purinoceptor in human platelets. Molecular cloning and functional characterization after heterologous expression. *J Biol Chem,* 273**,** 11544-7.

SURPRENANT, A., RASSENDREN, F., KAWASHIMA, E., NORTH, R. A. & BUELL, G. (1996) The cytolytic P2Z receptor for extracellular ATP identified as a P2X receptor (P2X7). *Science,* 272**,** 735-8.

SYED, N. I., BULLOCH, A. G. & LUKOWIAK, K. (1990) In vitro reconstruction of the respiratory central pattern generator of the mollusk Lymnaea. *Science,* 250**,** 282-5.

SYED, N. I. & WINLOW, W. (1991) Coordination of locomotor and cardiorespiratory networks of Lymnaea stagnalis by a pair of identified interneurones. *J Exp Biol,* 158**,** 37-62.

TABARA, H., GRISHOK, A. & MELLO, C. C. (1998) RNAi in C. elegans: soaking in the genome sequence. *Science,* 282**,** 430-1.

TASCHENBERGER, H., JUTTNER, R. & GRANTYN, R. (1999) Ca2+-permeable P2X receptor channels in cultured rat retinal ganglion cells. *J Neurosci,* 19**,** 3353-66.

TATE, C. G. (2001) Overexpression of mammalian integral membrane proteins for structural studies. *FEBS Lett,* 504**,** 94-8.

TINOCO, M. L., DIAS, B. B., DALL'ASTTA, R. C., PAMPHILE, J. A. & ARAGAO, F. J. In vivo trans-specific gene silencing in fungal cells by in planta expression of a double-stranded RNA. *BMC Biol,* 8**,** 27.

TITTLE, R. K., POWER, J. M. & HUME, R. I. (2007) A histidine scan to probe the flexibility of the rat P2X2 receptor zinc-binding site. *J Biol Chem,* 282**,** 19526-33.

TORRES, G. E., EGAN, T. M. & VOIGT, M. M. (1998a) Topological analysis of the ATP-gated ionotropic [correction of ionotrophic] P2X2 receptor subunit. *FEBS Lett,* 425**,** 19-23.

TORRES, G. E., EGAN, T. M. & VOIGT, M. M. (1999) Hetero-oligomeric assembly of P2X receptor subunits. Specificities exist with regard to possible partners. *J Biol Chem,* 274**,** 6653-9.

TORRES, G. E., HAINES, W. R., EGAN, T. M. & VOIGT, M. M. (1998b) Co-expression of P2X1 and P2X5 receptor subunits reveals a novel ATP-gated ion channel. *Mol Pharmacol,* 54**,** 989-93.

TSUDA, M., KUBOYAMA, K., INOUE, T., NAGATA, K., TOZAKI-SAITOH, H. & INOUE, K. (2009) Behavioral phenotypes of mice lacking purinergic P2X4 receptors in acute and chronic pain assays. *Mol Pain,* 5**,** 28.

UENO, T., UENO, S., KAKAZU, Y., AKAIKE, N. & NABEKURA, J. (2001) Bidirectional modulation of P2X receptor-mediated response by divalent cations in rat dorsal motor nucleus of the vagus neurons. *J Neurochem,* 78**,** 1009-18.

VALERA, S., HUSSY, N., EVANS, R. J., ADAMI, N., NORTH, R. A., SURPRENANT, A. & BUELL, G. (1994) A new class of ligand-gated ion channel defined by P2x receptor for extracellular ATP. *Nature,* 371**,** 516-9.

VALLEE, B. L. & AULD, D. S. (1990) Zinc coordination, function, and structure of zinc enzymes and other proteins. *Biochemistry,* 29**,** 5647-59.

VAN DER KLOOT, W. (2003) Loading and recycling of synaptic vesicles in the Torpedo electric organ and the vertebrate neuromuscular junction. *Prog Neurobiol,* 71**,** 269-303.

VAN NIEROP, P., BERTRAND, S., MUNNO, D. W., GOUWENBERG, Y., VAN MINNEN, J., SPAFFORD, J. D., SYED, N. I., BERTRAND, D. & SMIT, A. B. (2006) Identification and functional expression of a family of nicotinic acetylcholine receptor subunits in the central nervous system of the mollusc Lymnaea stagnalis. *J Biol Chem,* 281**,** 1680-91.

VEHOVSZKY, A. & ELLIOTT, C. J. (2001) Activation and reconfiguration of fictive feeding by the octopamine-containing modulatory OC interneurons in the snail Lymnaea. *J Neurophysiol,* 86**,** 792-808.

VEHOVSZKY, A., SZABO, H., HIRIPI, L., ELLIOTT, C. J. & HERNADI, L. (2007) Behavioural and neural deficits induced by rotenone in the pond snail Lymnaea stagnalis. A possible model for Parkinson's disease in an invertebrate. *Eur J Neurosci,* 25**,** 2123-30.

VIAL, C. & EVANS, R. J. (2000) P2X receptor expression in mouse urinary bladder and the requirement of P2X(1) receptors for functional P2X receptor responses in the mouse urinary bladder smooth muscle. *Br J Pharmacol,* 131**,** 1489-95.

VIAL, C., RIGBY, R. & EVANS, R. J. (2006) Contribution of P2X1 receptor intracellular basic residues to channel properties. *Biochem Biophys Res Commun,* 350**,** 244-8.

VIAL, C., ROBERTS, J. A. & EVANS, R. J. (2004) Molecular properties of ATP-gated P2X receptor ion channels. *Trends Pharmacol Sci,* 25**,** 487-93.

VIGNE, P., HECHLER, B., GACHET, C., BREITTMAYER, J. P. & FRELIN, C. (1999) Benzoyl ATP is an antagonist of rat and human P2Y1 receptors and of platelet aggregation. *Biochem Biophys Res Commun,* 256**,** 94-7.

VIRGINIO, C., CHURCH, D., NORTH, R. A. & SURPRENANT, A. (1997) Effects of divalent cations, protons and calmidazolium at the rat P2X7 receptor. *Neuropharmacology,* 36**,** 1285-94.

VIRGINIO, C., MACKENZIE, A., NORTH, R. A. & SURPRENANT, A. (1999) Kinetics of cell lysis, dye uptake and permeability changes in cells expressing the rat P2X7 receptor. *J Physiol,* 519 Pt 2**,** 335-46.

VON KUGELGEN, I. (2006) Pharmacological profiles of cloned mammalian P2Y-receptor subtypes. *Pharmacol Ther,* 110**,** 415-32.

VOROBJEV, V. S., SHARONOVA, I. N., SERGEEVA, O. A. & HAAS, H. L. (2003) Modulation of ATP-induced currents by zinc in acutely isolated hypothalamic neurons of the rat. *Br J Pharmacol,* 139**,** 919-26.

VULCHANOVA, L., ARVIDSSON, U., RIEDL, M., WANG, J., BUELL, G., SURPRENANT, A., NORTH, R. A. & ELDE, R. (1996) Differential distribution of two ATP-gated channels (P2X receptors) determined by immunocytochemistry. *Proc Natl Acad Sci U S A,* 93**,** 8063-7.

WALKER, J. E., SARASTE, M., RUNSWICK, M. J. & GAY, N. J. (1982) Distantly related sequences in the alpha- and beta-subunits of ATP synthase, myosin, kinases and other ATP-requiring enzymes and a common nucleotide binding fold. *EMBO J,* 1**,** 945-51.

WAN, H., MACKAY, B., IQBAL, H., NASKAR, S. & KEMENES, G. Delayed intrinsic activation of an NMDA-independent CaM-kinase II in a critical time window is necessary for late consolidation of an associative memory. *J Neurosci,* 30**,** 56-63.

WANG, T. L., HACKAM, A., GUGGINO, W. B. & CUTTING, G. R. (1995) A single histidine residue is essential for zinc inhibition of GABA rho 1 receptors. *J Neurosci,* 15**,** 7684-91.

WAREHAM, K., VIAL, C., WYKES, R. C., BRADDING, P. & SEWARD, E. P. (2009) Functional evidence for the expression of P2X1, P2X4 and P2X7 receptors in human lung mast cells. *Br J Pharmacol,* 157**,** 1215-24.

WERNER, P., SEWARD, E. P., BUELL, G. N. & NORTH, R. A. (1996) Domains of P2X receptors involved in desensitization. *Proc Natl Acad Sci U S A,* 93**,** 15485-90.

WHEELAN H.A., M. C. R. (1996) Food-related conditioning and neuronal correlates in the freshwater snail *Lymnaea Stagnalis*. *Journal of Molluscan Studies,* 62**,** 483-494.

WILDMAN, S. S., KING, B. F. & BURNSTOCK, G. (1997) Potentiation of ATP-responses at a recombinant P2x2 receptor by neurotransmitters and related substances. *Br J Pharmacol,* 120**,** 221-4.

WILDMAN, S. S., KING, B. F. & BURNSTOCK, G. (1998) Zn2+ modulation of ATP-responses at recombinant P2X2 receptors and its dependence on extracellular pH. *Br J Pharmacol,* 123**,** 1214-20.

WILDMAN, S. S., KING, B. F. & BURNSTOCK, G. (1999a) Modulation of ATP-responses at recombinant rP2X4 receptors by extracellular pH and zinc. *Br J Pharmacol,* 126**,** 762-8.

WILDMAN, S. S., KING, B. F. & BURNSTOCK, G. (1999b) Modulatory activity of extracellular H+ and Zn2+ on ATP-responses at rP2X1 and rP2X3 receptors. *Br J Pharmacol,* 128**,** 486-92.

WILEY, J. S., DAO-UNG, L. P., LI, C., SHEMON, A. N., GU, B. J., SMART, M. L., FULLER, S. J., BARDEN, J. A., PETROU, S. & SLUYTER, R. (2003) An

Ile-568 to Asn polymorphism prevents normal trafficking and function of the human P2X7 receptor. *J Biol Chem,* 278**,** 17108-13.

WILKINSON, W., GADEBERG, H., HARRISON, A., ALLEN, N., RICCARDI, D. & KEMP, P. (2009) Carbon monoxide is a rapid modulator of recombinant and native P2X(2) ligand-gated ion channels. *Br J Pharmacol*.

XIONG, K., PEOPLES, R. W., MONTGOMERY, J. P., CHIANG, Y., STEWART, R. R., WEIGHT, F. F. & LI, C. (1999) Differential modulation by copper and zinc of P2X2 and P2X4 receptor function. *J Neurophysiol,* 81**,** 2088-94.

YAMAMOTO, K., KORENAGA, R., KAMIYA, A., QI, Z., SOKABE, M. & ANDO, J. (2000) P2X(4) receptors mediate ATP-induced calcium influx in human vascular endothelial cells. *Am J Physiol Heart Circ Physiol,* 279**,** H285-92.

YAN, Z., LIANG, Z., TOMIC, M., OBSIL, T. & STOJILKOVIC, S. S. (2005) Molecular determinants of the agonist binding domain of a P2X receptor channel. *Mol Pharmacol,* 67**,** 1078-88.

YEGUTKIN, G. G. (2008) Nucleotide- and nucleoside-converting ectoenzymes: Important modulators of purinergic signalling cascade. *Biochim Biophys Acta,* 1783**,** 673-94.

YEOMAN, M. S., BRIERLEY, M. J. & BENJAMIN, P. R. (1996) Central pattern generator interneurons are targets for the modulatory serotonergic cerebral giant cells in the feeding system of Lymnaea. *J Neurophysiol,* 75**,** 11-25.

YEOMAN, M. S., KEMENES, G., BENJAMIN, P. R. & ELLIOTT, C. J. (1994a) Modulatory role for the serotonergic cerebral giant cells in the feeding system of the snail, Lymnaea. II. Photoinactivation. *J Neurophysiol,* 72**,** 1372-82.

YEOMAN, M. S., PARISH, D. C. & BENJAMIN, P. R. (1993) A cholinergic modulatory interneuron in the feeding system of the snail, Lymnaea. *J Neurophysiol,* 70**,** 37-50.

YEOMAN, M. S., PIENEMAN, A. W., FERGUSON, G. P., TER MAAT, A. & BENJAMIN, P. R. (1994b) Modulatory role for the serotonergic cerebral giant cells in the feeding system of the snail, Lymnaea. I. Fine wire recording in the intact animal and pharmacology. *J Neurophysiol,* 72**,** 1357-71.

YEOMAN, M. S., VEHOVSZKY, A., KEMENES, G., ELLIOTT, C. J. & BENJAMIN, P. R. (1995) Novel interneuron having hybrid modulatory-central pattern generator properties in the feeding system of the snail, Lymnaea stagnalis. *J Neurophysiol,* 73**,** 112-24.

YOUNG, M. T. (2009) P2X receptors: dawn of the post-structure era. *Trends Biochem Sci*.

YOUNG, M. T., FISHER, J. A., FOUNTAIN, S. J., FORD, R. C., NORTH, R. A. & KHAKH, B. S. (2008) Molecular shape, architecture, and size of P2X4 receptors determined using fluorescence resonance energy transfer and electron microscopy. *J Biol Chem,* 283**,** 26241-51.

YOUNG, M. T., PELEGRIN, P. & SURPRENANT, A. (2007) Amino acid residues in the P2X7 receptor that mediate differential sensitivity to ATP and BzATP. *Mol Pharmacol,* 71**,** 92-100.

ZIMMERMANN, H. (1996) Biochemistry, localization and functional roles of ecto-nucleotidases in the nervous system. *Prog Neurobiol,* 49**,** 589-618.

ZIMMERMANN, H. (2001) Ectonucleotidases: Some recent developments and a note on nomenclature *Drug Development Research,* 52**,** 44 - 56.